Alma Mater Studiorum – Università di Bologna

DOTTORATO DI RICERCA IN

SCIENZE DELLA TERRA, DELLA VITA E DELL'AMBIENTE

Ciclo 33

Settore Concorsuale: 04/A1 - GEOCHIMICA, MINERALOGIA, PETROLOGIA, VULCANOLOGIA, GEORISORSE ED APPLICAZIONI

Settore Scientifico Disciplinare: GEO/08 - GEOCHIMICA E VULCANOLOGIA

ERUPTIVE AND DEPOSITIONAL PROCESSES OF WIDELY DISPERSED VOLCANIC ASH: INSIGHTS FROM THE BROWN TUFFS (AEOLIAN ISLANDS)

Presentata da: Sara Meschiari

Coordinatore Dottorato

Maria Giovanna Belcastro

Supervisore

Federico Lucchi

Co-Supervisori

Roberto Sulpizio
Paul Albert
Marzia Rovere

Esame finale anno 2021

Alla mia famiglia

Table of Contents

Abstract

This is a multidisciplinary study of the Brown Tuffs (BT) ash deposits recognized in the stratigraphic sequences of most of the Aeolian Islands and the Capo Milazzo peninsula in northern Sicily and representing the most voluminous and widely distributed tephra deposit in the region under study. A large dataset of major and minor elements of the BT juveniles (glass) has defined a range from K-series (K_2O = 3.3-7.5 wt.%) basaltic-andesites and trachy-andesites through to tephri-phonolites and trachytes (SiO_2 = 49.9-64.1 wt.%; Na_2O + K_2O = 6.5-12.6 wt.%) that is entirely consistent with the Vulcano magmatic system. Combined with stratigraphic information and new radiocarbon ages, these compositional data have defined four stratigraphic macro-units, namely the Lower (80-56 ky; LBT), Intermediate (56-27 ky; IBT), Intermediate-upper (26-24 ky; IBT-upper) and Upper BT (24-6 ky; UBT), which are separated by the Ischia Tephra (56 ky), Monte Guardia pyroclastics from Lipari (27-26 ky), and Spiaggia Lunga scoriae on Vulcano (24 ky). These macro-units are furtherly subdivided into a number of depositional units by the occurrence of paleosols, reworked horizons and localized erosive surfaces, or the interbedding of tephra layers and other volcanic units. Glass compositional data provide constraints on proximal-distal correlations of the BT with deep-sea tephra layers in the Tyrrhenian and Adriatic Seas and give new insights on the definition of the dispersal area of the BT eruptions. Sedimentological evidence of massive to stratified deposits and shear-related structures, coupled with grain-size and componentry analyses on selected units and glass geochemistry, have allowed to interpret the Bt on Vulcano and Lipari as the result of laterally-spreading, concentrated ash-rich PDCs that were able to travel up to distances of (at least) 16-17 km from the source area with a high potential of erosion of the substratum and a substantial capacity of impact over the territory. In proximal areas, the persistent intermittent stratification of the UBT provides evidence of processes of post-depositional disruption of the primary deposits due to fluid escape related to dissipation of pore pressure between layers at different porosity. Shear-structures similar to those observed in the field in the BT deposits have been reproduced by small-medium scale laboratory experiments carried out on ash granular flows using natural volcanic material, which have also allowed to describe the behaviour of ash-rich PDcs and their mobility depending on variations of slope-ratio, grain size and flow channelization. The resulting integrated dataset, eventually assisted by new data and elaboration of the available ones, provides a substantial contribution to the knowledge of the BT eruptions and insights on long-term hazard assessment in the study

area. In particular, the eruptive dynamics of the BT may have a role in characterizing the whole magmatic system of the La Fossa Caldera on Vulcano, in the light of the geochemical link highlighted between the UBT macrounit and the early products of the La Fossa cone.

Introduction

This work focuses on the topic of widely dispersed volcanic ash and its source areas, eruptive dynamics and mechanisms of transport and deposition for the purpose of improving the knowledge of explosive volcanism, volcanic hazard evaluation and synchronization of paleoenvironmental archives.

Explosive volcanic eruptions are the most powerful and destructive type of volcanic activity and are responsible for the widespread and voluminous dispersal of particles of various sizes and shapes, known as tephra, produced by mechanical fragmentation of magma and/or country rock. Volcanic ash (<2 mm) can be transported by pyroclastic density currents (PDCs) and their co-ignimbrite clouds or ejected into the atmosphere by eruptive columns resulting in a widespread areal dispersal over tens to thousands of kilometers from their source, and cause several hazard impacts on human activities and the environment with a potential influence on climate variability (e.g. Biass et al., 2014; Dingwell and Rutgersson, 2014; Sulpizio et al., 2014). Tephra deposits from these eruptions may be fundamental for reconstructing the volcanic history of a volcano and understanding the frequency and the impact of its eruptive activity on the surrounding environment. Widespread ash produced from single eruptions can reach enormous distances from the source with a quasi-synchronous deposition and provides invaluable isochronous markers that are recorded in a variety of sedimentary archives. Where the age of the corresponding eruptions is known, *via* radiometric dating or proximal-to-distal correlations, ash deposits preserved in distal occurrences are also powerful chronological and stratigraphic markers to decipher complex stratigraphic sequences across the region under study (Machida, 1999; Narcisi, 1996; Shane, 2000), and can be used to synchronize various paleoclimate records (e.g. Paterne et al., 1986; Paterne et al., 1988; Zanchetta et al., 2011) and understand the timing and rates of rapid environmental changes. More recently, tephrostratigraphy has been used in archaeological settings being able to link environmental archives to anthropological evolutionary changes thus the tephrostratigraphy provides the exciting opportunity to assess human responses to abrupt climatic changes (Giaccio et al., 2006; Anikovich et al., 2007; Lowe et al., 2012).

An additional knowledge on the eruptive and depositional processes and dispersal areas of widely dispersed volcanic ash, is here provided by the Brown Tuffs (BT) outcropping on Aeolian Islands and representing the most voluminous and widely distributed tephra deposit in this sector of the southern Tyrrhenian Sea. The BT consist of reddish-brown ash deposits with metric thickness recognized in the stratigraphic sequences of most of the Aeolian Islands and on the Capo Milazzo peninsula in northern Sicily. Their interpretation as paleosols, reworked or primary pyroclastic products, as well as their vent locations, areal distribution, chronology and eruptive processes has been long debated, also because for a long time they have been studied on the scale of individual islands (Bergeat, 1899; Crisci et al., 1981; Crisci et al., 1983; Crisci et al., 1991; Keller, 1967; Keller, 1980a; Keller, 1980b; Manetti et al., 1988; Manetti et al., 1995; Morche, 1988; Pichler, 1980; Gioncada et al., 2003). Therefore, a large agreement on the distribution and source areas of these deposits and their correlation with proximal volcanic units on Vulcano is still lacking, together with information on their eruptive processes and magmatic plumbing system. Recent stratigraphic studies (Lucchi et al., 2008; 2013) have reconstructed a succession of 15 different BT depositional units in a time interval ranging from c. 70 to 8 ka, separated and identified by interlayered tephra units from Aeolian Islands or Campanian volcanoes, discontinuous erosive surfaces or paleosols. Three stratigraphic macro units, Lower (70-56 ka), Intermediate (56-27 ka) and Upper BT (27-8 ka) are distinguished by the interbedded, regional-scale Ischia Tephra and Monte Guardia tephra unit from Lipari (Lucchi et al., 2008). The BT have been intepreted as the result of deposition from PDCs and associated fallout produced from pulsating hydromagmatic activity of eruptive vents inside the La Fossa caldera on Vulcano (De Astis et al., 1997; Lucchi et al., 2008; 2013).

However, in this general framework, there is still a lot to understand on BT origin and their source areas, their areal distribution and eruptive dynamics, transport and depositional processes and characteristics of the magmatic feeding system. The open problems are particularly important from the point of view of volcanic hazard assessment in the region under study, considering that the youngest BT eruptions are slightly older than the eruptive activity of the pyroclastic cone of La Fossa on Vulcano. Furthermore, taking into account their regional areal distribution, the BT are still substantially undervalued as a potential producer of widespread ash, and the proximal-distal correlations between the BT and pyroclastic tephra levels in deep sea cores in the Tyrrhenian Sea remain almost entirely unexplored.

The results of this PhD project provide a multidisciplinary study of the stratigraphic, lithological, sedimentological and petrochemical features of the BT in order to interpret their eruption dynamics, and transportation and depositional mechanisms, and to reconstruct the distribution area of the main stratigraphic units of the BT in the Aeolian Islands and in distal areas of the Tyrrhenian Sea. The framework is set through a careful revision on the stratigraphic succession of the BT on Lipari, Vulcano and the other islands of the archipelago, with particular attention to the definition of potentially correlable units between different islands and the units to be sampled for the purpose of subsequent analyses. A sedimentological study of the BT is performed on selected, best-exposed BT units at variable distances from the source area and combined with grain-size and componentry analyses. The results are integrated by properly designed laboratory experiments on granular flows using natural volcanic material for the purpose of reproducing and verifying the the behavior of the PDCs during the BT eruptions. Detailed geochemical investigation of BT glass fragments using specific micro-analytical techniques with the EMPA electronic microprobe were performed to determining the major, minor and trace element contents of the main BT units in their proximal outcrop areas to define distinctive features and variability trends useful for the stratigraphic correlation of the units and their use as a proximal correlative of tephra levels in deep sea cores (or other tephrostratigraphic archives). For the purpose of proximal-distal correlation of BT deposits, the numerous data available in the literature for deep sea cores in the Tyrrhenian Sea and terrestrial and lake archives were used. Moreover, the research will involve the sampling of several marine sediment cores collected in the years 2010-2014 by ISMAR CNR in the area of the Gioia and Paola basins in the Tyrrhenian sea, at depths ranging from the upper escarpment to the basin, to verify the occurrences of BT deposits in distal basins. The chemical characterization of the BT is completed by in situ compositional analysis on the mineral phases of selected BT units through petrographic and morphoscopic SEM investigation and laser ablation analysis (LA-ICP-MS) performed to provide insights for the evolution of the BT in the magmatic plumbing system of the La Fossa Caldera and Vulcano. The resulting integrated dataset were used to characterize the eruptive dynamics, transport and depositional processes and magmatic processes of BT, and to define proximal-distal correlations in the region under study, eventually providing new insights on the assessment of volcanic hazard.

Thesis outline

The manuscript is structured as a collection of papers, one already published (Chapter 2) and two submitted manuscripts (Chapters 5, 7), three thematic chapters (Chapters 1, 3 and 6), one extended abstract (Chapter 4) and the final conclusions (Chapter 8), together with some future perspectives (Chapter 9) on the project.

In Chapter 1 (*"Aeolian Islands tephrostratigraphy")*, a review of the main stratigraphic, lithological and petrochemical features of all the tephra units that are interlayered within the BT stratigraphic succession is presented as a general framework for correlations. The data are related to tephra units cropping out on the islands of Vulcano, Lipari, Salina, Filicudi and Panarea, where the BT are best exposed, and comes from combined literature data and new data.

Chapter 2 is a published manuscript (*Meschiari S., Albert P.G., Lucchi F., Sulpizio R., Smith V.C., Kearney R., Tranne C.A.,* 2020. Frequent activity on Vulcano (Italy) spanning the last 80 ky: *New insights from the chemo-stratigraphy of the Brown Tuffs. J. Volcanol. Geotherm. Res. 406, 107079*) that provides a revised stratigraphic investigation of the BT and up-to-date constraints on their large-scale correlations and presents a large dataset of original major element volcanic glass compositional data for the whole stratigraphic succession and the different BT depositional units on Lipari and Vulcano islands.

Chapter 3 describes the main results of the compositional analysis on the mineral phases of the BT deposits carried out through petrographic and morphoscopic SEM investigation and laser ablation analysis (LA-ICP-MS) at the laboratories of the Institute of Geochemistry and Petrology, ETH Zürich, and the University of Keele (UK) for the purpose of characterizing the different BT stratigraphic units and study their magmatological evolution.

Chapter 4 is the abstract of a manuscript under preparation (*Albert P.G., Meschiari S., Lucchi F., Sulpizio R., Smith V.C., C.A. Tranne. New insights into the origin of external chrono-stratigraphic markers recorded on the Aeolian Islands)* regarding the definition of the age and source areas of a number of alkali-rich external tephra layers originating from explosive volcanism in the Campanian area that have been recognised in the proximal volcanic stratigraphies of the Aeolian Islands. This paper will provide new insights towards the definition of a general framework of correlations in the region under study.

Chapter 5 is a manuscript in a state of advanced preparation that is focused on the sedimentological features of the BT with special emphasis on the evidence for syn-depositional erosion and clast incorporation from the PDCs during the BT eruptions, and provides new insights on the transport and depositional behaviour of the BT in proximal to median occurrences from the source area of La Fossa caldera.

In Chapter 6, the main results of the laboratory experiments performed with the GRANFLOW simulator at UASLP (San Luis Potosì, Mexico) will be presented. These experiments were properly designed using natural volcanic material to simulate at a medium scale the depositional and erosive behaviour of ash-rich PDCs, and their runout, and compare the obtained results with the natural case of the PDCs during the BT eruptions.

Chapter 7 is a manuscript in a state of advanced preparation where some of the results of the laboratory experiments performed with the GRANFLOW simulator at UASLP are presented. The focus is on the runouts of channelized and unconfined flows using coarse and fine-grained volcanic material moving across a break in slope, and the results are interpreted to highlight significant feedbacks on flow mobility among slope changes, grain size and flow channelization, with insights for the comprehension of natural granular flows.

Chapter 8 (Conclusions) contains a summary of the main results at this stage of research.

It is to be noticed that the Covid-19 health crisis that has severely affected a large part of the Globe in the last year has strongly influenced the progress of the research, effectively preventing to carry out a series of analyses that were necessary to complete some branches of the research. For example, it was not possible to perform further laboratory experiments on the erosive behaviour of ash-rich granular flows to verify the field evidence from the BT deposits on Vulcano and Lipari. Also, some of the mineral chemistry analyses still have to be carried out, to complete the petrochemical framework of the BT that will allow to interpret them correctly from a magmatological point of view. Further, the chemical analyses of the tephra layers sampled in the marine cores in the area of the Gioia and Paola basins in the Thyrrhenian sea are still in progress, and this prevented possible proximal-distal correlations of the BT from being verified. Taking this into account, this thesis is accompanied by a final chapter of “Future Perspectives” (Chapter 9), which is a summary of the activities that can be carried out in the months to come using the data already available and new data still to be obtained.

References

Anikovich M.V., Sinitsyn A.A., Hoffecker J.F., Holliday V.T., Popov V.V., Lisitsyn S.N., Forman S.L., Levkovskaya G.M., Pospelova G.A., Kuz'mina I.E., Burova N.D., Goldberg P., Macphail R.I., Giaccio B., Praslov N.D., 2007. Early Upper Paleolithic in eastern Europe and implications for the dispersal of modern humans. Science 315, 223–226.

Bergeat, A., 1899. Die Äolischen Inseln (Stromboli, Panaria, Salina, Lipari, Vulcano, Filicudi
und Alicudi). Abh. Math. Phys. Kl. Kgl. Bayer. Akad. Wiss. 20, 274 I. Abt., München.

Biass S., Scaini C., Bonadonna C., Folch A., Smith K., Höskuldsson A., 2014. A multi-scale risk assessment for tephra fallout and airborne concentration from multiple Icelandic volcanoes-part 1: hazard assessment. Nat. Hazar. Earth Syst. Sci. discuss. 2, 2463–2529. Crisci et al., 1981; Crisci et al., 1983; Crisci et al., 1991;

De Astis G., Dellino P., De Rosa R., La Volpe L., 1997. Eruptive emplacement mechanism of fine grained pyroclastic deposits widespread on Vulcano Island. Bull. Volcanol. 59, 87–102.

Dingwell A., Rutgersson A., 2014. Estimating volcanic ash hazard in European airspace. J. Volcanol. Geotherm. Res. 286, 55–66.

Giaccio, B., Hajdas, I., Peresani, M., Fedele, F.G., Isaia, R., 2006. The Campanian Ignimbrite and its relevance for the timing of the Middle to Upper Palaeolithic shift. In: Conard, N.J. (Ed.), “When Neanderthals and Modern Humans Met”. Tübingen Publications in Prehistory. Kerns Verlag, Tübingen, pp. 343–375.

Gioncada A., Mazzuoli R., Bisson M., Pareschi M.T., 2003 Petrology of volcanic products younger than 42 ka on the Lipari-Vulcano complex (Aeolian Islands, Italy): an example of volcanism controlled by tectonics. Journal of Volcanology and Geothermal Research 122, 191–220.

Keller, J., 1967. Alter und Abfolge der vulkanischen Ereignisse auf den Äolischen Inseln Bericht Naturforschenden Gesellschaft Freiburg. 57 pp. 33–67.

Keller J., 1980a. The island of Vulcano. Rendiconti della Società Italiana di Mineralogia e Petrologia. 36, pp 369-414.

Keller J., 1980b. The island of Salina. Rendiconti della Società Italiana di Mineralogia e Petrologia. 36, pp 489–524.

Lowe J., Barton N., Blockley S., Ramsey C.B., Cullen V., Davies W., Gamble C., Grant K., Hardiman M., Housley R., Lane C.S., Lee S., Lewis M., MacLeod A., Menzies M., Muller W., Pollard M., Price C., Roberts A.P., Rohling E.J., Satow C., Smith V.C., Stringer C.B., Tomlinson E.L., White D., Albert P.G., Arienzo I., Barker G., Boric D., Carandente A., Civetta L., Ferrier C., Guadelli L., Karkanas P., Komiuzelis M., Muller C., Orsi G., Pross J., Rosi M., Shalamanov-Korobar L., Sirakov N., Tzedakis C., 2012. Volcanic ash layers illuminate the resilience of Neanderthals and early Modern Humans to natural hazards. PNAS 109 (34) 13432-13537.

Lucchi F., Tranne C.A., De Astis G., Keller J., Losito R., Morche W., 2008. Stratigraphy and significance of Brown Tuffs on the Aeolian Islands (southern Italy). J. Volcanol. Geotherm. Res. 177, 49–70.

Lucchi F., Keller J., Tranne C., 2013. Regional stratigraphic correlations across the Aeolian archipelago (southern Italy). Geol. Soc. Lond. Mem. 37, 55–81.

Machida H., 1999. The stratigraphy, chronology and distribution of distal marker tephras in and around Japan. Glob. Planet. Chang. 21, 71–94.

Manetti P., Pasquaré G., Tibaldi A., Tsegaye A., 1988. Geology of the island of Filicudi (Aeolian arc). Bollettino G.N.V. IV 368–382.

Manetti P., Pasquaré G., Tibaldi A., Tsegaye A., 1995. A new geo-vulcanological map of Filicudi island (Aeolian arc, Italy). Acta Vulcanol. 7, 1–5.

Morche W., 1988. Tephrochronologie der Aolischen Inseln. Unpublished PhD Thesis. Albert-Ludwigs-Universitat Freiburg, Germany.

Narcisi B., 1996. Tephrochronology of a late quaternary lacustrine record from the Monticchio maar (Vulture volcano, southern Italy). Quat. Sci. Rev. 15, 155–165.

Paterne M., Guichard F., Labeyrie J., Gillot P.Y., Duplessy J.C., 1986. Tyrrhenian Sea tephrochronology of the oxygen isotope record for the past 60,000 years. Mar. Geol. 72, 259–285.

Paterne M., Guichard F., Labeyrie J., 1988. Explosive activity of the South Italian volcanoes during the past 80,000 years as determined by marine tephrochronology. J. Volcanol. Geotherm. Res. 34, 153–172.

Pichler H., 1980. The Island of Lipari. Rend. Soc. Ital. Mineral. Petrol. 36, 415–440.

Shane P., 2000. Tephrochronology: a NewZealand case study. Earth Sci. Rev. 49, 223–259.

Sulpizio R., Zanchetta G., Caron B., Dellino P., Mele D., Giaccio B., Insinga D., Paterne M., Siani G., Costa A., Macedonio G., Santacroce R., 2014. Volcanic ash hazards in the Central Mediterranean assessed from geological data. Bull. Volcanol. 76, 866.

Zanchetta G., Sulpizio R., Roberts N., Cioni R., Eastwood W., Siani G., Caron B., Paterne M., Santacroce R., 2011. Tephrostratigraphy, chronology and climatic events of the Mediterranean basin during the Holocene: An overview. Holocene 21, 33–52.

Chapter 1

Aeolian Islands tephrostratigraphy

1. Introduction

Explosive volcanism is responsible for the injection of large amounts of gases and tephra of various sizes and shapes into the atmosphere, and the distal dispersal of volcanic ash. Distal occurrences of ash (and fine lapilli) are commonly preserved as tephra (or cripto-tephra) layers within marine and lake sedimentary archives at high distances from the source, and, where the age of the eruptions is known, they provide invaluable (chrono)stratigraphic markers for precisely synchronising various palaeoclimate records and constraining age-depth models. Moreover, distal tephrostratigraphy can help to better define the magnitude and frequency of explosive eruptions from active volcanoes, which is fundamental for hazard assessment and to define future eruption scenarios. This is particularly useful where the knowledge of the eruption history of a volcano is made difficult by an incomplete stratigraphic record due to poor exposure of proximal deposits depending on erosion, burial by more recent deposits, or deposition into the sea, as commonly occurs in island or coastal volcanoes.

However, the use of distal tephra layers for both dating of eruptive events and synchronising sedimentary archives depends substantially on the knowledge of the stratigraphy of proximal eruptive sequences and pyroclastic deposits and their glass compositions. Detailed characterisation of proximal volcanic glasses is in fact crucial for establishing proximal-to-distal correlations (e.g. Albert et al., 2017).

On this point, here a review of the characters of the most important tephra units cropping out proximally in the Aeolian Islands, combining literature data and new observations is presented. It is investigated particularly the time-stratigraphic interval almost corresponding to the Last Glacial period, which is that characterized by the deposition of the Brown Tuffs from Vulcano. This review refers specifically to the islands of Vulcano (source area of the Brown Tuffs), Lipari, Salina, Filicudi and Panarea, where the Brown Tuffs and interlayered local volcanic units are best exposed. The purpose of this contribution is to give information on the age and stratigraphy, distinctive lithological and volcanological features, and glass (or whole-rock) compositions of the proximal deposits of some of the largest explosive eruptions recorded on the Aeolian Islands over approximately the last 100-80 ky, as a general data repository that help assessing the proximal-to-distal tephra correlations. Distal occurrences of tephra related to the Aeolian Islands volcanoes are in fact reported within marine archives from the Tyrrhenian, Ionian and Adriatic seas (Paterne et al., 1986, 1988; Clift and Blusztajn, 1999; Siani et al., 2004; Di Roberto et al., 2008; Albert et al., 2012; Caron et al., 2012; Insinga et al., 2014; Matthews et al., 2015; Tamburrino et al., 2016; Albert et al., 2017). Moreover, this review can contribute to establish an integrated tephrostratigraphy for the Aeolian Islands, as well as to identify those diagnostic features useful in assigning the provenance sources to unknown distal tephras that presently are not related to a specific Aeolian Island, yet.

2. Geological Background

The Aeolian Islands (Alicudi, Filicudi, Salina, Lipari, Vulcano, Panarea and Stromboli) are the emerged volcanoes of the Aeolian Volcanic District, an active volcanic region located in the Southern Tyrrhenian Sea (Fig. 1). They are surrounded by seven volcanic seamounts: Eolo, Enarete, Sisifo to the NW; Lametini, Alcione, Palinuro to the NE; and Marsili to the north. The volcanic islands and seamounts represent the subaerial culminations of large, mainly submerged volcanic edifices rising 2000–2500 m above the seafloor (Romagnoli et al. 2013). Although its geodynamic significance is still not unequivocal, Aeolian magmatism is currently referred to a subduction-type scenario along the north-western margin of the Calabrian Arc, under control of regional fault systems (see De Astis et al. 2003, 2006b; Ventura 2013 for a review).

The Aeolian arc has been also divided into three main sectors, the western, the central and the eastern arcs, which are characterized by first-order volcanological, magmatic and structural differences (Peccerillo 2005; Ventura 2013). The volcanic islands and seamounts form an articulated arc-shaped structure that is transversely intersected in its central sector by the NNW–SSE-oriented Salina-Lipari-Vulcano volcanic belt developed along the Tindari–Letojanni regional fault system (Fig. 1). The islands of Alicudi and Filicudi together with the oldest part of Salina (western sector) are mostly controlled by a WNW–ESE-trending fault system, whereas the Panarea and Stromboli volcanoes (eastern sector) developed along a NE–SW tectonic trend.

Aeolian volcanism occurred entirely during the Quaternary as derived from the oldest radiometric age of c. 1.3 My measured on submarine lavas from the Sisifo seamount (Beccaluva et al., 1985). Subaerial volcanism has developed under strong control of regional stress fields from c. 270-250 ky (on Lipari, Salina and Filicudi) up to historical and present times on Lipari, Vulcano and Stromboli islands (Bigazzi and Bonadonna, 1973; Wagner et al., 1976; Condomines and Allegre, 1980; Keller, 1980a,b; Gillot and Villari, 1980; Crisci et al., 1981, 1983; Capaldi et al., 1985; Frazzetta et al., 1984, 1985; Arias et al., 1986; Gabbianelli et al., 1986; Gillot, 1987; Morche, 1988; De Astis et al., 1989; Gabbianelli et al., 1990; Crisci et al., 1991; Gillot and Keller, 1993; Hornig-Kjarsgaard et al., 1993; Kraml et al., 1997; Laj et al., 1997; Santo et al., 1995; Voltaggio et al., 1995; Calanchi et al., 1999; Lucchi, 2000; Rosi et al., 2000; Soligo et al., 2000; Keller, 2002; Bigazzi et al., 2003; De Rosa et al., 2003b; Arrighi et al., 2004; Speranza et al., 2004; Quidelleur et al., 2005; Dolfi et al., 2007; Arrighi et al., 2006; Speranza et al., 2008; Foeken et al., 2009; Calvari et al., 2011; Francalanci et al., 2011; Leocat, 2011; Zanchetta et al., 2011; Risica et al., 2019; Meschiari et al., 2020). The geological evolution of the Aeolian Islands volcanoes has been described by successive eruptive epochs subdivided by volcanic collapses or major quiescent (erosional) stages (De Astis et al., 2013; Forni et al., 2013; Francalanci et al., 2013; Lucchi et al., 2013a, c, d, e) (Fig. 2), at times associated with episodes of marine ingression and terrace formation during the major sea-level fluctuations (Keller, 1967, 1980a; Lucchi et al., 2004a,b; Lucchi et al., 2007; Lucchi, 2009). The best constrained are the marine terraces related to the last interglacial sea-level peaks of the marine oxygen-isotope stage (MIS) 5 (124-80 ky; Chappell and Shackleton, 1986; Waelbroeck et al., 2002; Rohling et al., 2014), which are recognized on Lipari, Filicudi, Panarea, Salina and Alicudi and play a primary role for correlations (Lucchi, 2009).

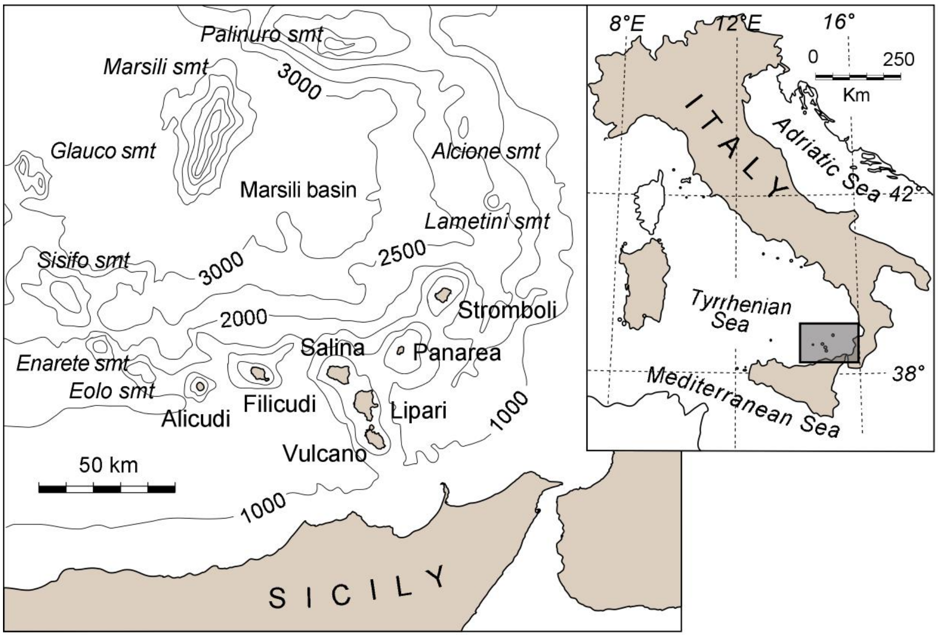

Fig. 1. Sketch map of the Aeolian Islands and seamounts in the southern Tyrrhenian sea (depth contour lines in meters below sea level). Coordinates conform to the Gauss-Boaga System (IGM).

The erupted melts in the Aeolian Islands range from basaltic andesites to rhyolites over a large range of differing magmatic suites from calc-alkaline (CA), high-K calc-alkaline (HKCA), shoshonitic (SHO) and K-Series (KS) (see Peccerillo et al., 2013 for a review) (Fig. 3). Older and more primitive CA basalt to basaltic andesite volcanic products related to Strombolian and effusive volcanic activity were emplaced on Lipari, Salina and Filicudi in a time span between c. 270 and 230 ky BP (Forni et al., 2013; Lucchi et al., 2013a, e). Volcanic activity started again between c. 220 ka BP and the Last Interglacial (c. 124 ky) on Lipari, Salina and Filicudi and Panarea (Forni et al., 2013; Lucchi et al., 2013a, c, e) with the emplacement of CA basaltic andesite to (minor) andesite/dacite volcanics related to mainly Strombolian and effusive activity, with a minor role for hydromagmatic eruptions. During the Last Interglacial (between 124 and 80 ky) HKCA andesite and subordinate dacite volcanic products related to both explosive (mainly hydromagmatic) and effusive volcanic activity were emplaced on Lipari, Panarea and Alicudi (Forni et al., 2013; Lucchi et al., 2013c, d), whilst on Vulcano SHO products were erupted together with the HKCA ones (De Astis et al., 2013). In this time span, the most primitive magmas were erupted on Alicudi Island, whose rocks are characterized by the major, trace element and isotopic signatures over the entire Aeolian archipelago (Lucchi et al., 2013d).

During the Last Glacial period (starting from c. 80 ky), more evolved CA and HKCA andesite to dacite/rhyolite products were erupted on Lipari, Salina, Filicudi, and Panarea (Forni et al., 2013; Lucchi et al., 2013a, c, e), all resulting from effusive activity (mainly dome-forming) and associated explosive eruptions. Vulcano and Stromboli were characterized by dominant SHO products together with the HKCA ones (De Astis et al., 2013; Francalanci et al., 2013). In particular, rhyolitic products occurred with highly variable volumes and dispersal areas on Salina, Lipari and Vulcano islands (and to a lesser extent Panarea) from c. 43-40 ky BP to historical times (De Astis et al., 2013; Forni et al., 2013; Lucchi et al., 2013a, c), as a result of magma differentiation processes in the central sector of the Aeolian archipelago. Stromboli and Vulcano were also characterized by a progressive transition from HKCA to SHO and KS magmas during the last 20 ky (De Astis et al., 2013; Francalanci et al., 2013). A few violent Strombolian to Subplinian eruptions involving dacite to rhyolite magmas have occurred on Lipari, Vulcano, Salina and Stromboli.

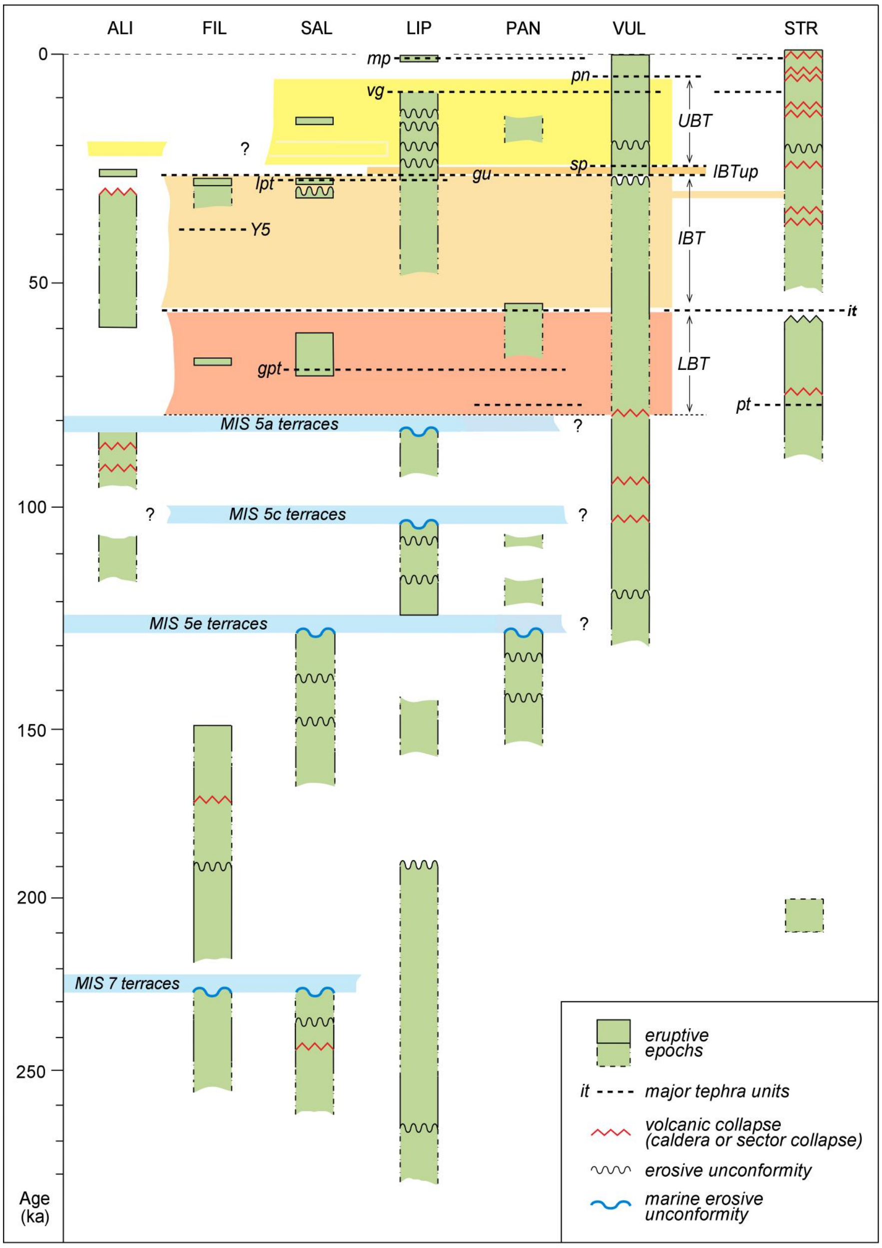

Fig. 2. Time-stratigraphic framework showing the simplified eruptive history of the Aeolian Islands (ALI=Alicudi; FIL=Filicudi; SAL=Salina; LIP=Lipari; PAN=Panarea; VUL=Vulcano; STR=Stromboli), based on the reconstructed stratigraphic successions, radiometric ages, and erosive and collapse unconformities (ALI=Lucchi et al. 2013c; FIL=Lucchi et al. 2013d; SAL=Lucchi et al. 2013a; LIP=Forni et al. 2013; PAN=Lucchi et al. 2013b; VUL=De Astis et al. 2013; STR=Francalanci et al. 2013). The major correlated tephra layers during the Last Glacial period are (in stratigraphic order): pt=Petrazza Tuffs; gpt=Grey Porri Tuffs; it=Ischia Tephra; Y5=Y5 tephra layer; lpt=Lower Pollara Tuffs; gu=Monte Guardia pumice; sp=Spiaggia Lunga scoria; vg=Vallone del Gabellotto pumice; pn=Punte Nere tuffs; mp=Monte Pilato pumice.

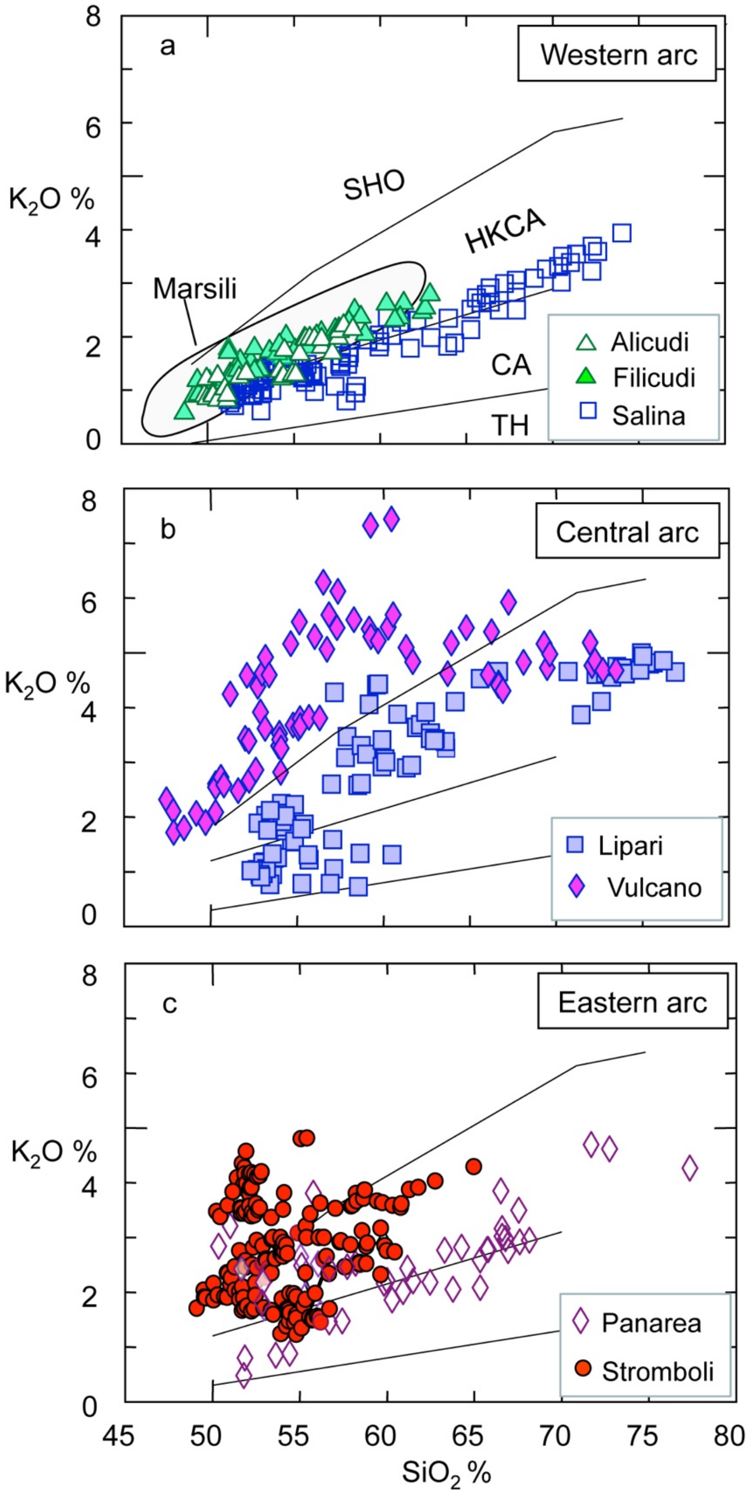

Fig. 3. K_2O vs. SiO_2 classification diagrams for the Aeolian Islands volcanics (from Peccerillo et al., 2013). Lines dividing arc tholeiitic (TH), calc-alkaline (CA), high-K calc-alkaline (HKCA) and shoshonitic (SHO) series are from Peccerillo and Taylor (1976).

3. Methods and Terminology

Stratigraphic analysis is based on classical lithostratigraphy and the lithofacies concept, combined with the identification of erosional unconformities and paleosoils along the volcanic successions as primary constraints to define the different tephra volcanic units, with a special emphasis on the their three-dimensional geometry and morphostratigraphic (lateral-vertical) relationships (see Lucchi, 2013 for a review). Stratigraphy is obviously supported by the available radiometric ages and magnetostratigraphic and tephrochronological age constraints.

The analysis of lateral and vertical lithofacies associations is a primary tool for reconstructing the architecture of the studied stratigraphic successions, and for providing their volcanological interpretation in terms of transport and emplacement mechanisms (fall, PDC, lahar, etc.) and time evolution of volcanic activity.

In this study the pyroclastic deposits are described by using the lithofacies (see Branney and Kokelaar, 2002; Sulpizio and Dellino, 2008 for reviews) and referring to the diagrams and nomenclature commonly used in the volcanological literature. They are described in terms of colour, nature and abundance of the juvenile components, grain size characteristics and sorting, thickness variations, texture, welding, stratification and depositional features. Lateral (and vertical) variations of the physical features of pyroclastic rocks related to time, paleo-topography, and increasing distance from the source (near-vent to distal) are primarily considered as as related to transport and emplacement mechanisms. According to their grain-size characteristics (Fisher 1966; Schmid 1981; Chough and Sohn 1990), the pyroclastic rocks are classified as tuffs (>75% ash), lapillistones (>75% lapilli), lapilli-tuffs (mixtures of ash and lapilli), tuff-breccias (mixtures of ash, lapilli and blocks or bombs) and pyroclastic-breccias or agglomerates for lithified or consolidated deposits, whereas the different grain size ranges are referred to for unconsolidated rocks (Schmid, 1981). Conforming with Fisher and Schmincke (1984), the pyroclastic-breccias are assumed to be consolidated accumulations of blocks (>75%), lapilli and ash, whereas the agglomerates are welded aggregates mostly consisting of bombs. The grain size of the studied deposits is generally estimated qualitatively using suitable comparators. The nomenclature of Ingram (1954) is adopted for bed thickness. The chemical classification of analyzed pyroclastic rocks (i.e. wr and glasses) was based on deposits (whole-rock, hereafter wr, or glass composition) refer to the Total Alkali Silica (TAS) diagram (Le Bas et al. 1986) and/or the diagram of Peccerillo and Taylor (1976), the latter being particularly focused on the classification of island-arc rocks.

Lithostratigraphic units (formation, member) are adopted as the basic units of stratigraphy in volcanic terrains, as in any other geological environments, to identify the main pyroclastic successions on the basis of their distinctive lithological features and stratigraphic position (and age) in a vertical succession of rocks (see Lucchi, 2013 for a review). A useful link between rock-stratigraphy and time-stratigraphy is established by introducing the concept of “eruption units” (sensu Fisher and Schmincke, 1984) as the pyroclastic material deposited during a single eruption. However, a certain pyroclastic succession, lithologically homogeneous or not, can be the result of an individual eruption, namely an eruption unit, or derive from a sequence of eruptions separated by short-lived interruptions of deposition at the considered time scale. Considering that the time duration of a stratigraphic hiatus is not achieved along a volcanic succession from the volcanic successions, it is preferred hereafter to define distinct depositional units when delimited by physical features indicative of interruptions in the deposition, e.g. erosive surfaces, paleosoils, angular discordances and/or detrital horizons, or even the occurrence of other interlayered volcanic units.

4. Stratigraphic overview

The Aeolian Islands host a high numer of tephra units recorded in the local stratigraphic successions referred to the time-stratigraphic interval that corresponds to the Last Glacial period (c. 100-80 ky), and partly correlated between distinct islands. These units are attributed to either Campanian-Roman or Neapolitan sources or distinct high-explosive eruptions from Aeolian Islands volcanoes. The latter are distinguished by a typical CA to HKCA magmatic signature, whereas Campanian-Roman or Neapolitan volcanoes are identified by a characteristic alkali-trachyte composition and sanidine as the major feldspar phase in the corresponding tephra layers (e.g. Keller 1981). A Pantelleria source was subordinately identified by Morche (1988) as dispersed glass shards in distinct stratigraphic positions. The tephra layers, both from Aeolian Islands volcanoes and external sources, are interbedded with successive depositional units of the Brown Tuffs from Vulcano (the main object of the present work), which are prominently documented in the stratigraphic profiles of most of the islands and on the Capo Milazzo peninsula (northern Sicily) related to the c. 80-6 ky time-stratigraphic interval.

Here we focus on the tephra units erupted from the Aeolian Islands volcanoes, whereas those from Campanian source areas will be the object of a companion paper (Albert et al., in prep.). Explosive eruptions in the Aeolian Islands are dominantly moderate to low intensity, Strombolian to Violent Strombolian, Vulcanian and Sub-Plinian eruptions, the largest of these producing c. 0.5 km^3 of pyroclastic material (Calanchi et al., 1993; De Rosa et al., 2003b; Dellino et al., 2011; Lucchi et al., 2013c). Tephra deposits are generally characterised by alternation of fall units from unsteady columns and units from small-volume, pyroclastic density currents (PDC). The proximal Aeolian tephra units are described in the following sections with particular focus on age and stratigraphy, their distinctive lithology and volcanological interpretation, and geochemical (bulk-rock or glass composition) and mineralogical fingerprint (in terms of distinctive minerals or their relative proportions). They are subdivided in major tephra layers that are characterized by a distribution over two or more islands and other pyroclastic units which are distributed only within a single island (at the present state of knowledge). The Ischia Tephra is discussed here because it plays a major role for correlations in the region under study. The Brown Tuffs are described in a separate section because they are the most voluminous and widely distributed tephra unit in the Aeolian Islands region. Figure 4 is a general framework of the stratigraphy in the islands of Lipari, Vulcano, Salina, Filicudi and Alicudi where the Brown Tuffs and the interbedded tephra layers are primarily documented. Whilst for the tephrostratigraphy of the Capo Milazzo site, in northern Siciliy, it is necessary to refer to Morche (1988) because the outcrops are currently largely eroded and partially destroyed by anthropogenic activity.

4.1. Brown Tuffs

The Brown Tuffs (BT) are reddish-brown to grey, massive pyroclastic ash deposits with metric thickness characterized by a wide areal distribution in the Aeolian Islands and the Capo Milazzo peninsula (Sicily). They are composed of glass shards, minor crystals (with dominant clinopyroxene) and a negligible lithic content. For a long time their interpretation has been controversial, particularly regarding their source area(s), areal distribution and eruptive dynamics (Bergeat 1899; Keller 1980a, b; Pichler 1980; Crisci et al., 1981, 1983, 1991; Manetti et al., 1988, 1995; Morche 1988; Losito 1989; De Astis et al., 1997a; Gioncada et al., 2003). Then, the BT have been chemo-stratigraphically referred to a source located inside the La Fossa caldera on Vulcano and hence correlated, with variable volumes and dispersal areas, on the islands of Vulcano, Lipari, Salina, Filicudi, Stromboli and Alicudi and the Capo Milazzo peninsula (Lucchi et al., 2008, 2013b), with distal occurrences also in Tyrrhenian and Adriatic Sea marine cores (Meschiari et al., 2020). They are characterized by glass compositions ranging from K-series (K_2O = 3.3-7.5 wt.%) basaltic-andesites and trachy-andesites through to tephri-phonolites and trachytes (SiO_2 = 49.9-64.1 wt.%; Na_2O + K_2O = 6.5-12.6 wt.%), which are entirely consistent with the Vulcano magmatic system (Meschiari et al., 2020). The BT are massive to plane-parallel and cross stratified (on Vulcano and and southern Lipari), with internal color and grain size (fine to coarse ash) banding and topography-controlled thickness variations, and are interpreted as the result of deposition from pyroclastic density currents (PDCs) and minor fallout related to a pulsating hydromagmatic explosive activity (De Astis et al, 1997a; Lucchi et al., 2008; Cicchino et al., 2011; De Rosa et al., 2016).

Based on these chemo-stratigraphy, Meschiari et al. (2020) have defined four stratigraphic macro-units, namely the Lower (80-56 ky; LBT), Intermediate (56-27 ky; IBT), Intermediate-upper (26-24 ky; IBT-upper) and Upper BT (24-6 ky; UBT), which are separated by the Ischia Tephra (56 ky), Monte Guardia pyroclastics from Lipari (27-26 ky), and Spiaggia Lunga scoriae on Vulcano (24 ky) (Fig. 4). Each of these macro-units is furtherly subdivided into a number of depositional units by the occurrence of paleosols, reworked horizons and localized erosive surfaces, or the interbedding of tephra layers and other volcanic units (Lucchi et al., 2008, 2013b; Meschiari et al., 2020). If these stratigraphic features are absent the distinct BT depositional units are amalgamated in thick successions with a very homogeneous lithology. The most complete BT stratigraphic succession is recognized on the island of Lipari where (at least) 16 depositional units are identified, whilst the UBT are best characterized on the island of Vulcano (Fig. 4). It is noteworthy that most BT depositional units on Vulcano and Lipari have transitional basal contacts with the underlying incoherent pyroclastic units derived from substrate erosion by the corresponding PDCs (in prep.). For a complete view of the BT units sampled and analyzed see Fig. 4 in Meschiari et al. 2020 (Chapter 2).

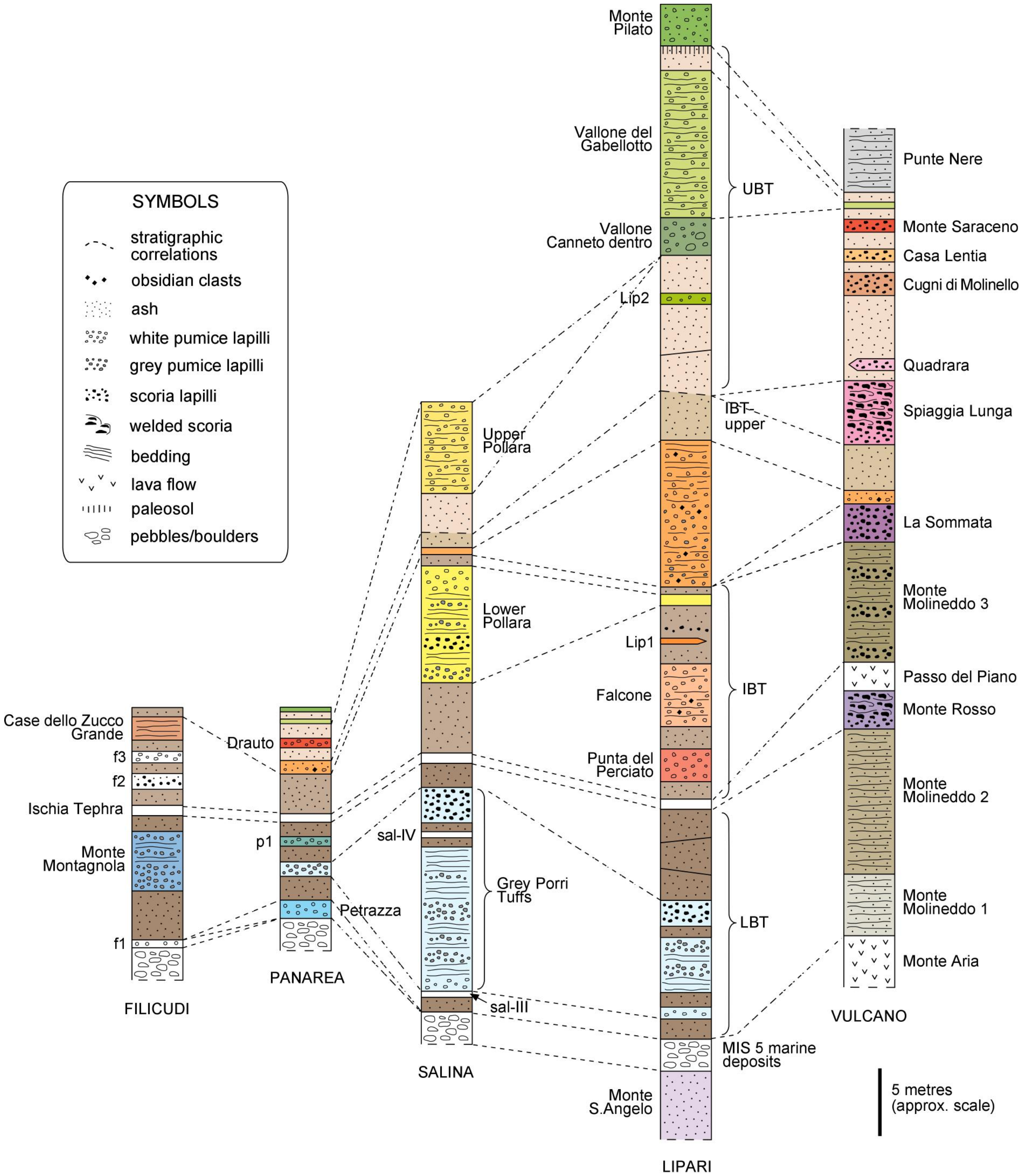

Fig. 4. Generalized stratigraphic succession of the Brown Tuffs and interlayered tephra layers during the past 100 ky derived from correlations between the islands of Vulcano, Lipari, Salina, Filicudi and Panarea. The Brown Tuffs are subdivided into the Lower (LBT), Intermediate (IBT), Intermediate-upper (IBT-upper) and Upper Brown Tuffs (UBT) macro-units, which are furtherly subdivided into a number of distinct depositional units by interlayered volcanic units and tephra layers, erosive surfaces and reworked horizons. References for the interlayered volcanic units are: De Astis et al., 2013 (Vulcano); Forni et al., 2013 (Lipari); Lucchi et al., 2013a (Salina); Lucchi et al., 2013c (Panarea); this work (Filicudi).

4.1.1. Lower Brown Tuffs (LBT, 80-56 ky)

The LBT are delimited at the base by late marine (oxygen) isotope stage (MIS) 5 (124-80 ky) and at the top by the Ischia Tephra (56 ky) (Fig. 5A). They generally consist of massive ash deposits with glass compositions ranging from basaltic trachy-andesites to trachy-andesites and tephri-phonolites (SiO_2 = 52.4–57.2 wt%; Na_2O+K_2O = 7.7–11.5 wt%) with a clear K-series affinity (K_2O = 4.2–6.3wt%) (Meschiari et al., 2020). Based on stratigraphy and geochemical overlap of the juvenile glass, the LBT are linked to the Monte Molineddo 2 pyroclastic succession as the near-source counterpart on Vulcano (§ 4.3.1).

The LBT are widely distributed on most of the Aeolian Islands (except Stromboli) and on the Capo Milazzo peninsula with thickness up to a 5-6 metres in southern Lipari, although sharp thickness variations are induced by topography-controlled depositional behaviour and substantial erosion of the primary deposits. The LBT are best recognized on Lipari (and Salina) where up to six distinct depositional units are separated by palaeosols and erosional unconformities and the wide interbedding of the Grey Porri Tuffs (70-67 ky) originated from Salina (§ 4.3.3) (Fig. 5A; 6D), which are important for stratigraphic correlations in the lower portion of the succession. Moreover, a tephra layer correlated to the Petrazza Tuffs from Stromboli (77-75 ky) (§ 4.2) is interbedded within the older portion of the LBT on Panarea (Fig. 6B) and Capo Milazzo, which helps to refine the lower chronological limit for the LBT.

4.1.2. Intermediate Brown Tuffs (IBT, 56-27 ky)

The IBT are defined between the Ischia Tephra (56 ky), at the base (Fig. 5B), and the Monte Guardia pyroclastic unit (27-26 ka), at the top (Lucchi et al., 2008, 2013b) (Fig. 5C). We use here the refined age assignment for the Monte Guardia provided by Meschiari et al. (2020) on the basis of a new calibration of radiocarbon ages (^{14}C) for charcoal remnants embedded within the BT below and above the marker bed. The youngest IBT are in fact ^{14}C dated on Lipari (Crisci et al. 1981, 1983; Morche 1988) and Salina (Keller 1980a; Calanchi et al. 1987), and then recalibrated to c. 27-28 ky according to the up-to-date IntCal20 Northern Hemisphere calibration curve of Reimer et al. (2020).

The IBT are made up of massive ash deposits with minor stratified lithofacies observed in the outcrops on the western sector of Vulcano. Glass compositions are K-series basaltic trachy-andesites to trachy-andesites and tephri-phonolites (SiO_2 = 50.8–57.2 wt%; Na_2O+K_2O = 7.0–12.3 wt%; K_2O = 3.6–7.5 wt%) largely mirroring the compositional field of the LBT, but they extend to more elevated K_2O contents than those of the LBT (Meschiari et al., 2020). A chronostratigraphic link and geochemical agreement exists between the IBT and the Monte Molineddo 3 pyroclastic succession as the near-source counterpart on Vulcano (§ 4.3.1) (Meschiari et al., 2020), which is also consistent with the occurrence of diffused Monte Molineddo 3 black/yellowish scoria lapilli within the IBT in some outcrops on Lipari and Vulcano.

The IBT are best exposed in the southern sector of Lipari where they are distinguished in (at least) 5 depositional units (Fig. 4; 5C) by the interlayering of the local pumiceous units of Punta di Perciato (undated), Falcone (44-40 ka) and Lip1 tephra (§ 4.3.2), and the Lower Pollara Tuffs from Salina (27.5 ka). Unfortunately these marker beds cannot be correlated between one island and another (except for the Lower Pollara Tuffs), and the IBT on Vulcano (in the western outcrops), Salina and Panarea are represented by a lithologically-homogeneous succession of amalgamated depositional units. Further subdivisions are possible on Filicudi where the IBT are split into 4 depositional units by other tephra layers (§ 4.3.4), although a one-to-one correlation with the depositional units defined on Lipari is not feasible.

4.1.3. Intermediate Brown Tuffs-upper (IBT-upper, 26-24 ky)

The IBT-upper correspond to the depositional unit located between the Monte Guardia pyroclastics (27-26 ky) (Fig. 5D) and the Spiaggia Lunga scoriae bed on Vulcano (24 ky). This depositional unit, previously included in the UBT macro-unit (Lucchi et al., 2008, 2013b), is in fact chemically consistent with the IBT (those deposits beneath the Monte Guardia) and consequently re-defined as the IBT-upper by Meschiari et al. (2020). The IBT-upper have juvenile glass components ranging from K-series trachy-andesites to higher alkali content tephri-phonolites (SiO_2 = 53.1–55.9 wt%; Na_2O+K_2O = 8.4–12.3 wt%; K_2O = 5.4–7.5 wt%) that are entirely consistent with the underlying IBT deposits. Charcoal within the IBT-upper on Lipari is dated at 25,800–26,190 cal y BP, in good agreement with the inferred Spiaggia Lunga boundary age (Meschiari et al. 2020).

The IBT-upper consist of typical massive ash deposits with minor stratification in the outcrops on the western sector of Vulcano, and have a thickness of 1-2 metres. They are best defined on Vulcano, where the stratigraphic boundaries are exposed, and then chemically correlated to various outcrops of the island of Lipari.

Fig. 5. Outcrop photographs of the Brown Tuffs. A) Lower Brown Tuffs (LBT) resting above MIS 5 marine coglomerates (co) at Panarea, near Drauto. The Grey Porri Tuffs (gpt) from Salina are interlayered in the basal portion of the LBT, whilst a pocket of Petrazza pumice lapilli (pt) from Stromboli is visible between the marine boulders. B) Lower (LBT) and Intermediate Brown Tuffs (IBT) separated by the Ischia Tephra (it) at Salina; the succession rests above the younger Monte dei Porri lava flows (mp). The camera bag for scale is 25 cm large. C) Intermediate Brown Tuffs (IBT) in central-eastern Lipari, delimited at the top by the Monte Guardia (gu) pyroclastic succession, and interlayered by the local Punta del Perciato (pe) and Falcone (fa) pumice layers. The scraper for scale is 30 cm high. D) Intermediate-upper (IBT-upper) and Upper Brown Tuffs (UBT) cropping out above the Monte Guardia marker unit (gu) at Lipari, near to Canneto. The distinction between the IBT-upper and UBT is geochemically established (Meschiari et al., 2020). E) Upper Brown Tuffs (UBT) on Vulcano, Il Piano locality, subdivided by the Cugni di Molinello scoria marker bed (cm). F) Upper Brown Tuffs (BT) on Vulcano, near to Passo del Piano, interlayered by the Vallone del Gabellotto (vg) pumice layer from Lipari and delimited at the top by the Punte Nere tuffs (pn).

4.1.4. Upper Brown Tuffs (UBT, 24-6 ky)

The UBT are chemo-stratigraphically defined above the Spiaggia Lunga scoriae maker bed on Vulcano (24 ky), and are recognized on the islands of Vulcano, Lipari, Salina, Panarea and Basiluzzo and on the Capo Milazzo peninsula (Lucchi et al. 2008) (Fig. 5D-F). They are typically pale-brown to brown-gray ash deposits, from massive to internally laminated with subparallel to inclined, truncated laminae and asymmetric bedforms in the outcrops of the central sector of the island of Vulcano. Compositionally, the UBT comprise the most evolved juvenile glasses (of the BT) ranging from K-series trachy-andesites through to trachytes (SiO_2 = 55.7–64.5 wt%; Na_2O + K_2O = 8.3–11.6 wt%; K_2O = 5.1–7.3 wt%), and extend to the highest contents of SiO_2 for similar CaO andMgO contents shown by the IBT and IBT-upper (Meschiari et al., 2020).

The best UBT outcrops visible on Vulcano (Fig. 5E), where they stratigraphically match the so-called Grotte dei Rossi Tuffs (Keller, 1980b) or Tufi di Grotte dei Rossi (De Astis et al., 1997a), corresponding to the Piano Grotte dei Rossi Formation in the geological map of De Astis et al. (2013). On Vulcano, they are subdivided by the widespread Cugni di Molinello scoria marker bed (§ 4.3.1). The UBT below Cugni di Molinello contain most of the deposit volume, with a maximum thickness of 8-10 m along the border of La Fossa caldera, whilst the UBT above the marker bed are only 2-3 m thick. The UBT above the Cugni di Molinello are furtherly subdivided in (at least) four depositional units by the interbedded local Casa Lentia (15 ky) and Monte Saraceno (8.3 ky) pyroclastic layers, and the Vallone del Gabellotto tephra from Lipari (8.7–8.4 ky) (Fig. 5F), and they are delimited at the top by the local Punte Nere Tuffs (5.5 ky) (Fig. 5F). The UBT depositional unit above Vallone del Gabellotto contains charcoal that has a re-calibrated ^{14}C age of 8305–8655 cal y BP (De Astis et al., 1997a; Meschiari et al., 2020). None of the individual UBT depositional units defined on Vulcano can be followed laterally over large areas (if not separated by the interbedded layers) and between the adjacent islands. On Lipari, the UBT are subdivided into four depositional units by a local erosional surface and the interlayering of the local Lipari products: Lip 2 (undated), Vallone Canneto dentro (undated) and Vallone del Gabellotto pumice layers. Most of the UBT on Lipari are found stratigraphically below the Vallone Canneto Dentro unit. The youngest UBT on Lipari are recognized below the widespread paleosol that separates the Vallone del Gabellotto and Monte Pilato pyroclastic units, which has a maximum age of 5445–5610 cal y BP based on re-calibration of the previous ^{14}C age determinations on charcoal embedded within the paleosol by Pichler (1980). Consistently, the youngest portion of the UBT can be dated by correlation with the marine tephra layers TIR2000–50 cm (~6.7 ky) and TIR2000-46 cm (~6.1 ky) in the Marsili Basin core TIR2000-C01 (Albert et al., 2012).

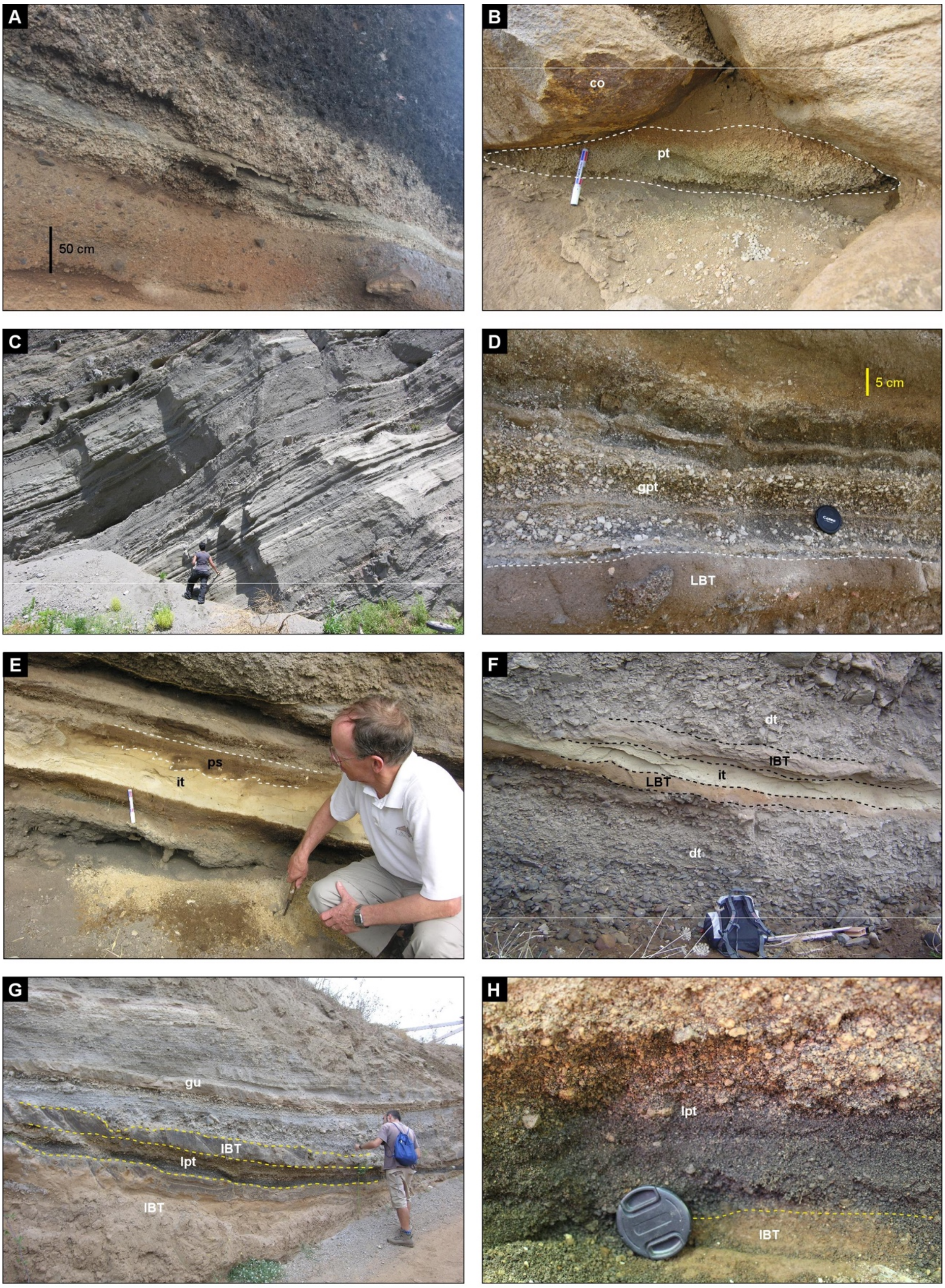

Fig. 6a. Outcrop photographs of the major tephra layers across the Aeolian Islands (in stratigraphic order). Proximal (A, La Petrazza, eastern Stromboli) and distal (B, Drauto, eastern Panarea) occurrences of the Petrazza Tuffs (pt) from Stromboli; in (B) a pocket of the Petrazza pumice lapilli is visibile between the boulders of the MIS 5 marine conglomerates (co). In (B) the pencil for scale is 10 cm high. Proximal (C, Malfa, northern

Salina) and mid-distal (D, Vallone dei Lacci, western Lipari) deposits of the Grey Porri Tuffs from Salina. In (D) the Grey Porri Tuffs (gpt) are interlayered with the Lower Brown Tuffs (LBT). Ischia Tephra in the outcrops of eastern Stromboli (E) and northern Salina (F). In (E) the Ischia Tephra (it) in interbedded within local deposits and characterized by an upper paleosol (ps), whilst in (F) it is interbedded within Lower (LBT) and Intermediate Brown Tuffs (IBT) and distinct horizons of paleo-detrital deposits (dt). Lower Pollara Tuffs from Salina representing a key marker bed on Lipari (G) and their detail view (H). The Lower Pollara Tuffs (lpt) are interlayered within the Intermediate Brown Tuffs (IBT), stratigraphically slightly below the Monte Guardia pumice unit (gu).

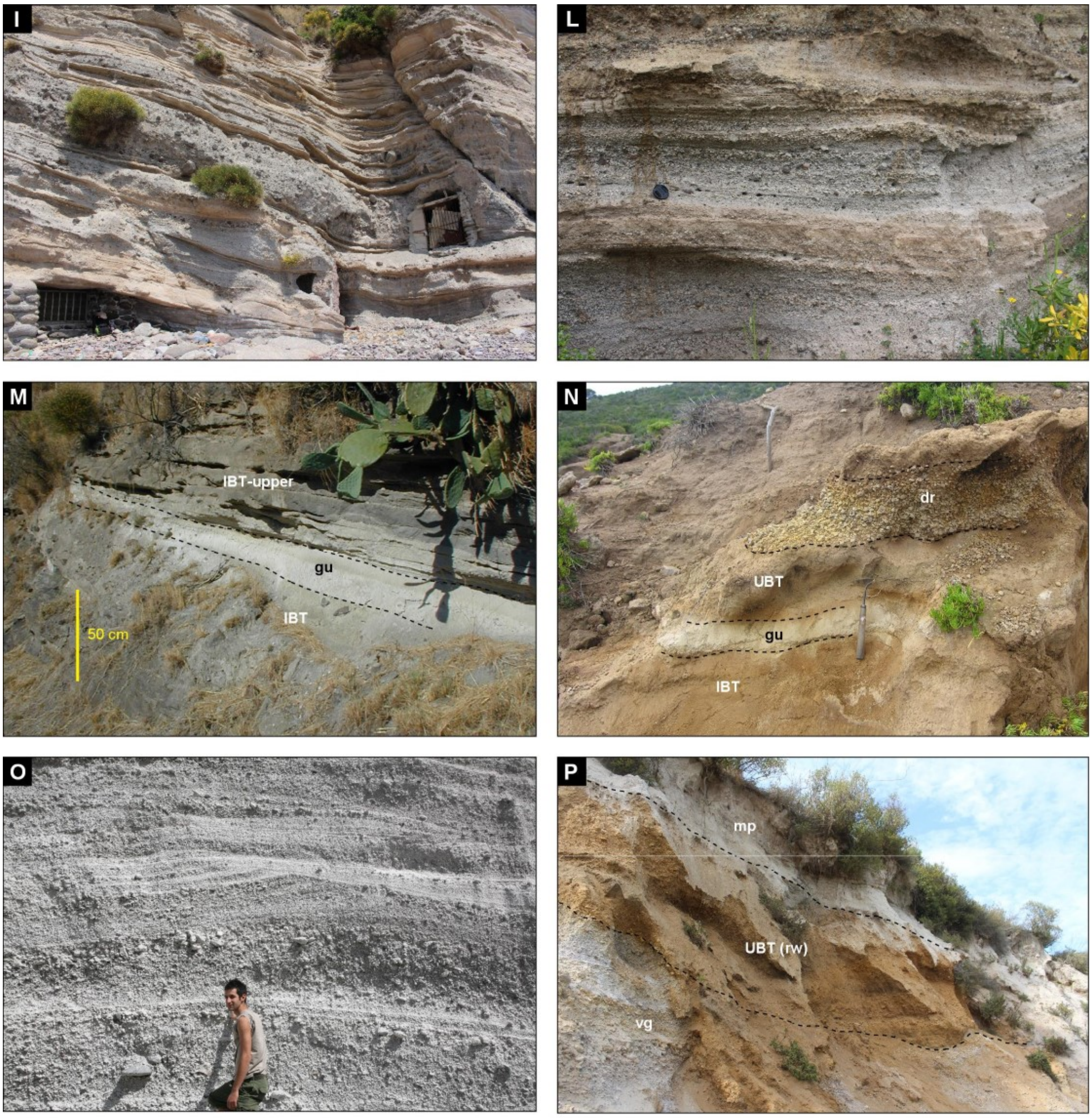

Fig. 6b. Proximal (I) and medial (L) outcrops of the Monte Guardia pumice succession on Lipari, and its distal correlatives on Vulcano, Gelso (M) and Panarea (N). In (M) the Monte Guardia unit (gu) is the marker between the Intermediate (IBT) and the Intermediate-upper Brown Tuffs (IBT-upper), whilst in (N) it is between the Intermediate (IBT) and the Upper Brown Tuffs (UBT), stratigraphically lower than the local Drauto pumice layer (dr). In (N) the scraper for scale is 20 cm high. (O) Vallone del Gabellotto pumice succession in its type locality in central Lipari. (P) Monte Pilato pumice and ash layer (mp) cropping out in central Lipari above reworked Upper Brown Tuffs (UBT-rw) and the Vallone del Gabellotto pumice (vg).

4.2. Major tephra layers

Six tephra layers relative to low- to mid-energy eruptions (Strombolian to Sub-Plinian) of Aeolian Islands volcanoes are characterized by a wide distribution with documented correlations between two or more islands of the Aeolian archipelago. In stratigraphic order, they are the Petrazza Tuffs (from Stromboli), Grey Porri Tuffs and Lower Pollara Tuffs (from Salina), M. Guardia (from Lipari), Vallone del Gabellotto and Monte Pilato (from Lipari). The Ischia Tephra is an additional major stratigraphic marker in the region under study.

4.2.1. Petrazza Tuffs (77-75 ky)

The Petrazza Tuffs are a thick pyroclastic succession derived from mid-explosive eruptions occurred on Stromboli (Hornig-Kjarsgaard et al. 1993), corresponding to the La Petrazza Formation in the mapping of the island (Francalanci et al. 2013). It mostly consists of thick fallout beds of bombs and lapilli of weakly vesicular to dense, black scoria and brown/grey pumice (diffusely characterized by an orange patina of oxidation) (Fig. 6A), with abundant heterolithologic lithic clasts in some layers. Juvenile clasts are HKCA basaltic–andesites to andesites (wr; Francalanci et al., 2013), whereas glass compositions are trachy-andesites to trachy-dacites (SiO_2 = 61.3–63.6 wt%, $Na_2O + K_2O$ = 7–8.2 wt%, K_2O = 3-4 wt%; Wulf et al., 2004), and the crystal content is of plagioclase, clino- and orthopyroxene, biotite, K-feldspar and apatite (Wulf et al., 2004).

Distal (terrestrial) equivalents of the Petrazza Tuffs are recognized by layers of loose, grey to brownish pumice lapilli on the island of Panarea (Lucchi et al. 2007) (Fig. 6B) and Capo Milazzo (Morche 1988). More distally, the Petrazza Tuffs are correlated with the Y9 marine tephra layer in the Ionian deep-sea cores (Wulf et al., 2004), which re-defines the Aeolian X-1 deep-sea tephra layer of Keller et al. (1978) and Paterne et al. (1988). Overall, these findings document a wide areal distribution towards the southwest and southeast.

The best age estimates for the Petrazza Tuffs are those obtained for the correlative Y9 marine tephra at 75.3 ky (core M25/4–12, Ionian Sea; Kraml et al., 1997) and at 77.1 ky (core KET 8003, Tyrrhenian Sea; Paterne et al., 1988) by means of the interpolation of astronomically calibrated time scales. Accordingly the Petrazza Tuffs eruption can be dated to the 77–75 ky time interval. This time interval is consistent with the finding by Morche (1988) of glass shards related to the ‘Ignimbrite Z’ of Pantelleria dated at 79.3±4.2 ky (Mahood and Hildreth 1986) within the Petrazza Tuffs succession in their main outcrop site on Stromboli. Moreover, the 77–75 ky age fits with the chronological interval defined proximally for the Petrazza Tuffs by the lava flows stratigraphically below and above

(Francalanci et al., 2013), dated to 85.3±2.0 ky and 64.3±4.9 ka (K–Ar; Gillot and Keller 1993; Hornig-Kjarsgaard et al. 1993), respectively.

4.2.2. Grey Porri Tuffs (70-67 ky)

The Grey Porri Tuffs (GPT) are a thick pyroclastic succession related to the highly explosive activity of the Monte dei Porri stratocone on the island of Salina (Keller 1980a), and correspond to the bulk of the Monte dei Porri succession (EU1-5) described by Sulpizio et al. (2016). The GPT consist of a thick succession (up to 25-30 m) of alternating fall and PDC deposits from Strombolian/Vulcanian to sub-Plinian/Plinian explosive eruptions (Fig. 6C). They are represented by massive to stratified units of moderately vesicular to dense brown/grey pumice and dark-grey to black scoria and highly vesicular, whitish pumice (in EU1 and EU5) with a variable content of lithic clasts (dominant lava clasts with some levels enriched by cumulates, granites and sedimentary rocks from the metamorphic basement, and quartz rich xenoliths). Glass compositions range from basaltic-andesites and andesites up to dacites (SiO_2 = 56.5–62.6 wt%; Na_2O + K_2O = 4.5–8.3wt%) with a transitional CA to HKCA affinity (Meschiari et al., 2020), while bulk-rock compositions are CA basaltic to HKCA dacites (Sulpizio et al., 2016). The most evolved compositions are observed in EU1 (i.e., whitish pumice), whereas EU2 contains the least evolved compositions (basalt and basaltic andesites). All the pumices and scoriae of the GPT are porphyritic (10–25% crystals) and contain plagioclase, clinopyroxene, orthopyroxene, oxides and accessory apatite, with widely present olivine crystals and scarce amphibole in some of the units (Sulpizio et al., 2016).

Based on tephrostratigraphy defined for Salina, it was possible to assess a relative age to the GPT are assigned (Keller 1981; Morche 1988). The Campanian tephra Sal-III, corresponding to the marine C(i)-8 tephra (72.7 ka; Paterne et al., 1988), is recognized below the Monte dei Porri succession, whereas the Sal-IV, coinciding with the marine C(i)-7 tephra (67.9 ka; Paterne et al., 1988), is interbedded within the upper portion of the GPT (EU4; Sulpizio et al., 2016). This provides an age interval of c. 70–67 ka for the GPT, which is also consistent with the K/Ar ages of 67–57 ka for the latest Monte dei Porri lava flows (Gillot, 1987; De Rosa et al., 2003b; Leocat, 2011).

The GPT are extensively documented on Lipari by a thick succession of massive to stratified lapilli-tuffs composed of dark grey scoria and grey pumice (Fig. 6D), characterized by a rapid west–to-east thickness decrease from a maximum of c. 15 m along the western coast down to c. 3 m on the eastern side. Both on Lipari and Salina the GPT are interbedded with distinct layers of the LBT from Vulcano, as an evidence of contemporaneous or alternating eruptions during a prolonged volcanic activity. The GPT are distally recognized on Panarea (Lucchi et al., 2007, 2008) (Fig. 5A) and the Capo Milazzo peninsula (Morche, 1988) by cm- to tens-of-cm thick massive beds of scoria and pumice lapilli and ash with a distinctive composition and mineralogic fingerprint. A layer of grey pumice lapilli showing the GPT glass composition is also observed on Vulcano within the Monte Molineddo 2 succession, which is the near-source equivalent of the LBT (Meschiari et al., 2020). Overall, these correlations outline a dominant NE- to SE-wards dispersal area.

4.2.3. Ischia Tephra (56 ky)

The Ischia Tephra is a white-yellowish ash bed cropping out on the islands of Stromboli, Salina, Filicudi, Lipari and Panarea (Keller, 1967, 1980b; Morche, 1988; Hornig-Kjarsgaard et al., 1993; Lucchi et al., 2008) (Fig. 6E-F), which is correlated to the widespread marine Y7 tephra (Keller et al. 1978). It has an average thickness of 25–30 cm all over the islands, with maximum values of c. 50 cm on Filicudi (probably due to secondary reworking). The tephra has a distinctive phono-trachytic glass composition with Na_2O slightly higher than K_2O (whilst tephras in the stratigraphic interval corresponding to the Y-zone generally have $K_2O \geq Na_2O$; Keller et al. 1978; Keller 1981), and mineralogic content of K-feldspar, biotite, plagioclase, clinopyroxene and the key tracer titanite (sphene, $CaTiSiO_5$) and yellow acmite in order of decreasing abundance (Tomlinson et al., 2014). The Y-7/Ischia Tephra is best correlated with the Monte Epomeo Green Tuff of Ischia (Tomlinson et al., 2014). The Monte Epomeo Green Tuff is directly dated to 55.4 ± 2.2 ka (K/Ar; Gillot 1984), whereas its distal equivalents are dated to 56 ± 4 ky ($^{40}Ar/^{39}Ar$, Ischia Tephra on Stromboli; Kraml, 1997) and 55 ± 2 ky ($^{40}Ar/^{39}Ar$, TM-19 layer in the Lago di Monticchio sediment core; Watts et al., 1996). This chronological constraint for the Y-7/Ischia Tephra is consistent with the interpolated ages of c. 50 ky from the astronomically calibrated sapropel chronology and oxygen isotope chronology for the Y-7 tephra (Kraml, 1997; Allen et al. 1999; Negri et al., 1999). Unequivocal geochemical and mineralogic identification, wide areal distribution and precise radiometric dating make the Y-7/Ischia Tephra a primary stratigraphic marker in the region under study (where it subdivides the LBT and IBT macro-units) and the entire Mediterranean Sea.

4.2.4. Lower Pollara Tuffs (27 ky)

The Lower Pollara Tuffs (LPT) are an up to 20 m thick pyroclastic succession formed by the early explosive activity from the Pollara crater on Salina (Keller 1980a; Calanchi et al. 1993), which correspond to the Punta delle Fontanelle Formation (Lucchi et al. 2013a). The LPT are made up of Strombolian to sub-Plinian fall layers with interlayered minor laminated PDC deposits, for a total volume of c. 2 km^3 of erupted magma (Calanchi et al., 1993). Juveniles are represented by dominant grey, vesicular pumice (partly banded), with a large amount of dense, highly porphyritic, poorly vesicular scoria in the mid-lower portion of the succession (and decreasing in abundance upwards), and highly vesicular, whitish pumice in the upper portion. Wr compositions range from basalts/basaltic andesites (black scoria) through andesites (grey pumice) to rhyolites (white pumice) belonging to the CA series (Calanchi et al., 1993), whereas glass compositions straddle the CA/HKCA boundary with dacites to rhyolites (SiO_2 = 68.2–75.1 wt%; CaO = 1.7–4.1 wt%; K_2O = 2.6–3.7 wt%) in the grey and white pumice (Albert et al., 2017; the analysis of the black crystal-rich scoria was not successful due to the absence of suitable matrix glass). Grey and black juveniles are characterized by phenocrysts of plagioclase, clinopyroxene, Fe-Ti oxides and olivine, with a distinctive content of hornblende crystals in the grey pumice (and subordinately in the white pumice), whereas whitish pumice are subaphyric to aphyric (Calanchi et al., 1993). Lithic clasts (lavas, scoriae, cumulates and metamorphic rocks) are abundant in some layers of the lower portion of the succession (decreasing to less than 10% vol. content towards the top).

The age of LPT is derived from a number of ^{14}C dates on charcoal fragments embedded within the IBT stratigraphically above and below the LPT on Salina and Lipari (cf. Keller 1980a; Crisci et al. 1981, 1983; Morche, 1988; Calanchi et al. 1993). The recent result proposed by Meschiari et al. (2020) using the IntCal20 Northern Hemisphere calibration curve (Reimer et al., 2020) provides an age of 26,425–27,585 cal y BP (95.4%) for the LPT eruption.

The LPT are correlated distally on Lipari where a tens-of-centimetre-thick fallout layer has a wide areal distribution on most of the island (Morche 1988; Crisci et al., 1991; Lucchi et al. 2008; Forni et al. 2013), representing a key marker bed for the correlations in the upper part of the IBT succession (Meschiari et al., 2020). This layer has a distinctive grading from dark scoria to whitish pumice lapilli from the base to the top (Fig. 6G-H), and a similar glass compositional range from CA/HKCA dacites to rhyolites (Albert et al., 2017) and phenocryst content. Such a wide compositional spectrum is also the reason why Di Roberto et al. (2008)

have attributed the tephra layer TIR2000-417 recognized in a deep-sea core in the northern Marsili to the LPT. These correlations suggest variable NW- to SE-wards dispersals during the LPT eruption.

4.2.5. Monte Guardia (27-26 ky)

The Monte Guardia pumice succession is the product of intense Sub-Plinian explosive activity in the southern (rhyolitic) dome complex of Lipari (Pichler 1980; Crisci et al. 1981; De Rosa and Sheridan, 1983; Colella and Hiscott 1997; De Rosa et al., 2003a), corresponding to the Monte Guardia Formation on the island map (Lucchi et al. 2010; Forni et al. 2013). It is thick (up to 50-60 m) and widespread succession of PDC deposits represented by lithic-rich tuff-breccias and massive, planar to cross-stratified lapilli-tuffs and tuffs with interlayered minor fallout beds (Colella and Hiscott 1997) (Fig. 6I-L). Juveniles clasts range from white, highly vesicular pumice to grey, dense to moderately vesicular pumice and banded pumice. White pumices have a distinctive low crystal content with crystals of K-feldspar, clinopyroxene, hornblende, sporadic biotite and minor Ti-magnetite, apatite and zircon, whilst grey pumice have a higher phenocryst abundance with crystals of clinopyroxene, plagioclase minor olivine and Ti-magnetite and apatite, and a microlite-rich groundmass (De Rosa et al. 2003a; Gioncada et al. 2003). Unaltered obsidian clasts are recognized throughout the succession, with the same mineralogy of white pumice (De Rosa et al., 2003a). Wr compositions range from latites to high-K dacites (grey pumice) to rhyolites (white pumice) (De Rosa et al., 2003a), whereas glass compositions yield significant chemical heterogeneity through the stratigraphic succession in the field of rhyolites (Albert et al., 2017): a larger chemical heterogeneity is recorded in the banded pumice (SiO_2 = 70.2–76.8 wt%; K_2O = 4.9–6.3 wt%) from the lower succession, whilst more evolved rhyolites are present in the middle portion (SiO_2 = 74.3–76.7 wt%; K_2O = 2–6.1 wt%) and the most evolved occur in the uppermost part of the succession (SiO_2 = 75.9–76.8 wt%; K_2O = 5.0–5.6 wt%), with a clear inflection to lower K_2O in the glass compositions at ca. 72–74 wt% SiO_2 (Albert et al., 2017). Lithic clasts, which are abundant particularly in the basal breccia layers, consists of older lava and pyroclastic fragments together with subordinate crystalline rocks from the basement (De Rosa et al., 2003a).

The age of the Monte Guardia eruption is defined on the basis of the ^{14}C dates of charcoal fragments embedded within the BT below and above the corresponding pumice deposit in distinct outcrops on the island of Lipari (cf. Crisci et al. 1981; 1983; Meschiari et al., 2020). Calibration of these radiocarbon ages according to IntCal20 Northern Hemisphere calibration curve of Reimer et al. (2020) has provided a restricted time interval ranging 25,920–27,025 cal y BP for the Monte Guardia eruption (Meschiari et al., 2020).

The Monte Guardia pyroclastic succession is widely distributed across the entire island of Lipari, and is distally correlated over most of the Aeolian archipelago and the Capo Milazzo peninsula, representing a major stratigraphic key-bed for correlations in the region under study (Lucchi et al. 2008, 2013b). In particular, the Monte Guardia marker bed was defined by Lucchi et al. (2008) as the stratigraphic boundary between the IBT and UBT, whereas it has been recently adopted to subdivide the IBT and IBT-upper macro-units (Meschiari et al., 2020). Distal fallout layers (up to tens-of-centimetres thick) on Vulcano (Gelso) (Fig. 6M), Salina, Panarea and Basiluzzo (Fig. 6N) and (probably) on Capo Milazzo are made up of normal-graded pumice lapilli and ashes and obsidian fragments with distinctive chemical composition and mineralogical content (Lucchi et al. 2008). More distally, the Monte Guardia has been identified in the T2 tephra layer in the sediment core of the Lago di Pergusa, Sicily (Narcisi, 2002), although the established chronology between 23,555 and 25,860 cal yrs BP is not entirely consistent. Overall, the recognition of the Monte Guardia deposits on Panarea, Vulcano and Sicily is indicative of a large (northern to southern) dispersal area.

4.2.6. Vallone del Gabellotto (8.7-8.4 ky)

The Vallone del Gabellotto pumice succession is the result of a high explosive eruption in north-eastern Lipari (Gabellotto–Fiume Bianco tephra of Cortese et al. 1986; Vallone del Gabellotto Formation of Lucchi et al. 2010; Forni et al. 2013). It has a maximum thickness of c. 130 m and consists of massive to planar and cross-stratified PDC deposits of lapilli and ash with large-scale wavy bedforms interlayered with minor fallout beds (Fig. 6O). The main component is represented by whitish pumice, from highly vesicular to moderately vesicular and blocky, and minor obsidian clasts. A very homogeneous HKCA rhyolite glass composition with no chemostratigraphic variation characterizes these pumices wich are typically aphyric (Albert et al., 2017). Compared to the older Lipari's rhyolites, the Vallone del Gabellotto pumice have consistently lower SiO_2 contents, and lower K_2O at comparable SiO_2 values, together with enrichment of a number of trace elements (Zr, LREE and Th; Albert et al., 2017).

The Vallone del Gabellotto pumice are widely distributed in the entire northern-central part of Lipari (below the Monte Pilato pyroclastic series), with cm-thick distal fallout beds or scattered lapilli and ash identified on Vulcano, Panarea and Stromboli (Keller 1980b; Lucchi et al., 2007, 2008, 2013b, c; De Astis et al., 2013; Francalanci et al., 2013), thus representing a widespread stratigraphic marker in the region under study. The Vallone del Gabellotto is also an important marker bed for correlations in the upper portion of the UBT on Lipari and Vulcano (Meschiari et al., 2020) (Fig. 5F). More distally, the Vallone del Gabellotto pumice has been correlated with the E-1 marine tephra layer documented in the early-Holocene Sapropel sediments of the central Mediterranean including Tyrrhenian, Adriatic and Ionian Seas cores (Paterne et al., 1988; Fontugne et al. 1989; Siani et al., 2004; Caron et al., 2012). Moreover, a Vallone del Gabellotto tephra layer has been recognized in a deep-sea core in the northern Marsili basin (TIR2000-93; Di Roberto et al. 2008), whilst a cryptotephra with its distinctive composition has been recognized in a marine core in the southernmost Ionian Sea (M25/4-12-28 cm; Albert et al., 2017).

The widely accepted Vallone del Gabellotto eruption age is that of its marine equivalent E-1 recognized in the middle of Sapropel 1 at 8430–8730 cal yrs BP (7770±40 14C yrs BP; Siani et al., 2004; Zanchetta et al., 2011). This age entirely fits the fission-track ages of 8.6±1.6 ky (Arias et al. 1986) and 8.6±1.5 ky (Wagner et al. 1976) for the overlying Pomiciazzo obsidian flow on Lipari, whilst the Pomiciazzo ages of 11.4±1.8 ky (Bigazzi and Bonadonna 1973) and 7.17±0.72 ky (Bigazzi et al. 2003) are considered less reliable.

4.2.7. Monte Pilato (776 CE)

The Monte Pilato pumice succession (Monte Pilato tephra of Cortese et al., 1986; Monte Pilato–Rocche Rosse unit of Dellino and La Volpe, 1995; Sciarra dell'Arena Formation of Lucchi et al. 2010 and Forni et al. 2013) is the main product of the intense explosive eruptions that resulted in the building of the Monte Pilato pumice cone in north-eastern Lipari. It has a maximum thickness of c. 150 m, and is composed of alternating PDC deposits represented by massive to planar bedded lapilli-tuffs and tuffs and fallout beds. Juvenile clasts are predominantly represented by whitish, highly to weakly (from the base to the top of the succession) vesicular pumice with spherical to elongated vesicles, and abundant lava lithic clasts with minor obsidian clasts (more abundant in the higher portion). Pumice are aphyric, and have rhyolitic glass compositions with subtly higher SiO_2 and lower levels of incompatible trace element in the lower portion of the succession (Albert et al., 2017).

The Monte Pilato ash (and lapilli) crop out widely along the north-eastern sector of the island of Lipari (Fig. 6P), mantling the topography above a reddish to dark-coloured, humic-rich, laterally-persistent paleosol formed on the Vallone del Gabellotto pumice succession.

Distal centimetre-thick fallout beds of ash and minor lapilli are recognized on Stromboli (Bertagnini et al. 2011) and Panarea (Romano, 1973; Lanzafame and Rossi, 1984; Lucchi et al., 2007), although the latter is no longer exposed in the field. A Monte Pilato tephra layer was also reported along La Fossa and Vulcanello successions (Keller, 1980b; De Astis et al., 2013), but this correlation seems more questionable in the light of a possible attribution of this tephra layer to the younger Rocche Rosse eruption (1220 CE; Lucchi et al., 2007) based on different chronological constraints (Gurioli et al., 2012, Di Traglia et al., 2013, Rosi et al., 2018). More distally, the Monte Pilato ash is a widespread marker bed in the marine sediment records of the Tyrrhenian (Paterne et al., 1988; Albert et al., 2012) and Ionian (Caron et al., 2012) Seas, and in a sedimentary sequence in Albania (Bescoby et al., 2008). Furtherly, a turbidite bed derived from reworking of Monte Pilato deposits has been recognized in a deep-sea core in the northern Marsili basin (TIR2000-IV-7 cm; Di Roberto et al. 2008). Overall, these findings indicate a dominant north-, northeastern- to east-wards dispersal of the Monte Pilato tephra, which is also consistent with the distribution of the succession in the proximal areas of Lipari island (Forni et al., 2013).

The Monte Pilato eruption is dated to 776 CE (1241 ± 31 yrs BP) by the calibrated ^{14}C age obtained for short-lived, carbonized plant material embedded within the base of the pumice succession (Keller, 2002). This age is comparable to another radiocarbon age of to 780-785 CE previously provided by Keller (1970). This age attribution is also consistent with the findings of Monte Pilato pumice deposits above Greco-Roman ruins dated to the 4–5th centuries CE in the archeological site of Contrada Diana in Lipari (Keller 1970) and above Late Antique Butrint archeological excavations dated to the 4–6th centuries CE in Albania (Bescoby et al., 2008). Further chonological information is derived from the interpretation of historical reports. The 776 CE age is in agreement with the description of explosive activity on Lipari given by monk Gregorius in 787 CE (Bernabò Brea, 1989). In this report there is also a reference to what seems the emission of a blackish lava into the sea, which is consistent with the occurrence of remnants of an obsidian lava flow above the Monte Pilato succession along the lowered, northeastern side of the crater (cf. Sciarra dell'Arena Formation, sa_1 member; Forni et al., 2013). Intense explosive eruptions during the Early Middle Ages are also suggested as the main cause for the long-lasting demographic crisis occurred on Lipari between the 6th and 11th centuries CE (Manni et al. 2019). It is notable that the description of explosive activity on Vulcano in 729 CE from the Anglo-Saxon bishop Willibald (Iadanza, 2011) was instead attributed to Monte Pilato by Bernabò Brea (1978), but this interpretation is considered questionable from the historical point of view (see also Keller, 2002).

4.3. Other tephra layers

In addition to the major tephra layers described above, there are a number of other eruptions of Aeolian Islands volcanoes that have produced pyroclastic deposits with a remarkable areal distribution, and a potential for correlations between one island and another or more distally in marine and lake sedimentary archives. Hereafter we assess the diagnostic stratigraphy, age, lithological and volcanological features, and geochemical to mineralogic information which can help in identifying the different tephra units interlayered in the local BT stratigraphic successions, described in stratigraphic order for the islands of Vulcano, Lipari, Salina, Panarea and Filicudi.

4.3.1. Vulcano

The BT deposits are recognized at different stratigraphic intervals across the central, western and southern sectors of the island of Vulcano. A subdivision between LBT/IBT deposits and the IBT-upper macro-unit is made possible by the occurrence of the Monte Guardia tephra layer from Lipari. The UBT instead rest above the Spiaggia Lunga scoria deposit, and they are bounded at the top by the Punte Nere Tuffs. The La Sommata scoria are interlayered within the IBT, whereas the Quadrara pumice and scoria unit, Cugni di Molinello scoria, Casa Lentia pumice and Monte Saraceno scoria are interbedded to the UBT. On Vulcano the LBT are linked to the Monte Molineddo 2 Tuffs as their more probable near-source counterpart, with a possible link between the Monte Molineddo 1 Tuffs and the earliest LBT, and the IBT are chronostratigraphically associated to the Monte Molineddo 3 Tuffs.

Hereafter, the local tephra units on Vulcano that have stratigraphic relationships with the BT are described in stratigraphic order.

4.3.1.1. Monte Molineddo 1 tuffs

This is a thick pyroclastic succession cropping out in the flattish area of il Piano ("Upper Grey Sandtuffs", Keller 1980b; Monte Molineddo 1 Formation, De Astis et al., 2013), which has been linked to an undefined eruptive vent(s) inside the La Fossa caldera (De Astis et al., 2013). It has a maximum thickness of 8 metres and consists mostly of PDC deposits represented by planar to cross laminated grey ashes with interlayered minor fallout beds (Fig. 7A). Juvenile clasts are glass fragments and dark grey to grey scoria lapilli, frequently characterized by a yellowish patina, whilst mm-sized, euhedral clinopyroxene crystals are abundant. Scoria lapilli have relatively homogeneous trachy-andesite glass compositions (56.0–58.4 wt% SiO_2; Na_2O+K_2O=9.1–10.5 wt%) with a clear K-series affinity (5.3–6.2 wt% K_2O) (Meschiari et al., 2020).

The Monte Molineddo 1 tephra is not directly dated, but it is stratigraphically recognized above the Monte Aria/Timpa del Corvo lava flows, dated to 78.5–77 ky (K/Ar; Frazzetta et al., 1985; Gillot, 1987; De Astis et al., 1989), and below the Monte Rosso, Monte Luccia and Passo del Piano units, dated to 53.7–48.5 ky (De Astis et al., 1989). The corresponding eruption(s) are thus attributed to the 77-53.7 ky time interval (De Astis et al., 2013).

On this basis, the Monte Molineddo 1 was discussed as the proximal counterpart on Vulcano of the LBT, which have a compatible chrono-stratigraphic position and share many lithological and textural features (Lucchi et al., 2008; 2013b). A link with the earliest LBT cannot be completely excluded based on some overlap between the glass compositions of the Monte Molineddo 1 and the LBT, but this is not the preferred interpretation based on the available data (Meschiari et al., 2020).

4.3.1.2. Monte Molineddo 2 tuffs

The Monte Molineddo 2 pyroclastic succession (“Varicolored Tuffs”, Keller, 1980b; Monte Molineddo 2 Formation; De Astis et al., 2013) unconformably rests above the Monte Molineddo 1 (Fig. 7A) and share the same provenance from a vent(s) inside the La Fossa caldera (De Astis et al., 2013). It has a maximum thickness of 25–30 m and consists of PDC deposits of varicoloured, planar to cross-laminated ash and lapilli (Fig. 7B), with some interlayered fallout beds of scoria lapilli in the upper portion. Scoria lapilli have variable glass compositions ranging from phono-tephrites and tephri-phonolites to trachy-andesites (SiO_2 = 51.4–55.7 wt%; Na_2O + K_2O = 9.2–11 wt%), with a clear K-series affinity (K_2O = 5.2–6.1 wt%), although few data are available, likely not fully representative of the compositional variability of this thick eruptive succession (Meschiari et al., 2020).

The Monte Molineddo 2 tephra is stratigraphically defined in the same 77-53.7 ky interval of the Monte Molineddo 1 (De Astis et al., 2013), and is considered as the most probable near-source counterpart of the LBT on Vulcano based on the reconstructed chronostratigraphy and geochemical overlap of the available glass data (Meschiari et al., 2020).

4.3.1.3. Monte Molineddo 3 tuffs

This is a thick (up to 22 m) pyroclastic succession widely distributed in the central sector of Vulcano (“Molineddu Tuffs”, De Astis et al., 1989; Monte Molineddo 3 Formation, De Astis et al., 2013), and linked to a source area inside the La Fossa Caldera (De Astis et al., 2013). It consists of alternating PDC deposits of planar to cross laminated ash and fallout beds of dark-grey scoria lapilli (moderately to highly vesicular) very often with a yellowish patina (Fig. 7C). The uppermost portion of the succession is a 6-m-thick layer of scoria lapilli and bombs with abundant (10–15%) lava lithics. Millimetre-sized euhedral clinopyroxene are present in the entire succession. The Monte Molineddo 3 scoria have glass compositions dominated by tephri-phonolites which straddle the trachy-andesite classification boundary (SiO_2 = 52.9-54.8 wt.%; Na_2O + K_2O = 9.3-12.7 wt.%) and show a K-series affinity (K_2O = 5.6-7.4 wt.%) (Meschiari et al., 2020).

The Monte Molineddo 3 tephra is stratigraphically recognized above the Monte Rosso, Monte Luccia and Passo del Piano units, dated to 53.7–48.5 ky (K/Ar; De Astis et al., 1989), and below the Spiaggia Lunga scoria, dated to 24.0±5.0 ky (U/series; Soligo et al., 2000). The corresponding eruption(s) are thus constrained to the 48.5-24.0 ky time interval (De Astis et al., 2013), which is largely consistent with that of the IBT. Moreover, glass compositions of the Monte Molineddo 3 reveal a substantial compositional variability, which appears to correspond to a significant proportion of the overall IBT chemical variability. Scoria lapilli correlated to the Monte Molineddo 3 are also recognized interbedded within the IBT in southern Lipari and Vulcano (Gelso). This supports the chronostratigraphic link between the IBT and the Monte Molineddo 3 as their near-source counterpart on Vulcano (Meschiari et al., 2020), although it is notable that the available data are not considered fully representative of the stratigraphic succession in the proximal areas.

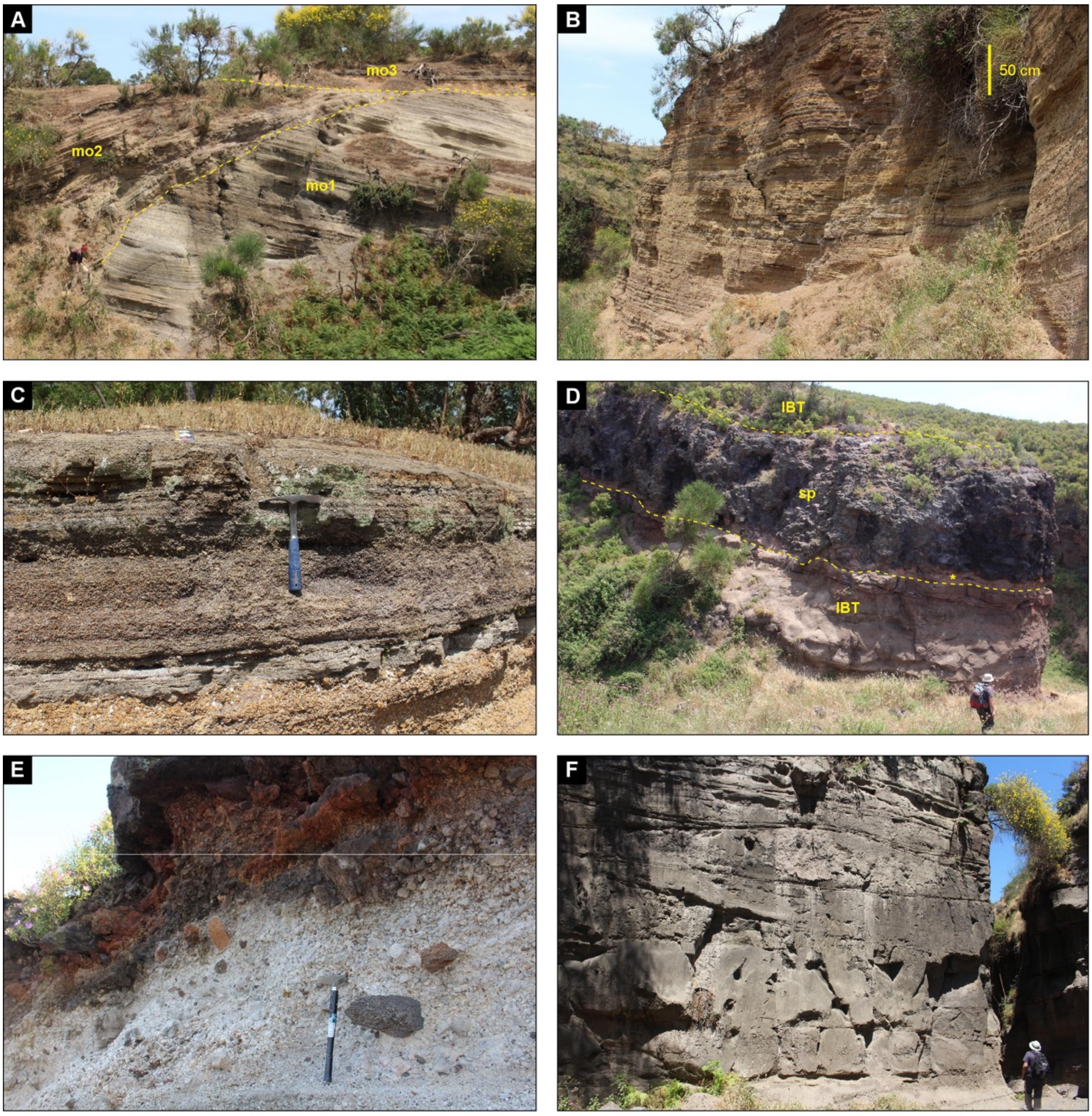

Fig. 7. Outcrop photographs of the major tephra units interlayered within the BT on Vulcano (in stratigraphic order). A) Monte Molineddo 1 tuffs (mo1) in their type locality in central Vulcano. They are unconformably covered by the Monte Molineddo 2 (mo2) and Monte Molineddo 3 (mo3) tuffs. B) Monte Molineddo 2 tuffs in the same locality of Figure 7A. C) Monte Molineddo 3 tuffs in their type locality near to Capo Grillo, central-northern Vulcano. D) Spiaggia Lunga scoria blanket (sp) in the area of Grotta dei Pisani, western Vulcano, showing a laminated tuff layer at the base (*). This unit defines the lower boundary of the Upper Brown Tuffs (UBT) on Vulcano, and delimits at the top the Intermediate (and Intermediate-upper) Brown Tuffs (IBT). E) Quadrara pumice and scoria unit near to Piano d'Alighieri, south-western Vulcano. F) Punte Nere tuffs along the Rio Grande valley, near to the southern border of the La Fossa caldera.

4.3.1.4. La Sommata scoriae

The La Sommata pyroclastic succession crops out in the south sector of il Piano area on Vulcano (La Sommata Formation, De Astis et al. 2013), and consists of Strombolian fallout deposits of loose, dense to highly vesicular, black scoriaceous lapilli and bombs. These deposits build up two NNE–SSW-aligned scoria cones. Juvenile scoriae are low porphyritic to sub-aphyric, and have a wr basaltic composition showing either SHO or HKCA affinities (SiO2 = 48.0-52.4 wt%; Na_2O + K_2O = 3.9–6.0 wt %; K_2O = 1.9-3.0 wt%), with the highest MgO contents (up to 8.69 wt %) and the lowest $^{87}Sr/^{86}Sr$ values among the Vulcano products (De Astis et al., 2013). Distinct layers of La Sommata scoriae lapilli are interlayered within the IBT (56-27 ky) in mid-distal areas.

4.3.1.5. Spiaggia Lunga scoriae (24.0 ky)

This is a well-known pyroclastic succession outcropping along the western coastal sector of the island of Vulcano (“Spiaggia Lunga–Saraceno blanket” of Keller 1980b; “Spiaggia Lunga Scoriae” of De Rosa et al. 1988; Spiaggia Lunga Formation of De Astis et al., 2013). It mostly consists of two wide, red-brownish weakly to intensely welded scoria blankets (45 and 8 m thick) produced by fountain-fed fallout coupled with scoria flow processes during Strombolian-Hawaiian eruptions (De Astis et al., 2013) (Fig. 7D). A distinctive PDC deposit (locally up to 3 m thick) consisting of planar to low-angle (or wavy) laminated and varicoloured ash with interlayered fall beds of scoria lapilli is visible at the base of the succession (Fig. 7D), together with a lithic-rich layer containing quartzitic and monzogabbroid blocks related to the conduit-opening phase (De Astis et al., 2013). The Spiaggia Lunga activity is related by De Astis et al. (2013) to an eruptive fissure parallel to the southwestern border of the La Fossa Caldera, whilst Nicotra et al. (2020) have suggested that these deposits are directly representative of one of the caldera-forming eruptions. The Spiaggia Lunga scoria have a homogeneous SHO basalt to shoshonite wr composition (SiO_2 = 49.7–51.7 wt%; Na_2O + K_2O = 5.7–7.2 wt %; K_2O = 2.3-2.7 wt%; De Astis et al., 2013; Nicotra et al., 2020), with the typical mineral content of basaltic products (plagioclase, clinopyroxene, olivine and oxides).

The Spiaggia Lunga scoria have a radiometric age of 24.0±5.0 ky (U-series; Soligo et al. 2000) and have been adopted by Meschiari et al. (2020) as the main chemo-stratigraphic marker bed to subdivide the IBT-upper and UBT macro-units on Vulcano (Fig. 7D).

4.3.1.6. Quadrara pumice and scoriae (21.3±3.4 ky)

This is a distinctive pyroclastic unit that mantles the southwestern flanks of the island of Vulcano ("Quadrara blanket" of Keller, 1980b; Quadrara Formation of De Astis et al., 2013). It consists of an inversely-graded layer (c. 1 m thick) of whitish pumice lapilli and bombs with abundant xenoliths at the base, which gradually passes upwards to a brown to reddish, welded scoria blanket (15 m thick) (Fig. 7E). They are the product of fallout coupled with scoria flow processes during a violent Strombolian to sub-Plinian eruption (De Astis et al., 2013; Albert et al., 2017). Juveniles have wr compositions ranging from trachytes (pumice) to shoshonites and latites (scoria) (De Astis et al., 2013; Nicotra et al., 2020), whilst glass compositions range from trachyte (SiO_2 = 63.4–63.6 wt%; Na_2O + K_2O = 10.4-10.9 wt % K_2O = 5.7-6.2 wt%) in the pumice to trachy-andesite in the scoria (SiO_2 = 58.1–60.2 wt%; Na_2O + K_2O = 8.5-9.4 wt % K_2O = 4.9-5.0 wt%), both showing a clear SHO affinity (Albert et al., 2017). Pumice have distinctive K-feldspar and biotite crystals content.

The Quadrara unit has a radiometric age of 21.3±3.4 ky (U-series; Soligo et al. 2000), and are proximally interlayered within the lower portion of the UBT (Meschiari et al., 2020). A distal occurrence of Quadrara is recognized by pumice interlayered within the UBT on Capo Milazzo (Morche, 1988; Albert et al., 2017), documenting a dominant southerly dispersal. On the other hand, proposed correlations of Quadrara with the trachytic EL4 layer on Panarea (De Rita et al., 2008) and the T-3 tephra layer in the lacustrine sediments of Lago Pergusa, Sicily (Narcisi, 2002) are considered chemically and/or stratigraphically not consistent by Albert et al. (2017).

4.3.1.7. Cugni di Molinello scoriae

This unit is a fallout bed (up to 2 m thick) of black, highly vesicular scoria lapilli probably due to a violent strombolian activity and widely distributed in the central sector of Vulcano (Cugni di Molinello Formation; De Astis et al., 2013) (Fig. 5E). The venting area of the Cugni di Molinello scoria remains uncertain, but a more probable origin from inside the La Fossa caldera is outlined by a slight NE- and SW-wards grain size and thickness decrease in the outcrops exposed in the area of Il Piano (Dellino et al., 2011; 2013). Scoria have shoshonite wr composition (De Astis et al., 2013) and relatively homogeneous basaltic trachy-andesite glass composition (52.3–54.3 wt% SiO_2) with a K-series affinity (5.2–6.2 wt% K_2O), and most significant variability in their MgO (2.9–4.0 wt%) and CaO (6.3–8.0 wt%) contents (Meschiari et al., 2020).

The Cugni di Molinello scoria is a key marker bed within the UBT on Vulcano that subdivides a lower and an upper portion of this succession (corresponding to the lower and upper "Tufi di Grotta dei Rossi" in De Astis et al., 1997a) (Fig. 5E). Note that these scoriae display the more primitive chemical features than all the UBT deposits (Meschiari et al., 2020).

4.3.1.8. Casa Lentia (15-13 ky)

The Casa Lentia pyroclastic succession (up to 4 m thick) consists of a loose to weakly agglutinated fallout deposits made up of weakly vesicular pumice and lava lithics. Pumice have glass compositions that straddle the boundary between trachytes and rhyolites (SiO_2 = 68.7–70.49 wt%; Na_2O + K_2O = 9.8–10.4 wt %), with a clear shoshonitic affinity (K_2O = 6-6.4 wt%) (Albert et al., 2017), and contain phenocrysts of plagioclase, clinopyroxene, olivine and K-feldspar. The Casa Lentia pyroclastic succession crops out uniquely along the western border of the La Fossa caldera in Vulcano, resting above the Monte Lentia lava domes, and is related to an undefined vent(s) within the caldera that is presently dismantled by following erosional and collapse processes (De Astis et al., 2013). The pyroclastic deposits are associated to a couple of dark-grey trachytic (wr) aa-type lava flows that are exposed also in the area of Passo del Piano inside the La Fossa caldera.

There is no direct age attribution for the Casa Lentia pyroclastic deposits and lavas. However, the underlying Monte Lentia lava domes are dated to 15.5±1.0 ky (paleomagnetism; Laj et al. 1997), 13.0±3.0 ky (U-series; Soligo et al., 2000) and 13.0±1.0 ky (K/Ar; De Rosa et al., 2003b), whereas a K/Ar age of 15.5±1.3 ky (average; Gillot, 1987) is available for latite lavas of uncertain location in the same area. We thus assume an approximate age of 15-13 ky for the Casa Lentia eruption.

Glass fragments with the distinctive Casa Lentia compositions are recognized embedded within the upper portion of the UBT in the sector of Passo del Piano on Vulcano and in the northern sector of Lipari (Meschiari et al., 2020), thus documenting a substantial distribution of the ash produced during the eruption.

4.3.1.9. Monte Saraceno scoriae (8.3 ky)

This is a tephra layer (Monte Saraceno Formation, ms_1 member; De Astis et al.. 2013) related to an eruptive fissure localized at the junction between the il Piano and La Fossa caldera structures on Vulcano, which has also produced thin aa lava flows. Tephra consists of a Strombolian-hawaiian fallout bed of welded to loose scoria lapilli and bombs. Scoria have shoshonite (wr) composition (SiO_2 = 51.7-52.6 wt%; $Na_2O + K_2O$ = 6.8-7.6 wt % K_2O = 3.4-4.3 wt%), whilst lava is shoshonite to latite (De Astis et al., 2013).

The Monte Saraceno scoria bed is interlayered within the upper portion of the UBT, immediately below the Vallone del Gabellotto tephra layer from Lipari (Lucchi et al., 2008, 2013). This stratigraphic position is approximately in agreement with the radiometric age of the Monte Saraceno lava to 8.3±1.6 ky (K/Ar; De Astis et al., 1989).

4.3.1.8. Punte Nere tuffs (5.5 ky)

The Punte Nere pyroclastic succession (Punte Nere succession, Dellino and La Volpe, 1997; Punte Nere Formation, De Astis et al. 2013) is the oldest unit that is firmly attributed to the currently active La Fossa cone, Vulcano (De Astis et al. 2013). The bulk of the succession (up to 150 m thick) consists of PDC deposits of massive and planar to cross-laminated grey-black ashes with minor interlayered fallout beds of pumice lapilli (Fig. 7F). A distinctive metre-thick layer of welded scoria lapilli and bombs is recognized. Glass fragments from the lower portion of the succession have compositions ranging from K-series trachy-andesites and trachytes (SiO_2 = 58.5-63.8 wt.%; $Na_2O + K_2O$ = 9.7-11.3 wt.%; K_2O = 5.6-7.1 wt.%) to tephri-phonolites and phonolites (SiO_2 = 55.0-58.5 wt.%; $Na_2O + K_2O$ = 9.4-12.5 wt.%; K_2O = 6.9-8.3 wt.%) (Meschiari et al., 2020). These heterogeneous Punte Nere data are consistent with glass data for Punte Nere published by Lucchi et al. (2008), which also extend towards the rhyolites.

The Punte Nere scoria are dated to 5.5 (+2.2/-1.1) ky (U-series, Soligo et al., 2000). In addition, radiometric ages of 5.5-3.8 ky were obtained for the lava flows attributed to the Punte Nere activity (K/Ar, Frazzetta et al., 1985; Gillot, 1987; U-series, Soligo et al., 2000), but they have been recently called into question due to a different paleomagnetic age to 1170 CE (Arrighi et al. 2006). We thus use an age of 5.5 ky for the Punte Nere explosive eruption(s), although this chronological assignment is not yet so solid.

The Punte Nere tephra is generally adopted as the upper stratigraphic constraint for the UBT on Vulcano (Lucchi et al., 2008, 2013), although the direct relationships between the two successions are not well exposed in the field. It is notable that the two successions share on Vulcano very similar lithofacies of massive to laminated grey to dark grey ash deposits, which makes difficult to recognize stratigraphic contacts between them. Moreover, there is a large geochemical similarity between the glass compositions of the UBT (trachy-andesites to trachytes) and the earliest Punte Nere tephra, which indicates that the two successions likely shared the same magmatic plumbing system (Meschiari et al., 2020). On the other hand, it cannot be completely excluded that some of the older Punte Nere deposits may actually equate to the uppermost UBT in the field.

4.3.2. Lipari

The island of Lipari shows the most complete BT succession, which is constrained by late MIS 5 marine deposits at the base and the Monte Pilato Tuffs at the top. In the internal areas of the island (where the MIS 5 marine deposits are not present) the lower boundary of the LBT is marked by the Monte S.Angelo Tuffs. The LBT, IBT and IBT-upper macro-units are defined by the interlayered Ischia Tephra and Monte Guardia pumice, whereas the subdivision between the IBT-upper and the UBT is established geochemically following Meschiari et al. (2020). The GPT and Lower Pollara Tufffs from Salina and the Vallone del Gabellotto pumice are important markers for correlations in the lower, intermediate and upper portion of the BT succession. Moreover, the Punta di Perciato and Falcone pumice and the Lip 1 ash layer are recognized within the IBT, and Lip 2 and Vallone Canneto dentro are interbedded to the UBT.

Hereafter, the local tephra units on Lipari that have stratigraphic relationships with the BT (in addition to the major Monte Guardia, Vallone del Gabellotto and Monte PIlato pumice layers) are described in stratigraphic order.

4.3.2.1. Monte S. Angelo tuffs (104 ky)

Thick and widespread pyroclastic deposits built up the bulk of the Monte S.Angelo stratocone on Lipari, and are widely distributed on most of the island representing an important stratigraphic horizon. Two major pyroclastic successions (Timpone Pataso and Serra Pirrera formations; Forni et al., 2013) are separated by a laterally persistent reddish palaeosol. The two successions have tens-of-metres thickness and consist of PDC deposits of massive to planar and cross-stratified, grey to pink lapilli-tuffs with interlayered minor Strombolian fallout beds of scoria lapilli (Fig. 8A). At the foot of the flanks of Monte S.Angelo the primary deposits pass into two massive sheet-like horizons (15-25 m thick each) of grey massive lapilli-tuffs embedding numerous unburnt fossil plant relicts ("leaf-bearing pyroclastics", Ricci Lucchi et al., 1988).

The Monte S.Angelo tuffs are not directly dated, but they are covered by distinctive blocky lava flows ("cordierite-rich lavas"; Forni et al., 2013) dated to 105±19 ky (K/Ar; Crisci et al., 1991) and 104.0±3.5 ky (Ar/Ar; Lucchi, 2009). An age reference of 104 ky is here assumed for the Monte S.Angelo (grey) tuffs.

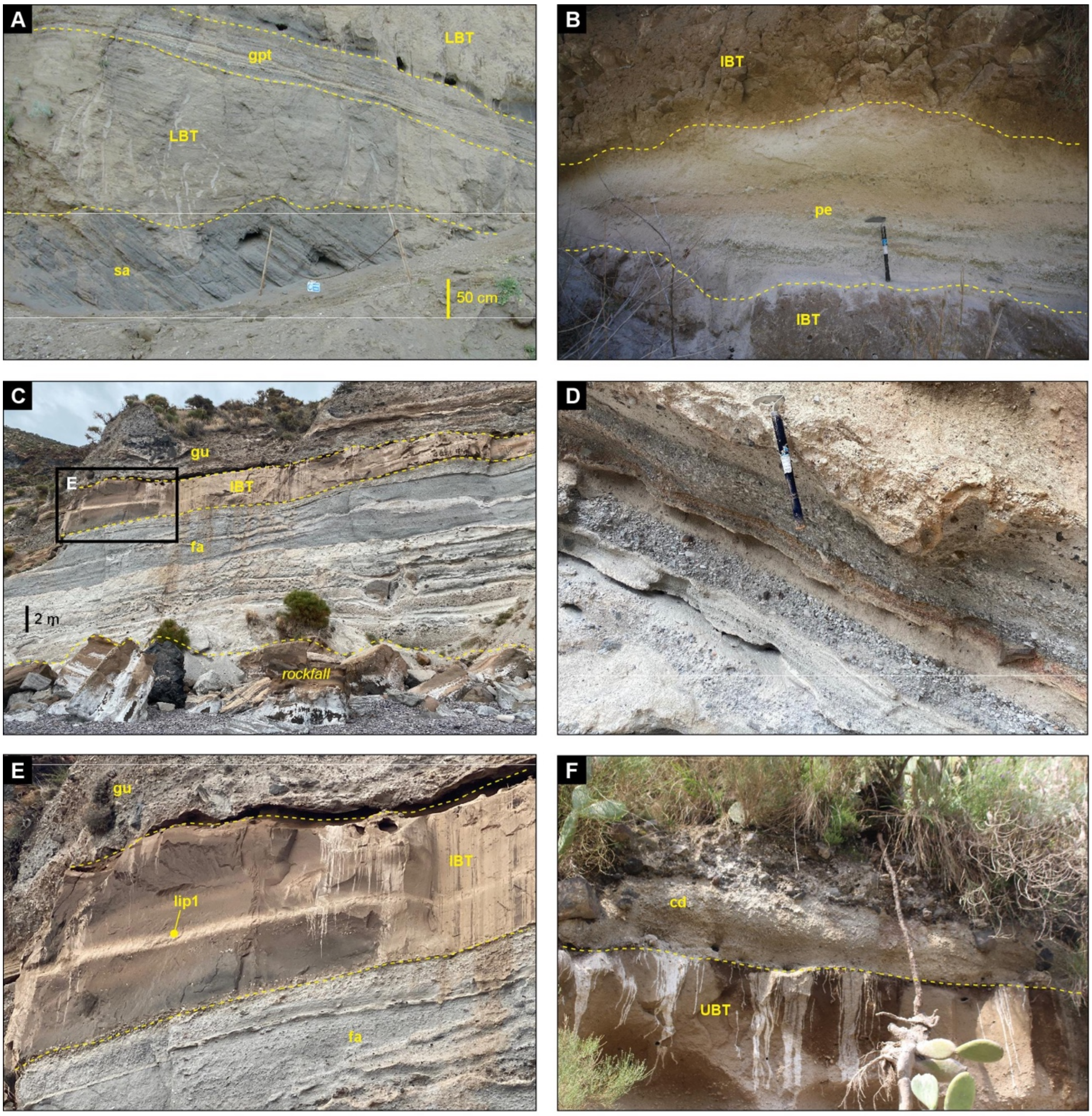

Fig. 8. Outcrop photographs of the major tephra units interlayered within the BT on Lipari (in stratigraphic order). A) The Monte S.Angelo tuffs (sa) crop out below the Lower Brown Tuffs (LBT) at Madoro, in the internal sector of Lipari. The LBT are interlayered by the Grey Porri Tuffs from Salina (gpt). B) Punta del Perciato pumice layer (pe) interlayered within the Intermediate Brown Tuffs (IBT) along the Valle Muria valley, south-west Lipari. C) Natural stratigraphic section exposed along the coastal cliff of Scogliera sotto il Monte, south-west Lipari, showing the Falcone (fa) and Monte Guardia (gu) pumice succession interlayered by the Intermediate Brown Tuffs (IBT). D) Falcone pumice deposits along the Valle Muria valley. E) Detail of Figure 8C where the Lip1 ash layer is interbedded within the Intermediate Brown Tuffs (IBT) stratigraphically below Monte Guardia (gu) and above Falcone (fa). F) Vallone Canneto dentro pumice deposits (cd) resting above the Upper Brown Tuffs (UBT) near to Canneto, eastern Lipari.

4.3.2.2. Punta del Perciato pumice

This is the oldest tephra unit related to volcanic activity in the southern rhyolite dome field of Lipari, and is associated to the remnants of two endogenous NNW–SSE-aligned lava domes cropping out along the southwestern coastal cliff of Scogliera sotto il Monte (Punta del Perciato Formation, pe_1 and pe_2 members; Lucchi et al., 2010; Forni et al., 2013). The tephra unit (up to 2 m thick) consists dominantly of PDC deposits of massive (lithic-rich) pyroclastic-breccias passing laterally to massive to planar and cross-stratified whitish ash and lapilli (Fig. 8B). Juvenile clasts are represented by white pumice that are generally highly vesicular (Forni et al., 2013), scarcely porphyritic (K-feldspar, plagioclase, hornblende, minor biotite, Ti-magnetite; Gioncada et al., 2005) and have a very homogeneous HKCA rhyolite (glass) composition (SiO_2 = 76.3-76.5 wt.%; Na_2O + K_2O = 9.0-9.1 wt.%; K_2O = 5.7 wt.%) (Albert et al., 2017). Scarce, frequently brecciated, obsidian fragments (up to a few cms in diameter) are present.

The Punta del Perciato eruptions are not yet precisely dated, but the corresponding tephra unit is stratigraphically interbedded within the lower portion of the IBT (Fig. 8B), between the underlying 56 ka Ischia Tephra and the 43–40 ka Falcone domes. The Punta del Perciato pumice layer is mostly recognized in southern-central Lipari.

4.3.2.3. Falcone pumice

The Falcone pumice succession are associated to the intermediate NNW–SSE aligned lava domes of the southern rhyolite dome field of Lipari (Falcone Formation, fa_1 and fa_2 members; Lucchi et al., 2010; Forni et al., 2013). The tephra unit has a maximum thickness of 15 metres and consists of PDC deposits of massive lithic-rich tuff-breccias passing laterally to massive, planar and cross-stratified lapilli-tuffs interlayered with minor fallout beds of pumice lapilli (and bombs) (Fig. 8C-D). The pumices are moderately to highly vesicular, with dominant whitish pumice clasts and dense to moderately vesicular grey pumices, with minor banded pumice and lava lithics (up to 30% in the tuff-breccia layers), whilst obsidian clasts with a diameter in the range of 5-10 cm, are present in the near-vent outcrops and become less abundant and smaller in size towards distal areas. Grey pumice are porphyritic with phenocrysts of clinopyroxene, plagioclase, olivine and Ti-magnetite, whereas whitish pumice are low porphyritic and contain few crystals of plagioclase, K-feldspar, hornblende and sporadic biotite (Gioncada et al., 2003; 2005). The Falcone pumice display a range of glass compositions from trachytes to rhyolites that is consistent with the presence of both grey and white pumice (Albert et al., 2017). The Falcone glass analysis show more variation in trace element concentrations, and subtly higher concentrations of La and Ce, compared to the older Punta del Perciato ones (owing to the presence of lower silica rhyolites), although the contents are largely indistinguishable (Albert et al., 2017).

The Falcone pumice layer is widely interlayered within the intermediate portion of the IBT succession in most of the central-southern sector of Lipari (Fig. 8C), in a stratigraphic position higher than the Punta del Perciato one. The Falcone tephra is not directly dated, but the associated lava domes display a series of radiometric ages: 43±1 ky, 42±1 ky (K/Ar; Leocat, 2011), 42.0±0.3 ky (K/Ar; Crisci et al., 1991), 41.0±3.8 ky and 40.0±2.5 (K/Ar; Gillot, 1987). This provides a robust age assignment to 43-40 ky for both the Falcone lava domes and associated pumice deposits.

4.3.2.4. Lip 1 ash layer

This is a bed of whitish ash (up to 10 cm thick) recognized along the western coastal cliff of the southern dome field of Lipari (Fig. 8E). Glass compositions are homogeneously rhyolites (SiO_2 = 75.5-76.7 wt.%; Na_2O + K_2O = 7.7-9.2 wt.%; K_2O = 4.9-5.6 wt.%).

The Lip 1 ash layer is interlayered within the intermediate portion of the IBT succession in a stratigraphic position between the older Falcone (43-40 ky) and younger Monte Guardia (27-26 ky) pumice units (Fig. 8E). Based on consistent glass compositions and stratigraphic position, we suggest here that the Lip 1 ash layer is correlated distally to the E-11 tephra layer identified by Paterne et al. (1988) in the Tyrrhenian Sea core KET8003, which was attributed unequivocally to Lipari by Albert et al. (2017) but missing of a proximal equivalent until now. The E-11 tephra is dated to 37.7 ky (Paterne et al., 1988) and occurs directly above the 40 ky BP Campanian Ignimbrite (Y-5; De Vivo et al., 2001). E-11 correlatives in the Ionian and Adriatic Sea marine records have been dated to 34.1 ky (I-2 tephra, KC01B core; Insinga et al., 2014) and 33,711–35,163 cal yrs BP (T1535 tephra, SA03-11 core; Matthews et al., 2015). An age of 37-34 ky for the Lip 1 (E-11) ash layer gives chronological information about a previously unknown (rhyolite) explosive eruption of the southern dome-field of Lipari (preceding the major Monte Guardia eruption). This eruption have no substantial proximal occurrence, probably because the subsequent intense Monte Guardia eruption has buried or destroyed most of the products in near-vent areas.

4.3.2.5. Lip 2 tephra layer

This tephra layer (corresponding to the I_3 layer of Forni et al., 2013) is recognized in the central-eastern sector of Lipari near to Vallonaccio. It has a thickness of 1-2 m and consists of massive and planar to cross-stratified, whitish pumice lapilli-tuffs with a substantial content of obsidian fragments. Pumice are aphyric and have homogeneously rhyolite glass compositions (SiO_2 = 74.9-75.8 wt.%; Na_2O + K_2O = 8.8-9.1 wt.%; K_2O = 4.9-5.1 wt.%; Meschiari et al., 2020).

The Lip 2 tephra layer is not directly dated, but it is interbedded within the UBT in a stratigraphic position higher than Monte Guardia and lower than the Vallone Canneto dentro (undated) and Vallone del Gabellotto (8.7-8.4 ky) units. Moreover, charcoal dated from within the IBT-upper below the Lip 2 tephra is dated to 25,800–26,190 cal y BP (Meschiari et al., 2020). As such, Lip 2 is poorly constrained to between 26 ky and 8.7 ky, and represents the oldest unit of rhyolite aphyric pumice in the northeastern sector of Lipari. In this time-stratigraphic interval the only exposed proximal unit in this sector is represented by the strongly hydrothermally altered, rhyolite lava domes of Capo Rosso (Capo Rosso Formation, Forni et al., 2013), which are recognized along the coastal cliff north of Canneto. It can be suggested here that the Lip 2 tephra is the result of explosive eruptions associated to the Capo Rosso lava domes, but it cannot be discounted that it is produced from another vent in the vicinity of the outcrop site. Note that an obsidian (lithic) clast within the Vallone del Gabellotto pumice succession near Acquacalda gave a fission track age of 21±4 ky (Bigazzi and Bonadonna 1973). This could be related to the explosive activity that resulted in the Lip 2 tephra, thus providing a generic chronological constraint for the onset of rhyolite activity in the northeastern sector of Lipari.

4.3.2.6. Vallone Canneto Dentro pumice

This is a pyroclastic succession ("Canneto Dentro tephra"; Cortese et al., 1986) that underlies the endogenous lava dome of Vallone Canneto dentro, in the central-eastern sector of Lipari (Vallone Canneto Dentro Formation, cd_1 and cd_2 members; Forni et al., 2013. It has a maximum thickness of 4 metres and mostly consists of PDC deposits of massive to stratified, obsidian-rich, whitish pumice tuff-breccias and lapilli-tuffs (Fig. 8F). Pumice are aphyric and have homogeneous rhyolite glass compositions (SiO_2 = 74.6-75.6 wt.%; Na_2O + K_2O = 8.7-9.4 wt.%; K_2O = 4.9-5.3 wt.%; Meschiari et al., 2020).

The Vallone Canneto Dentro tephra is currently undated, but it is stratigraphically constrained within the upper portion of the UBT (Fig. 8F), immediately below the Vallone del Gabellotto unit (8.7-8.4 ky). In particular, there are no other BT units nor evidence of erosion or pedogenization between the Vallone Canneto Dentro and Vallone del Gabellotto units, which suggests that they were erupted in a close time-stratigraphic window. Further chronologic information can be derived from a proposed distal correlation of the Vallone Canneto Dentro with a cryptotephra in a marine core in the Ionian Sea (M25/4-12; Albert et al., 2017). The cryptotephra M25/4-12-44 cm, stratigraphically older than the M25/4-12-28cm/Vallone del Gabellotto, is in fact HKCA rhyolitic (Albert et al., 2017), and it is largely consistent with the glass composition of the Vallone Canneto Dentro pumice presented here. It is thus suggested here a correlation between Vallone Canneto Dentro and the cryptotephraM25/4-12-44 cm, which falls in the Late-glacial period of the record based on the oxygen isotope stratigraphy (Negri et al., 1999). Accordingly, the Vallone Canneto Dentro unit would be dated to c. 15-12 ky.

4.3.3. Salina

The BT deposits occur in the northern and eastern coastal sectors of Salina, and preferentially accumulate in the morphological depression of Valdichiesa (central Salina). They are constrained by the late MIS 5 marine deposits at the base whilst the upper stratigraphic boundary is represented by the Upper Pollara Tuffs. The LBT and IBT macro-units are well distinguished by the widespread interlayering of the Ischia Tephra, whereas the upper boundary of the IBT is made evident only discontinuously by the Monte Guardia pumice bed. Above Monte Guardia, only UBT deposits are recognized (with no geochemical evidence of the IBT-upper). The GPT and Lower Pollara Tuffs are widely interbedded within the LBT and IBT, respectively.

Hereafter the Upper Pollara Tuffs are described.

4.3.3.1. Upper Pollara Tuffs (15.5 ky)

The Upper Pollara Tuffs (cf. Keller, 1980a; Vallone del Pozzo Formation, Lucchi et al., 2013a) are the product of the late explosive eruption(s) from the Pollara crater, and the latest activity on Salina. They are a thick pyroclastic succession (up to 200 metres) mostly consisting of PDC deposits of massive tuff-breccias passing laterally to planar- and cross-stratified lapilli-tuffs and massive tuffs, with Vulcanian lithic-rich fallout deposits at the base of the succession (Sulpizio et al., 2008) (Fig. 9). Massive, weakly lithified and zeolitized yellowish lapilli tuffs are recognized on the inward-dipping slopes of the Pollara crater. Juveniles mostly consist of white pumice with variable vesicularity and minor amounts of grey and banded pumices (increasing with stratigraphic heights), loose crystals and lithic fragments in the basal portion (Keller, 1980a; Sulpizio et al., 2008). Bulk rock compositions range over a large interval from HKCA dacites to rhyolites (SiO_2=65-74 wt.%) (Sulpizio et al., 2008), whilst pumice have mostly rhyolite glass compositions with a HKCA affinity, with a large geochemical variation (SiO_2 = 71.4–77.6 wt%; CaO = 0.9–3.0 wt%; K_2O = 3.4–4.4 wt%) consistent with the occurrence of white and grey pumice (Albert et al., 2017). Glass compositions reported in Sulpizio et al. (2008) extend to less evolved (HKCA) dacites and andesites. Whitish pumice are low porphyritic (10%) and contain crystals of plagioclase, amphibole and biotite, less-abundant clinopyroxene, orthopyroxene and rare xenocrystic olivine, whilst grey pumice have a higher crystal content with plagioclase, amphibole, clinopyroxene and rare olivine (Keller 1980; Donato et al. 2006; Sulpizio et al. 2008). Upper Pollara is the only unit on Salina that contains biotite as a major phenocryst phase (Keller 1980a).

The Upper Pollara Tuffs are widely distributed in the northern sector of the island above the UBT succession. The Upper Pollara eruption is radiocarbon dated to 15,000–16,090 cal yrs BP (Albert et al., 2017) on charcoal embedded at the base of the unit (uncalibrated age of 12.97±0.18; Keller, 1980a). No BT deposits are recognized above Upper Pollara on Salina, probably due to subsequent erosion of the loose ash (primary) deposits along steep slopes.

Albert et al. (2017) have suggested that Upper Pollara is correlated distally with the E-2 tephra layer in the southern Tyrrhenian marine core KET8003 reported by Paterne et al. (1988). Correlation is supported by consistent HKCA rhyolite glass composition with higher CaO at overlapping FeOt contents compared to the typical Lipari glasses.

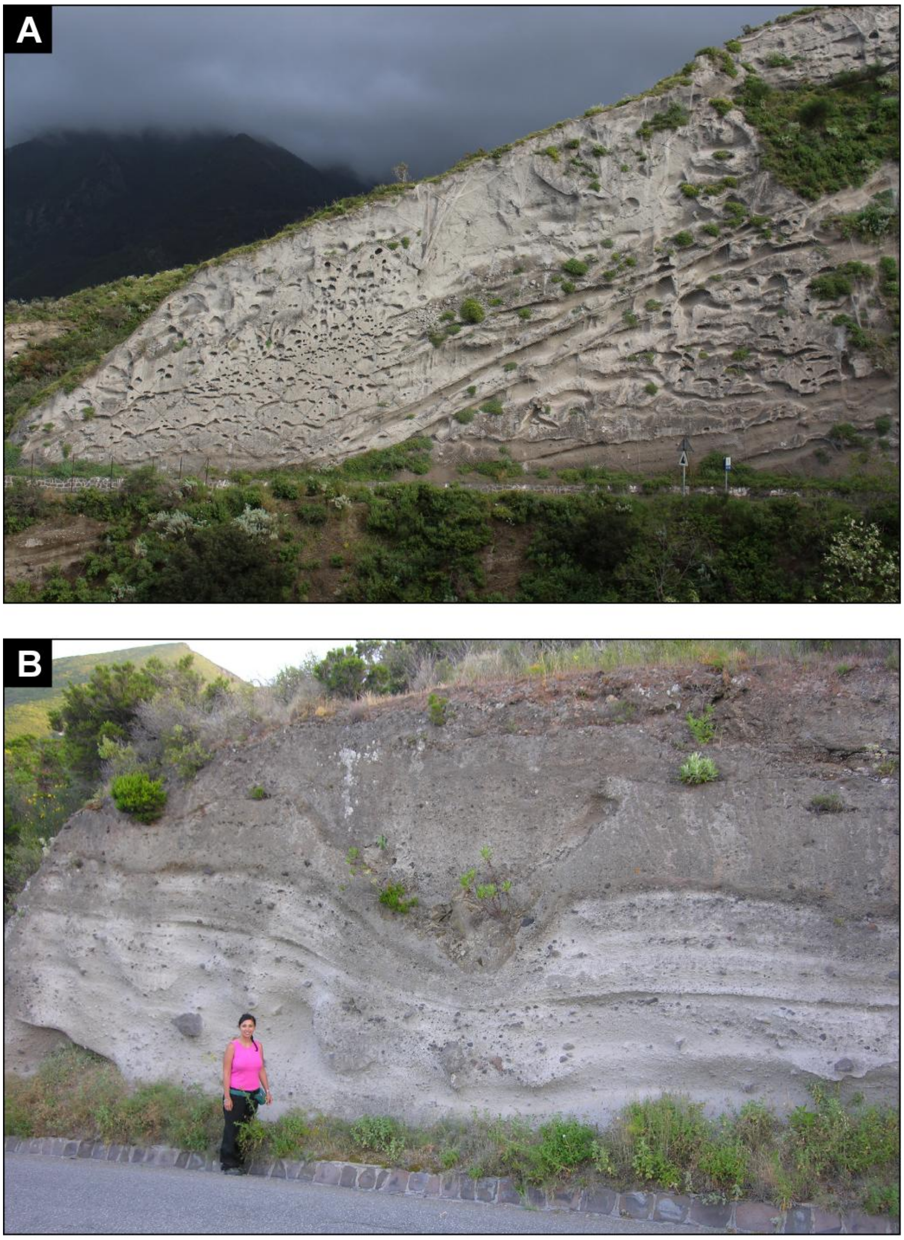

Fig. 9. Outcrop photographs of the Upper Pollara Tuffs on Salina, along the Malfa-Pollara road (A) and near to the Semaforo di Pollara locality (B).

4.3.4. Filicudi

The BT deposits discontinuously crop out across the entire island of Filicudi, invariably above the late MIS 5 marine deposits (Fig. 10A). The LBT and IBT macro-units are best distinguished by the interbedded Ischia Tephra, whilst no other major tephra makers are recognized. No chemical compositions of the UBT have been currently recognized. The Monte Montagnola Tuffs are interlayered within the IBT, whereas the f2 and f3 tephra layers, and the Case dello Zucco Grande Tuffs are embedded within the IBT. At the base of the LBT in the western sector of Filicudi there is an horizon of rounded pumice with a typical Campanian glass composition (f1 tephra), which is not discussed here. Other tephra layers were recognized by Morche (1988) interbedded within the BT succession in an outcrop at Vallechiesa, which is unfortunately currently no more available. In particular, Morche (1988) signalled the occurrence of dispersed glass shards with the distinctive trachyte-phonolite composition of the Y5 marine tephra layer embedded within the IBT. Note that the Y5 tephra layer is the distal equivalent of the 40 ky Campanian Ignimbrite from the Phlegrean Fields (Keller et al. 1978; Pyle et al. 2006; De Vivo et al. 2001), and is a major chronostratigraphic marker in the entire Mediterranean.

The local tephra units on Filicudi that have stratigraphic relationships with the BT are hereafter described in stratigraphic order.

4.3.4.1. Monte Montagnola Tuffs (64±18 ky)

This is the pyroclastic deposit relative to the Vulcanian/Strombolian explosive eruption that preceded the emission of the Monte Montagnola lava dome, in the central-western sector of Filicudi (Monte Montagnola Formation, mo_1 and mo_2 members; Lucchi et al., 2013e). The Monte Montagnola Tuffs have a maximum thickness of 20 metres and consist of thick fallout beds of pumice lapilli and bombs interlayered with some layers of PDC deposits of planar to cross-laminated lapilli-tuffs and tuffs (Fig. 10B). Juveniles are represented by light grey to dark-grey pumice, mildly to highly vesicular, together with banded pumice and several bread-crust bombs. Heterolithological lava lithic fragments are particularly abundant in the near-vent areas. Pumice have a wr HKCA andesite composition, and contain phenocrysts of plagioclase, clinopyroxene, orthopyroxene, and magnetite. Peculiarly, they are characterized by scarce amphibole phenocrysts, which are instead abundant in the overlying lava dome (Bilharz 2000; Sgattoni, 2008).

The Monte Montagnola lava dome is dated to 64±18 ky (K/Ar; Leocat, 2011), which is also adopted as an age constraint for the underlying tuffs. Accordingly, the Monte

Montagnola products are found interlayered within the IBT, as clearly demonstrated by the occurrence of the Ischia Tephra in a very representative outcrop on the summit of the lava dome. An older age of 101±4 ky for the Monte Montagnola lava dome (K/Ar; De Rosa et al., 2003b) is considered not reliable based on these chronostratigraphic relationships. Tephra layers linked to the Monte Montagnola activity are currently not known in the IBT outcrops distant from the source area.

4.3.4.2. f_2 tephra layer

This is a thick (up to 40 cm) bed of fallout pumice lapilli gradually passing upwards to massive fine lapilli and ash that is exposed in the outcrops of Siccagni (Fig. 10C) and Filicudi Porto. Pumice are light grey to grey, and dense to moderately vesicular. This pumice bed is interlayered within the lower portion of the IBT (in a stratigraphic position slightly higher than the Ischia Tephra). Morche (1988) reports the occurrence of tephra layers with similar lithological features below the (40 ky) Y5 stratigraphic marker. This constrains the time-stratigraphic interval of deposition of the f_2 tephra layer to 56-40 ky.

4.3.4.3. f_3 tephra layer

This thick (up to 45 cm) bed of fallout pumice lapilli is currently recognized in the outcrop of Filicudi Porto (corresponding to the f_5 tephra layer of Lucchi et al., 2013). Pumice are whitish to light grey, moderately vesicular, and they show a wr CA andesite composition (Lucchi et al., 2013e) with phenocrysts of plagioclase, clino- and orthopyroxene, amphibole, titanite and olivine. This pumice bed is interlayered within the upper portion of the IBT. In particular, it was signalled in a stratigraphic position slightly higher than the Y5 occurrence in the Vallechiesa outcrop by Morche (1988). Accordingly, the f_3 tephra layer would be younger than 40 ky.

4.3.4.4. Case dello Zucco Grande tuffs

This a 4 m thick pyroclastic succession exposed with very limited areal dispersal in the central-eastern sector of Filicudi, and linked with the activity of an isolated vent. It consists mostly of PDC deposits of massive to planar laminated tuffs (Fig. 10D), in places showing intense hydrothermal alteration. Grey, poorly vesicular pumice are diffused, together with abundant lava lithics. Pumice have a (wr) CA to HKCA andesite composition (Lucchi et al., 2013e).

The Case dello Zucco Grande tuffs are currently undated. They are generically interbedded within the IBT (younger than 56 ky), but there are no stratigraphic relationships with the other tephra layers recognized in distant outcrops.

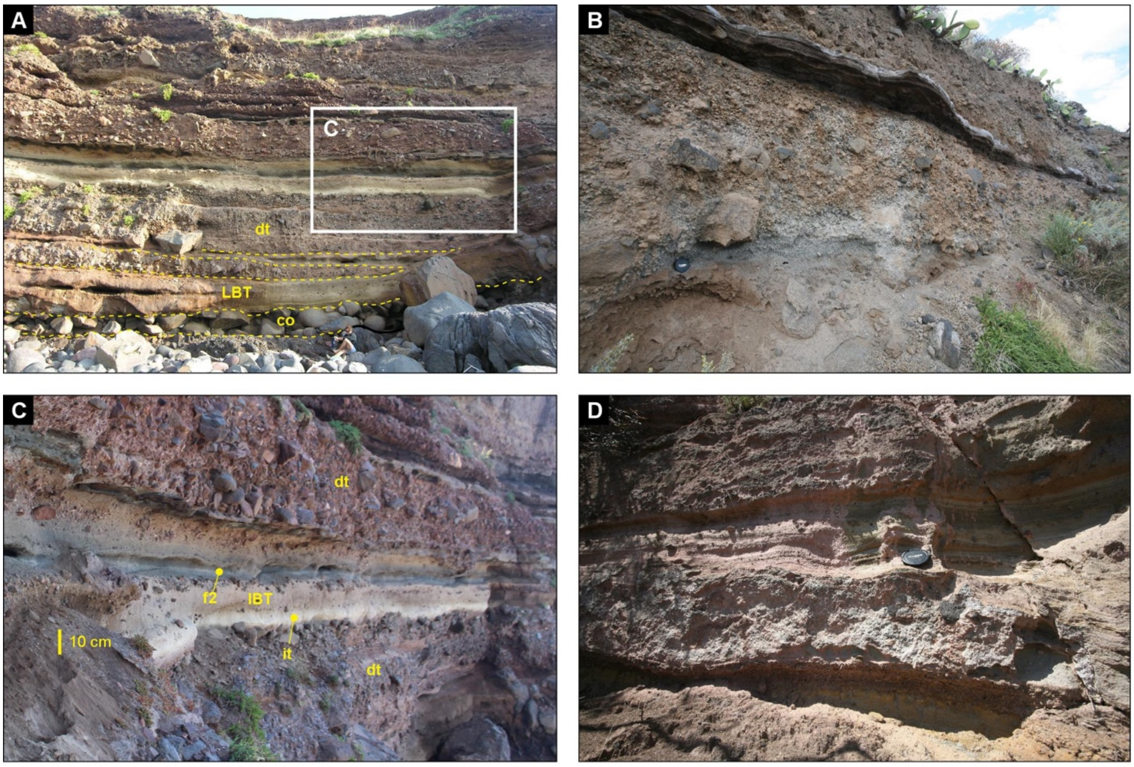

Fig. 10. Outcrop photographs of the major tephra units interlayered within the BT on Filicudi (in stratigraphic order). A) Natural stratigraphic section exposed along the coastal cliff of Siccagni, west Filicudi, showing the Lower Brown Tuffs (LBT) that rest above marine conglomerate deposits (co) referred to the late MIS 5. The Lower Brown Tuffs are interlayered with distinct horizons of paleo-detrital deposits (dt). B) Monte Montagnola pyroclastic deposits along the road to Pecorini a Mare, south Filicudi. C) Detailed view of Figure 10A showing the Ischia Tephra (it) interlayered between paleo-detrital deposits (dt) and a depositional unit of the Intermediate Brown Tuffs (IBT), and the f2 tephra layer located stratigraphically slightly higher. D) Case dello Zucco Grande tuffs exposed near to their type locality, central-east Filicudi.

4.3.5. Panarea

The BT deposits are widely present along the slopes of the island of Panarea (and Basiluzzo), resting above the late MIS 5 marine deposits and the Petrazza Tuffs from Stromboli. The LBT/IBT and IBT/IBT-upper subdivisions can be made due to the occurrence of the Ischia Tephra and Monte Guardia marker beds, whilst the typical chemical compositions of the UBT are recognized in the upper portion of the succession (Meschiari et al., 2020). The GPT are interbedded in the lower portion of the LBT (Fig. 11A), whilst the Vallone del Gabellotto tephra layer is discontinuoly recognized in the upper portion of the UBT. Moreover, the local p_1 pumice layer and Drauto pumice are recognized embedded within the LBT and UBT, respectively.

The local tephra units on Panarea that have stratigraphic relationships with the BT (in addition to the major pumice layers listed above) are hereafter described in stratigraphic order.

4.3.5.1. p_1 pumice

This fallout layer (10 cm thick) of pumice lapilli ($Ø_{average}$ = 2–2.5 cm) is recognized in the stratigraphic profile of Drauto. Pumice have a (glass) composition of shoshonites to latites (Morche, 1988). The p_1 layer is interlayered within the basal portion of the LBT, between the 70–67 ka Grey Porri Tuffs and the 56 ka Ischia Tephra. It is more likely related to an explosive eruption from a proximal source located in the area of the minor islets of Panarea, as consistent with the coarse grain size and the similar shoshonite composition of lava rocks and volcanic xenoliths (Calanchi et al. 2002; Lucchi et al., 2007; 2013c). However, the precise position of the eruptive vent of the p_1 pumice is still uncertain.

4.3.5.2. Drauto pumice

This is a massive layer (10-25 cm thick) composed of two fallout beds of moderately vesicular, light grey pumiceous lapilli (Ømax = 1.5-3 cm) (Fig. 11B) that is exposed in a number of stratigraphic profiles of the islands of Panarea and Basiluzzo (Drauto Formation; Lucchi et al, 2013c). Pumice have a wr latite to trachyte composition and HKCA to SHO affinity, with a distinctive content of biotite and amphibole phenocrysts (Lucchi et al., 2013c). This pumice layer is currently undated, but it is interlayered within the UBT between the Monte Guardia (27-26 ky) and Vallone del Gabellotto (8.7-8.4 ky) marker beds. Its provenance is still uncertain, but an origin from an eruptive vent(s) through a Strombolian eruption in the area of the minor islets seems probable in the light of a sharp east–west decrease of grain size (from pumice diameter of 3 cm on Basiluzzo to 1.5 cm on Panarea) and thickness (from c. 25 cm on Basiluzzo to 10 cm on Panarea) (Lucchi et al., 2013c). An origin from the area of the minor islets would be also supported by the similar chemical composition and mineralogic content of the Drauto pumice and some volcanic products of the Lisca Bianca and Bottaro islets (Calanchi et al., 2002).

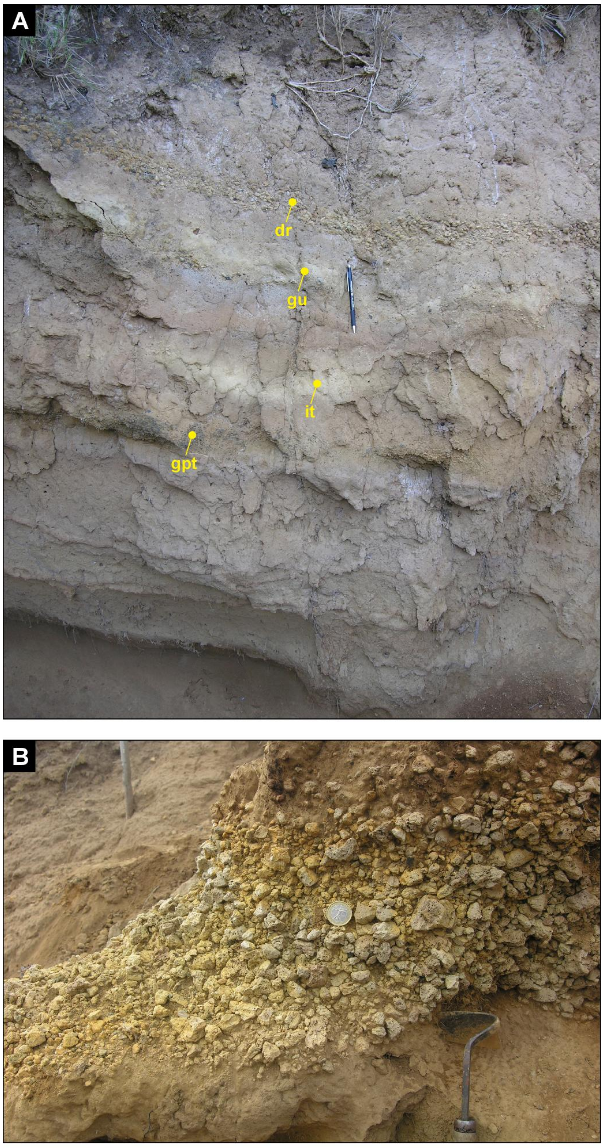

Fig. 11. Outcrop photographs of the major tephra units interlayered within the BT on Panarea (in stratigraphic order). A) Natural stratigraphic section of the BT exposed near to the summit of Panarea, Castello di Salvamento, showing the interlayered Grey Porri Tuffs (gpt), Ischia Tephra (it), Monte Guardia pumice (gu) and Drauto pumice (dr). B) Close view of the Drauto pumice layer at Basiluzzo.

References

Albert, P.G., Tomlinson, E.L., Smith, V.C., Di Roberto, A., Todman, A., Rosi, M., Marani, M., Muller, W., Menzies, M.A., 2012. Marine-continental tephra correlations: volcanic glass geochemistry from the Marsili Basin and the Aeolian Islands, Southern Tyrrhenian Sea, Italy. J. Volcanol. Geotherm. Res. 229-230, 74-94.

Albert, P.G., Tomlinson, E.L., Smith, V.C., Di Traglia, F., Pistolesi, M., Morris, A., Donato, P., De Rosa, R., Sulpizio, R., Keller, J., Rosi, M., Menzies M., 2017. Glass geochemistry of pyroclastic deposits from the Aeolian Islands in the last 50 ka: a proximal database for tephrochronology. J. Volcanol. Geotherm. Res. 336, 81-107.

Allen, J.R.M., Brandt, U., Brauer, A., Hubberten, H.-W., Huntley, B., Keller, J., Kraml, M., Mackensen, A., Mingram, J., Negendank, J.F.W., Nowaczyk, N.R., Oberh.ansli, H., Watts, W.A., Wulf, S., Zolitschka, B., 1999. Rapid environmental changes in southern Europe during the last glacial period. Nature 400, 740–743.

Arias, C., Bigazzi, G., Bonadonna, F. P., Cipollini, M., Hadler, J. C., Lattes, C.M. G., Radi, G., 1986. Fission-track dating in archaeology: a useful application. In: Parrini, P. (ed.) Scientific Methodologies Applied to Works of Art. Proceedings of the Symposium, Florence, Italy, 2–5 May 1984. Montedison, Progetto Cultura, Milano, 151–159.

Arrighi, S., Rosi, M., Tanguy, J.-C. & Courtillot, V. 2004. Recent eruptive history of Stromboli (Aeolian Islands, Italy) determined from high-accuracy archeomagnetic dating. Geophys. Res. Lett. 31, L19603.

Arrighi, S., Tanguy, J., Rosi, M., 2006. Eruptions of the last 2200 years at Vulcano and Vulcanello (AeolianIslands, Italy) dated by highaccuracy archeomagnetism. Phys. Earth Planet. Inter., 159, 225–233.

Bergeat, A., 1899. Die Äolischen Inseln (Stromboli, Panaria, Salina, Lipari, Vulcano, Filicudi und Alicudi), Abh. Math. Phys. Kl. Kgl. Bayer. Akad. Wiss., vol. 20 I. Abt., München, 274.

Bernabo`-Brea, L., 1978. Lipari, i vulcani, l'inferno e San Bartolo. In: Le Isole Eolie dal tardo antico ai Normanni. Archivio Storico Siracusano, Nuova Serie, 5, 25–89.

Bertagnini, A., Di Roberto, A., Pompilio, M., 2011. Paroxysmal activity at Stromboli: lessons from the past. Bull. Volcanol. 73, 1229–1243.

Bescoby, D., Barclay, J., Andrews, J. 2008. Saints and Sinners: a tephrochronology for Late Antique landscape change in Epirus from the eruptive history of Lipari, Aeolian Islands. J. Archaeol. Sci. 35, 2574–2579.

Bigazzi, G., Bonadonna, F.P., 1973. Fission track dating of the obsidian of Lipari Island (Italy). Nature, 242, 322–323.

Bigazzi, G., Coltelli, M., Norelli, P., 2003. Nuove eta` delle ossidiane di Lipari determinate con il metodo delle tracce di fissione. GeoItalia, 4th Forum FIST, Bellaria, 16–18 September, Abstract Volume, 444–446.

Bilharz, B., 2000. Vulkanologische Entwicklung und zeitliche Stellung des Montagnola-Domes auf Filicudi, Aolische Inseln. Diploma thesis, University of Freiburg, Germany.

Branney, M.J., Kokelaar, P., 2002. Pyroclastic Density Currents and the Sedimentation of Ignimbrites. Geol. Soc. Lond. Mem. 27

Calanchi, N., De Rosa, R., Mazzuoli, R., Ricci Lucchi, F., Rossi, P.L., Santacroce, R., 1987. L'attivita` del centro di Pollara (Salina, Isole Eolie). Bollettino GNV, 187–213.

Calanchi, N., De Rosa, R., Mazzuoli, R., Rossi, P.L., Santacroce, R., Ventura, G., 1993. Silicic magma entering a basaltic magma chamber: eruptive dynamics and magma mixing – an example from Salina (Aeolian Islands, southern Tyrrhenian Sea). Bull. Volcanol. 55, 504–522.

Calanchi, N., Tranne, C.A., Lucchini, F., Rossi, P.L., Villa, I.M. 1999. Explanatory notes to the geological map (1:10 000) of Panarea and Basiluzzo Islands, Aeolian Arc, Italy. Acta Vulcanologica 11, 223–243.

Calanchi, N., Peccerillo, A. et al. 2002. Petrology and geochemistry of volcanic rocks from the island of Panarea: implications for mantle evolution beneath the Aeolian island arc (southern Tyrrhenian sea). J. Volcanol. Geoth. Res. 115, 367–395.

Calvari, S., Branca, S. et al. 2011. Reconstruction of the eruptive activity on the NE sector of Stromboli volcano: timing of flank eruptions since 15 ka. Bull. Volcanol. 73, 101–112.

Capaldi, G., Civetta, L., Gillot, P.-Y. 1985. Geochronology of Plio-Pleistocene volcanic rocks from southern Italy. Rend. Soc. It. Mineral. Petrol. 40, 25–44.

Caron, B., Siani, G., Sulpizio, R., Zanchetta, G., Paterne, M., Santacroce, R., Tema, E., Zanella, E., 2012. Late Pleistocene to Holocene tephrostratigraphic record from the Northern Ionian Sea. Mar. Geol. 311-314, 41-51.

Chough, S.K., Sohn, Y.K., 1990. Depositional mechanics and sequences of base surges, Songaksan tuff ring, Cheju Island, Korea. Sedimentology 37, 1115–1135.

Cicchino, A., Zanella, E., De Astis, G., Lanza, R., Lucchi, F., Tranne, C.A., Airoldi, G., Mana S., 2011. Rock magnetism and compositional investigation of Brown Tuffs deposits at Lipari and Vulcano (Aeolian Islands – Italy) J. Volcanol. Geotherm. Res. 208, 23-28.

Clift, P., Blusztajn, J., 1999. The trace-element characteristics of Aegean and Aeolian volcanics arc marine tephra. J. Volcanol. Geotherm. Res. 92, 321–374.

Colella, A., Hiscott, R.N., 1997. Pyroclastic surges of the Pleistocene Monte Guardia sequence (Lipari Island, Italy): depositional processes. Sedimentology 44, 47–66.

Condomines, M., Allegre, C.J 1980. Age and magmatic evolution of Stromboli volcano from $^{230}Th/^{238}U$ disequilibrium data. Nature 288, 354–357.

Cortese, M., Frazzetta, G., La Volpe, L., 1986. Volcanic history of Lipari (Aeolian islands, Italy) during the last 10 000 years. J. Volcanol. Geoth. Res. 27, 117–133.

Crisci, G.M., De Rosa, R., Lanzafame, G., Mazzuoli, R., Sheridan, M.F., Zuffa, G.G., 1981. Monte Guardia Sequence: a Late-Pleistocene Eruptive Cycle on Lipari (Italy). Bull. Volcanol. 44, 241-255.

Crisci, G.M., Delibrias, G., De Rosa, R., Mazzuoli, R., Sheridan, M.F., 1983. Age and petrology of the Late-Pleistocene Brown Tuffs on Lipari, Italy. Bull. Volcanol 46, 381-391.

Crisci, G.M., De Rosa, R., Esperanca, S., Mazzuoli, R., Sonnino, M., 1991. Temporal evolution of a three component system: the island of Lipari (Aeolian Arc, southern Italy). Bull. Volcanol. 53, 207-221.

De Astis, G., Frazzetta, G., La Volpe, L., 1989. I depositi di riempimento della caldera del Piano ed i depositi della Lentia. Bollettino GNV 2, 763–778.

De Astis, G., Dellino, P., De Rosa, R., La Volpe, L., 1997a. Eruptive emplacement mechanism of fine grained pyroclastic deposits widespread on Vulcano Island. Bull. Volcanol. 59, 87-102.

De Astis, G., La Volpe, L., Peccerillo, A., Civetta, L., 1997b. Volcanological and petrological evolution of Vulcano Island (Aeolian Arc, southern Tyrrhenian Sea). J. Geophys. Res. 102, 8021–8050.

De Astis, G., Ventura, G., Vilardo, G. 2003. Geodynamic significance of the Aeolian volcanism (Southern Tyrrhenian Sea, Italy) in light of structural, seismological and geochemical data. Tectonics 22, 1040–1057.

De Astis, G., Lucchi, F., Tranne, C. A. 2006. The Aeolian volcanic district: volcanism and magmatism. Acta Vulcanologica 18, 79–104.

De Astis, G., Lucchi, F., Dellino, P., La Volpe, L., Tranne, C.A., Frezzotti, M.L., Peccerillo, A., 2013. Geology, volcanic history and petrology of Vulcano (central Aeolian archipelago). Geol. Soc. Lond. Mem. 37, pp. 281–348.

De Rita, D., Dolfi, D., Cimarelli, C., 2008. Occurrence of Somma- Vesuvio fine ashes in the tephrostratigraphic record of Panarea, Aeolian Islands. J. Volcanol. Geotherm. Res. 177, 197–207.

De Rosa, R., Frazzetta, G., La Volpe, L., Mazzuoli, R., 1988. The Spiaggia Lunga scoriae deposits: an example of fissural type eruption at Vulcano, Aeolian Islands, Italy. Rend. Soc. It. Mineral. Petrol. 43, 1059–1068.

De Rosa, R., Donato, P., Gioncada, A., Masetti, M., Santacroce, R. 2003a. The Monte Guardia eruption (Lipari, Aeolian Islands): an example of a reversely zoned magma mixing sequence. Bull. Volcanol. 65, 530–543.

De Rosa, R., Guillou, H., Mazzuoli, R., Ventura, G., 2003b. New unspiked K-Ar ages of volcanic rocks of the central and western sector of the Aeolian Islands: reconstruction of the volcanic stages. J. Volcanol. Geoth. Res. 120, 161–178.

De Rosa, R., Donato, P., Scarciglia, F., 2016. On the origin and post-depositional history of widespread massive ash deposits: the case of Intermediate Brown Tuffs (IBT) of Lipari (Aeolian Islands, Italy). J. Volcanol. Geotherm. Res. 327, 135-151.

Di Roberto, A., Rosi, M., Bertagnini, A., Marani, M.P., Gamberi, F., Del Principe, A., 2008. Deep water gravity core from the Marsili Basin (Tyrrhenian Sea) records Pleistocene-Holocenic explosive events and instabilities of the Aeolian Island Archipelago, (Italy). J. Volcanol. Geotherm. Res. 177 (1), 133-144.

Di Traglia, F., Pistolesi, M., Rosi, M., Bonadonna, C., Fusillo, R., Roverato, M., 2013. Growth and erosion: the volcanic geology and morphological evolution of La Fossa (Island of Vulcano, Southern Italy) in the last 1000 years. Geomorphology 194, 94–107

Dellino, P., Nuccio, M., Privitera, E. & Sbrana, A. (eds) Progetto Vulcano: Risultati dell’attivita` di ricerca 1993–1995. CNR – Gruppo Nazionale per la Vulcanologia, Felici Editore, Pisa, 214–237.

Dellino, P., and L. La Volpe, 1997. Stratigrafia, dinamiche eruttive e deposizio-nali, scenario eruttivo e valutazioni di pericolosita` a La Fossa di Vulcano,C.N.R. Gruppo Nazionale per la Vulcanologia, volume speciale Vulcano,pp. 207 – 213, Felici Editore, Pisa.

Dellino, P., De Astis, G., La Volpe, L.,Mele, D., Sulpizio, R., 2011. Quantitative hazard assessment of phreatomagmatic eruptions at Vulcano (Aeolian Islands, Southern Italy), as obtained by combining stratigraphy, event statistics and physical modelling. J. Volcanol. Geotherm. Res. 201, 264-384.

De Vivo, B., Rolandi, G., Gans, P.B., Calvert, A., Bohrson, W.A., Spera, F.J., Belkin, H.E., 2001. New constraints on the pyroclastic eruptive history of the Campanian Volcanic Plain (Italy). Mineral. Petrol. 73, 47–65.

Dolfi, D., de Rita, D., Cimarelli, C., Mollo, S., Soligo, M., Fabbri, M.. 2007. Dome growth rates, eruption frequency and assessment of volcanic hazard: Insights from new U/Th dating of the Panarea and Basiluzzo dome lavas and pyroclastics, Aeolian Islands, Italy. Quat. Int. 162/163, 182–194.

Donato, P., Behrens, H., De Rosa, R., Holtz, F., Parat, F., 2006. Crystallization conditions in the Upper Pollara magma chamber, Salina Island, Southern Tyrrhenian Sea. Mineral. Petrol. 86, 89–108.

Fisher, R.V., 1966. Rocks composed of volcanic fragments. Earth-Sci. Rev. 1, 287–298.

Fisher, R. V., Schmincke, H.-U., 1984. Pyroclastic Rocks. Springer Verlag, Berlin, Heidelberg, pp. 472.

Foeken, J.P.T., Stuart, F.M., Francalanci, L., 2009. Dating Holocene lavas on Stromboli, Italy using cosmogenic He. Quat. Geochron. 4, 517–524.

Fontugne, M., Paterne, M., Calvert, S.E., Murat, A., Guichard, F., Arnold, M., 1989. Adriatic deep water formation during the Holocene: implication for the reoxygenation of the deep Eastern Mediterranean sea. Paleoceanography 4, 199–206.

Forni, F., Lucchi, F., Peccerillo, A., Tranne, C.A., Rossi, P.L., Frezzotti, M.L., 2013. Stratigraphic and geological evolution of the Lipari volcanic complex (central Aeolian archipelago). Geol. Soc. Lond. Mem. 37, 213-279.

Francalanci, L., Lucchi, F., Keller, J., De Astis, G., Tranne, C.A., 2013. Eruptive, volcano-tectonic and magmatic history of the Stromboli volcano (north-eastern Aeolian archipelago). Geol. Soc. Lond. Mem. 37, 395–469.

Frazzetta, G., Gillot, P.-Y., La Volpe, L., Sheridan, M.F., 1984. Volcanic hazards of Fossa di vulcano: data from the last 6,000 years. Bull. Volcanol. 4, 105–124.

Frazzetta, G., Gillot, P.Y., La Volpe, L., 1985. The Island of Vulcano. IAVCEI Scientific Association Excursion Guidebook, 125–140.

Gabbianelli, G., Gillot, P.-Y., Lanzafame, G., Ligi, M., Postpisch, D., Rossi, P.L., 1986. Controllo strutturale nell'evoluzione vulcanica di Panarea (Isole Eolie). CNR (Consiglio Nazionale delle Ricerche), IIV Open File Report, 4/86, 27.

Gabbianelli, G., Gillot, P.-Y., Lanzafame, G., Romagnoli, C., Rossi, P.L., 1990. Tectonic and volcanic evolution of Panarea (Aeolian Islands, Italy). Mar. Geol. 92, 313–326.

Gillot, P.Y., 1984. Datations par la methode du potassium-argon des roches volcaniques re´centes (Pleistocene et Holocene). Contribution a` l'e´tude chronostratigraphique et magmatique des provinces volcaniques de Campanie, des iles Eoliennes, de pantelleria (italie du Sud) et de la Re´union (Oce´an Indien). Unpublished PhD thesis, University of Paris-Sud.

Gillot, P.Y., 1987. Histoire volcanique des Iles Eoliennes: arc insulaire ou complexe oroge´nique anulaire? Documents et Travaux, IGAL (Institut Ge´ologique Albert-de-Lapparent), Paris, 11, 35–42.

Gillot, P.-Y., Villari, L., 1980. K/Ar geochronological data on the Aeolian Arc Volcanism. A preliminary report. CNR-IIV, Open file report 145

Gillot, P.-Y., Keller, J., 1993. Radiochronological dating of Stromboli. Acta Vulcanologica 3, 69–77.

Gioncada, A., Mazzuoli, R., Bisson, M., Pareschi, M.T., 2003. Petrology of volcanic products younger than 42 ka on the Lipari-Vulcano complex (Aeolian Islands, Italy): an example of volcanism controlled by tectonics. J. Volcanol. Geotherm. Res. 122, 191–220.

Gioncada, A., Mazzuoli, R., Milton, A.J., 2005. Magma mixing at Lipari (Aeolian Islands, Italy): insights from textural and compositional features of phenocrysts. J. Volcanol. Geoth. Res. 145, 97–118.

Gurioli, L., Zanella, E., Gioncada, A., Sbrana, A., 2012. The historic magmatic–hydrothermal eruption of the Breccia di Commenda, Vulcano, Italy. Bull. Volcanol. 74, 1235–1274.

Hornig-Kjarsgaard, I., Keller, J., Koberski, U., Stadlbauer, E., Francalanci, L., Lenhart, R., 1993. Geology, stratigraphy and volcanological evolution of the island of Stromboli, Aeolian arc, Italy. Acta Vulcanologica, 3, 21–68.

Iadanza, M., 2011. Hugeburg di Heidenheim: Vita Willibaldi episcopi Eichstetensis. Firenze, Edizioni del Galluzzo, pp. CCCXIV-114. ISBN 978-88-8450-414-2.

Ingram, R.L., 1954. Terminology for the thickness of stratification and parting units in sedimentary rocks. Geol. Soc. Am. Bull. 65, 937–938.

Insinga, D.D., Tamburrino, S., Lirer, F., Vezzoli, L., Barra, M., De Lange, G.J., Tiepolo, M., Vallefuoco, M., Mazzola, S., Sprovieri, M., 2014. Tephrochronology of the astronomically- tuned KC01B deep-sea core, Ionian Sea: insights into the explosive activity of the Central Mediteranean area during the last 200 ka. Quat. Sci. Rev. 85, 63–84.

Keller, J., 1967. Alter und Abfolge der vulkanischen Ereignisse auf den Aolischen Inseln. Berichte der Naturforschenden Gesellschaft zu Freiburg i. Br., 57, 33–67.

Keller, J., 1970. Datierung der Obsidiane und Bimstuffe von Lipari. Neues Jahrbuch fu¨r Geologie und Pala¨ontologie, Monatshefte, Jahrgang, 1970, 90–101.

Keller, J., 1980a. The island of Salina. Rend. Soc. It. Mineral. Petrol. 36, 489-524.

Keller, J., 1980b. The Island of Vulcano. Rend. Soc. It. Mineral. Petrol. 36, 369-414.

Keller, J., 1981. Quaternary tephrochronology in the Mediterranean region. In: Self, S. & Sparks, S. R. J. (eds) Tephra Studies. NATO, Advanced Study Institutes Series C 75, D. Reidel Publishing Company, Dordrecht, 227-244.

Keller, J., 2002. Lipari's fiery past: dating the medieval pumice eruption of Monte Pelato. International Conference 'The fire between air and water', UNESCO-Regione Siciliana, Lipari, 29 September–2 October, Abstracts.

Keller, J., Ryan, W.B.F., Ninkovich, D., Altherr, R., 1978. Explosive volcanic activity in the Mediterranean over the past 200 000 yr as recorded in deep-sea sediments. Geol. Soc. Am. Bull. 89, 591–604.

Kraml, M., 1997. Laser 40Ar/39Ar-Datierungen an distalen marinen Tephren des jungquarta¨ren mediterranean Vulkanismus (Ionisches Meer, Meteor-Fahrt 25/4). PhD Thesis, Albert-Ludwigs-Universita¨t Freiburg, Germany.

Kraml, M., Keller, J., Henjes-Kunst, F., 1997. Dating of Upper Quaternary deep-sea sediments from the Ionian Sea (Eastern Mediterranean) with laser 40Ar/39Ar analyses on prominent tephra layers. EUG 9 (European Union of Geosciences), Strasbourg (France) 23–27 March 1997, Terra Nova 9, Abstract Supplement 1, 406.

Lanzafame, G., Rossi, P.L., 1984. Evidenze di attivita´ tettonica recente a Panarea (Eolie): implicazioni vulcanologiche. Geol. Romana 23, 131–139.

Laj, C., Rais, A., Surmont, J., Gillot, P.Y., Guillou, H., Kissel, C., Zanella, E., 1997. Changes of the geomagnetic field vector obtained from lava sequences on the island of Vulcano (Aeolian Islands, Sicily). Phys. Earth Planet. Int. 99, 161–177.

Le Bas, M.J., Le Maitre, R.W., Streckeisen, A., Zanettin, B., 1986. A chemical classification of volcanic rocks on the total alkali - silica diagram. J. Petrol. 27, 745–750.

Leocat, E., 2011. Histoire eruptive des volcans du secteur occidental des Iles Eoliennes (Sud de la Mer Tyrrhenienne, Italie). PhD thesis, University of Paris 11, Orsay.

Losito, R., 1989. Stratigrafia, caratteri deposizionali e aree sorgente dei tufi bruni delle Isole Eolie. Unpublished PhD Thesis, University of Bari, Italy.

Lucchi, F., 2000. Evoluzione dell’attivita` vulcanica e mobilita` verticale delle Isole Eolie nel tardo Quaternario.Unpublished PhD thesis, University of Bologna, Italy, 186 p.

Lucchi, F., 2009. Late-Quaternary marine terrace deposits as tools for wide-scale correlation of unconformity-bounded units in the volcanic Aeolian archipelago (southern Italy). Sed. Geol. 216, 158–178.

Lucchi, F., 2013. Stratigraphic methodology for the geological mapping of volcanic areas: insights from the Aeolian archipelago (southern Italy). Geol. Soc. Lond. Mem. 37, 37–55.

Lucchi, F., Tranne, C.A. et al. 2004a. Stratigraphic constraints to date late-Quaternary ancient shorelines and to evaluate vertical movements at Lipari (Aeolian Islands). Quat. Int. 115/116, 105–115.

Lucchi, F., Tranne, C.A., Calanchi, N., Rossi, P.L. 2004b. Late Quaternary fossil shorelines in the Aeolian Islands (Southern Tyrrhenian Sea): evaluation of long-term vertical displacements. In: Antonioli, F. & Monaco, C. (eds) Contribution from the Study of Ancient Shorelines to Understanding the Recent Vertical Motions. Field trip across the Messina Straits. Quaternaria Nova, VIII, Casa Editrice Il Calamo, Roma, 115–137.

Lucchi, F., Tranne, C.A., Calanchi, N., Keller, J., Rossi, P.L., 2007. The stratigraphic role of marine deposits in the geological evolution of the Panarea volcano (Aeolian Islands, Italy). J. Geol. Soc. Lond. 164/5, 983–996.

Lucchi, F., Tranne, C.A., De Astis, G., Keller, J., Losito, R., Morche, W., 2008. Stratigraphy and significance of Brown Tuffs on the Aeolian Islands (southern Italy). J. Volcanol. Geotherm. Res. 177, 49-70.

Lucchi, F., Tranne, C.A., Rossi, P.L., 2010. Stratigraphic approach to geological mapping of the late-Quaternary volcanic island of Lipari (Aeolian archipelago, Southern Italy). In: Groppelli, G. & Viereck-Goette, L. (eds) Stratigraphy and Geology of Volcanic Areas. Geol. Soc. Am. Spec. Pap. 464, 1–32.

Lucchi, F., Gertisser, R., Keller, J., Forni, F., De Astis, G., Tranne, C.A., 2013a. Eruptive history and magmatic evolution of the island of Salina (central Aeolian archipelago). Geol. Soc. Lond. Mem. 37, 155-211.

Lucchi, F., Keller, J., Tranne, C., 2013b. Regional stratigraphic correlations across the Aeolian archipelago (southern Italy). Geol. Soc. Lond. Mem. 37, 55-81.

Lucchi, F., Tranne, C.A., Peccerillo, A., Keller, J., Rossi, P.L., 2013c. Geological history of the Panarea volcanic group (eastern Aeolian archipelago). Geol. Soc. Lond. Mem. 37, 349-393.

Lucchi, F., Peccerillo, A., Tranne, C. A., Rossi, P. L., Frezzotti, M. L. & Donati, C. 2013d. Volcanism, calderas, and magmas of the Alicudi composite volcano (western Aeolian archipelago). Geol. Soc. Lond. Mem. 37, 83–111.

Lucchi, F., Santo, A.P., Tranne, C.A., Peccerillo, A., Keller, J., 2013e. Volcanism, magmatism, volcano-tectonics and sea-level fluctuations in the geological history of Filicudi (western Aeolian archipelago). Geol. Soc. Lond. Mem. 37, 113-153.

Mahood, G.A., Hildreth, W., 1986. Geology of the peralkaline volcano at Pantelleria, Strait of Sicily. Bull. Volcanol. 48, 143–172.

Manetti, P., Pasquaré, G., Tibaldi, A., Tsegaye, A., 1988. Geology of the island of Filicudi (Aeolian arc). Bollettino G.N.V. IV, 368-382.

Manetti, P., Pasquaré, G., Tibaldi, A., Tsegaye, A., 1995. A new geo-vulcanological map of Filicudi island (Aeolian arc, Italy). Acta Vulcanologica 7, 1-5.

Manni, M., Coltelli, M., Martinelli, M.C., 2019. Volcanic events that have marked the anthropic history of the Aeolian Islands. Ann. Geophys. 62/1, VO08. doi: 10.4401/ag-7716

Matthews, I.P., Trincardi, F., Lowe, J.J., Bourne, A.J., MacLeod, A., Abbott, P.M., Anderson, N., Asioli, A., Blockley, S.P.E., Lane, C.S., Oh, Y.A., Satow, C.S., Staff, R.A.,Wulf, S., 2015. Developing a robust tephrochronological framework for Late Quaternary marine records in the Southern Adriatic Sea: new data from core station SA03-11. Quat. Sci. Rev. 118, 84–104.

Meschiari, S., Albert, P.G., Lucchi, F., Sulpizio, R., Smith, V.C., Kearne, R., Tranne, C.A., 2020. Frequent activity on Vulcano (Italy) spanning the last 80 ky: New insights from the chemo-stratigraphy of the Brown Tuffs. J. Volcanol. Geotherm. Res. 406.

Morche, W., 1988. Tephrochronologie der Aolischen Inseln. (Unpublished PhD Thesis). Albert-Ludwigs-Universitat Freiburg, Germany.

Narcisi, B., 2002. Tephrostratigraphy of the Late Quaternary lacustrine sediments of Lago di Pergusa (central Sicily). Boll. Soc. Geol. Ital. 12 (2), 211–219.

Negri, A., Capotondi, L., Keller, J., 1999. Calcareous nannofossils, planktonic foraminifera and oxygen isotopes in the Late Quaternary Sapropels of the Ionian Sea. Mar. Geol. 157, 89–103.

Nicotra, E., Minniti, M., Donato, P., De Rosa, R., 2020. Insights into the eruptive dynamics of small caldera-forming eruptions: the case study of the welded scoriae of Vulcano (Aeolian Islands, Italy). Front. Earth Sci. 8, 223.

Paterne, M., Guichard, F., Labeyrie, J., Gillot, P.Y., Duplessy, J.C., 1986. Tyrrhenian Sea tephrochronology of the oxygen isotope record for the past 60,000 years. Mar. Geol. 72, 259–285.

Paterne, M., Guichard, F., Labeyrie, J., 1988. Explosive activity of the South Italian volcanoes during the past 80 000 years as determined by marine tephrochronology. J. Volcanol. Geotherm. Res. 34, 153–172.

Peccerillo, A., Taylor, S.R., 1976. Geochemistry of Eocene calc-alkaline rocks from Kastamonu area, Northern Turkey. Contrib. Mineral. Petrol. 58, 63–81.

Peccerillo, A., De Astis, G., Faraone, D., Forni, F., Frezzotti, M.L., 2013. Compositional variations of magmas in the Aeolian arc: implications for petrogenesis and geodynamics. Geol. Soc. Lond. Mem. 37 489–508.

Pichler, H., 1980. The Island of Lipari. Rendiconti della Società Italiana di Mineral. Petrol. 36, 415-440.

Pyle, D.M., Ricketts, G.D., Margari, V., van Andela, T.H., Sinitsyn, A.A., Praslov, N.D., Lisitsyn, S., 2006. Wide dispersal and deposition of distal tephra during the Pleistocene 'Campanian Ignimbrite/Y5' eruption, Italy. Quat. Sci. Rev. 25, 2713–2728.

Quidelleur, X., Gillot, P.-Y., Filoche, G., Lefèvre, J.-C., 2005. Fast geochemical changes and rapid lava accumulation at Stromboli Island (Italy) inferred from K-Ar dating and paleomagnetic variations recorded at 60 and 40 ka. J. Volcanol. Geotherm. Res. 141, 177–193.

Reimer, P., Austin, W., Bard, E., Bayliss, A., Blackwell, P., Bronk Ramsey, C., Butzin, M., Cheng, H., Edwards, R., Friedrich, M., Grootes, P., Guilderson, T., Hajdas, I., Heaton, T., Hogg, A., Hughen, K., Kromer, B., Manning, S., Muscheler, R., Palmer, J., Pearson, C., van der Plicht, J., Reimer, R., Richards, D., Scott, E., Southon, J., Turney, C., Wacker, L., Adolphi, F., Büntgen, U., Capano, M., Fahrni, S., Fogtmann-Schulz, A., Friedrich, R., Köhler, P., Kudsk, S., Miyake, F., Olsen, J., Reinig, F., Sakamoto, M., Sookdeo, A., & Talamo, S. (2020). The IntCal20 Northern Hemisphere radiocarbon age calibration curve (0–55 cal kBP). Radiocarbon, 62.

Ricci Lucchi, F., Calanchi, N., Lanzafame, G., Rossi, P.L., 1988. Plant-rich pyroclastic deposits of Monte S.Angelo, Lipari (Aeolian Island). Rend. Soc. It. Mineral. Petrol. 43, 1227–1251.

Romagnoli, C., Casalbore, D. et al. 2013. Bathy-morphological setting of the Aeolian Islands. Geol. Soc. Lond. Mem. 37, 27–36.

Romano, R., 1973. Le isole di Panarea e Basiluzzo. Contributo alla conoscenza geo-vulcanologica e magmatologica delle Isole Eolie. Rivista Mineraria Siciliana, 24, 3–40.

Rosi, M., Bertagnini, A., Landi, P., 2000. Onset of the persistent activity at Stromboli volcano (Italy). Bull. Volcanol. 62, 294–300.

Rosi, M., Di Traglia, F., Pistolesi, M., Esposti Ongaro, T., de' Michieli Vitturi, M., 2018. Dynamics of shallow hydrothermal eruptions: new insights from Vulcano's Breccia di Commenda eruption. Bull. Volcanol. 80: 83. doi.org/10.1007/s00445-018-1252-y

Santo, A., Chen, Y., Clark, A. H., Farrar, E., Tsegaye, A., 1995. $^{40}Ar/^{39}Ar$ ages of the Filicudi volcanics: implications for volcanological history of the Aeolian Arc, Italy. Acta Vulcanologica 7, 13–18.

Schmid, R., 1981. Descriptive nomenclature and classification of pyroclastic deposits and fragments: recommendations of the IUGS Subcommission on the Systematics of igneous rocks. Geology 9, 41–43.

Sgattoni, G., 2008. Analisi stratigrafica e petrochimica dei depositi dell'attivita` vulcanica recente (,100 ka) dell'isola di Filicudi (Isole Eolie). Unpublished Degree thesis, University of Bologna.

Siani, G., Sulpizio, R., Paterne, M., Sbrana, A., 2004. Tephrostratigraphy study for the last 18,000 14C years in a deep-sea sediment sequence for the South Adriatic. Quat. Sci. Rev. 23, 2485-2500.

Soligo, M., De Astis, G., Delitala,M C., La Volpe, L., Taddeucci, A., Tuccimei, P., 2000. Uranium-series disequilibria in the products from Vulcano Island (Sicily, Italy): isotopic chronology and magmatological implications. Acta Vulcanologica 12, 49–59.

Speranza, F., Pompilio, M., Sagnotti, L., 2004. Paleomagnetism of spatter lavas from Stromboli volcano (Aeolian Islands, Italy): implications for the age of paroxysmal eruptions. Geophys. Res. Lett. 31, L02607.

Speranza, F., Pompilio, M., D'Ajello Caracciolo, F., Sagnotti, L., 2008. Holocene eruptive history of the Stromboli volcano: constraints from paleomagnetic dating. J. Geophys. Res. 113, B09101.

Sulpizio, R., De Rosa, R., Donato, P., 2008. The influence of variable topography on the depositional behaviour of pyroclastic density currents: the examples of the Upper Pollara eruption (The island of Salina, southern Italy). J. Volcanol. Geotherm. Res. 175, 367–385.

Sulpizio, R., Dellino, P., 2008. Sedimentology, depositional mechanisms and pulsating behaviour of pyroclastic density currents. Developments in Volcanology 10, 57–96.

Sulpizio, R., Forni, F., Lucchi, F., Massaro, S., Tranne, C., 2016. Unravelling the effusive-explosive transitions and the construction of a volcanic cone from geological data: the example of Monte dei Porri, Salina Island (Italy). J. Volcanol. Geoth. Res. 327, 1-22.

Tamburrino, S., Insinga, D.D., Pelosi, N., Kissel, C., Laj, C., Capotondi, L., Sprovieri, M., 2016. Tephrochronology of a ~ 70 ka-long marine record in the Marsili basin (southern Tyrrhenian Sea) J. Volcanol. Geotherm. Res. 327, 23–39.

Tomlinson, E.L., Albert, P.G.Wulf, S., Brown, R., Smith, V.C., Keller, J., Orsi, G., Bourne, A.J., Menzies, M.A., 2014. Age and geochemistry of tephra layers from Ischia, Italy: constraints from proximal-distal correlations with Lago Grande di Monticchio. J. Volcanol. Geotherm. Res. 287, 22-39.

Ventura, G., 2013. Kinematics of the Aeolian volcanism (Southern Tyrrhenian Sea) from geophysical and geological data. Geol. Soc. Lond. Mem. 37, 3–11.

Voltaggio, M., Branca, M., Tuccimei, P., Tecce, F., 1995. Leaching procedure used in dating young potassic volcanic rocks by the $^{226}Ra/^{230}Th$ method. Earth Planet. Sci. Lett. 136, 123–131.

Zanchetta, G., Sulpizio, R., Roberts, N., Cioni, R., Eastwood, W., Siani, G., Caron, B., Paterne, M., Santacroce, R., 2011. Tephrostratigraphy, chronology and climatic events of the Mediterranean basin during the Holocene: An overview. Holocene 21, 33-52.

Wagner, G.A., Storzer, C., Keller, J., 1976. Spaltspurendatierung quarta¨rer Gesteinsgla¨ser aus dem Mittelmeerraum. Neues Jahrbuch fu¨r Mineralogie Monatshefte 2, 84–94.

Watts, W.A., Allen, J.R.M., Huntley, B., 1996. Vegetation history and palaeoclimate of the last glacial period at Lago Grande di Monticchio, southern Italy. Quat. Sci. Rev. 15, 133–153.

Wulf, S., Kraml, M., Brauer, A., Keller, J. & Negendank, J. F. W. 2004. Tephrochronology of the 100 ka lacustrine sediment record of Lago Grande di Monticchio (southern Italy). Quat. Int. 122, 7-30.

Chapter 2

Frequent activity on Vulcano (Italy) spanning the last 80 ky: New insights from the chemo-stratigraphy of the Brown Tuffs

Meschiari S.[1], Albert P.G. [2,3], Lucchi F.[1], Sulpizio R.[4], Smith V.C. [3], Kearney R. [3], Tranne C.A. [1].

[1] Dipartimento di Scienze Biologiche Geologiche ed Ambientali, Piazza di Porta San Donato, 1, 40126, Bologna, Italy

[2] Department of Geography, Swansea University, Singleton Park, Swansea SA2 8PP, UK

[3] Research Laboratory for Archaeology and the History of Art (RLAHA), University of Oxford, Dyson Perrins Building, South Parks Road, Oxford OX1 3QY, UK

[4] Dipartimento di Scienze della Terra e Geoambientali, via Orabona 4, 70125, Bari, Italy

Published in Journal of Volcanology and Geothermal Research 406, November 2020, Article 107079.

Journal of Volcanology and Geothermal Research 406 (2020) 107079

Contents lists available at ScienceDirect

Journal of Volcanology and Geothermal Research

journal homepage: www.elsevier.com/locate/jvolgeores

Frequent activity on Vulcano (Italy) spanning the last 80 ky: New insights from the chemo-stratigraphy of the Brown Tuffs

S. Meschiari [a,*], P.G. Albert [b,c], F. Lucchi [a], R. Sulpizio [d], V.C. Smith [c], R. Kearney [c], C.A. Tranne [a]

[a] Dipartimento di Scienze Biologiche, Geologiche e Ambientali, Università di Bologna, Piazza Porta S. Donato 1, 40126 Bologna, Italy
[b] Department of Geography, Swansea University, Singleton Park, Swansea SA2 8PP, UK
[c] Research Laboratory for Archaeology and the History of Art (RLAHA), University of Oxford, Dyson Perrins Building, South Parks Road, Oxford OX1 3QY, UK
[d] Dipartimento di Scienze della Terra e Geoambientali, Universitá di Bari, via Orabona 4, 70125 Bari, Italy

ARTICLE INFO

Article history:
Received 17 June 2020
Received in revised form 2 October 2020
Accepted 4 October 2020
Available online 8 October 2020

ABSTRACT

The Brown Tuffs (BT) are widespread reddish-brown to grey, ash-rich pyroclastic deposits recognized in the stratigraphic sequences of the Aeolian Islands and Capo Millazzo peninsula (Sicily) that span the last 80 ky. They have very homogeneous lithological, textural and sedimentological features which make it difficult to reliably correlate units on the islands to proximal units in the source areas. Here we carefully re-interpret the stratigraphic profiles of the BT on Vulcano and Lipari where the deposits are thickest and present the most complete succession. The investigation is based on a large dataset of major and minor element geochemistry of juvenile glass components for the majority of the recognized BT depositional units, whilst also providing new radiocarbon ages. The distinctive chemical groupings observed within the glass analyses, both temporally and spatially, allow us to fingerprint the three main stratigraphically defined macro-units in which the BT succession can be subdivided using prominent tephra marker beds, the Ischia Tephra (Monte Epomeo Green Tuff; 56 ky) and Monte Guardia pyroclastics from Lipari (herein radiocarbon dated to 27–26 ky). The Lower (80–56 ky; LBT), Intermediate (56–27 ky; IBT) and Upper BT (here dated at 24–6 ky; UBT) macro-units display K-series volcanic glasses ranging from basaltic trachy-andesites, through trachy-andesites, to more evolved trachytes, all consistent with an origin on Vulcano. The UBT are clearly distinguished from the lower macro units by their higher-SiO_2 trachy-andesite to trachytic glasses, which extend to noticeably lower TiO_2, CaO and MgO contents. These features make it possible to re-define the geochemical-evolutionary boundary between IBT and UBT as corresponding to the 24 ky Spiaggia Lunga scoria bed on Vulcano, which is stratigraphically higher (and younger) than the previous boundary marker (Monte Guardia). The glass compositions of the LBT, IBT and UBT are used to: (1) assess links to known proximal eruption units outcropping on Vulcano; (2) validate medial-distal BT occurrences across the Aeolian archipelago (Salina, Filicudi and Panarea) and on Capo Millazzo; (3) confirm that the BT are responsible for distal volcanic ash layers preserved in Central Mediterranean marine sedimentary archives. Interestingly, the glass compositions of the UBT are very similar to those of the Punte Nere unit, the earliest pyroclastic products erupted from the currently active La Fossa cone on Vulcano, indicating the corresponding magmatic system has likely erupted similar melts and products over the last 24 ky and thus extending its life cycle. Such information is crucial for evaluating the long-term eruption scenarios underpinning hazard assessment of the La Fossa caldera magmatic system.

1. Introduction

Explosive volcanic eruptions can disperse volcanic ash (< 2 mm) to distances of tens to thousands of kilometers from their source and cause multi-hazard impacts on human activities and the environment, potentially forcing climate variability (e.g. (Biass et al., 2014; Bonasia et al., 2012; Dingwell and Rutgersson, 2014; Le Pennec et al., 2012; Martin et al., 2009; Scaini et al., 2014; Sulpizio et al., 2012; Sulpizio et al., 2014)). Pyroclastic deposits from these eruptions are crucial for reconstructing the volcanic history of a volcano, and understanding the frequency and the impact of its eruptive activity on the surroundings. Where the age of the corresponding eruptions is known, ash (tephra) deposits preserved in distal sedimentary records are also powerful chronological and stratigraphic markers in complex stratigraphic sequences across the region (Machida, 1999; Narcisi, 1996; Shane, 2000), and can be used in age-depth models and to synchronize disparate sedimentary palaeoclimate archives (Paterne et al., 1986; Paterne et al., 1988; Sulpizio et al., 2010; Zanchetta et al., 2011).

* Corresponding author.
E-mail address: sara.meschiari4@unibo.it (S. Meschiari).

https://doi.org/10.1016/j.jvolgeores.2020.107079
0377-0273/

In this paper, the Brown Tuffs (BT) are presented as a case study of widespread, ash-rich pyroclastic deposits. These deposits have metric thickness and are recognized in the stratigraphic sequences of most of the Aeolian Islands and on the Capo Milazzo peninsula in northern Sicily. Their interpretation as paleosols, reworked or primary pyroclastic products, as well as their vent locations, areal distribution, chronology and eruptive processes has been long debated (Bergeat, 1899; Crisci et al., 1981; Crisci et al., 1983; Crisci et al., 1991; Keller, 1967; Keller, 1980a; Keller, 1980b; Manetti et al., 1988; Manetti et al., 1995; Morche, 1988; Pichler, 1980; Gioncada et al., 2003). Stratigraphic and tephrochronological studies have suggested that the BT are composed of a number of depositional units emplaced in the 80–5 ky time interval by pyroclastic density currents (PDCs) and fallout from hydromagmatic explosive activity of a vent (or multiple vents) located within the La Fossa caldera on Vulcano (Lucchi et al., 2008; Lucchi et al., 2013b). This is also confirmed by measurements of the anisotropy of magnetic susceptibility of BT sequences on Lipari and Vulcano (Cicchino et al., 2011) and combined textural, petrological methods on glass fragments of the BT on Lipari (De Rosa et al., 2016). However, in most outcrops the BT show a very homogeneous lithology, whilst sedimentological characteristics and textural features, reflecting similar eruptive mechanisms, transport and deposition. Moreover, preliminary glass compositional data indicate the deposits have a dominant, albeit variable, trachy-andesite glass composition and overall K-series affinity, extending towards subsidiary rhyolitic components (Lucchi et al., 2008). As a consequence, the individual BT depositional units generally cannot be distinguished from each other, and only separated by localized erosive surfaces or reworked horizons and the interbedding of other volcanic units or exotic tephra deposits erupted from within, and outside the Aeolian Islands. A stratigraphic subdivision into three macro-units, namely the Lower (LBT), Intermediate (IBT) and Upper BT (UBT), has been proposed by Lucchi et al., (2008); Lucchi et al., (2013b) based on the interbedding of two stratigraphic markers correlated on a regional scale, namely the i) Ischia Tephra (56 ky) from Campania and the ii) Monte Guardia pyroclastics (27–24 ky) from Lipari. Unfortunately, the discontinuous recognition of these marker-beds makes difficult to correlate directly the BT macro-units between one island and another, and throughout the Aeolian archipelago. The similar componentry and mineral assemblage, and the rather small glass compositional variability reported so far (De Rosa et al., 2016; Lucchi et al., 2008; Lucchi et al., 2013b), has meant that the LBT, IBT and UBT could not be clearly discriminated or correlated across the islands in the absence of the interlayered marker-beds. Because of all these difficulties and fragmentary stratigraphic, petrological and geochemical data, a largely accepted framework of the distribution and depositional area of these units and their correlation to proximal counterparts on the island of Vulcano (for the LBT and IBT) has been missing.

Here we present a large dataset of major and minor element geochemistry of juvenile glass components for most BT depositional units using grain-specific micro-analytical techniques. The BT were sampled from exposed stratigraphic profiles on the islands of Vulcano and Lipari, which are fully representative of the complete stratigraphic succession, together with selected stratigraphic sections from the islands of Salina, Filicudi, Panarea and on Capo Milazzo peninsula (northern Sicily) for strengthening the correlations. A revised stratigraphic analysis of the BT exposures has taken advantage of the local successions, new radiocarbon ages and correlation of marker beds to the regional tephrostratigraphy (e.g. (Albert et al., 2017)). This provides an improved reconstruction of the stratigraphy, dispersal and chronology of the different BT depositional units. The LBT, IBT and UBT macro-units are geochemically fingerprinted in order to investigate the compositional variability both temporally and spatially, supporting inter-island and regional correlations. Previously the BT were largely overlooked as correlatives of volcanic ash recorded in distal land and deep-sea archives (Albert et al., 2012; Caron et al., 2012; Di Roberto et al., 2008; Insinga et al., 2014; Matthews et al., 2015; Paterne et al., 1986; Paterne et al., 1988; Siani et al., 2004; Tamburrino et al., 2016), mostly due to an inadequate characterization of their glass geochemistry. This contribution instead illustrates that the BT are potentially proximal (high-volume) equivalents of widespread ash dispersals, with the associated tephra layers being suitable to correlate volcanic and tectonic events across the whole Aeolian archipelago and southern Tyrrhenian Sea. Finally, the glass geochemical data of the LBT, IBT and UBT, combined with stratigraphic and lithological information, are also used to infer links to proximal units on Vulcano, providing insights into the eruptive and magmatic history and long-term hazard assessment in the La Fossa caldera magmatic system.

2. Study area

The Aeolian Islands (Alicudi, Filicudi, Salina, Lipari, Vulcano, Panarea and Stromboli; Fig. 1a), and the surrounding seamounts, are an active volcanic system in the southern Tyrrhenian Sea (Barberi et al., 1973; Beccaluva et al., 1985; Chiarabba et al., 2008; De Astis et al., 2003; Ventura, 2013). Subaerial volcanism developed from c. 270–240 ky to the present (Leocat, 2011; Lucchi et al., 2013b), through successive eruptive epochs subdivided by volcanic collapses or major quiescent (erosional) stages (De Astis et al., 2013; Forni et al., 2013; Francalanci et al., 2013; Lucchi et al., 2013a; Lucchi et al., 2013c; Lucchi et al., 2013d; Lucchi et al., 2013e), and the erupted melts range from basaltic andesites to rhyolites, covering a large spectrum of differing magmatic suites from calc-alkaline (CA), high-K calc-alkaline (HKCA), shoshonitic (SHO) and K-Series (KS) (Ellam et al., 1988; Francalanci et al., 1993; Peccerillo et al., 2013). Vulcano, which is the suggested source area of the Brown Tuffs (BT), is a complex volcanic system made up of various eruptive centres and two multi-stage calderas (Il Piano and La Fossa), and characterised by the active La Fossa cone (De Astis et al., 2013). The BT have been deposited during distinct time intervals over the last c. 80 ky (Lucchi et al., 2008; Lucchi et al., 2013b), and are interlayered with widespread fall deposits from major explosive eruptions of Lipari, Stromboli, Salina and Campania (Albert et al., 2017; Keller, 1981; Lucchi et al., 2013b).

3. Methods

3.1. Fieldwork

Stratigraphic analysis and sampling was conducted principally on the islands of Vulcano and Lipari, whilst also on Salina, Panarea, Filicudi and Capo Milazzo peninsula following the correlations between islands as defined by Lucchi et al., (2008); Lucchi et al., (2013b). Stratigraphic logging and lithostratigraphy focussed on identifying all the individual depositional units of the BT, and obtain a comprehensive set of samples of the tephra deposits. Following Lucchi, (2013), a “depositional unit” is generically referred to as the pyroclastic material deposited during an individual, relatively continuous eruptive event (PDC or fallout), and is delimited by features indicative of interruptions of deposition or energy variations (e.g. erosive surfaces, paleosols, reworked horizons, angular discordances, sharp grain-size variations, fine ash layers), or other volcanic units.

Once the stratigraphic correlations of the BT across the islands had been fixed, 65 ash deposits were sampled covering most of the BT depositional units that were stratigraphically recognized, together with several lapilli (12) and ash (19) samples from the interbedded tephra layers. We also sampled near-vent pyroclastic deposits on Vulcano which either represent potential proximal equivalents of the BT (Monte Molineddo 1–3 and Punte Nere formations; (De Astis et al., 2013)), and/or offer useful constraints on the known chemical signature of the volcano.

3.2. Laboratory analyses

Juvenile (glass) fragments from the selected samples were washed, dried and mounted in Streurs epoxy resin. Mounts were ground,

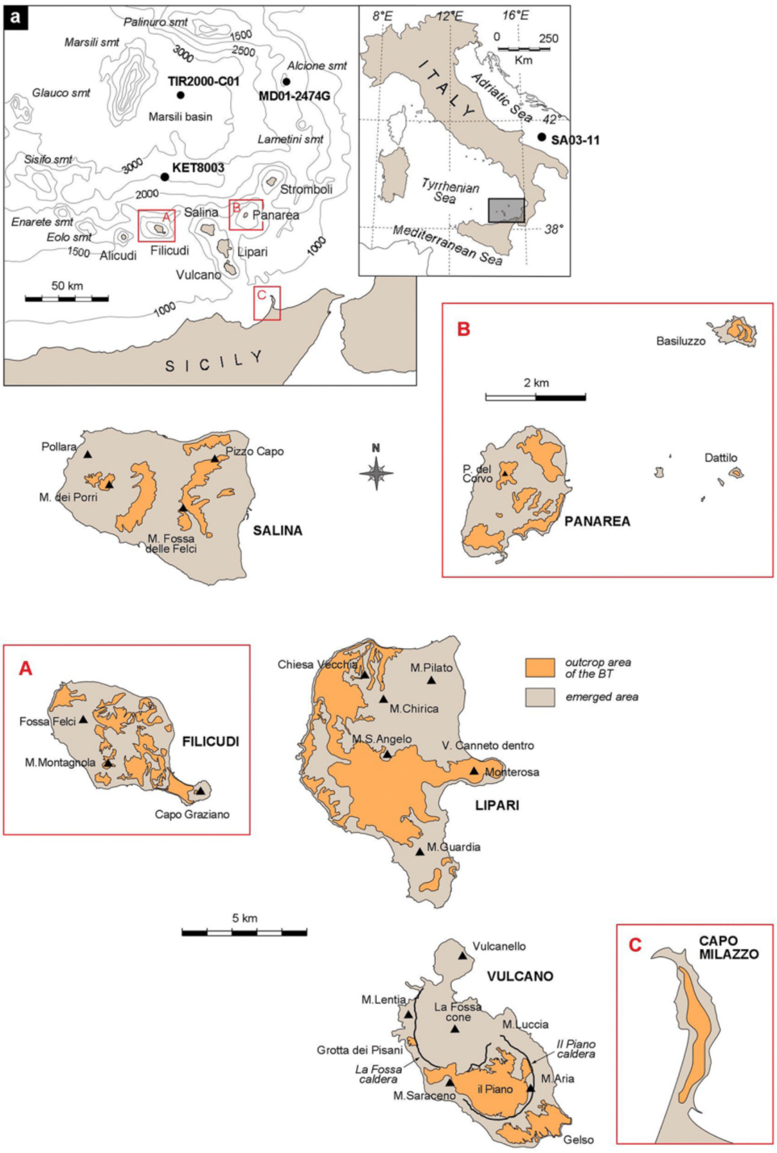

Fig. 1. Sketch maps of the islands of Vulcano, Lipari, Salina, Filicudi and Panarea (Aeolian archipelago) and the Capo Milazzo in northern Sicily showing the outcrop areas of the BT. The inset (a) shows the location of the Aeolian Islands and seamounts in the southern Tyrrhenian sea (depth contour lines in metres below sea level). Coordinates conform to the Gauss-Boaga System (IGM). The sites of marine cores TIR200-C01 (Albert et al., 2012), KET8003 (Paterne et al., 1988), MD01–2474G (Tamburrino et al., 2016) and SA03–11 (Matthews et al., 2015), that have BT units, are also outlined.

polished and carbon coated in preparation for chemical analysis. Major and minor element micron-beam volcanic glass data was determined using the wavelength-dispersive JEOL 8600 and the JEOL 8200 electron microprobes (WDS-EMP) at the Research Laboratory for Archaeology and the History of Art (RLAHA), University of Oxford. Details of the analytical operating conditions, monitoring of data accuracy and precision, and post-analysis data treatment are provided in Supplementary Material A.1. The full geochemical dataset, along with MPI-DING reference glasses (Jochum et al., 2006) run alongside the unknown samples are available in Supplementary Material B. Data presented in plots are normalised (e.g., water-free) and error bars represent reproducibility, calculated as 2 x standard deviation of replicate analysis of StHs6/80-G reference glass.

Charcoal fragments embedded within the BT deposits were collected for radiocarbon (^{14}C) dating to provide further age constraints. Charcoals were chemically pre-treated at the Oxford Radiocarbon Accelerator Unit (ORAU) using the acid- base-acid (ABA) methodology outlined by Brock et al., (2010). The ^{14}C analyses were subsequently performed using a 2.5 MV HVEE tandem Accelerator Mass Spectrometry (AMS) system at ORAU (Ramsey et al., 2004). These new radiocarbon ages, together with previously published BT radiocarbon ages (Crisci et al., 1981; Crisci et al., 1983; De Astis et al., 1997; Pichler, 1980), were then calibrated and modelled using the Bayesian statistical program of OxCal v4.4 (Bronk Ramsey, 2009), using the IntCal20 Northern Hemisphere calibration curve (Reimer et al., 2020).

4. Results

4.1. Overview of the stratigraphy and age of the Brown Tuffs (BT)

The BT are made up of reddish-brown to grey fine to coarse ash in weakly coherent to coherent depositional units, which comprise glass shards, minor crystals (with abundant clinopyroxene) and a negligible lithic content. They form thick massive successions (up to 15–25 m on Vulcano and Lipari) with considerable thickness variations due to the paleo-topography and erosion. In some exposures on Vulcano and southern Lipari there are internal grain size variations, color banding and plane-parallel to cross bedding stratification (De Astis et al., 1997; Lucchi et al., 2008). The stratigraphy of the BT has been reviewed through a careful investigation of the majority of the outcrops on the islands of Vulcano and Lipari (Fig. 1), where the BT obtain their maximum thickness, and where there are radiocarbon (^{14}C) age constraints. Outcrops on Salina, Filicudi, Panarea and Capo Milazzo (Fig. 1) were also studied to verify BT occurrences and extend the correlations established on Vulcano and Lipari. The outcrops of the BT on Capo Milazzo, originally described by Morche (1988), are now largely eroded and partially destroyed by anthropogenic activity. The BT outcropping on the islands of Alicudi and Stromboli are not considered here due to their poor stratigraphic and chronologic constraints (Francalanci et al., 2013; Lucchi et al., 2013d). The most important features of the Campanian and Aeolian tephra layers ultimately used to subdivide and correlate the BT are provided in Table 1, and the suite of radiocarbon ages adopted in the present work is provided in Table 2.

The most complete succession of the BT is reconstructed on the island of Lipari, furtherly detailing the stratigraphy previously proposed by Lucchi et al., (2008); Lucchi et al., (2013b) by identifying a few more interlayered tephra beds and localized erosional surfaces. The BT succession is distinguished into (at least) 16 depositional units (Fig. 2), superimposed on the three-fold subdivision into the Lower (LBT), Intermediate (IBT) and Upper BT (UBT) macro-units based on the interbedded Ischia Tephra and Monte Guardia pyroclastics from Lipari (see (Lucchi et al., 2013b) and references therein). The most important features of this succession are hereafter described, outlining correlations between the main outcrops on Lipari and Vulcano, and the other Aeolian Islands and the Capo Milazzo peninsula. Correlations with the island of Vulcano are described below in Section 4.1.1.

The LBT are constrained at the base by the late marine (oxygen) isotope stage (MIS) 5 conglomerate deposits (c. 80 ky) along the west coast of Lipari, as well as on Salina, Filicudi, Panarea and the Capo Milazzo peninsula. A lower chronological boundary is also provided by lapilli and ash correlated to the 77–75 ky Petrazza Tuffs from Stromboli found at the base of the LBT succession on Panarea and Capo Milazzo ((Lucchi et al., 2008) and references therein). The Grey Porri Tuffs (GPT) from Salina (70–67 ky; (Sulpizio et al., 2016) and references therein) are important for stratigraphic correlations in the lower portion of the LBT on Salina and Lipari, with distal occurrences on Panarea and Capo Milazzo.

The IBT are defined as above the Ischia Tephra, which is widely exposed on Lipari, Salina, Filicudi and Panarea. This marker bed is the distal equivalent of the Monte Epomeo Green Tuff of Ischia (Tomlinson

Table 1
Main characteristics of tephra layers and marker beds used for the subdivisions of BT depositional units and correlations (listed in stratigraphic order starting from the older one). Recognition area: Str = Stromboli, Pan = Panarea, Sal = Salina, Lip = Lipari, Vul = Vulcano, Fil = Filicudi, Ali = Alicudi; Mil = Capo Milazzo. Chemical composition of juvenile glass fragments (w.r = whole rock) is reported by referring to: [(1)] present work; [(2)] (Albert et al., 2017); [(3)] (De Astis et al., 2013): CA = calcalkaline, HKCA = high-k calcalkaline, SHO = shoshonite series; Bas = basalt, Bas-And = basaltic andesite, And = andesite, Dac = dacite, Rhy = rhyolite, Lat = latite, Sho = shoshonite, Tra = trachyte). Correlations with proximal stratigraphic units refer to: [(1)] (Lucchi et al., 2008); [(2)] (Forni et al., 2013); [(3)] (Lucchi et al., 2013a); [(4)] (De Astis et al., 2013). Age references: [(1)] (Morche, 1988); [(2)] (De Astis et al., 1989); [(3)] (Soligo et al., 2000); [(4)] (Siani et al., 2004); [(5)] (Leocat, 2011); [(6)] (Lucchi et al., 2013a; Lucchi et al., 2013b); [(7)] (Sulpizio et al., 2016); [(8)] (Giaccio et al., 2017); [(9)] present work.

Tephra	Marine Tephra	Lithology	Dispersal area	Chemistry (glass)	Source area	Proximal stratigraphic unit	Age (ky)
Grey Porri Tuff		Grey (to whitish) scoria and pumice lapilli and ash	Sal, Lip, Pan, Mil	CA Bas-And to Dac	Sal	Rocce di Barcone Fm. [(3)]	70–67 [(1,6,7)]
		Grey fine to coarse ashes, with abundant mm-sized cpx crystals and interlayered yellowish scoriaceous lapilli	Vul		Vul	M. Molineddo 1 [(4)]	
		Varicoloured ash, locally with beds of scoriaceous lapilli and isolated bombs	Vul		Vul	M. Molineddo 2 [(4)]	
Ischia Tephra	Y-7	White-yellowish ash	Str, Pan, Sal, Lip, Fil	Tra-Pho [(1)]	Ischia	Epomeo Green Tuff –Monte Sant'Angelo [(1)]	56.1 ± 1.0 [(8)]
		Black to yellowish scoriaceous lapilli and bombs and grey coarse to fine ashes with abundant mm-sized euhedral cpx crystals	Vul		Vul	M. Molineddo 3 [(4)]	
Punta di Perciato		Whitish pumice lapilli and ash	Lip	Rhy [(1,2)]	Lip	Punta di Perciato Fm., member pe_2 [(2)]	
Falcone		Whitish pumice lapilli and ash	Lip	Rhy [(1,2)]	Lip	Falcone Fm., member fa_1 [(2)]	43–40 [(5)]
lip1		Whitish ash	Lip	Rhy [(1)]	Lip		
Lower Pollara Tuff		Lapilli and ash of yellow pumice and black scoria	Sal, Lip	CA- to HKCA Bas-And to And	Sal	Punta Fontanelle Form. [(3)]	27.6–26.4 [(9)]
Monte Guardia		White and grey pumice (and obsidian) lapilli and ash	Lip, Vul, Sal, Pan	Rhy [(1,2)]	Lip	Monte Guardia Fm. [(2)]	27–26 [(9)]
Spiaggia Lunga		Red to black scoria lapilli and bombs	Vul	SHO Bas to Sho (w.r.) [(3)]	Vul	Spiaggia Lunga Fm. [(4)]	24 ± 5 [(3)]
Cugni di Molinello		Black scoria lapilli	Vul	Sho	Vul	Cugni di Molinello Fm. [(4)]	
lip2		Pumice and obsidian lapilli and ash	Lip	Rhy [(1)]	Lip		
Monte Saraceno		Red to black scoria lapilli	Vul	Sho (w.r.) [(3)]	Vulc	Monte Saraceno Fm., member sa_1 [(4)]	8.3 ± 1.6 [(2)]
Vallone Canneto dentro		Pumice and obsidian lapilli and ash	Lip	Rhy [(1)]	Lip	Vallone Canneto dentro Fm., member cd_1 [(2)]	
Vallone del Gabellotto	E-1	White pumice ash and lapilli	Lip, Pan, Vul, Str	Rhy [(1,2)]	Lip	Vallone del Gabellotto Fm. [(2)]	8.7–8.4 [(4)]
Punte Nere		Dark grey lapilli and ash	Lip	Tra-Pho [(1)]	Vul	Punte Nere Fm., member pn_1 [(4)]	5.3 + 2.2/−1.1 [(3)]

Table 2
Radiocarbon age determinations of charcoals sampled from within the BT succession and the paleosol overlying the UBT. (A) Radiocarbon age determinations presented here from between the Monte Guardia Tephra and the Vallone Cannetto Dentro on Lipari Island. Charcoal LIP14/17 was collected at Location 9 (Fig. 3) and LIP07/17 was collected at Location 8 (Fig. 3). Ages are calibrated using IntCal20 (Reimer et al., 2020) and OxCal v4.4. Calibrated age-distribution plots are provided in supplementary information A. (B) Radiocarbon ages from the literature recalibrated using IntCal20 (Un-modelled), while some of the age determinations have been incorporated into an Bayesian age-depth model which is used to provide new age constraints on the Monte Guardia and Lower Pollara eruption deposits used as chrono-stratigraphic markers in the Aeolian Islands. Detaiils of the Bayesian age model are reported in Supplementary Material A. * Age range represents 82.2% probability, with 8.7% probability range of 5325–5390 cal y BP.

Eruption Unit	Location	Sample ID	Material	Oxford Lab Code	^{14}C age	Error (68.2%)	$\delta^{13}C$	Cal y BP (95.4%; IntCal20) (Un-modelled)	Cal y BP (95.4%; IntCal20) Modelled Age	Reference
(A) This study										
IBT *Upper*	Lipari	LIP014/17	Charcoal	OxA-36,000	20,020	90	−24.83	23,830–24,240	23,830–24,260	This Study
IBT *Upper*	Lipari	LIP07/17	Charcoal	OxA-35,999	21,760	100	−24.73	25,845–26,310	25,830–26,295	This Study
(B) Re-calibrated published data + Bayesian Modelling										
–	Lipari	–	palaesol (bulk Sed)	–	4810	60	–	5445*–5610*	--	(Pichler, 1980)
UBT	Vulcano	–	Charcoal	–	7680	100	–	8305–8655	---	(De Astis et al., 1997)
UBT	Lipari	–	Charcoal	–	16,800	200	–	19,825–20,845	---	(Crisci et al., 1983)
IBT *Upper*	Lipari	–	Charcoal	–	20,500	200	–	24,155–25,200	24,240–25,240	(Crisci et al., 1983)
IBT *Upper*	Lipari	–	Charcoal	–	20,300	700	–	22,950–26,005	24,110–25,980	(Crisci et al., 1983)
Monte Guardia *(mg)*									25,920–27,025	This Study
IBT	Lipari	–	Charcoal	–	22,480	1100	–	24,570–29,500	26,125–27,295	(Crisci et al., 1983)
IBT	Lipari	–	Charcoal	–	22,600	300	–	26,100–27,460	26,300–27,275	(Crisci et al., 1981)
Lower Pollara Tuff *(lpt)*									26,425–27,585	This Study
IBT	Lipari	–	Charcoal	–	22,940	340	–	26,445–27,770	26,575–27,760	(Morche, 1988)
IBT	Lipari	–	Charcoal	–	23,500	900	–	26,085–29,850	26,495–28,100	(Crisci et al., 1983)

et al., 2014), and dated distally in Lake Fucino (Italy) at 56.1 ± 1.0 ky [2σ] (Giaccio et al., 2017). The IBT are best exposed in southern-central Lipari (Fig. 3A-B) where they are split into (at least) 6 depositional units by the local pumiceous successions of Punta di Perciato (undated) and Falcone (43–40 ky; (Forni et al., 2013) and references therein), the Lower Pollara Tuffs from Salina and a couple of other tephra layers (Fig. 2, Table 1). Particularly, the Lip1 tephra has a rhyolitic composition (cf. 4.2.2.1) and provides evidence of a previously unknown explosive eruption in the southern dome-field of Lipari.

The IBT and UBT macro-units are subdivided on Lipari (Fig. 3A-D) and across much of the archipelago by the Monte Guardia marker bed (Lucchi et al., 2008), until now dated to between 27 and 24 ky ((Albert et al., 2017; Lucchi et al., 2013b) and references therein). Here we provide new radiocarbon ages of charcoal remnants embedded within the BT above the Monte Guardia (Table 2), yielding calibrated (IntCal20) eruption ages of 25,845–26,310 cal y BP (95.4%; sample LIP07/17) and 23,830–24,240 cal y BP (95.4%; sample LIP14/17) for the host BT depositional unit. Here we incorporate these new ages, together with all the available and stratigraphically relevant BT ^{14}C ages from the literature (Table 2), into the Bayesian age-model developed by Albert et al., (2017) (Supplementary Material A.3) to provide a more precise age of between 25,920–27,025 cal y BP (95.4%) for the Monte Guardia eruption. The modelling also provides an age of 26,425–27,585 cal y BP (95.4%) for the Lower Pollara eruption (Salina).

The youngest UBT units, above the Monte Guardia marker-bed, are best exposed in the north-eastern sector of Lipari, where they are further subdivided into (at least) 4 distinct depositional units by local pyroclastic deposits (Fig. 2). Most of the UBT are found stratigraphically below the Vallone Canneto Dentro pyroclastic unit (currently undated) (Fig. 3D), with no occurrences between Vallone Canneto Dentro and the widespread Vallone del Gabellotto pyroclastic marker bed (8430–8730 cal y BP; (Albert et al., 2017; Siani et al., 2004)). The most recent UBT depositional unit is recognized between Vallone del Gabellotto and the Monte Pilato pyroclastic unit (dated to 776 CE; (Forni et al., 2013), and references therein) (Fig. 3E), and is capped by an irregularly thick reddish paleosol with a maximum age of 5445–5610 cal y BP based on previous ^{14}C age determinations ((Pichler, 1980); Table 2).

4.1.1. Stratigraphy and age of the BT on Vulcano

The BT deposits are recognized in different sectors of Vulcano, interlayered between various other local volcanic units at different stratigraphic levels (Fig. 2). They do not outcrop in the northern sector of the island (except to the south of M. Lentia) and within the La Fossa caldera owing to their burial by the most recent volcanic products related to the La Fossa and Vulcanello eruptive centres (younger than 5.5 ky).

The youngest UBT are best exposed in the central sector of Il Piano, beyond the south-eastern rim of the La Fossa caldera, and match stratigraphically and lithologically the so-called Piano Grotte dei Rossi tuffs ((Lucchi et al., 2008) and references therein). The UBT are subdivided by the widespread Cugni di Molinello scoria fallout layer that is the marker bed (currently undated) separating the lower and upper portions of the Piano Grotte dei Rossi tuffs ('Tufi di Grotte dei Rossi' in (De Astis et al., 1997)). As with the UBT, the source area of the Cugni di Molinello unit is interpreted as being within the La Fossa caldera (De Astis et al., 2013; Dellino et al., 2011). The UBT below Cugni di Molinello contain most of the deposit volume (Fig. 2), with a maximum thickness of 8–10 m along the border of La Fossa caldera, whilst the UBT above the marker bed are only 2–3 m thick and are further subdivided into (at least) 3 depositional units based on the interlayered Monte Saraceno unit (8.3 ky; (De Astis et al., 1989)) and the Vallone del Gabellotto tephra layer from Lipari (8.7–8.4 ky). Outside of the main depositional area of Il Piano, the UBT are recognized above the Monte Guardia in the areas of Gelso (south-east) and Monte Luccia (central-north Vulcano), and above the Spiaggia Lunga unit (24 ky; (Soligo et al., 2000)) along the western slopes of the island (Fig. 3F), cropping out very discontinuously due to erosion along steep and exposed slopes. The UBT are not recognized along the western rim of La Fossa caldera, stratigraphically above the intermediate Monte Lentia lava domes (15–13 ky). This suggests that most of the UBT were emplaced before 15–13 ky, likely corresponding to the part of UBT below the Cugni di Molinello marker bed. One of the youngest UBT depositional units has a calibrated radiocarbon age of 8305–8655 cal y BP (Table 2). At the top, the UBT are unconformably covered by the Grotta dei Palizzi 1 and 2 pyroclastic successions from the intermediate La Fossa cone (2.9–2.1 ky; (De Astis et al., 2013) and references therein) along the border of La Fossa caldera, whereas there are no clear stratigraphic contacts or field-based correlations with the Punte Nere pyroclastics (Fig. 2) that represent the oldest portion of La Fossa cone succession (5.5–3.8 ky; (De Astis et al., 2013) and references therein).

Delimiting the areal distribution of LBT and IBT on Vulcano is challenging, and their separation is made difficult by the absence of the Ischia Tephra marker bed. LBT-IBT deposits with a maximum thickness

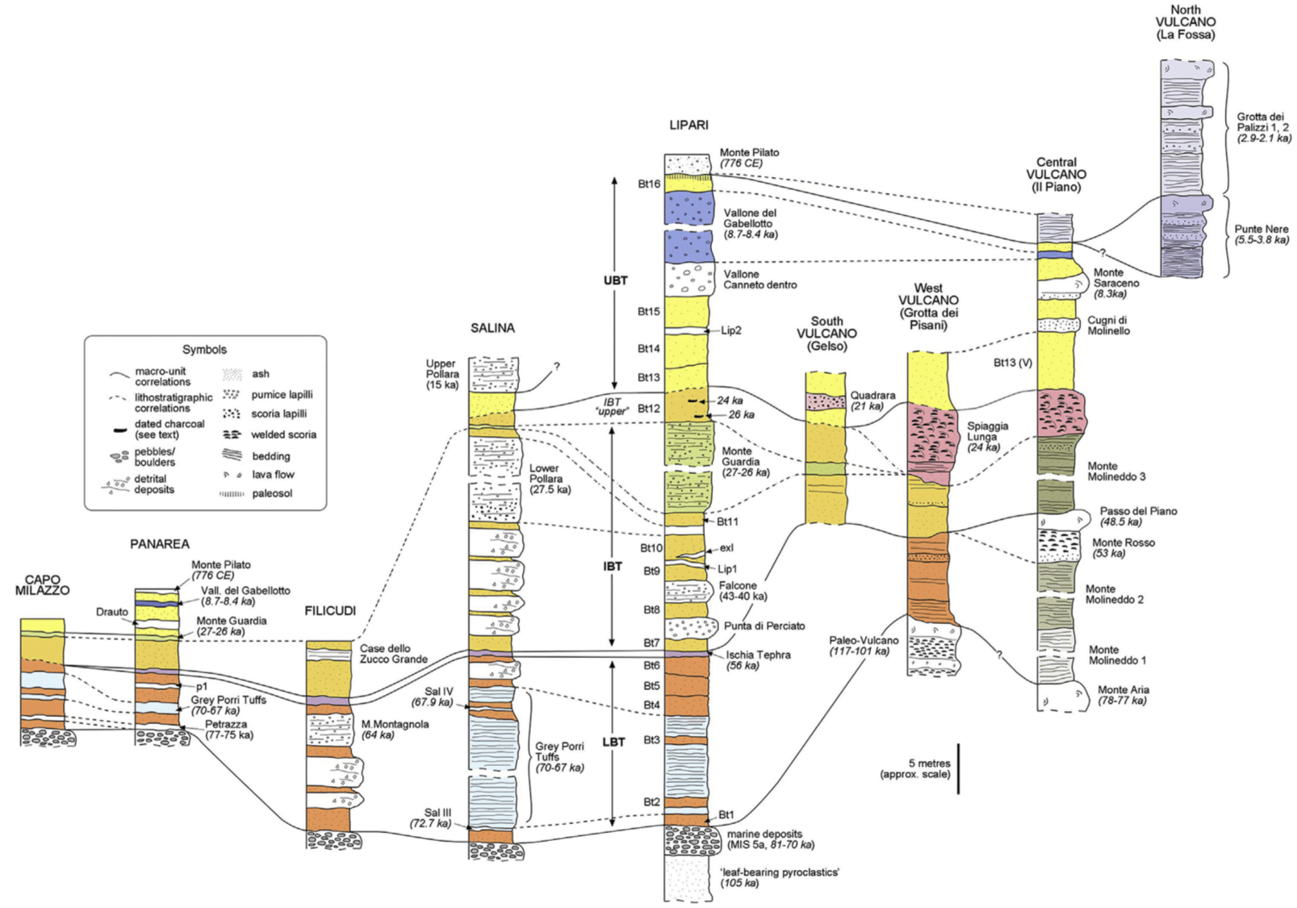

Fig. 2. Generalized stratigraphic correlations of the BT successions and age constraints in the study area. The most complete BT succession is recognized on the island of Lipari, subdivided into several depositional units (Bt1–16) superposed to the LBT, IBT and UBT macro-units by means of interlayered volcanic units and tephra layers, erosive surfaces and reworked horizons. The Bt12 depositional unit immediately overlying the Monte Guardia tephra is considered as part of the IBT (namely IBT 'Upper') following the chemical evidence presented here (whilst it was part of the UBT macro unit as defined by (Lucchi et al., 2008)). The LBT, IBT and UBT are then correlated with distinct sectors of the island of Vulcano, the islands of Salina, Filicudi, Panarea and the Capo Milazzo peninsula. Please note that the recognized depositional units are a minimum number as some lithologically-homogeneous units could have be amalgamated. References for the stratigraphic units in the different sites are: (Forni et al., 2013) (Lipari); (De Astis et al., 2013) (Vulcano); (Lucchi et al., 2013a) (Salina); (Lucchi et al., 2013e) (Filicudi); (Lucchi et al., 2013c) (Panarea); (Morche, 1988) (Capo Milazzo). The Lip1 and Lip2 tephras are described in Table 1, whilst 'ext' is an external tephra not discussed here. On Salina, the Sal III and Sal IV tephra layers ((Lucchi et al., 2008) and references therein) are correlated with tephra layers C(i)-8 and C(i)-7 in the Tyrrhenian sea core KET 8011 (Paterne, 1985; (Paterne et al., 1988)). Some additional tephra layers interlayered within the BT succession (not displayed here) provide stratigraphic boundaries between distinct depositional units of BT (not correlated between the islands), and based on their glass geochemistry they are likely to correlate with widespread central Mediterranean isochronous markers derived from the Campanian volcanic zone and recorded in marine and lacustrine successions.

of 5–6 m are found in south Vulcano near Gelso, below the Monte Guardia marker bed. Whilst, they are generically recognized below the Spiaggia Lunga scoriae in west Vulcano near to Grotta dei Pisani (Fig. 3G), where they show a thickness of 7–8 m, and the absence of the Monte Guardia makes it difficult to define the boundary with the UBT. In this outcrop the LBT-IBT boundary is represented by a high-angle erosional unconformity.

Noteworthy, there are no typical LBT-IBT deposits in the area of il Piano, where the stratotype of UBT is identified. There, three thick pyroclastic successions (Fig. 3H), namely the Monte Molineddo (MM) 1–3 formations (De Astis et al., 2013), are stratigraphically recognized above the Monte Aria/Timpa del Corvo lava flows (78–77 ky; (De Astis et al., 2013) and references therein) and below the UBT, matching the stratigraphic position of the LBT-IBT units. Local volcanic units (Monte Rosso, Monte Luccia, Passo del Piano) dated to 53–48 ky ((De Astis et al., 2013), and references therein) are interlayered between the MM1–2 and MM3 successions (Fig. 2). The MM1–3 are massive to stratified, grey to varicoloured ash successions with interlayered layers of black to yellow scoria lapilli, which are related to an undefined source area within the La Fossa caldera based on a substantial south-eastwards thickness and grain size decrease (De Astis et al., 2013). They share some lithofacies observed in LBT-IBT deposits, but a clear lithostratigraphic correlation has not yet been defined. Remarkably, black to yellow scoria lapilli resembling those of the MM3 succession are found embedded, in places aligned in trails, within the IBT in south Lipari (above the Falcone domes) and near Grotta dei Pisani and Gelso on Vulcano, thus suggesting a possible correlation between the MM3 and IBT.

4.2. Volcanic glass geochemistry of the BT

Following the stratigraphy outline above, in the following sections we report the compositional data (major and minor elements) of volcanic glass (ash and scoria) sampled from throughout the BT successions outcropping on Vulcano and Lipari. Owing to more extensive exposures the chemical analysis of the LBT and IBT stratigraphic macro-units concentrated predominantly on outcrops studied on Lipari, whilst chemical

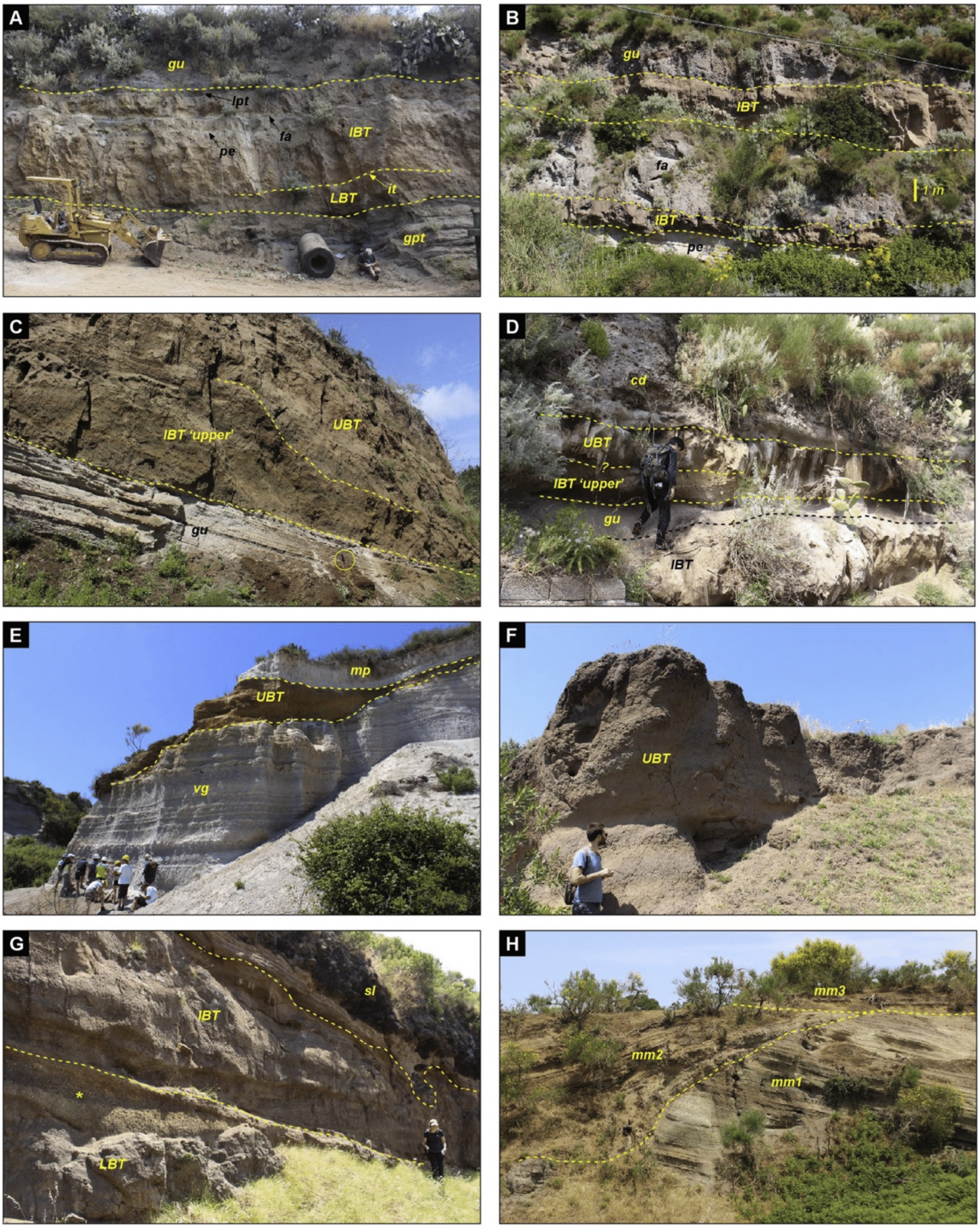

Fig. 3. Field evidence and main sampling outcrops of the BT on Lipari and Vulcano. A) Vallone Canneto Dentro, central-eastern Lipari: LBT and IBT macro-units with interlayered Grey Porri Tuffs (gpt), Ischia Tephra (it) and the local Punta di Perciato (pe), Falcone (fa) and Monte Guardia pumice pyroclastics (gu). B) Valle Muria, south-western Lipari: IBT interlayered with the local Punta di Perciato (pe), Falcone (fa) and Monte Guardia pumice pyroclastics (gu). C) Canneto, eastern Lipari: IBT 'upper' (see the text for explanation) and UBT above the Monte Guardia marker bed (gu). D) Vallone Canneto Dentro, central-eastern Lipari: IBT 'upper' and UBT above the Monte Guardia marker bed (gu), bounded at the top by the local Vallone Cannetro Dentro (cd) pumice succession. E) Vallone Fiume Bianco, central-northern Lipari: top portion of the UBT interlayered between the local Vallone del Gabellotto (vg) and Monte Pilato (mp) pumice successions. F) Grotta dei Pisani, western Vulcano: UBT located above the Spiaggia Lunga scoria marker bed. G) Grotta dei Pisani, western Vulcano: IBT and LBT below the Spiaggia Lunga scoria marker bed (sl), characterised by massive ash deposits alternated with scoria lapilli layers (*). H) Il Piano, central Vulcano: Monte Molineddo 1, 2, 3 (mm3) pyroclastic successions outcropping in the stratigraphic window of the LBT and IBT.

investigations of the UBT instead largely focused on the outcrops exposed on Vulcano (Fig. 4).

For each stratigraphically defined macro-unit outlined below, in the first instance we report the glass data relating to dominant glass component or melt composition tapped during the eruptions responsible for the emplacement of the BT deposits. Overall the juvenile BT glasses range from basaltic trachy-andesites through trachy-andesites to more evolved trachytes (Fig. 5A) and show a clear K-series affinity (Fig. 5B). Major and minor element glass analyses of representative BT depositional units analysed are reported in Tables 3 and 4, whilst the full glass dataset is reported in the Supplementary Material B.

Separately, some minor chemical components with distinct compositions are observed within some of the individual BT depositional units (Table 5) and are also described below. We attribute these chemical components to the stratigraphic units underlying the BT, and as such are considered 'secondary' components unrelated to the juvenile products of the BT source eruptions. Specifically, some depositional units in the IBT and UBT contain HKCA rhyolitic glasses, whilst transitional CA to HKCA andesite to dacitic glasses are recognized in some LBT depositional units (Fig. 5A).

To assess links between the BT depositional units and proximal eruptive units on Vulcano we provide additional major and minor element glass data for the Monte Molineddo (MM) 1–3 successions, and the Punte Nere Formation (Table 6). A detailed description of their glass compositions is reported in Supplementary Material A.2.

4.2.1. Glass geochemistry of the LBT outcropping on Lipari and Vulcano

The sampled units representative of the LBT (Bt1–6) outcropping on Lipari are dominated by volcanic glass compositions ranging from basaltic trachy-andesites to trachy-andesites and tephri-phonolites (SiO_2 = 52.4–57.2 wt%; $Na_2O + K_2O$ = 7.7–11.5 wt%; [$n = 109$] Fig. 5A), and these glasses have a clear K-series affinity (K_2O = 4.2–6.3 wt%; Fig. 5B). Using increasing SiO_2 content as a fractionation index for the LBT glasses, CaO (4.9–7.5 wt%), MgO (1.8–3.5 wt%), and Na_2O (2.8–5.9 wt%) contents noticeably decrease, whilst K_2O content increases. There is no evidence of clear chemo-stratigraphic variation in the glass compositions of the LBT depositional units (Table 3). Trachy-andesite glasses ($n = 22$) from the limited LBT exposures accessible on Vulcano, at Grotta dei Pisani, display a consistent K-series affinity, and evolutionary trends similar to those from LBT deposits examined on Lipari (Fig. 5-8).

A secondary glass component ($n = 14$), with glasses ranging from andesite through to dacite (SiO_2 = 56.5–62.6 wt%; $Na_2O + K_2O$ = 4.5–8.3 wt%) and a transitional CA to HKCA affinity (Fig. 5A), is observed in the LBT units outcropping on Lipari interlayered with (Bt3) and overlying (Bt4) the GPT (Fig. 2).

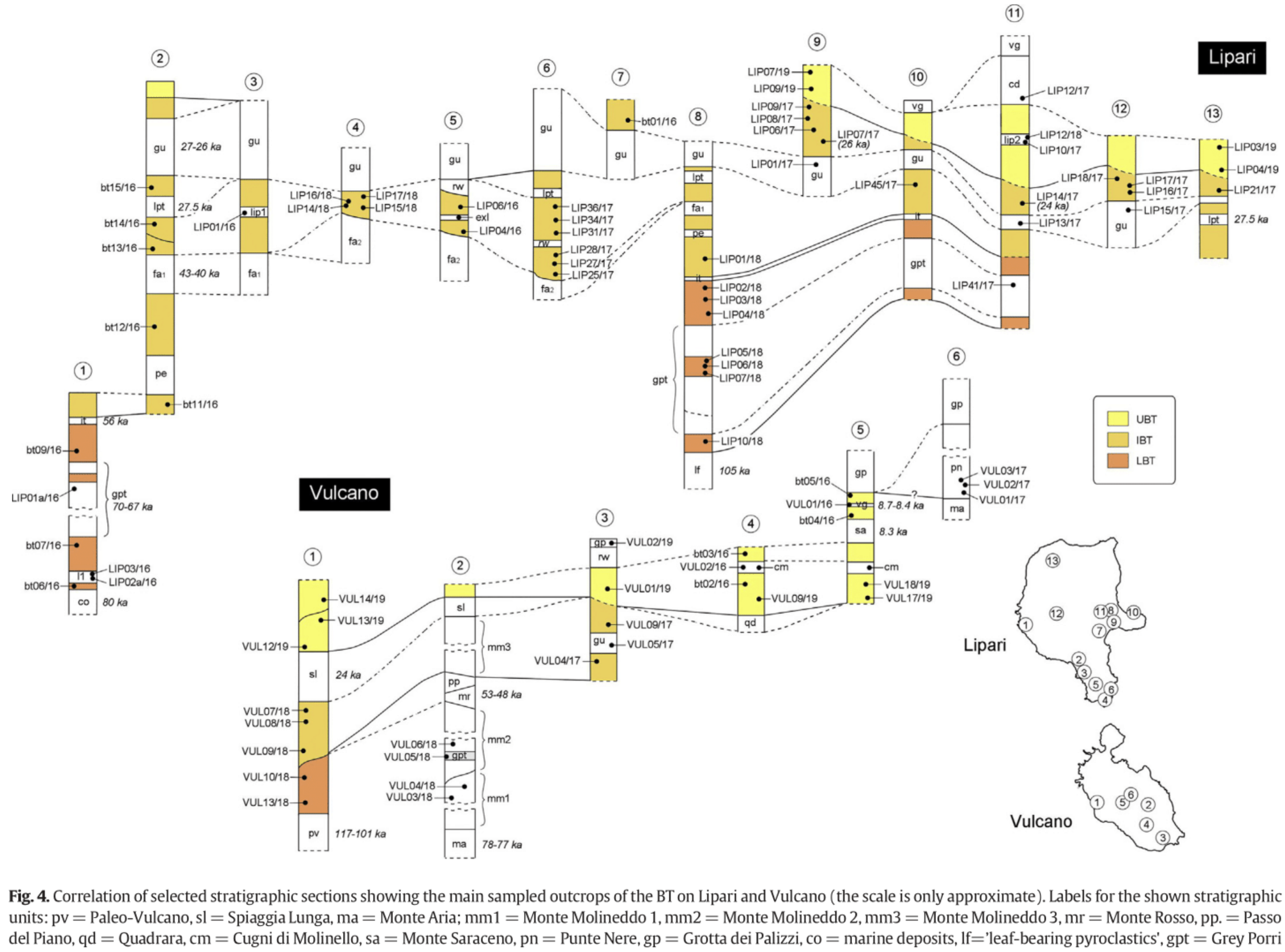

Fig. 4. Correlation of selected stratigraphic sections showing the main sampled outcrops of the BT on Lipari and Vulcano (the scale is only approximate). Labels for the shown stratigraphic units: pv = Paleo-Vulcano, sl = Spiaggia Lunga, ma = Monte Aria; mm1 = Monte Molineddo 1, mm2 = Monte Molineddo 2, mm3 = Monte Molineddo 3, mr = Monte Rosso, pp. = Passo del Piano, qd = Quadrara, cm = Cugni di Molinello, sa = Monte Saraceno, pn = Punte Nere, gp = Grotta dei Palizzi, co = marine deposits, lf='leaf-bearing pyroclastics', gpt = Grey Porri Tuffs, it = Ischia-Tephra, pe = Punta di Perciato, fa1 = Falcone pumice, fa2 = Falcone domes, lip1 = lip1 tephra, exl = external tephra (not discussed here), lpt = Lower Pollara Tuffs, gu = Monte Guardia, lip2 = lip2 tephra, cd = Vallone Canneto dentro, vg = Vallone del Gabellotto, rw = reworked horizon. References for the stratigraphic units herein are (Forni et al., 2013) (Lipari) and (De Astis et al., 2013) (Vulcano).

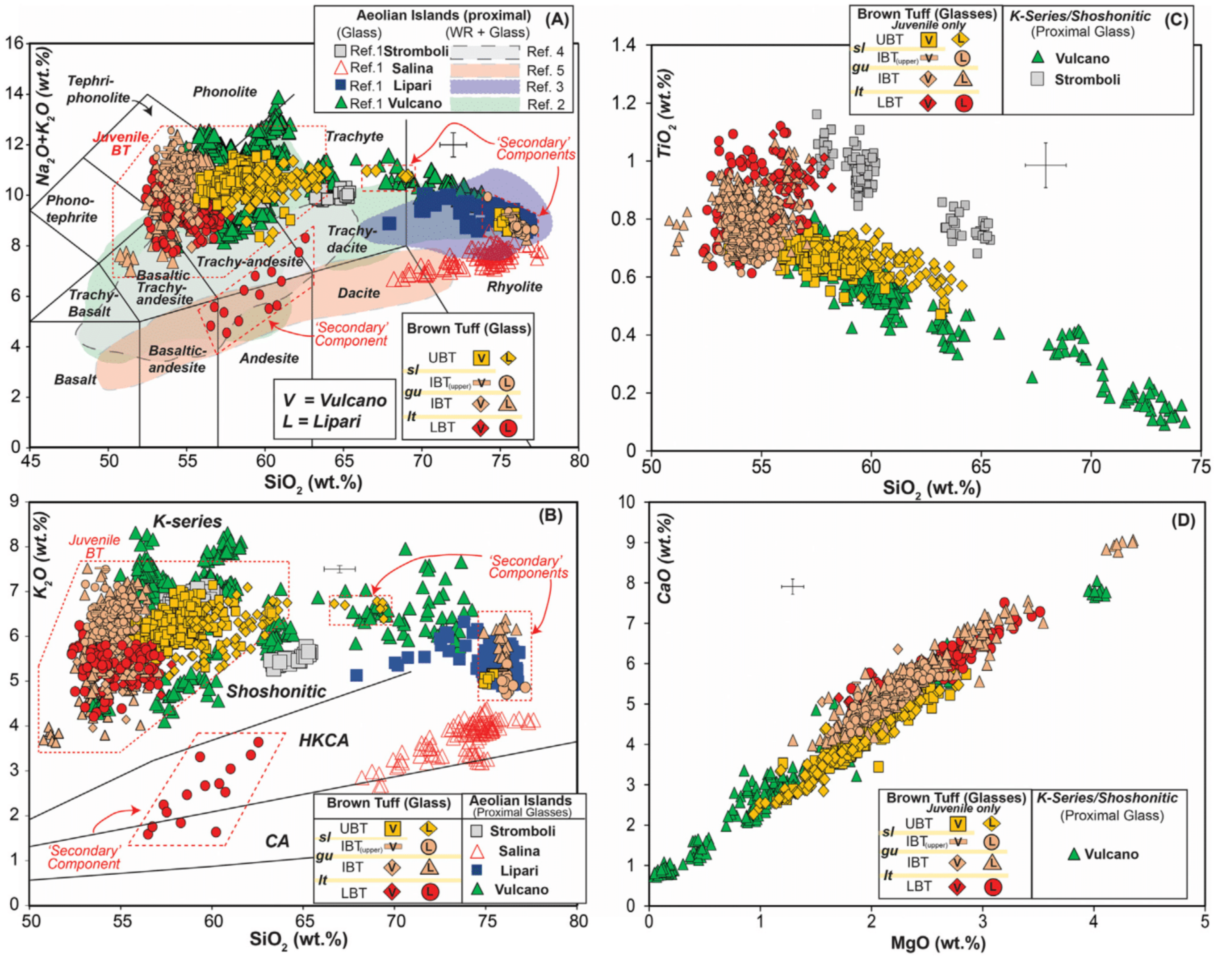

Fig. 5. Major element (wt%) glass geochemical variations of the BT glasses analysed in this study compared to the volcanic glasses of explosive eruption deposits produced on Vulcano, Lipari, Salina and Stromboli during the last 50 ky. (A) TAS classification diagram of BT glasses, also shown are the compositional ranges of the whole rock (WR) data for Vulcano, Lipari, Salina and Stromboli; (B) SiO_2 vs K_2O classification diagram; (C) SiO_2 vs. TiO_2 diagnostic plot used for distinguishing the potassic eruptive products of Vulcano and Stromboli, and illustrating the BT clear link to volcanism on Vulcano and useful when considering the provenance of distal marine tephra layers; (D) MgO vs. CaO plot further illustrating that the BT juvenile glasses conform to the compositions of eruptive products known to have been produced on Vulcano (including the Quadrara Formation, Casa Lentia, Grotta dei Palizzi 1 and 2, Caruggi formation/Breccia di Commenda, Lower and Upper Pietre Cotte). Error bars represented 2*standard deviations of replicated analyses of the StHs6/80-G secondary standard glass run alongside the BT samples. References: (1) (Albert et al., 2017); (2) (De Astis et al., 2013); (3) (Forni et al., 2013); (4) (Francalanci et al., 2013); and (5) (Lucchi et al., 2013a).

4.2.2. Glass geochemistry of the IBT outcropping on Lipari and Vulcano

The sampled units representative of the IBT (Bt7–11) that outcrop on Lipari are dominated by volcanic glass compositions ranging from basaltic trachy-andesite to trachy-andesites and tephri-phonolites (SiO_2 = 50.8–57.2 wt%; $Na_2O + K_2O$ = 7.0–12.3 wt%; [n = 279] Fig. 5A), and these glasses display a clear K-series affinity (K_2O = 3.6–7.5 wt%; Fig. 5B). Using increasing SiO_2 content as a fractionation index the IBT glasses show decreasing CaO (4.0–9.1 wt%) and MgO (1.3–4.4 wt%) content, while K_2O increases with evolution (Fig. 5B). The FeOt, TiO_2, Na_2O and Al_2O_3 contents remain broadly constant with increasing SiO_2. No clear chemo-stratigraphic relationship exists in the IBT succession on Lipari (Table 3). The least evolved products observed within the IBT relate to layers of diffuse scoria lapilli (Fig. 7-8; Table 3). The limited IBT exposures on Vulcano at Grotta dei Pisani are relatively homogeneous and chemically consistent with the trachy-andesite/tephri-phonolitic glasses of the IBT on Lipari (Fig. 5A), and these glasses conform to the same evolutionary trends (Fig. 8).

Minor secondary glass components (n = 34) observed in distinct IBT depositional units sampled on Lipari (bt8–10) are homogeneous high-SiO_2 rhyolites (SiO_2 = 76.0 ± 0.4 wt%; $Na_2O + K_2O$ = 8.9 ± 0.3 wt%; Fig. 5A), and are characterised by variable K_2O contents, but all show a clear HKCA affinity (K_2O = 5.6 ± 0.8 wt% [2 s.d.]; Fig. 5B). No rhyolitic glasses were observed in the IBT (Bt7) that underly the lowermost Punta di Perciato pumice deposits in southern Lipari (Fig. 2). Separating Bt9 and Bt10 in southern Lipari (Fig. 4; Loc. 3) a previously unreported whitish tephra layer (Lip1, sample LIP01/16; Table 1) was identified, which displays a homogeneous HKCA rhyolitic glass composition (SiO_2 = 75.8 ± 0.6 wt% [2 s.d.]; K_2O = 5.3 ± 0.4 wt% [2 s.d.]; n = 15; Supplementary Material 2).

4.2.2.1. IBT 'upper' unit that outcrops on Lipari and Vulcano. A further subdivision of the BT succession is introduced here on the basis of the presented volcanic glass chemistry. The glasses analysed from the basal portion of the UBT macro-unit, as previously defined by Lucchi et al., (2008) immediately overlying the Monte Guardia tephra on Lipari and Vulcano (Gelso), and labelled the Bt12 depositional unit here, are actually chemically consistent with the underlying IBT compositions described above (Section 4.2.2; Fig. 6), and distinct from the UBT (Bt13–16). Thus, we prefer to attribute the Bt12 deposits, directly overlying the Monte Guardia, to the IBT macro-unit, and herein name them as the IBT 'upper'.

Table 3
Average of major and minor element composition (normalised) of juvenile glass of selected Lower and Intermediate Brown Tuffs units included in the study. Totals are pre-normalised analytical totals. n = number of analyses used to calculate the average, Φ = sample grain size. Locality is referred to Fig. 4. A complete geochemical dataset is provided in Supplementary material B.

Macro Unit	LOWER BROWN TUFF													
Locality	1 (Lipari)		8 (Lipari)		8 (Lipari)		1 (Lipari)		8 (Lipari)		8 (Lipari)		1 (Vulcano)	
Unit	bt 1		bt 1/2		bt 3		bt 4		bt 4		bt 6		?	
Sample	bt06/16 (L) 2φ		LIP10/18 3φ		LIP05/18 3φ		bt09/16 (L) 3φ		LIP04/18 3φ		LIP02/18 3φ		VUL10/18 3φ	
Material	ash		ash		ash		ash		ash		ash		ash	
n	10		10		11		8		19		11		16	
	mean	1σ	mean	1σ	mean	1σ	mean	1σ	mean	1σ	mean	1σ	mean	1σ
(wt%)														
Total	96.83	1.50	96.70	0.60	97.07	1.80	97.57	1.11	97.66	1.40	98.19	0.78	98.66	1.15
SiO_2	54.68	0.80	54.01	0.62	56.68	0.33	56.13	0.42	53.76	0.49	53.41	0.93	56.77	1.10
TiO_2	0.99	0.03	0.84	0.10	0.87	0.07	0.99	0.09	0.79	0.05	0.73	0.11	0.97	0.05
Al_2O_3	16.58	0.13	17.03	0.63	16.44	0.38	16.39	0.20	17.55	0.38	17.78	0.91	16.35	0.37
FeO	9.22	0.61	8.63	0.64	8.18	0.38	8.83	0.35	8.03	0.26	8.02	1.08	8.15	0.56
MnO	0.21	0.05	0.19	0.03	0.20	0.04	0.22	0.04	0.16	0.02	0.17	0.05	0.16	0.03
MgO	2.76	0.37	2.83	0.17	2.13	0.20	2.29	0.26	2.69	0.15	2.78	0.39	2.09	0.38
CaO	6.09	0.64	6.24	0.26	5.38	0.21	5.54	0.40	6.02	0.28	6.23	0.67	5.22	0.68
Na_2O	3.61	0.25	4.19	0.32	3.89	0.23	3.57	0.45	4.50	0.25	4.43	0.74	3.97	0.25
K_2O	5.10	0.58	5.16	0.37	5.33	0.23	5.16	0.22	5.66	0.25	5.63	0.49	5.47	0.45
P_2O_5	0.61	0.05	0.69	0.04	0.66	0.07	0.68	0.04	0.68	0.03	0.70	0.09	0.67	0.03
Cl	0.15	0.02	0.20	0.04	0.23	0.07	0.19	0.06	0.15	0.03	0.12	0.03	0.18	0.05
Macro Unit	INTERMEDIATE BROWN TUFF													
Locality	2 (Lipari)		4 (Lipari)		10 (Lipari)		6 (Lipari)		6 (Lipari)		2 (Lipari)		1 (Vulcano)	
Unit	bt 7		bt 9		bt 8/9		bt 9		bt 10		bt 11		?	
Sample	bt11/16 (L)		LIP14/18 3φ		LIP45/17		LIP27/17		LIP36/17 -1φ		bt15/16 (L) 2 φ		VUL09/18 2φ	
Material	ash		ash		scoria		scoria		ash		ash		ash	
n	10		27		10		18		20		10		10	
	mean	1σ	mean	1σ	mean	1σ	mean	1σ	mean	1σ	mean	1σ	mean	1σ
(wt%)														
Total	97.46	1.27	96.19	0.91	98.59	0.74	97.01	1.18	98.16	0.62	97.83	1.28	99.07	0.83
SiO_2	54.77	0.45	54.17	0.57	51.15	0.69	53.61	0.54	53.85	0.40	54.44	0.41	55.12	0.32
TiO_2	0.83	0.05	0.77	0.05	0.77	0.07	0.90	0.03	0.82	0.05	0.75	0.05	0.85	0.05
Al_2O_3	17.21	0.40	17.25	0.36	17.22	0.48	17.17	0.17	17.02	0.27	17.35	0.26	16.59	0.31
FeO	8.24	0.29	8.14	0.37	9.34	0.52	8.68	0.29	8.64	0.27	8.21	0.32	8.65	0.20
MnO	0.18	0.05	0.20	0.04	0.19	0.04	0.18	0.06	0.19	0.06	0.21	0.06	0.19	0.04
MgO	2.20	0.29	2.19	0.17	4.21	0.59	3.05	0.24	2.60	0.31	2.09	0.16	2.29	0.05
CaO	5.31	0.56	5.38	0.23	8.86	0.87	6.92	0.43	5.88	0.45	5.25	0.36	5.52	0.14
Na_2O	4.00	0.35	4.75	0.17	3.72	0.32	3.95	0.28	4.20	0.18	4.27	0.31	4.17	0.18
K_2O	6.26	0.49	6.02	0.16	3.88	0.53	4.65	0.27	5.87	0.34	6.46	0.47	5.61	0.18
P_2O_5	0.75	0.05	0.83	0.06	0.49	0.08	0.60	0.04	0.73	0.05	0.71	0.03	0.73	0.02
Cl	0.25	0.04	0.31	0.03	0.17	0.02	0.29	0.02	0.20	0.04	0.25	0.04	0.28	0.02

On Lipari, the IBT 'upper' have a dominant juvenile glass component that ranges from trachy-andesites to higher alkali content tephri-phonolites (SiO_2 = 53.1–55.9 wt%; $Na_2O + K_2O$ = 8.4–12.3 wt%; [n = *157*] Fig. 5A), and these glasses display a clear K-series affinity (K_2O = 5.4–7.5 wt%; Fig. 5B). At Gelso on Vulcano (VUL09/17), the IBT 'upper' is characterised by tephri-phonolitic glasses (Fig. 5A), with a K-series affinity (Fig. 5B), that are consistent with the IBT 'upper' glasses observed on Lipari. With increasing SiO_2 content these IBT 'upper' glasses show broadly increasing K_2O content, decreasing CaO and MgO, whilst FeOt, TiO_2, Na_2O and Al_2O_3 contents remain largely constant. The evolutionary trends of the IBT 'upper' glasses characterised here on both Lipari and Vulcano are entirely consistent with the underlying IBT deposits (Section 4.2.2; Fig. 6).

Minor secondary glass components (n = *19*) observed in the IBT 'upper'on Lipari and Gelso (Vulcano), above the Monte Guardia marker bed, are relatively homogeneous high-SiO_2 rhyolites (SiO_2 = 74.2–77.2 wt%; $Na_2O + K_2O$ = 8.5–9.9 wt%; Fig. 5A), these glasses show a clear HKCA affinity (K_2O = 4.8–6.0 wt%; Fig. 5B).

4.2.3. Glass geochemistry of the UBT

4.2.3.1. UBT units that outcrop on Vulcano, and the Cugni di Molinello Formation. Here we refer to the UBT depositional units (from Bt13 upwards) as those above the IBT 'upper' (Bt12) (Fig. 2). Overall the juvenile glass compositions of the UBT on Vulcano show a considerable range in evolution and are dominated by trachy-andesitic through to trachytic glasses (SiO_2 = 55.7–64.5 wt%; $Na_2O + K_2O$ = 8.3–11.6 wt%; n = *242*; Fig. 5A), all showing a clear K-series affinity (K_2O = 5.1–7.3 wt%; Fig. 5B). The UBT glass compositions display increasing K_2O and decreasing CaO (2.6–5.7 wt%), MgO (1.3–2.9 wt%), and FeOt (3.9–7.3 wt%) with increasing SiO_2 content, whilst Na_2O (2.6–4.8 wt%), TiO_2 (0.5–0.8 wt%; Fig. 5C) and Al_2O_3 (16.4–18.1 wt%) contents remains broadly constant. They plot along a distinct evolutionary trend with higher SiO_2 contents at overlapping CaO and MgO contents relative to the IBT and IBT 'upper' glasses (Fig. 6).

The most voluminous UBT, corresponding to unit Bt13, likely results from numerous amalgamated depositional units, and was sampled directly above the Spiaggia Lunga (24 ky) marker bed at Grotta dei Pisani. Glass compositions of Bt13 extend to the most evolved products observed in the entire Vulcano UBT succession (58.1–63.3 wt% SiO_2). Where Bt13 glasses overlap in SiO_2 content with the younger BT depositional units, the latter are typically dominated by glasses with higher K_2O content (e.g., Bt15; Fig. 6). The highest SiO_2 glasses observed within the Bt13 samples display the lowest CaO, FeOt and MgO contents within the entire UBT succession (Fig. 6). Stratigraphically higher in the Bt13 unit on Vulcano, above the Quadrara marker bed (21 ky), glasses are more restricted in their degree of evolution (VUL09/19; 56.1–59.3 wt% SiO_2). Whilst, the uppermost portion of Bt13 on Vulcano (sample bt02/16), collected immediately below the Cugni di Molinello scoria bed, displays some of the least evolved compositions observed through the entire Bt13 unit (55.7–58.5 wt% SiO_2).

The Cugni di Molinello scoria is a key marker bed within the UBT succession on Vulcano (Fig. 2). Here we present glass data for the Cugni di Molinello scoria to help assess their geochemical relationship. Glasses ($n = 19$) are relatively homogeneous trachy-andesites (52.3–54.3 wt% SiO_2) with a K-series affinity (5.2–6.2 wt% K_2O), and show most significant variability in their MgO (2.9–4.0 wt%) and CaO (6.3–8.0 wt%) contents (Fig. 6). The Cugni di Molinello scoria are more primitive than all the UBT deposits.

Above the Cugni di Molinello scoria bed, the UBT (Bt14) are quite homogenous (55.9–57.9 wt% SiO_2) (Fig. 6). The Bt15 unit displays some of the most potassic glasses throughout the UBT macro-unit, with a dominant population containing ca. 7 wt% K_2O. Juvenile glasses from both the Bt15 (56.3–60.7 wt% SiO_2) and Bt16 (56.9–61.2 wt% SiO_2) units are more heterogeneous than those of Bt14, and display some of the most evolved UBT glass compositions after the basal portions of the Bt13 unit (Fig. 6).

A minor, silicic, secondary glass component is identified in the Bt16 depositional unit sampled on Vulcano immediately above the Vallone del Gabellotto tephra erupted from Lipari. These secondary rhyolitic glasses ($SiO_2 = 75.0 \pm 0.3$ wt%; $Na_2O + K_2O = 9.2 \pm 0.5$ wt%; Fig. 5A) display a clear HKCA affinity ($K_2O = 5.3 \pm 0.5$ wt%; Fig. 5B). Also, two glass analyses (ca. 53 wt% SiO_2) from the Bt14 unit are chemically consistent with the underlying Cugni di Molinello scoria (Fig. 6),

4.2.3.2. UBT units that outcrop on Lipari. The UBT on Lipari are sampled above the IBT 'upper', exclusively belonging to the Bt13 depositional unit. Overall the juvenile glasses sampled at Chiesa Vecchia (north Lipari) and Vallone Canneto Dentro (central-eastern) are broadly consistent, with a heterogeneous composition ranging from tephri-phonolites to trachytes ($SiO_2 = 57.7$–64.2; $Na_2O + K_2O =$ 8.2–11.3 wt%; $n = 63$; Fig. 5A) and a K-series affinity ($K_2O =$ 5.1–7.1 wt%; Fig. 5B). With increasing SiO_2 content these UBT juvenile glass display decreasing CaO (2.3–5.5 wt%; Fig. 6B), FeOt (4.4–6.7 wt %), MgO (0.9–2.8 wt%; Fig. 6C), TiO_2 (0.5–0.8 wt%) and Al_2O_3 (15.5–17.7 wt%) content, whilst K_2O content increases, and Na_2O (2.9–4.6 wt%) remains broadly constant. In central-eastern Lipari, the juvenile glasses of the basal Bt13 unit (LIP09/19) are largely distinct from those overlying (LIP07/19), whereby the latter are typically offset to higher SiO_2 at overlapping CaO, MgO and K_2O contents (Fig. 6). The same compositional heterogeneity is shown by glasses of the Bt13 unit collected at Chiesa Vecchia (north Lipari). A secondary component of higher SiO_2 glasses (66.1–68.8 wt%; $n = 7$) is observed in the upper sample of Bt13 sampled at Chiesa Vecchia (LIP03/19), recognized on the basis of a clear compositional gap (ca.64–66 wt%; Fig. 6) which separates them from the dominant juvenile component.

5. Discussion

Stratigraphic relationships and detailed geochemical characterization of the BT on Lipari and Vulcano are integrated to give constraints on their areal distribution and correlations with proximal near-source units. This provides the basis for proximal-medial-distal tephra correlations, and fundamental insights into hazard assessment in this active sector of the Aeolian Islands.

5.1. Geochemical characteristics of the BT volcanic glasses and a proximal link to Vulcano

Major and minor element glass geochemistry of the juvenile component of individual BT depositional units reveals that they are relatively homogeneous with K-series populations ranging from basaltic trachy-andesites, through trachy-andesites and tephri-phonolites, up to more evolved trachytes (Fig. 5A). The minor outlying HKCA rhyolitic glasses, and CA to HKCA andesite to dacite glasses recognized in some depositional units of the LBT, IBT and UBT are considered as "secondary" components, which do not reflect the juvenile magmas feeding the BT. Their origin is discussed in Section 5.2. Consequently, the overall compositional field of BT volcanic glasses is significantly more restricted when compared to the one proposed by Lucchi et al., (2008). A narrower compositional range centred exclusively around K-series volcanic glasses reinforces the correlation of the BT with the Vulcano magmatic system. During its intermediate to youngest stages of evolution, Vulcano has been the dominant source of K-series products within the Aeolian archipelago (Fig. 5A-C). The evolutionary trends observed here within the overall BT dataset are entirely consistent with the previously characterised near-source Vulcano volcanic glasses (Fig. 5C-D). Indeed, the only other source of K-series magmas within the archipelago, and similar to those of the BT, is the Stromboli volcano, specifically during the Neostromboli period (~13–4 ky; (Albert et al., 2017; Francalanci et al., 2013); Fig. 5). An association between the BT and eruptive activity on Stromboli is, however, implausible owing to their greater thicknesses on Vulcano and Lipari relative to the rest of the archipelago (including Stromboli). Furthermore, K-Series activity on Stromboli is temporally incompatible with the longer-term emplacement of the BT succession. Finally, in terms of glass compositions, at overlapping SiO_2 content, the BT glasses display TiO_2 content more consistent with Vulcano products (lower-TiO_2) rather than those erupted on Stromboli (Fig. 5C). This final observation is pertinent when assessing the provenance of distal K-series marine tephra layers which might be related to the eruptions responsible for the BT.

Resolving unique geochemical fingerprints for the LBT and IBT glasses is a significant challenge given their large degree of chemical overlap. They are broadly consistent in terms of their SiO_2 content (~52–57 wt%), and across most other major and minor elements (Fig. 8). Some subtle differences may offer potential to help provenance medial-distal equivalents of the BT deposits, particularly where chronostratigraphy is poorly constrained. The least evolved IBT glasses contain higher MgO, CaO and FeOt relative to those analysed throughout the LBT (Figs. 5 and 8). More useful is that the IBT glasses range to higher K_2O content than those of the LBT, thus at overlapping SiO_2, where K_2O content exceeds 6.3 wt%, an attribution to the IBT is more likely (Fig. 7C).

The UBT glasses can be distinguished from those of the IBT (and LBT) owing to their higher SiO_2, trachy-andesitic to trachytic compositions (Fig. 5). The UBT glasses extend to lower TiO_2 contents compared to the underlying IBT units, again consistent with the overall trends observed in the glasses of known Vulcano erupted products (Fig. 5C). The UBT glasses also plot on subtly different evolutionary trends from those of the IBT, and this is well illustrated by CaO and MgO content plotted against SiO_2 (Fig. 6), where both CaO and MgO contents of the UBT extend to lower values than those of the IBT glasses (Fig. 6).

The stratigraphic boundary between the IBT and UBT macro-units had been previously defined by the identification of the widespread Monte Guardia tephra marker bed (Lucchi et al., 2008) and dated here at 25,920–27,025 cal y BP. The observed geochemical distinction between the IBT and UBT makes it possible to define a different geochemical-evolutionary boundary between the two successions. The lowermost depositional unit (Bt12) of the stratigraphically defined UBT macro-unit, immediately overlying the Monte Guardia tephra on both Vulcano (Gelso) and at various locations across Lipari (Fig. 6), is in fact chemically consistent with the IBT (those deposits beneath the Monte Guardia; Fig. 6), and consequently this depositional unit is re-defined in this study as the IBT '*upper*'. On Vulcano, the IBT/UBT chemical transition is observed relative to the Spiaggia Lunga scoria unit in the western sector of the island, whereby IBT type compositions are not observed in BT deposits above the Spiaggia Lunga, instead exclusively evolved UBT compositions are recognized. The age of 24 ± 5 ky for Spiaggia Lunga (Soligo et al., 2000) allows us to redefine the chronological boundary between IBT (56–24 ky) and UBT (24–8 ky).

Table 4
Average of major and minor element composition (normalised) of juvenile glass of selected Intermediate Brown Tuff 'Upper' and Upper Brown Tuffs units included in the study. Totals are pre-normalised analytical totals. n = number of analyses used to calculate the average, Φ = sample grain size. Locality is referred to Fig. 4. A complete geochemical dataset is provided in Supplementary material B.

Macro Unit	INTERMEDIATE BROWN TUFF 'UPPER'									
Locality	7 (Lipari)		12 (Lipari)		9 (Lipari)		13 (Lipari)		3 (Vulcano)	
Unit	bt 12		bt 12		bt 12		bt 12		bt 12	
Sample	bt01/16 (L) 3 φ		LIP18/17 1φ		LIP06/17 -1φ		LIP21/17 -1φ		VUL09/17 1φ	
n	11		17		26		24		10	
	mean	1σ	mean	1σ	mean	1σ	mean	1σ	mean	1σ
(wt%)										
Total	97.10	1.26	97.73	0.64	97.18	0.96	97.88	0.61	97.83	0.97
SiO_2	54.55	0.68	54.26	0.62	54.89	0.38	54.73	0.42	54.09	0.49
TiO_2	0.78	0.05	0.71	0.03	0.71	0.03	0.73	0.05	0.72	0.05
Al_2O_3	17.48	0.14	17.77	0.21	17.64	0.18	17.67	0.23	17.86	0.34
FeO	8.19	0.32	7.65	0.24	7.70	0.21	7.62	0.19	7.73	0.34
MnO	0.21	0.06	0.19	0.04	0.19	0.03	0.18	0.04	0.16	0.07
MgO	2.10	0.22	2.13	0.22	1.95	0.15	2.00	0.10	2.18	0.17
CaO	5.15	0.42	5.03	0.40	4.74	0.32	4.80	0.19	5.15	0.22
Na_2O	4.45	0.39	4.72	0.24	4.56	0.29	4.58	0.59	4.71	0.23
K_2O	6.08	0.50	6.51	0.24	6.57	0.30	6.66	0.25	6.42	0.30
P_2O_5	0.73	0.06	0.80	0.05	0.79	0.04	0.79	0.05	0.76	0.07
Cl	0.29	0.04	0.24	0.03	0.25	0.02	0.23	0.04	0.21	0.02
Macro Unit	UPPER BROWN TUFF									
Locality	9 (Lipari)		5 (Vulcano)		4 (Vulcano)		5 (Vulcano)		5 (Vulcano)	
Unit	bt 13		bt 13		bt 14		bt 15		bt 16	
Sample	LIP07/19		VUL17/19		bt03/16 (V) 2 φ		bt04/16 (V) 2 φ		bt05/16 (V) 3 φ	
n	17		17		17		19		17	
	mean	1σ	mean	1σ	mean	1σ	mean	1σ	mean	1σ
(wt%)										
Total	97.90	1.00	99.17	1.03	97.82	0.79	98.31	0.61	98.00	1.06
SiO_2	60.80	1.95	59.12	0.65	56.96	1.03	58.16	0.87	58.06	1.38
TiO_2	0.64	0.04	0.65	0.05	0.68	0.05	0.68	0.03	0.68	0.04
Al_2O_3	16.37	0.41	17.30	0.36	17.12	0.26	17.14	0.17	17.47	0.41
FeO	5.72	0.61	5.94	0.56	6.88	0.53	6.32	0.38	6.28	0.28
MnO	0.11	0.02	0.12	0.04	0.16	0.05	0.15	0.05	0.15	0.04
MgO	1.85	0.52	1.78	0.11	2.20	0.29	1.86	0.29	1.94	0.27
CaO	3.89	0.97	3.87	0.19	4.73	0.53	3.99	0.59	4.25	0.58
Na_2O	4.09	0.43	4.38	0.14	4.24	0.19	4.39	0.25	4.27	0.45
K_2O	5.85	0.48	6.19	0.21	6.18	0.24	6.53	0.38	6.12	0.34
P_2O_5	0.43	0.06	0.47	0.07	0.61	0.04	0.57	0.04	0.54	0.05
Cl	0.23	0.02	0.18	0.05	0.24	0.04	0.21	0.02	0.25	0.01

Unfortunately, where the Spiaggia Lunga scoria is not present, the IBT to UBT chemo-stratigraphic boundary is more difficult to identify, and this is the case on Lipari where no obvious unconformities are recognized at the corresponding stratigraphic level. However, charcoal dated from within the IBT 'upper' on Lipari is dated here at 25,800–26,190 cal y BP and this eruption age is in good chrono-stratigraphic agreement with the inferred Spiaggia Lunga boundary-transition age on Vulcano. The Spiaggia Lunga scoria unit crops out along the south-western border of the La Fossa caldera, which is the likely source area of the BT. Interestingly, Nicotra et al. (2020) have proposed that the emplacement of the Spiaggia Lunga scoria unit is directly linked to a volcano-tectonic (caldera) collapse event on Vulcano. It can be thus postulated that a collapse of the La Fossa caldera has coincided with a reconfiguration of this magmatic system, and the production of more evolved magmas which feed the UBT.

The more evolved depositional units that form the UBT (Bt13–16) show considerable compositional variability (Fig. 6). The most evolved glasses erupted within the UBT are associated with the most voluminous and oldest portion of Bt13, below the Cugni di Molinello scoria marker bed (Fig. 6). There is clear chemical overlap between the Bt13 depositional unit sampled on Vulcano and further north on Lipari. For instance the lowermost Bt13 samples from Vallone Canneto Dentro on Lipari (LIP09/19) are very consistent with the analysed deposits from the lowest portions of Bt13 on Vulcano. However, there are some noticeable spatio-chemical variations associated with unit Bt13. The remaining Lipari Bt13 samples (LIP07/19, LIP04/19 and LIP03/19) are dominated by glasses which reside on a subtly distinct evolutionary trend to those prevalent in the Vulcano deposits, this is best illustrated by a subtle offset to higher SiO_2 at overlapping K_2O, CaO and MgO content (Fig. 6). Importantly, from a correlation and provenance perspective, these higher SiO_2 glasses are also observed in the basal Bt13 deposit closer to source on Vulcano, albeit as a lower proportion of the glasses analysed. Published data (sample VL328) stratigraphically equivalent to Bt13 reported on Vulcano (Lucchi et al., 2008) is also consistent with the data presented here from Lipari. The most obvious explanation for a lower proportion of higher SiO_2 UBT glasses in our Vulcano dataset is because our sampling concentrated at the top and bottom of the thick Bt13 depositional unit, whereby the intermediate portion was not analysed. In contrast on Lipari, further from vent, this depositional unit is thinner and more compact, for instance at Vallone Canneto Dentro the analyses appear to reveal a more heterogeneous Bt13 signature, with data reflecting both the subtly offset UBT evolutionary trends (Fig. 6). There is a return to less evolved trachy-andesite compositions (ca. 57 wt%) in the uppermost portion of unit Bt13 (sample bt02/16), directly underlying the Cugni di Molinello scoria bed. This variability suggests that Bt13 does not represent a single depositional unit, but an amalgamation of lithologically homogeneous deposits, as also testified by the occurrence of localized erosional surfaces throughout the thickness of Bt13. The upper portion of Bt13 and Bt14 on Vulcano are indistinguishable in their composition, and are merely stratigraphically separated by the less

Table 5
Average of major and minor element composition of secondary glass components inside Brown Tuffs units across the macro units included in the study. Totals are pre-normalised analytical totals. n = number of analyses used to calculate the average, Φ = sample grain size. Locality is referred to Fig. 4. A complete geochemical dataset is provided in Supplementary material B.

Corresponding Pyroclastic Unit	Grey Porri Tuff		Grey Porri Tuff		Grey Porri Tuff		Perciato		Falcone	
Locality	8 (Lipari)		8 (Lipari)		1 (Lipari)		2 (Lipari)		4 (Lipari)	
Unit	bt 1/2		bt 3		bt 4		bt 8		bt 9	
Sample	LIP10/18 3φ		LIP07/18 3φ		bt09/16 (L) 3φ		bt12/16 (L)		LIP16/18 3φ	
n	3		2		3		15		4	
	mean	1σ	mean	1σ	mean	1σ	mean	1σ	mean	1σ
(wt%)										
Total	97.18	0.40	98.68	0.17	97.76	0.17	96.08	0.97	93.94	0.65
SiO_2	58.19	1.48	57.08	0.43	59.07	0.43	75.92	0.37	76.05	0.30
TiO_2	1.17	0.13	1.14	0.34	0.91	0.34	0.07	0.02	0.05	0.02
Al_2O_3	16.53	1.80	17.18	2.16	16.11	2.16	12.65	0.15	12.49	0.21
FeO	7.44	1.26	7.72	1.52	8.49	1.52	1.36	0.10	1.48	0.08
MnO	0.13	0.04	0.14	0.04	0.22	0.04	0.04	0.03	0.04	0.05
MgO	2.70	0.64	3.25	0.44	2.59	0.44	0.02	0.02	0.02	0.02
CaO	7.27	1.69	7.38	0.46	6.71	0.46	0.70	0.06	0.69	0.02
Na_2O	3.47	0.27	3.44	0.50	3.01	0.50	2.94	0.31	3.75	0.11
K_2O	2.47	0.85	2.02	0.35	2.30	0.35	5.99	0.27	5.10	0.14
P_2O_5	0.50	0.07	0.48	0.08	0.35	0.08	0.01	0.02	0.02	0.01
Cl	0.14	0.06	0.16	0.01	0.24	0.01	0.30	0.03	0.31	0.03

Corresponding Pyroclastic Unit	Monte Guardia		Monte Guardia		Monte Guardia		Vallone Del Gabellotto	
Locality	7 (Lipari)		12 (Lipari)		3 (Vulcano)		5 (Vulcano)	
Unit	bt 12		bt 12		bt 12		bt 16	
Sample	bt01/16(L)		LIP17/17		VUL09/17 -1φ		bt05/16 (V)	
n	17		8		3		3	
	mean	1σ	mean	1σ	mean	1σ	mean	1σ
(wt%)								
Total	94.44	1.10	96.43	0.61	94.39	0.91	97.53	0.69
SiO_2	76.10	0.27	76.42	0.42	75.55	0.16	75.37	0.42
TiO_2	0.07	0.02	0.05	0.02	0.05	0.05	0.05	0.06
Al_2O_3	12.51	0.07	12.28	0.29	12.59	0.08	12.72	0.32
FeO	1.37	0.10	1.49	0.12	1.45	0.08	1.53	0.16
MnO	0.08	0.04	0.05	0.02	0.05	0.04	0.05	0.01
MgO	0.01	0.01	0.01	0.01	0.01	0.01	0.02	0.01
CaO	0.69	0.04	0.67	0.05	0.72	0.04	0.71	0.04
Na_2O	3.77	0.13	3.72	0.18	3.97	0.07	4.07	0.05
K_2O	5.03	0.21	4.94	0.15	5.26	0.01	5.10	0.23
P_2O_5	0.01	0.02	0.02	0.02	0.01	0.01	0.00	0.00
Cl	0.35	0.04	0.35	0.03	0.34	0.02	0.38	0.02

evolved Cugni di Molinello scoria (Fig. 6), seemingly sourced from a separate vent within the La Fossa caldera (Dellino et al., 2011). Bt15 and Bt16 return to more evolved trachytic glass compositions, more consistent with those deposits from Bt13 (Fig. 6), making independent stratigraphic control important when distinguishing depositional units throughout the UBT. Bt15 is distinctive in terms of its prevalence of higher-K_2O glasses at overlapping SiO_2 content relative to other UBT deposits, a feature that is also apparent in published data from the same stratigraphic level (sample VL151; (Lucchi et al., 2008)).

5.2. The secondary glass compositions: Insight into the BT depositional mechanisms

In addition to the dominant juvenile K-series glass components of the BT, a small proportion of chemical outliers are recognized in some depositional units of the LBT, IBT and UBT on both Vulcano and Lipari. These glasses are genetically unrelated to magmas feeding the eruptions responsible for the BT and are termed here as "secondary glasses". HKCA rhyolitic glass compositions identified in some IBT and UBT units are entirely consistent with the silicic activities on Lipari during the past ca. 50 ka (Fig. 5A-B). Specifically, the rhyolitic glasses observed in the depositional units Bt8 and Bt9–10 of the IBT on Lipari, Bt12 of the newly defined IBT 'upper' on Lipari and Bt16 of the UBT on Vulcano. Lipari HKCA rhyolitic glasses can be most easily distinguished using their SiO_2 and K_2O content. On this basis we see that the rhyolitic glasses observed as secondary glasses can be compositionally linked to the pumice beds stratigraphically underlying each of the above-mentioned BT depositional units. The Bt8 and Bt9–10 depositional units of IBT contain high-SiO_2 (~76 wt%) rhyolites with high K_2O (~5.5–6.2 wt%), largely consistent with the underlying Falcone and Punta di Perciato tephra deposits related to eruptive activity in southern Lipari (Fig. 9A-B). There is also a degree of chemical overlap with rhyolitic glasses of the Lip1 tephra. This newly identified tephra layer separating the Bt9 and Bt10 depositional units, clearly documents a previously un-reported explosive eruption in the southern dome-field of Lipari given its glass composition spans those of the underlying (Falcone) and overlying (Monte Guardia) eruption units (Fig. 9A-B). The Bt12 (IBT 'upper') deposits across Lipari and in southern Vulcano (Gelso) contain minor components of high-SiO_2 rhyolites (~76 wt%) with far more variable K_2O content (4.7–6.0- wt%), consistent with the pumice and ash compositions of the underlying Monte Guardia eruption deposits (Fig. 9A-B). Whilst the HKCA rhyolitic glasses within the Bt16 unit of UBT on Vulcano are more consistent with the underlying Vallone del Gabellotto tephra deposits from Lipari (Fig. 9).

Similarly, CA to HKCA andesitic glass compositions are identified in the depositional units Bt3–4 of the LBT that outcrop on Lipari and are

Table 6
Average of major and minor element glass composition (normalised) of near-source Vulcano pyroclastic units included in the study. Totals are pre-normalised analytical totals. n = number of analyses used to calculate the average, Φ = sample grain size. Locality is referred to Fig. 4. A complete geochemical dataset is provided in Supplementary material B.

Pyroclastic unit	Monte Molineddo 1		Monte Molineddo 1		Monte Molineddo 2		Monte Molineddo 3	
Locality	2 (Vulcano)		2 (Vulcano)		2 (Vulcano)		3 (Vulcano)	
Sample	VUL03/18 3φ		VUL04/18 2φ		VUL06/18 2φ		VUL04/17 1φ (component 1)	
n	23		6		10		10	
	mean	1σ	mean	1σ	mean	1σ	mean	1σ
(wt%)								
Total	96.29	0.81	98.54	1.05	98.58	1.23	97.96	1.60
SiO_2	57.43	0.33	56.73	1.16	53.08	1.35	53.33	0.31
TiO_2	0.98	0.05	0.99	0.08	0.86	0.07	0.76	0.04
Al_2O_3	16.09	0.33	16.28	0.69	17.06	0.56	17.56	0.24
FeO	7.96	0.19	8.15	0.82	9.09	0.70	8.28	0.33
MnO	0.17	0.03	0.19	0.03	0.17	0.04	0.22	0.04
MgO	1.85	0.14	1.97	0.28	2.66	0.22	2.43	0.11
CaO	4.61	0.14	5.14	0.61	6.39	0.38	5.38	0.80
Na_2O	4.12	0.12	4.05	0.18	4.25	0.30	4.56	0.32
K_2O	5.85	0.14	5.60	0.29	5.51	0.26	6.39	0.55
P_2O_5	0.76	0.03	0.69	0.05	0.69	0.04	0.73	0.06
Cl	0.19	0.02	0.22	0.08	0.26	0.04	0.36	0.08
Pyroclastic unit	Monte Molineddo 3		Punte Nere		Punte Nere		Punte Nere	
Locality	6 (Vulcano)		6 (Vulcano)		6 (Vulcano)		6 (Vulcano)	
Sample	BT03/20		VUL03/17 1φ		VUL02/17 1φ		VUL01/17 1φ	
n	42		13		14		9	
	mean	1σ	mean	1σ	mean	1σ	mean	1σ
(wt%)								
Total	97.79	0.30	97.06	1.17	97.19	1.39	98.54	1.18
SiO_2	53.51	0.28	56.87	0.55	56.09	0.44	60.32	1.72
TiO_2	0.73	0.04	0.68	0.04	0.67	0.04	0.60	0.06
Al_2O_3	17.18	0.14	18.18	0.23	18.03	0.17	16.76	0.35
FeO	8.24	0.24	6.14	0.17	6.38	0.50	5.73	0.58
MnO	0.16	0.02	0.16	0.05	0.15	0.04	0.10	0.07
MgO	3.05	0.15	1.66	0.09	1.82	0.18	1.71	0.37
CaO	6.63	0.23	3.74	0.21	4.07	0.32	3.59	0.66
Na_2O	3.91	0.13	4.37	0.59	4.46	0.43	4.23	0.20
K_2O	5.82	0.15	7.39	0.30	7.50	0.39	6.28	0.51
P_2O_5	0.52	0.05	0.52	0.03	0.54	0.02	0.50	0.11
Cl	0.24	0.02	0.29	0.04	0.28	0.02	0.19	0.06

either interbedded within, or directly overly the GPT deposits from neighboring Salina (Fig. 9, C-D). These glass compositions are entirely consistent with the GPT deposits characterised proximally on Salina (Sulpizio et al., 2016), but also include new glass data for the proximal GPT, and medial-distal occurrences sampled on Lipari (LIP41/17; SME4/5), Vulcano (VUL05/18) and Panarea (PAN07/17). The additional occurrence of basaltic-andesite to andesite glass compositions consistent with the GPT in the depositional units Bt1–2 of the LBT in western Lipari (Fig. 9C-D) is instead likely to be attributed to an underlying tephra deposit (reported as I1 tephra by (Forni et al., 2013)) which shares a similar composition to the products of the GPT (Fig. 9C-D).

Furthermore, unit Bt14 of the UBT on Vulcano contains a minor component of K-series glasses which are entirely consistent with the juvenile products of the underlying, more primitive, Cugni di Molinello scoria bed (Fig. 6).

The presence of a minor component of glass fragments within some BT depositional units that compositionally correlate to the underlying pyroclastic units is the result of clast-embedding, ripped up from the incoherent substratum by PDCs laterally spreading from the source area on Vulcano. This is clearly observed in the field where pumice and/or scoria from the underlying incoherent pyroclastic units are ripped-up and embedded at the base of the individual BT depositional units in the sampled outcrops, a feature first observed by Lucchi et al., (2008); Lucchi et al., (2013b). These authors suggested that PDC erosion and abrasion was limited to proximal to mid-proximal areas, whereas here we suggest that clast-embedding could be effective even at a greater distance up to at least the northern sector of Lipari (more than 10 km from the source).

5.3. BT links with proximal units on Vulcano

Here our volcanic glass dataset for the LBT, IBT and UBT is used to assess correlations with proximal units on Vulcano, to further constraint source/vent location. For this purpose we discuss the geochemical affinity of the LBT, IBT and UBT with the volcanic units belonging to the corresponding chrono-stratigraphic windows that currently outcrop along the borders of the La Fossa caldera, which have been considered as the most probable BT source area (Lucchi et al., 2008; Lucchi et al., 2013b). Lucchi et al., (2008); Lucchi et al., (2013b) established a univocal lithostratigraphic correlation between the UBT and the Piano Grotte dei Rossi Tuffs, which are best exposed along the south-eastern rim of La Fossa caldera, in the area of Il Piano and crop out discontinuously on western and southern Vulcano. These show a regular decrease of deposit thickness from the caldera rim towards southern Vulcano that indicate an origin from a (undefined) vent within the La Fossa caldera.

Instead, there remains a challenge in defining correlations and areal distributions of the LBT-IBT (80–24 ky) because deposits with their typical lithofacies are absent in the area of Il Piano, given the UBT stratotype is observed here, it should represent the main depositional area of the LBT-IBT units, assuming that their source area has not changed over time. In this area, the MM1–3 pyroclastic successions occupy the chrono-stratigraphic window corresponding to the LBT-IBT (in addition to other minor units). Specifically, the MM1–2 are found interlayered between Vulcano products dated at 78–77 ky and 53–48 ky, which broadly corresponds to the 80–56 ky chrono-stratigraphy of the LBT, whilst the IBT (56–24 ky) are more likely to correspond to the MM3 that is loosely defined in the stratigraphic interval above 53–48 ky and

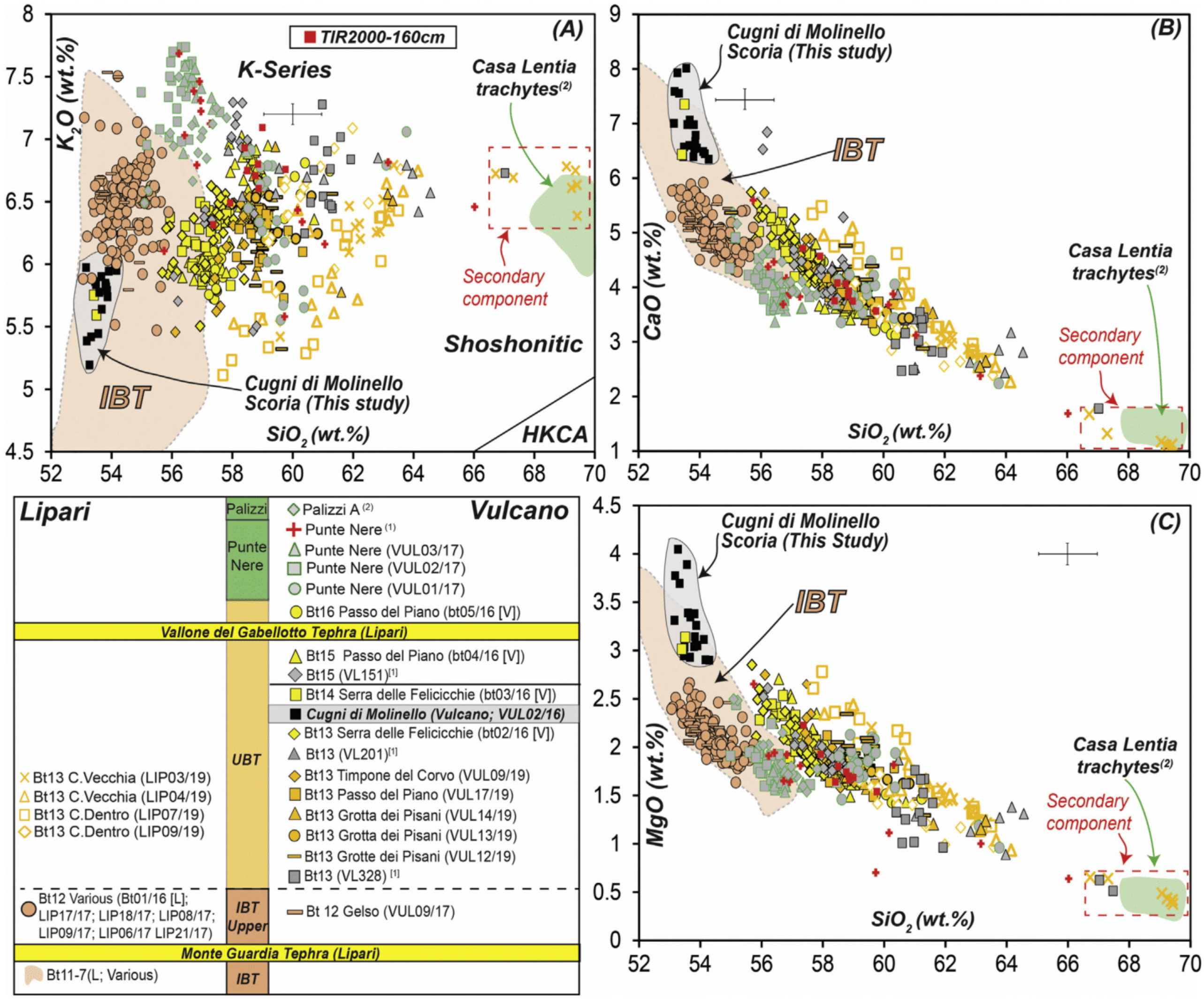

Fig. 6. Major element (wt%) glass geochemical variation diagrams (A-C) showing the different UBT depositional units sampled on Vulcano and Lipari (D). Shown are the compositions of the newly defined IBT 'upper' which immediately overly the Monte Guardia tephra at various outcrops on Lipari and Vulcano (Gelso). These deposits are re-classified as the IBT 'upper' owing to their chemical similarity to the IBT found below the Monte Guardia marker bed. A minor secondary components of more evolved trachyte is shown within the Bt13 (LIP03/19) deposits at Chiesa Vecchia, Lipari and these share a similar chemical affinity to the explosive products of the Casa Lentia eruptive succession on Vulcano. HKCA rhyolitic secondary glass component are also observed in Bt16 on Vulcano, these are not shown here, instead refer to Fig. 9. New glass data is presented for the Cugni di Molinello scoria bed which is interbedded between the Bt12 and Bt13 depositional units on Vulcano, these more primitive fall out scoria deposit are also believed to derive from activity within the La Fossa caldera, albeit erupted from a separate vent area to the UBT (Dellino et al., 2011). Glass data collected from a marine ash sample TIR2000-160 cm taken from the Marsili Basin marine core is also shown to have a clear UBT affinity. Error bars represented 2*standard deviations of replicated analyses of the StHs6/80-G secondary standard glass run alongside the BT samples. References: (1) (Lucchi et al., 2008) and (2) (Albert et al., 2017).

the UBT (<24 ky). In addition to a compatible chrono-stratigraphic position, the MM1–3 share many lithological and textural features with the LBT-IBT deposits, consisting of massive ash with discontinuous lamination and planar to inclined bedding, with abundant clinopyroxene crystals and internal banding of color and grain-size. Furthermore, distinctive black to yellowish scoria lapilli of MM3 are recognized in a number of stratigraphic positions within the IBT including at Grotta dei Pisani and Gelso on Vulcano, or along the southern sector of Lipari. These lines of evidence were responsible for Lucchi et al., (2008); Lucchi et al., (2013b) proposing that the MM1–3 could represent the near source counterpart of the LBT-IBT units. However, a clear lithostratigraphic correlation between the LBT-IBT units and the MM1–3 has not yet been established, and thus geochemical support becomes particularly important.

The K-series basaltic trachy-andesitic, tephri-phonolitic and trachy-andesitic glasses of the LBT and IBT are indeed broadly consistent with the volcanic glasses erupted during the emplacement of the proximal MM1–3 (Fig. 7-8). Our samples and subsequent glass analyses, reported in Supplementary A, are unlikely to be representative of the full compositional variability of these thick eruptive successions, particularly owing to the poor preservation of the hydrothermally altered MM3 deposits. Regardless of this, the MM1 glasses show some overlap with both the LBT and IBT, although they are dominated by subtly more evolved glass compositions, particularly with respect to those LBT-IBT on Lipari (Fig. 8). There is significant geochemical overlap between the LBT and MM2 glasses (Fig. 8), whilst the IBT appear to show subtle offsets, for instance MM2 glasses do not fully satisfy the higher K_2O (Fig. 7C) or lower TiO_2 observed in the IBT glasses. Whilst a link between the MM1

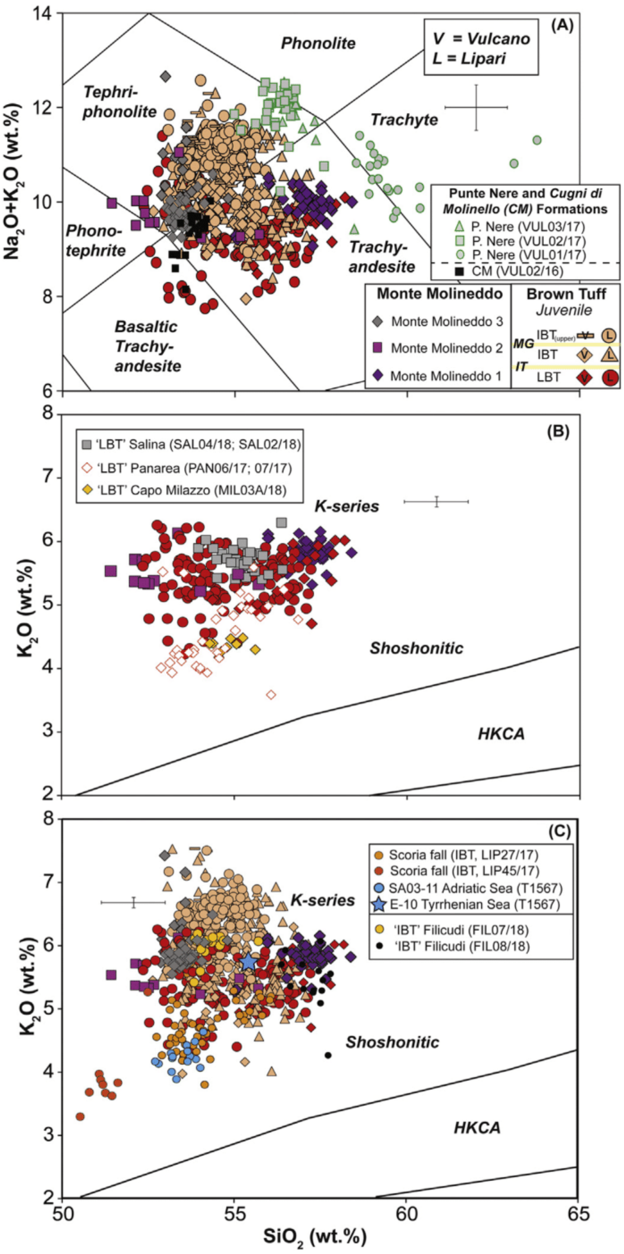

Fig. 7. Major element glass geochemical variation diagrams for the juvenile component of the LBT, IBT and IBT 'upper' outcropping on Lipari and Vulcano compared to near-vent deposits on Vulcano and distal tephra layers. The near-vent eruption deposits on Vulcano considered responsible for the LBT and IBT are Monte Molineddo 1–3. Also shown are the proximal deposit of the younger Punte Nere succession and the Cugni di Molinello (CM). Here more distal occurrences of the LBT and IBT units focus on deposits found outcropping across the archipelago on Salina, Panarea, Filicudi and Capo Milazzo (Sicily). The similarity between fallout components of the IBT deposits and a distal marine tephra layers in the Tyrrhenian (Paterne et al., 1988) and Adriatic Seas (Matthews et al., 2015) is explored. (A) TAS classification diagram of LBT and IBT glasses, (B, C) SiO_2 vs K_2O classification diagrams of the LBT and IBT deposits and distal equivalents. Error bars represented 2*standard deviations of replicated analyses of the StHs6/80-G secondary standard glass run alongside the BT samples.

and the earliest LBT cannot be completely excluded, an assignment of the MM2 as a near-source counterpart of the LBT on Vulcano seems the most probable, consistent with the reconstructed chrono-stratigraphy. Indeed, the correlation is also supported by the occurrence of a layer of grey pumice lapilli (VUL05/18) observed within the MM2 (Fig. 4; sec. 2 on Vulcano). These lapilli display glass compositions consistent with those of the GPT from Salina, which critically is also found interlayered within the LBT on Lipari (Fig. 9), Salina and Panarea (See Section 5.4).

Coarse proximal MM3 scoria fall (sample BT03/20), along with the more evolved component of a black to yellowish MM3 scoria fall deposits traced to southern Vulcano (Gelso; VUL04/17), are consistent with the IBT (Fig. 7-8). The proximal MM3 (BT03/20) glasses are chemically consistent with the least evolved ash deposits of the IBT observed on both Vulcano and Lipari (Fig. 8), while the most evolved scoria (54.4 wt% SiO_2) analysed displays higher K_2O, and lower CaO and MgO content consistent with the dominant IBT glass compositions (Fig. 8D-F). These proximal MM3 scoria fall (BT03/20) also shows broad chemical consistency with the scoria fall identified within the IBT on Lipari (Fig. 8), albeit these MM3 glasses are offset to higher K_2O content (Fig. 7C). MM3 fall sampled in southern Vulcano (Gelso) is bimodal, while one population is more primitive (~ 49 wt% SiO_2) than the IBT deposits, the second is chemically consistent with the IBT glasses, even extending to the same more elevated K_2O contents, and further supporting a link between the MM3 and the IBT (Fig. 7C; 8D-F). Combining the proximal and medial MM3 scoria fall data reveals a substantial compositional variability, and this variability appears to correspond to a significant proportion of overall IBT chemical variability observed. However some of the more evolved IBT glass compositions are not satisfied by the available MM3 data, and again this is likely to reflect MM3 preservation related sampling biases. Both in terms of limited stratigraphic coverage of the proximal MM3 succession sampled, and the associated difficulties of being able to chemically compare the same lithofacies. For instance, proximal MM3 alternates between scoria fall and ash-rich PDC deposits, here we are only able to analyse the fresh scoria fall, whilst the IBT characterised clearly relate to PDCs. Overall, there is sufficient chemical agreement to support the chrono-stratigraphic link between the MM3 and the IBT.

Our geochemical dataset shows that the juvenile UBT glasses (trachy-andesites to trachytes) are very similar to glass compositions of the early to intermediate products of La Fossa cone, namely the Punte Nere and Grotta dei Palizzi deposits (Fig. 6). Interestingly, volcanic glasses of the Punte Nere pyroclastic succession can be chemically distinguished and lie on separate evolutionary trends (Fig. 6). The lowermost Punte Nere (VUL01/17) deposits, and ultimately the earliest La Fossa products recognized in the volcanic stratigraphy, are entirely consistent with the UBT (Fig. 6). Whilst these lowermost Punte Nere deposits are slightly more evolved than the products of the youngest UBT depositional unit (Bt16), they are entirely consistent with the older Bt13 deposits sampled across Vulcano and Lipari, and the Bt15 deposits (Fig. 6). This geochemical link is important given that the Punte Nere pyroclastics are massive to cross-laminated, dark grey ash deposits, lithologically very similar to UBT, yet direct stratigraphical relationships between the two successions are lacking in the field (Fig. 2). The geochemical similarity between the UBT and the earliest Punte Nere products suggests that the UBT may be associated with the earliest activities of the La Fossa cone too, probably sharing the same magmatic plumbing system. It is even plausible that some of the older Punte Nere products recognized in the field may actually equate to the uppermost UBT. Either way this outlines a direct relationship between the UBT and the active La Fossa cone which was not fully demonstrated by previous studies, and illustrates a possible continuity in the evolution of the magmatic and eruptive system of La Fossa cone starting (at least) from the onset of UBT activity at ~24 ky, which extends its life cycle.

As highlighted, the glass compositions within the basal Punte Nere succession are variable. Whilst the oldest Punte Nere deposits (VUL01/17), are chemically consistent with the UBT, the overlying Punte Nere glasses analysed (VUL02/17; VUL03/17) are offset in terms of their CaO, MgO and K_2O content (Fig. 6). Interestingly, these glasses, and those of the younger Grotta dei Palizzi successions (cf. (Albert et al., 2012)), lie on the same evolutionary trends as the older IBT glasses,

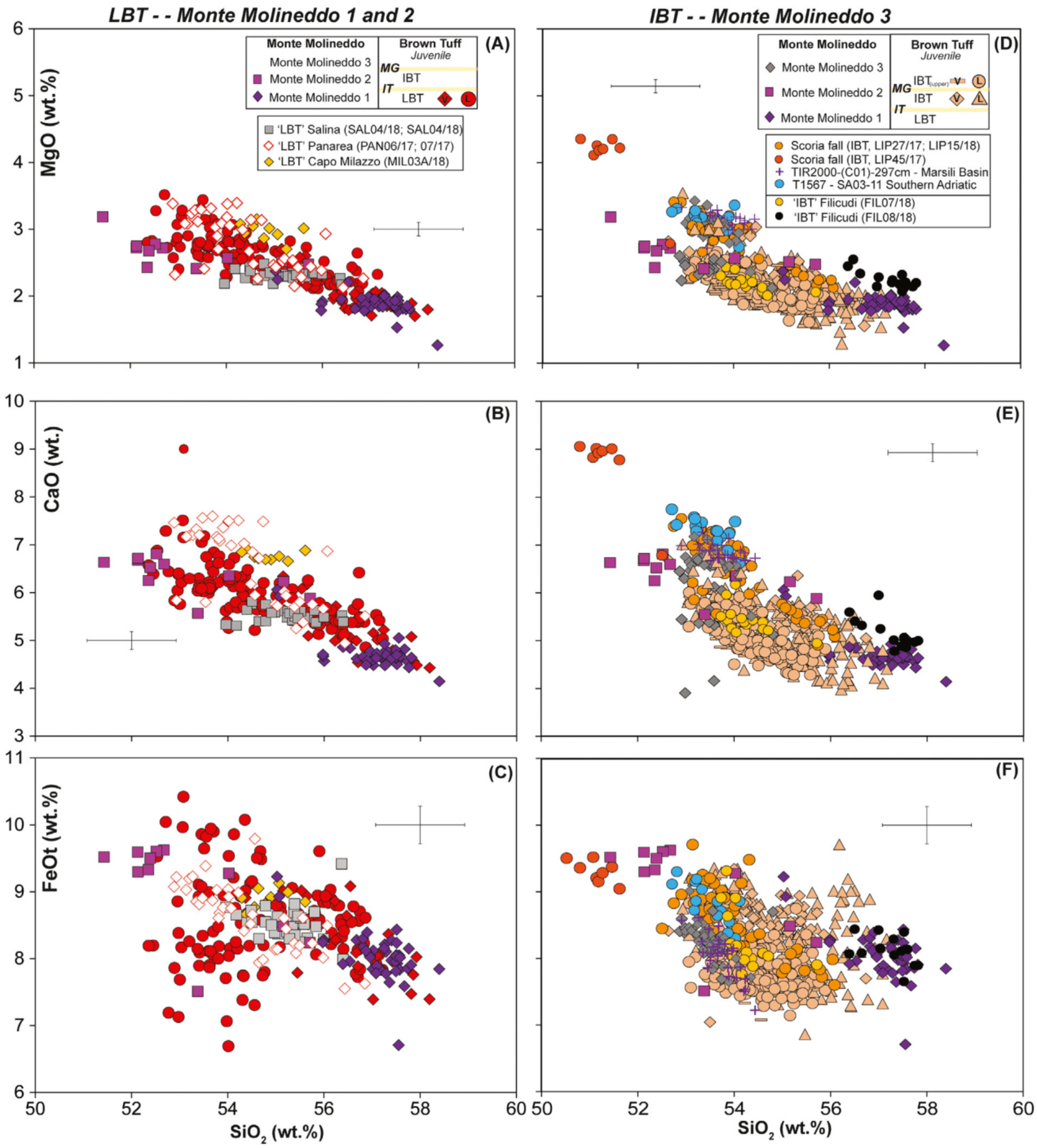

Fig. 8. Major element glass geochemical variation diagrams for the juvenile component of the LBT, IBT and IBT 'upper' outcropping on Lipari and Vulcano compared to near-vent deposits on Vulcano and distal tephra layers found on the neighboring islands and in the marine setting. LBT are considered in the context of Monte Monlineddo 1 and 2 units on Vulcano, whilst the IBT are compared to the limited glass data available for the Monlineddo 3 unit. Error bars represented 2*standard deviations of replicated analyses of the StHs6/80-G secondary standard glass run alongside the BT samples.

albeit extending to more evolved end-member (Fig. 6). Our heterogeneous Punte Nere data, which are consistent with published Punte Nere and Grotta dei Palizzi glass data (Fig. 6), suggest that the La Fossa explosive activity at this time was fed by a complex magmatic system comprising of more than one magma batch.

5.4. Proximal-medial-distal correlations

5.4.1. BT occurrences on Salina, Panarea, Filicudi and Capo Milazzo (Sicily)

Here we use new glass analyses (Supplementary Material B) of BT occurrences from across the Aeolian archipelago (Salina, Filicudi and Panarea) and Capo Millazzo (Sicily) to help constrain the dispersal of volcanic ash associated with the successive eruptions on Vulcano. Considerable geochemical overlap between the juvenile glass components of the LBT and IBT macro units (Section 5.1) means that correlations rely on the stratigraphic context at individual localities throughout the Aeolian islands, and often relying upon key stratigraphic markers beds (e.g., the Ischia Tephra or GPT).

BT depositional units observed on Salina underlying the Ischia tephra in the stratigraphic window of the LBT have relatively homogeneous glass chemistries that overlap with the glasses of the LBT elsewhere, and the proximal MM1–2 on Vulcano (Fig. 7B; Fig. 8A-C). These LBT deposits observed on Salina lack secondary glass components from the underlying strata, coherent with their occurrence on the lava flows related to the

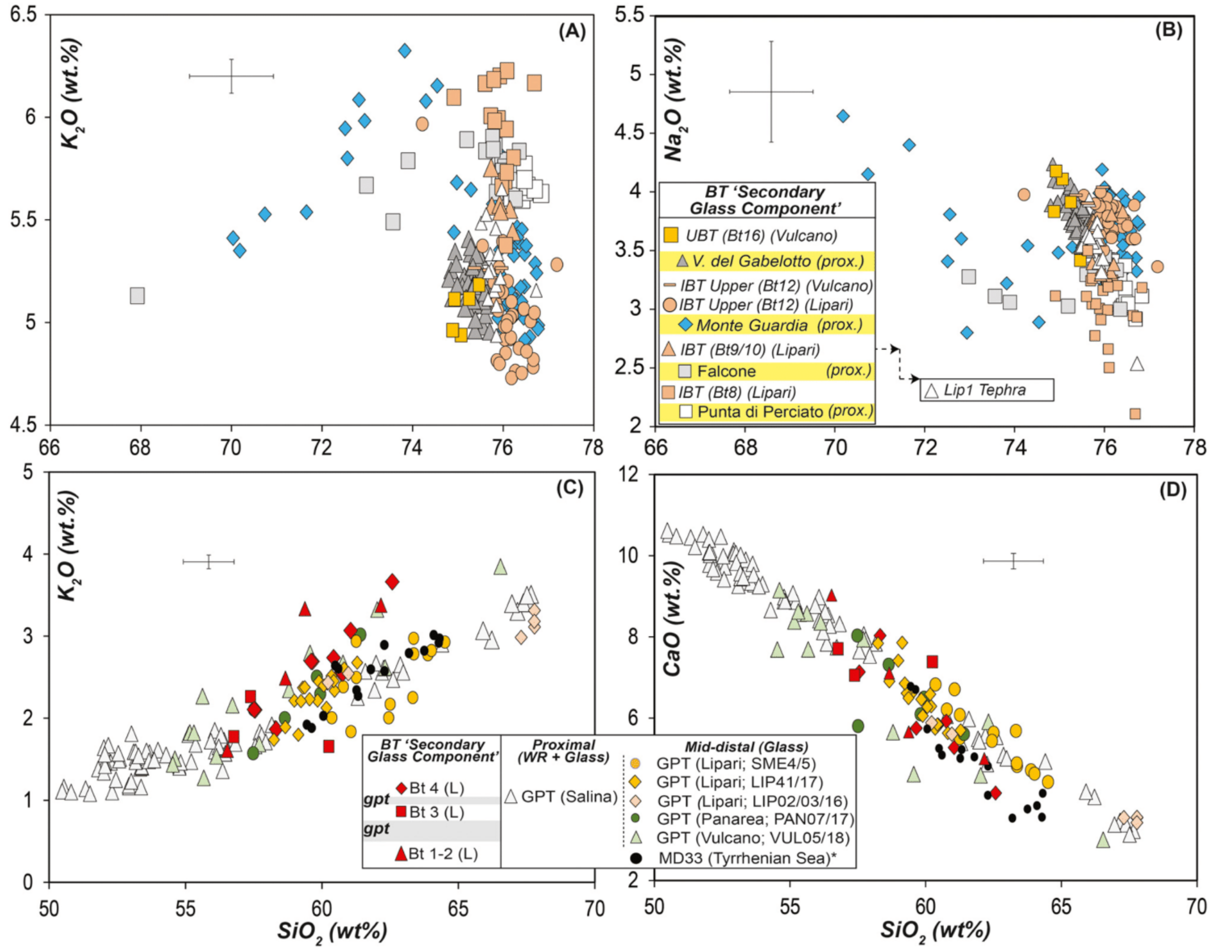

Fig. 9. Major element geochemical variability diagram of the secondary glass components found within a selection of BT depositional units outcropping primarily on Lipari, but also Vulcano. These minor populations are chemically related to the underlying stratigraphic units which were subject to clast embedding and erosion processes. Error bars represented 2*standard deviations of replicated analyses of the StHs6/80-G secondary standard glass run alongside the BT samples.

final activity of Monte dei Porri stratocone dated at 67–57 ky (Lucchi et al., 2013a) and the absence of significant abrasion effects.

Ash deposits chemically consistent with the LBT and IBT are recognized on Panarea and these are attributed to the former owing to the presence of GPT from Salina interbedded within (Fig. 7B; 8A-C). Deposits with relatively homogeneous glasses consistent with the LBT also outcrop on Capo Milazzo peninsula (Fig. 7B; 8A-C), although without the stratigraphic constraints coming from other tephra marker beds, a link to the IBT cannot be excluded. This highlights the importance of external chrono-stratigraphic markers, or dating (^{14}C) to constrain the timing of the source eruptions on Vulcano and their associated ash dispersals.

K-series ash deposits on Filicudi island (FIL07/18), northwest of Vulcano, are entirely consistent with the LBT and IBT glass compositions (Fig. 7C; Fig. 8D-F). However, based on their stratigraphic position above the Ischia tephra these deposits are firmly attributed to the activity of the IBT. A second Filicudi ash unit (FIL08/18) is also interpreted as IBT based on its position above the Ischia tephra and its glass compositions being broadly consistent with the most evolved IBT (Fig. 8D-F).

5.4.2. Possible BT occurrences in the sedimentary records of the Central Mediterranean

Given their significant near-source thickness on Vulcano and Lipari and wide distribution throughout the Aeolian Islands (Salina, Panarea and Filicudi), the successive BT depositional units potentially represent the source equivalents of volcanic ash layers recorded in sedimentary archives (marine and lacustrine) across the Central Mediterranean. The region has a well-established distal tephrostratigraphic framework (e.g., Keller et al., 1978; Calanchi et al., 1998; Giaccio et al., 2017; Paterne et al., 1988; Kraml et al., 1997; Sulpizio et al., 2010; Wulf et al., 2004) with many widespread ash layers tied into the well-dated eruption stratigraphies of the productive central Mediterranean volcanoes, particularly those in Campania (e.g., Campi Flegrei, Ischia). Therefore, the identification of BT deposits within this tephrostratigraphic framework would not only provide information on the distribution and scale of explosive activity on Vulcano, it also offers chronological constraints on the timing of eruptions on the island. With some exceptions, the presence of BT deposits in regional sedimentary archives is largely underexplored (e.g. (Albert et al., 2012; Calanchi et al., 1994; Di Roberto et al., 2008; Paterne et al., 1988; Tamburrino et al., 2016)), probably due to an inadequate knowledge of their stratigraphy, and most importantly their geochemical (juvenile glass) signatures, essential to reliable source attributions. Here we use our extensive volcanic glass dataset to evaluate the distribution and timing of distal BT occurrences.

In the chrono-stratigraphic window of the LBT (80–56 ky), Tyrrhenian (and Adriatic) Sea marine cores, including those investigated by Paterne et al., (1986); Paterne et al., (1988), do not reveal any obvious ash layers candidates for distal LBT in the deep-sea realm. In terms of IBT and UBT occurrences, Tamburrino et al., (2016) explored the ash deposits preserved in the Marsili Basin core, MD01–2474G (Fig. 1a), situated on a topographic high. They proposed the possible occurrence of ash layers associated with the IBT (MD27, MD22, MD15) and UBT (MD11 and MD3) eruptions, although it is worth noting that these correlations were made in the absence of reliable BT reference glass data. Albert et al., (2012) reported the occurrence of 'pre-La Fossa' Vulcano tephra (TIR2000–50 cm) in another Marsili Basin core, TIR2000-C01 (Fig. 1a), situated more than 20 km ENE of the Stromboli Canyon mouth, a major source of volcaniclastic material into the Basin. The Marsili Basin captures volcaniclastic turbidites relating to pyroclastic material deposited on the islands, and directly into the marine environment, consequently we carefully re-evaluate the available data from these Marsili cores. Unfortunately, with TIR2000-C01, the age of ash layers below the Soccavo 1 tephra (Campi Flegrei) at ~12 ky (TIR2000-93 cm) were not well constrained in the absence of reliable chrono-stratigraphic or biostratigraphic markers. Conversely, the Marsili core MD01–2474G has a more reliable chronology developed using radiocarbon dating, and orbitally-tuned chronological tie-points (Tamburrino et al., 2016). Broad agreement exists between the independent chronology of the record and the preferred ages of key chrono-stratigraphic markers, particularly those in the deeper portion of the core. For instance, layer MD28 (54.8 ky) correlates to the widespread marine ash layer, the Y-7, equivalent to the Ischia Tephra, dated at 56.1 ± 1.0 ky (Giaccio et al., 2017), thus providing a direct tie-point between the onland BT stratigraphy and the marine core. Furthermore, our GPT (Salina) glass data corroborates its distal occurrence in MD01–2474G (MD33 [58.9 ky]; Fig. 9C-D), offering another terrestrial-marine chrono-stratigraphic tie point. Crucially, co-located tephras in the Marsili cores now facilitate the transfer of age information from MD01–2474G to TIR2000-CO1.

The oldest ash layer in MD01–2474G, MD27, previously linked to the IBT (Tamburrino et al., 2016), comprises a dominant component of transitional HKCA/SHO trachy-andesitic glasses. This layer is dated using the cores age-model at 42.7 ky, an age which is further corroborated by the presence of a secondary Pantellerite glass shards linked to the Pantelleria Green Tuff (Tamburrino et al., 2016) that is $^{40}Ar/^{39}Ar$ dated at 45.7 ± 1.0 ky ([95.4%]; (Scaillet et al., 2013)). Compared to our juvenile BT data it is apparent that these SHO glasses are generally too low in K_2O content, and too high in TiO_2 to be associated with IBT activity on Vulcano (Fig. 10). Glass data indicates they reside on an evolutionary trend more akin to glasses erupted on Stromboli during the Paleostromboli epoch, rather than the central sector of the Aeolian archipelago.

Ash layer MD22 (MD01–2474G) dated at 36.9 ky was linked to the IBT (Tamburrino et al., 2016), our data clearly indicate that this layer is inconsistent with the IBT the and Vulcano magmatic system (Fig. 10). Tamburrino et al. (Tamburrino et al., 2016) linked this 8.3 cm thick tephra deposit to a layer in TIR2000-C01, namely TIR2000–417 cm. Here we suggest that there is better chemical agreement between MD22 and the overlying tephra in TIR2000-C01, TIR2000–398 cm, a 20 cm thick coarse-grained volcaniclastic turbidite (Albert et al., 2012; Di Roberto et al., 2008). MD22 appears to contain both chemical components of the TIR2000–398 cm deposit (Fig. 10), the transitional CA/HKCA glasses which extend from basaltic-andesites through andesites and dacites, to a low-SiO_2 rhyolites (Component-1), and HKCA basaltic-andesites (Component-2). This clear chronological tie-point between MD01–2474G and TIR2000-C01 means we can import the MD01–2474G age of 36.9 ky to the TIR2000–398 cm tephra unit. This offers useful chronology to the basal sediments of TIR2000-C01, critical when assessing the age of other ash deposits in this core. The sedimentological features of MD22/TIR2000–398 cm, including grain-size and layer thickness, combined with the different chemical arrays observed, indicate this deposit is linked with a major volcanic collapse. The data from this deposit are clearly inconsistent with Vulcano and the central sector of the Aeolian archipelago. The high TiO_2 content of the glasses (Fig. 10B) may prompt future investigations of a link to one of the many collapse events to have occurred on Stromboli island (Francalanci et al., 2013).

MD15 (29.7 ky) in MD01–2474G, a 10.8 cm thick tephra, was linked to IBT activity on Vulcano, its trachy-andesitic glasses are transitional between HKCA/SHO (Tamburrino et al., 2016). Importantly these glasses display lower K_2O content than the IBT volcanic glasses at overlapping SiO_2 content, and more elevated TiO_2 content is again inconsistent with the BT and Vulcano (Fig. 10). Two trachy-andesite ash layers, MD11 (16.7 ky) and MD3 (6.9 ky), in the MD01–2474G core were attributed to the 'Tufi di Grotte dei Rossi inferiori', here equivalent to the UBT (Tamburrino et al., 2016). Whilst both layers display glasses that overlap with those of the UBT, they show more elevated TiO_2 content at particular SiO_2 contents, which is again more consistent with Stromboli than the UBT and Vulcano (Fig. 10B).

Returning to Marsili core TIR2000-C01, in light of new age constraints, with 36.9 ky placed on the coarse-grained volcaniclastic turbidite (CGVT; TIR2000–398 cm = MD22), we are able to evaluate the timing of potential distal BT deposits found in the core stratigraphically above this CGVT. Between the Campi Flegrei tephra Soccavo 1 (TIR2000-93 cm) found at 93 cm depth in TIR2000-C01, and the CGVT (TIR2000–398) at 398 cm a crude sedimentation rate of 12.4 cm/ky^{-1} is calculated. This is a noticeable increase from a rate of 7.72 cm/ky^{-1} observed in the upper portion of the core between the 776 CE Monte Pilato tephra from Lipari (TIR2000-7 cm), found at depth of 7 cm, and the Soccavo 1 (TIR2000-93 cm). However, given the frequent occurrence of volcaniclastic turbidity current deposits (Di Roberto et al., 2008), a highly variable sedimentation rate is expected; indeed, such variability was also recognized in Marsili core MD01–2474G (Tamburrino et al., 2016). Without calculating an event-free sedimentation rate, our TIR2000-C01 tephra age estimates are tentative.

Many ash rich, volcaniclastic turbidites within TIR2000-C01 have not been chemically characterised (Albert et al., 2012; Di Roberto et al., 2008), here we provide new glass data from some which reinforce the occurrence of marine deposits chemically consistent with the BT in the Marsili Basin, and highlight the need for future investigations of similar sedimentary successions from the southern Tyrrhenian Sea. A thin (3 mm) ash deposit sampled at a depth of 297 cm, TIR2000-297 cm, has a homogeneous K-Series (Fig. 10), basaltic trachy-andesite to trachy-andesite affinity, with an age of ~28.7 ky. The glass compositions are generally consistent with the eruptive products of the IBT on Lipari, and in particular the diffuse scoria fall (LIP27/17; Fig. 8D-F) observed in the depositional unit above the Falcone dome (~43–40 ky), although we must acknowledge a subtle offset in FeOt content (Fig. 8F). With an age of ~28.7 ky for TIR2000-297 cm we tentatively suggest this marine tephra pre-dates the widespread 25,885–27,055 cal y BP Monte Guardia eruption, and therefore it is plausible that the tephra relates to IBT activity preserved on Lipari Island between the local Falcone and Monte Guardia tephra beds (Bt10 or Bt11).

Stratigraphically higher in the TIR2000-C01 succession, a thin (2 mm) ash rich tephra, TIR2000-160 cm, has a relatively heterogeneous (57.4–61.4 wt% SiO_2) K-series (Fig. 10), trachy-andesite to trachyte compositions with an age of ~16.7 ky. These glasses are entirely consistent with the UBT on Vulcano, whilst restricted by a limited number of analyses the compositional variability and chrono-stratigraphic position means a link to the eruptions responsible for Bt13 is most likely (Fig. 6). This marine tephra reinforces a chemical link to the La Fossa magmatic system deeper in time.

The K-series trachytic tephra TIR2000–50 (Fig. 10) has an age of ~6.7 ky, and its origin was the focus of previous debate. (Di Roberto et al., 2008) initially attributed this layer to a collapse during the Secche di Lazzaro eruption on Stromboli (Neostromboli epoch). However, chemical investigations revealed that this tephra was actually more

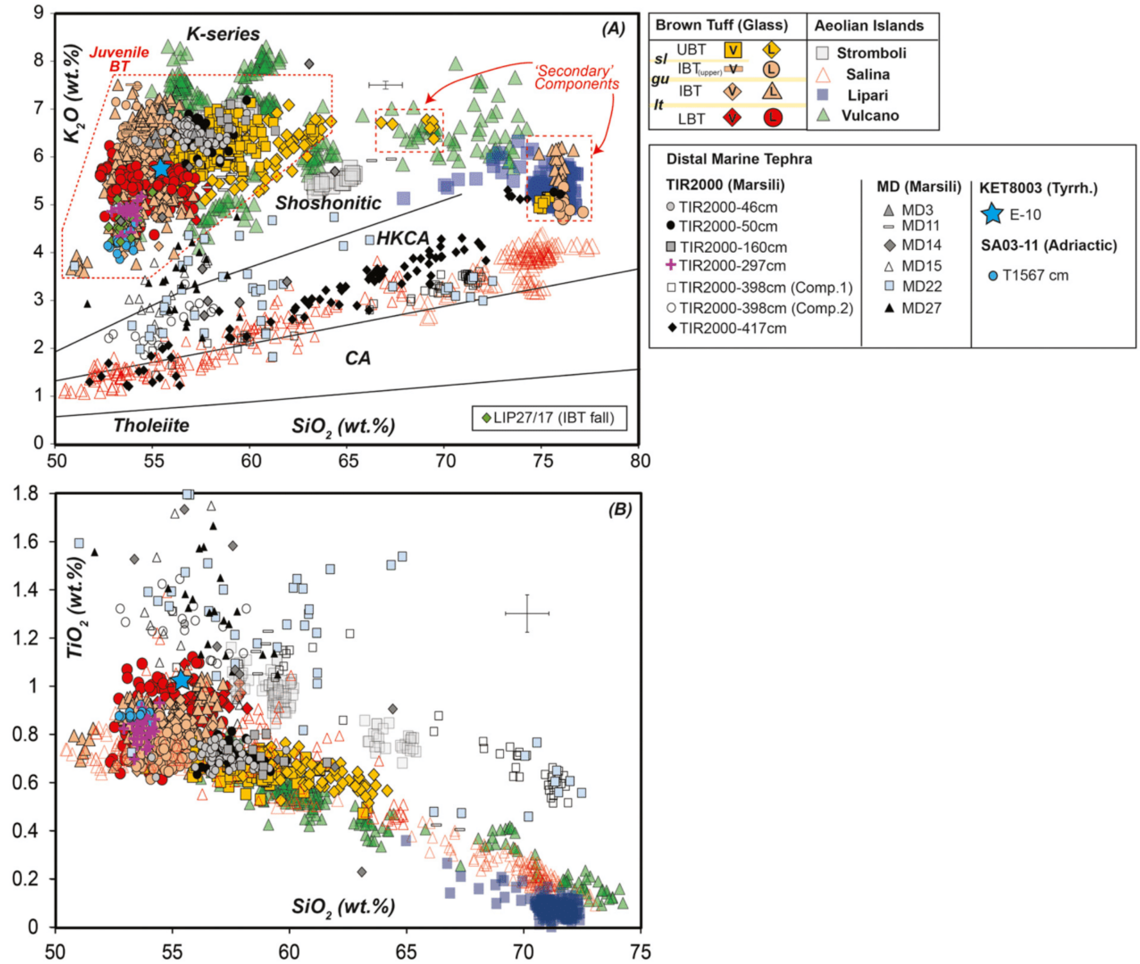

Fig. 10. Major element geochemical variability of the BT deposits compared to marine tephra deposits considered here to be related to the BT eruption units, or have been previously ascribed as distal BT deposits in the literature. (A) SiO_2 vs K_2O classification diagram; (B) SiO_2 vs. TiO_2 diagnostic plot used for distinguishing the potassic eruptive products of Vulcano and Stromboli, and very useful when considering the provenance of distal marine tephra layers associated with the two islands. Error bars represented 2*standard deviations of replicated analyses of the StHs6/80-G secondary standard glass run alongside the BT samples. TIR2000 Marsili Basin cores samples are from Albert et al., (2012) and Albert (2012) (Thesis); the MD Marsili Basin marine tephra layers are from Tamburrino et al., (2016), the marine layers E-11 (Tyrrhenian Sea) and T1567 (Adriatic) are reported in Paterne et al., (1988) and Matthews et al., (2015) respectively.

consistent with the eruptive products of Vulcano (Albert et al., 2012; Albert et al., 2017). Based on the diagnostic lower TiO_2 content of these volcanic glasses they were akin to the evolutionary trend of Vulcano products and thus suggested pre- or early La Fossa activity (Fig. 10B). Interestingly, the dominant K-series glasses are consistent with the UBT (Fig. 10A), whilst a secondary glass component of HKCA rhyolites are consistent with those of the Vallone del Gabellotto (Lipari). This feature is consistent with the onland Bt16 depositional unit, immediately overlying the Vallone del Gabellotto (8.7–8.4 ky) tephra on Vulcano. A correlation of TIR2000–50 cm to Bt16 would be consistent with the chrono-stratigraphy given the marine tephra deposits age (~6.7 ky). The overlying TIR2000-46 cm unit is compositionally indistinguishable from the dominant K-series component of the underlying TIR2000–50 (Fig. 10), although this younger tephra (~6.1 ky) has no secondary rhyolitic component. It is plausible that this tephra also relates to the Bt16, and would imply that Bt16 depositional unit is the product of more than one eruption. These correlations give us new age constraints for the youngest portion of the UBT on Vulcano, which post-date the 8.5 ky (radiocarbon) age obtained by De Astis et al., (1997).

Away from the Marsili Basin, two noticeable distal occurrences of potential IBT are worthy of discussion. The E-10 Tyrrhenian Sea ash layer preserved in KET8003 north of Salina (Fig. 1a) and dated to 35.2 ky (Paterne et al., 1988) appears to have a glass chemistry (Fig. 10) and chrono-stratigraphic position consistent with the IBT positioned between the Falcone and Monte Guardia tephra deposits outcropping on Lipari. Matthews et al., (2015) reported a basaltic trachy-andesite tephra, T1567, dated at between 35,693–34,064 cal y BP in the Southern Adriatic (core SA03–11; Fig. 1a) and positioned immediately above the 40 ky Campanian Ignimbrite (Y-5/C-13) tephra. The glass compositions of this tephra are entirely consistent with those of the IBT, and specifically to the diffuse scoria fall observed in the IBT above the 43–40 ky Falcone dome on Lipari (LIP27/17; LIP15/18; LIP16/18). The chrono-stratigraphy of this correlation is compelling and indicates a widespread ash fall event associated with the IBT at ~35 ky. Whilst there are clear chemical differences between the E-10 and T1567, their ages (~ 35 ky) are entirely compatible, indicating that the two distal tephra layers may reflect either; (1) closely spaced eruptions or eruptive phases on Vulcano, which cumulatively form part of the IBT eruptive cycle; or (2) different eruptive processes during the same IBT eruption. According to this hypothesis, the E-10 (Tyrrhenian Sea) marine tephra, which is chemically compatible with the IBT emplaced from PDCs across Lipari at this time, may relate to ash fall from a co-PDC plume. While in contrast T1567 (Adriatic Sea), is compositionally consistent with a phase of scoria fall embedded within these PDC deposits on Lipari and perhaps reflects ash dispersed from a quasi-sustained eruptive column. This would be consistent with the observed lithological features of the IBT and their likely proximal counterpart in Vulcano, the MM3, which are characterised by ash layers from PDCs, alternated with scoria lapilli fall.

6. Conclusions

Revised stratigraphic investigations combined with new radiocarbon ages and a large dataset of grain-specific volcanic glass compositional data for the different depositional units of the ash-rich Brown Tuffs (BT) on Lipari and Vulcano provide constraints on their large-scale correlations across the Aeolian archipelago and the southern Tyrrhenian Sea, along with insights for hazard assessments. The main outcomes of this work are the following:

(1) Juvenile BT eruptive material displays relatively homogeneous glass compositions, particularly in the case of individual depositional units. Overall these units range from basaltic trachy-andesites and trachy-andesites to trachytes, broadly evolving through the succession, with the most evolved glass compositions observed in the UBT macro unit. The LBT (80–56 ky) and IBT (56–24 ky) macro units are most challenging to chemically distinguish, with alkali variability most diagnostic. While the UBT macro unit can be distinguished on the basis that their glasses display higher SiO_2 and extend to lower TiO_2, CaO, MgO and FeOt contents.

(2) Secondary glass compositions within some of the BT depositional units are related to a minor component of embedded pumice and/or scoriae from the underlying incoherent pyroclastic units during the emplacement of the PDCs that deposited the BT in proximal-medial areas.

(3) The time interval of the eruptions that deposited the UBT has been re-defined to between 24 and 6 ky based on the observed chemo-stratigraphic transitions which coincides with the age of the Spiaggia Lunga marker bed on Vulcano, and thus replaces the older previously adopted Monte Guardia stratigraphic marker.

(4) Correlations between the LBT, IBT and UBT macro-units and proximal units on Vulcano are proposed, providing a more robust framework for the long-term hazard assessment related to explosive activity within the La Fossa Caldera. A clear geochemical link is suggested between the UBT and the early products of the La Fossa cone, suggesting a shared magmatic system during the last 24 ky, and thus extending the life cycle of this currently active eruptive source area.

(5) Unequivocal evidence that ash deposits preserved across the Aeolian archipelago and in Tyrrhenian and Adriatic Sea marine cores are chemically consistent with the IBT and UBT erupted on Vulcano offers important insights into the scale of these eruptions and the associated hazards.

Declaration of Competing Interest

The authors declare that they have no known competing financial interests or personal relationships that could have appeared to influence the work reported in this paper.

Acknowledgements

SM funded through a PhD Scholarship of the University of Bologna-Alma Mater Studiorum. PGA is funded through a UKRI Future Leaders Fellowship (MR/S035478/1). We thank Gianfilippo De Astis and another Anonymous Reviewer for their constructive comments.

Appendix A. Supplementary data

Supplementary data to this article can be found online at https://doi.org/10.1016/j.jvolgeores.2020.107079.

References

Albert, P.G., Tomlinson, E.L., Smith, V.C., Di Roberto, A., Todman, A., Rosi, M., Marani, M., Muller, W., Menzies, M.A., 2012. Marine-continental tephra correlations: volcanic glass geochemistry from the Marsili Basin and the Aeolian Islands, Southern Tyrrhenian Sea, Italy. J. Volcanol. Geotherm. Res. 229-230, 74–94.

Albert, P.G., Tomlinson, E.L., Smith, V.C., Di Traglia, F., Pistolesi, M., Morris, A., Donato, P., De Rosa, R., Sulpizio, R., Keller, J., Rosi, M., Menzies, M., 2017. Glass geochemistry of pyroclastic deposits from the Aeolian Islands in the last 50 ka: a proximal database for tephrochronology. J. Volcanol. Geotherm. Res. 336, 81–107.

Barberi, F., Gasparini, P., Innocenti, F., Villari, L., 1973. Volcanism of the Southern Tyrrhenian Sea and its geodynamic implications. J. Geophys. Res. 78, 5221–5232.

Beccaluva, L., Gabbianelli, G., Lucchini, F., Rossi, P.L., Savelli, C., 1985. Petrology and K/Ar ages of volcanics dredged from the Aeolian Seamounts: implications for geodynamic evolution of the southern Tyrrhenian basin. Earth Planet. Sci. Lett. 74, 187–208.

Bergeat, A., 1899. Die Äolischen Inseln (Stromboli, Panaria, Salina, Lipari, Vulcano, Filicudi und Alicudi). Abh. Math. Phys. Kl. Kgl. Bayer. Akad. Wiss. 20, 274 I. Abt., München.

Biass, S., Scaini, C., Bonadonna, C., Folch, A., Smith, K., Höskuldsson, A., 2014. A multi-scale risk assessment for tephra fallout and airborne concentration from multiple Icelandic volcanoes-part 1: hazard assessment. Nat. Hazar. Earth Syst. Sci. discuss. 2, 2463–2529.

Bonasia, R., Costa, A., Folch, A., Macedonio, G., Capra, L., 2012. Numerical simulation of tephra transport and deposition of the 1982 El Chichón eruption and implications for hazard assessment. J. Volcanol. Geotherm. Res. 231-232, 39–49.

Brock, F., Higham, T., Ditchfield, P., Ramsey, C.B., 2010. Current pretreatment methods for AMS radiocarbon dating at the Oxford Radiocarbon Accelerator Unit (ORAU). Radiocarbon 52, 103–112.

Bronk Ramsey, C., 2009. Bayesian analysis of radiocarbon dates. Radiocarbon 51 (1), 337–360.

Calanchi, N., Gasparotto, G., Romagnoli, C., 1994. Glass chemistry in volcaniclastic sediments of ODP Leg 107, Site 650, sedimentary sequence: provenance and chronological implications. J. Volcanol. Geotherm. Res. 60, 59–85.

Calanchi, N., Cattaneo, A., Dinelli, E., Gasparotto, G., Lucchini, F., 1998. Tephra layers in Late Quaternary sediments of the central Adriatic Sea. Mar. Geol. 149, 191–209.

Caron, B., Siani, G., Sulpizio, R., Zanchetta, G., Paterne, M., Santacroce, R., Tema, E., Zanella, E., 2012. Late Pleistocene to Holocene tephrostratigraphic record from the Northern Ionian Sea. Mar. Geol. 311-314, 41–51.

Chiarabba, C., De Gori, P., Speranza, F., 2008. The Southern Tyrrhenian Subduction Zone: deep geometry, magmatism and Plio-Pleistocene evolution. Earth Planet. Sci. Lett. 268, 408–423.

Cicchino, A., Zanella, E., De Astis, G., Lanza, R., Lucchi, F., Tranne, C.A., Airoldi, G., Mana, S., 2011. Rock magnetism and compositional investigation of Brown Tuffs deposits at Lipari and Vulcano (Aeolian Islands – Italy). J. Volcanol. Geotherm. Res. 208, 23–28.

Crisci, G.M., De Rosa, R., Lanzafame, G., Mazzuoli, R., Sheridan, M.F., Zuffa, G.G., 1981. Monte guardia sequence: a late-pleistocene eruptive cycle on lipari (Italy). Bull. Volcanol. 44, 241–255.

Crisci, G.M., Delibrias, G., De Rosa, R., Mazzuoli, R., Sheridan, M.F., 1983. Age and petrology of the Late-Pleistocene Brown Tuffs on Lipari. Italy. Bull. Volcanol 46, 381–391.

Crisci, G.M., De Rosa, R., Esperanca, S., Mazzuoli, R., Sonnino, M., 1991. Temporal evolution of a three component system: the island of Lipari (Aeolian Arc, southern Italy). Bull. Volcanol. 53, 207–221.

De Astis, G., Frazzetta, G., La Volpe, L., 1989. I depositi di riempimento della caldera del Piano ed i depositi della Lentia. Bollettino GNV 2, 763–778.

De Astis, G., Dellino, P., De Rosa, R., La Volpe, L., 1997. Eruptive emplacement mechanism of fine grained pyroclastic deposits widespread on Vulcano Island. Bull. Volcanol. 59, 87–102.

De Astis, G., Ventura, G., Vilardo, G., 2003. Geodynamic significance of the Aeolian volcanism (Southern Tyrrhenian Sea, Italy) in light of structural, seismological, and geochemical data. Tectonics 22 (4), 1–17.

De Astis, G., Lucchi, F., Dellino, P., La Volpe, L., Tranne, C.A., Frezzotti, M.L., Peccerillo, A., 2013. Geology, volcanic history and petrology of Vulcano (central Aeolian archipelago). Geological Society, London. Memoirs 37, 281–348.

De Rosa, R., Donato, P., Scarciglia, F., 2016. On the origin and post-depositional history of widespread massive ash deposits: the case of Intermediate Brown Tuffs (IBT) of Lipari (Aeolian Islands, Italy). J. Volcanol. Geotherm. Res. 327, 135–151.

Dellino, P., De Astis, G., La Volpe, L., Mele, D., Sulpizio, R., 2011. Quantitative hazard assessment of phreatomagmatic eruptions at Vulcano (Aeolian Islands, Southern Italy), as obtained by combining stratigraphy, event statistics and physical modelling. J. Volcanol. Geotherm. Res. 201, 264–384.

Di Roberto, A., Rosi, M., Bertagnini, A., Marani, M.P., Gamberi, F., Del Principe, A., 2008. Deep water gravity core from the Marsili Basin (Tyrrhenian Sea) records Pleistocene-Holocenic explosive events and instabilities of the Aeolian Island Archipelago, (Italy). J. Volcanol. Geotherm. Res. 177 (1), 133–144.

Dingwell, A., Rutgersson, A., 2014. Estimating volcanic ash hazard in European airspace. J. Volcanol. Geotherm. Res. 286, 55–66.

Ellam, R.M., Menzies, M.A., Hawkesworth, C.J., Leeman, W.P., Rosi, M., Serri, G., 1988. The transition from calc-alkaline to potassic orogenic magmatism in the Aeolian Islands, Southern Italy. Bull. Volcanol. 50, 387–398.

Forni, F., Lucchi, F., Peccerillo, A., Tranne, C.A., Rossi, P.L., Frezzotti, M.L., 2013. Stratigraphic and geological evolution of the Lipari volcanic complex (central Aeolian archipelago). Geol. Soc. Lond. Mem. 37, 213–279.
Francalanci, L., Taylor, S.R., McCulloch, M.T., Woodhead, J.D., 1993. Geochemical and isotopic variations in the calc-alkaline rocks of Aeolian arc, southern Tyrrhenian Sea, Italy: constraints on magma genesis. Contrib. Mineral. Petrol. 113, 300–313.
Francalanci, L., Lucchi, F., Keller, J., De Astis, G., Tranne, C.A., 2013. Eruptive, volcano-tectonic and magmatic history of the Stromboli volcano (north-eastern Aeolian archipelago). Geol. Soc. Lond. Mem. 37, 397–471.
Giaccio, B., Hajdas, I., Isaia, R., Deino, A., Nomade, S., 2017. High-precision 14C and 40Ar/39Ar dating of the Campanian Ignimbrite (Y-5) reconciles the time-scales of climatic-cultural processes at 40 ka. Sci. Rep. 7.
Gioncada, A., Mazzuoli, R., Bisson, M., Pareschi, M.T., 2003. Petrology of volcanic products younger than 42 ka on the Lipari–Vulcano complex (Aeolian Islands, Italy): an example of volcanism controlled by tectonics. J. Volcanol. Geotherm. Res. 122, 191–220.
Insinga, D.D., Tamburrino, S., Lirer, F., Vezzoli, L., Barra, M., De Lange, G.J., Tiepolo, M., Vallefuoco, M., Mazzola, S., Sprovieri, M., 2014. Tephrochronology of the astronomically- tuned KC01B deep-sea core, Ionian Sea: insights into the explosive activity of the Central Mediteranean area during the last 200 ka. Quat. Sci. Rev. 85, 63–84.
Jochum, K.P., Stoll, B., Herwig, K., Willbold, M., Hofmann, A.W., Amini, M., Aarburg, S., Abouchami, W., Hellebrand, E., Mocek, B., Raczek, I., Stracke, A., Alard, O., Bouman, C., Becker, S., Dücking, M., Brätz, H., Klemd, R., de Bruin, D., Canil, D., Cornell, D., de Hoog, C., Dalpé, C., Danyushevsky, L., Eisenhauer, A., Gao, Y., Snow, J.E., Groschopf, N., Günther, D., Latkoczy, C., Guillong, M., Hauri, E., Höfer, H.E., Lahaye, Y., Horz, K., Jacob, D.E., Kasemann, S.A., Kent, A.J.R., Ludwig, T., Zack, T., Mason, P.R.D., Meixner, A., Rosner, M., Misawa, K., Nash, B.P., Pfänder, J., Premo, W.R., Sun, W.D., Tiepolo, M., Vannucci, R., Vennemann, T., Wayne, D., Woodhead, J.D., 2006. MPI-DING reference glasses for in situ microanalysis: 581 New reference values for element concentrations and isotope ratios. Geochem. Geophys. Geosyst. 7 (2).
Keller, J., 1967. Alter und Abfolge der vulkanischen Ereignisse auf den Äolischen Inseln Bericht Naturforschenden Gesellschaft Freiburg. 57 pp. 33–67.
Keller, J., 1980a. The island of Salina. Rend. Soc. Ital. Mineral. Petrol. 36, 489–524.
Keller, J., 1980b. The Island of Vulcano. Rend. Soc. Ital. Mineral. Petrol. 36, 369–414.
Keller, J., 1981. Quaternary tephrochronology in the Mediterranean region. In: Self, S., Sparks, S.R.J. (Eds.), Tephra Studies. NATO, Advanced Study Institutes Series C 75. D. Reidel Publishing Company, Dordrecht, pp. 227–244.
Keller, J., Ryan, W.B.F., Ninkovich, D., Altherr, R., 1978. Explosive volcanic activity in the Mediterranean over the past 200,000 years as recorded in deep-sea sediments. Geol. Soc. Am. Bull. 89, 591–604.
Kraml, M., Keller, J., Henjes-Kunst, F., 1997. Dating of Upper Quaternary Deep-sea Sediments from the Ionian Sea (Eastern Mediterranean) with Laser 40Ar/39Ar Analyses on Prominent Tephra Layers. EUG 9 (European Union of Geosciences), Strasbourg (France) 23–27 March 1997. Terra Nova 9, Abstract Supplement. 1 p. 406.
Le Pennec, J.L., Ruiz, G.A., Ramón, P., Palacios, E., Mothes, P., Yepes, H., 2012. Impact of tephra falls on Andean communities: The influences of eruption size and weather conditions during the 1999-2001 activity of Tungurahua volcano, Ecuador. J. Volcanol. Geotherm. Res. 217-218, 91–103.
Leocat, E., 2011. Histoire eruptive des volcans du secteur occidental des Iles Eoliennes (Sud de la Mer Tyrrhenienne, Italie). PhD thesis. University of Paris 11, Orsay.
Lucchi, F., 2013. Stratigraphic methodology for the geological mapping of volcanic areas: insights from the Aeolian archipelago (southern Italy). Geol. Soc. Lond. Mem. 37, 37–53.
Lucchi, F., Tranne, C.A., De Astis, G., Keller, J., Losito, R., Morche, W., 2008. Stratigraphy and significance of Brown Tuffs on the Aeolian Islands (southern Italy). J. Volcanol. Geotherm. Res. 177, 49–70.
Lucchi, F., Gertisser, R., Keller, J., Forni, F., De Astis, G., Tranne, C.A., 2013a. Eruptive history and magmatic evolution of the island of Salina (central Aeolian archipelago). Geol. Soc. Lond. Mem. 37, 155–211.
Lucchi, F., Keller, J., Tranne, C., 2013b. Regional stratigraphic correlations across the Aeolian archipelago (southern Italy). Geol. Soc. Lond. Mem. 37, 55–81.
Lucchi, F., Tranne, C.A., Peccerillo, A., Keller, J., Rossi, P.L., 2013c. Geological history of the Panarea volcanic group (eastern Aeolian archipelago). Geol. Soc. Lond. Mem. 37, 349–393.
Lucchi, F., Peccerillo, A., Tranne, C.A., Rossi, P.L., Frezzotti, M.L., Donati, C., 2013d. Volcanism, calderas, and magmas of the Alicudi composite volcano (western Aeolian archipelago). Geol. Soc. Lond. Mem. 37, 83–111.
Lucchi, F., Santo, A.P., Tranne, C.A., Peccerillo, A., Keller, J., 2013e. Volcanism, magmatism, volcano-tectonics and sea-level fluctuations in the geological history of Filicudi (western Aeolian archipelago). Geol. Soc. Lond. Mem. 37, 113–153.
Machida, H., 1999. The stratigraphy, chronology and distribution of distal marker tephras in and around Japan. Glob. Planet. Chang. 21, 71–94.
Manetti, P., Pasquaré, G., Tibaldi, A., Tsegaye, A., 1988. Geology of the island of Filicudi (Aeolian arc). Bollettino G.N.V. IV 368–382.
Manetti, P., Pasquaré, G., Tibaldi, A., Tsegaye, A., 1995. A new geo-vulcanological map of Filicudi island (Aeolian arc, Italy). Acta Vulcanol. 7, 1–5.
Martin, R.S., Watt, S.F.L., Pyle, D.M., Mather, T.A., Matthews, N.E., Georg, R.B., Day, J.A., Fairhead, T., Witt, M.L.I., Quayle, B.M., 2009. Environmental effects of ashfall in Argentina from the 2008 Chaitén volcanic eruption. J. Volcanol. Geotherm. Res. 184, 462–472.
Matthews, I.P., Trincardi, F., Lowe, J.J., Bourne, A.J., MacLeod, A., Abbott, P.M., Anderson, N., Asioli, A., Blockley, S.P.E., Lane, C.S., Oh, Y.A., Satow, C.S., Staff, R.A., Wulf, S., 2015. Developing a robust tephrochronological framework for Late Quaternary marine records in the Southern Adriatic Sea: new data from core station SA03-11. Quat. Sci. Rev. 118, 84–104.
Morche, W., 1988. Tephrochronologie der Aolischen Inseln. Unpublished PhD Thesis. Albert-Ludwigs-Universitat Freiburg, Germany.
Narcisi, B., 1996. Tephrochronology of a late quaternary lacustrine record from the Monticchio maar (Vulture volcano, southern Italy). Quat. Sci. Rev. 15, 155–165.
Nicotra, E., Minniti, M., Donato, P., De Rosa, R., 2020. Insights into the eruptive dynamics of small caldera-forming eruptions: the case study of the welded scoriae of Vulcano (Aeolian Islands, Italy). Front. Earth Sci. 8, 223.
Paterne, M., Guichard, F., Labeyrie, J., Gillot, P.Y., Duplessy, J.C., 1986. Tyrrhenian Sea tephrochronology of the oxygen isotope record for the past 60,000 years. Mar. Geol. 72, 259–285.
Paterne, M., Guichard, F., Labeyrie, J., 1988. Explosive activity of the South Italian volcanoes during the past 80,000 years as determined by marine tephrochronology. J. Volcanol. Geotherm. Res. 34, 153–172.
Peccerillo, A., De Astis, G., Faraone, D., Forni, F., Frezzotti, M.L., 2013. Compositional variation of magmas in the Aeolian arc: implications for petrogenesis and geodynamics. Geological Society, London, Memoirs, pp. 489–508.
Pichler, H., 1980. The Island of Lipari. Rend. Soc. Ital. Mineral. Petrol. 36, 415–440.
Ramsey, C.B., Higham, T.F.G., Leach, P., 2004. Towards high-precision AMS; progress and limitations. Radiocarbon 46, 17–24.
Reimer, P., Austin, W., Bard, E., Bayliss, A., Blackwell, P., Bronk Ramsey, C., Butzin, M., Cheng, H., Edwards, R., Friedrich, M., Grootes, P., Guilderson, T., Hajdas, I., Heaton, T., Hogg, A., Hughen, K., Kromer, B., Manning, S., Muscheler, R., Palmer, J., Pearson, C., van der Plicht, J., Reimer, R., Richards, D., Scott, E., Southon, J., Turney, C., Wacker, L., Adolphi, F., Büntgen, U., Capano, M., Fahrni, S., Fogtmann-Schulz, A., Friedrich, R., Köhler, P., Kudsk, S., Miyake, F., Olsen, J., Reinig, F., Sakamoto, M., Sookdeo, A., Talamo, S., 2020. The IntCal20 Northern Hemisphere radiocarbon age calibration curve (0–55 cal kBP). Radiocarbon 62.
Scaillet, S., Vita-Scaillet, G., Rotolo, S.G., 2013. Millennial-scale phase relationships between ice-core and Mediterranean marine records: insights from high-precision 40Ar/39Ar dating of the Green Tuff of Pantelleria, Sicily Strait Quat. Sci. Rev. 78, 141–154.
Scaini, C., Biass, S., Galderisi, A., Bonadonna, C., Folch, A., Smith, K., Hoskuldsson, A., 2014. A multi-scale risk assessment for tephra fallout and airborne concentration frommultiple Icelandic volcanoes-part 2: vulnerability and impact. Nat. Hazar. Earth Syst. Sci. Discuss. 2, 2531–2595.
Shane, P., 2000. Tephrochronology: a New Zealand case study. Earth Sci. Rev. 49, 223–259.
Siani, G., Sulpizio, R., Paterne, M., Sbrana, A., 2004. Tephrostratigraphy study for the last 18,000 14C years in a deep-sea sediment sequence for the South Adriatic. Quat. Sci. Rev. 23, 2485–2500.
Soligo, M., De Astis, G., Delitala, M.C., La Volpe, L., Tadderucci, A., Tuccimei, P., 2000. Disequilibri nella serie dell uranio nei prodotti dell isola di Vulcano: cronologia isotopica e implicazioni magmatologiche. 2 Forum Italiano di Scienze della Terra Riassunti. Plinus. 22, 347–349.
Sulpizio, R., Zanchetta, G., D'Orazio, M., Vogel, H., Wagner, B., 2010. Tephrostratigraphy and tephrochronology of lakes Ohrid and Prespa, Balkans. Biogeosciences 7, 3273–3288.
Sulpizio, R., Folch, A., Costa, A., Scaini, C., Dellino, P., 2012. Hazard assessment of far-range volcanic ash dispersal from a violent Strombolian eruption at Somma-Vesuvius volcano, Naples, Italy: implications on civil aviation. Bull. Volcanol. 74, 2205–2218.
Sulpizio, R., Zanchetta, G., Caron, B., Dellino, P., Mele, D., Giaccio, B., Insinga, D., Paterne, M., Siani, G., Costa, A., Macedonio, G., Santacroce, R., 2014. Volcanic ash hazards in the Central Mediterranean assessed from geological data. Bull. Volcanol. 76, 866.
Sulpizio, R., Forni, F., Lucchi, F., Massaro, S., Tranne, C., 2016. Unravelling the effusive-explosive transitions and the construction of a volcanic cone from geological data: the example of Monte dei Porri, Salina Island (Italy). J. Volcanol. Geotherm. Res. 327, 1–22.
Tamburrino, S., Insinga, D.D., Pelosi, N., Kissel, C., Laj, C., Capotondi, L., Sprovieri, M., 2016. Tephrochronology of a ~ 70 ka-long marine record in the Marsili basin (southern Tyrrhenian Sea) J. Volcanol. Geotherm. Res. 327, 23–39.
Tomlinson, E.L., Albert, P.G., Wulf, S., Brown, R., Smith, V.C., Keller, J., Orsi, G., Bourne, A.J., Menzies, M.A., 2014. Age and geochemistry of tephra layers from Ischia, Italy: constraints from proximal-distal correlations with Lago Grande di Monticchio. J. Volcanol. Geotherm. Res. 287, 22–39.
Ventura, G., 2013. Kinematics of the Aeolian volcanism (Southern Tyrrhenian Sea) from geophysical and geological data. In: Lucchi, F., Peccerillo, A., Keller, J., Tranne, C.A., Rossi, P.L. (Eds.), The Aeolian Islands Volcanoes. 37. Geological Society, London, Memoirs, pp. 3–11.
Wulf, S., Kraml, M., Brauer, A., Keller, J., Negendank, J.F.W., 2004. Tephrochronology of the 100 ka lacustrine sediment record of Lago Grande di Monticchio (southern Italy). Quat. Int. 122, 7–30.
Zanchetta, G., Sulpizio, R., Roberts, N., Cioni, R., Eastwood, W., Siani, G., Caron, B., Paterne, M., Santacroce, R., 2011. Tephrostratigraphy, chronology and climatic events of the Mediterranean basin during the Holocene: An overview. Holocene 21, 33–52.

Chapter 3

Petrography, mineral chemistry and melt inclusion compositions of the Brown Tuffs

1. Introduction

The most energetic eruptions in the Aeolian Islands were erupted from the northern Vulcano multiphase caldera system and led to the Brown Tuffs (BT) eruptions, which produced a long sequence of pyroclastic ash deposits, never investigated for what concern their magma source, covering a wide time span (from 80 to 6 ky), spread over most of the archipelago and the Capo Milazzo peninsula on Sicily (Lucchi et al., 2008). Meschiari et al. (2020) discussed the geochemical affinity of the main stratigraphic macro-units, Lower BT, Intermediate and Intermediate-upper BT and Upper BT, those proximal volcanic units on Vulcano placed in the corresponding chrono-stratigraphic windows and cropping out along the borders of the La Fossa Caldera, which has been considered as the most probable BT source area (Lucchi et al., 2008; Lucchi et al., 2013b). In particular, an unequivocal correlation between the Upper BT and the Piano Grotte dei Rossi Tuffs have been established, with a regular decrease of deposit thickness and grain size from the caldera rim towards southern Vulcano that has irrefutably confirmed an origin from an undefined vent(s) within the La Fossa caldera. Moreover, the entire dataset of glass composition obtained for the Lower BT and Intermediate BT macro units are consistent with that of the products erupted during the emplacement of the proximal Monte Molineddo 1–3 formations (Meschiari et al., 2020). Furthermore, the Upper BT glasses (trachy-andesites to trachytes) are largely similar to those of the early to intermediate products of the La Fossa cone (i.e. the Punte Nere and Grotta dei Palizzi pyroclastic deposits, Meschiari et al., 2020). This geochemical link suggests that the UBT not only preclude the early La Fossa activities but probably share the same magmatic plumbing system. Interestingly, the glass compositions within the basal Punte Nere succession, are variable. Whilst the oldest Punte Nere deposits are chemically consistent with the UBT, the overlying Punte Nere glasses are in offset and lie on the same evolutionary trends as the older IBT glasses togheter with those of the younger Grotta dei Palizzi successions (Meschiari et al., 2020), suggesting that the La Fossa explosive activity was fed by a complex magmatic system comprising of more than one magma batch.

Based on these considerations, it is crucial to unravel how the magmatological evolution of the BT can be inserted into the general framework of the magma plumbing system of Vulcano, bearing in mind that even the latest articles (Nicotra et al., 2020; Palummo et al., 2020) do not consider the data deriving from BT, with a possible underestimation of the role they play in magmatological terms. Considering that Vulcano is an active volcanic system that last erupted in 1888-1890 this can be fundamental to further establish monitoring strategies and forecasting volcanic eruption scenarios.

In this view, the lack of petrological data on the BT precludes a full interpretation of the magmatic system of the La Fossa Caldera during the last 80 ka, and also the pre-eruptive storage conditions of the magmas feeding the BT eruptions. Therefore, petrography, mineral chemistry and melt inclusions data were obtained for selected samples of the BT on the islands of Lipari and Vulcano, to be merged with the major and trace elements compositional glass data.

2. Methods

Laboratory investigation were focused on selected samples representative of the most defined BT depositional units on Lipari and Vulcano (Table 1) and included: grain size and component analysis, morphological and textural particle characterization by scanning electron microscope (SEM). The samples were previously cleaned, dried and sieved at 1Φ (phi) intervals from −1 to 4 Φ (2–0.0625 mm). 53 polished thin sections mounted on glass slides, which are representative of all the BT macro-units and the ash size fraction (2Φ), have been prepared and analysed under a polarising optical microscope. The nature, texture and morphological properties of the glass fragments and crystals forming the samples were analyzed using a TM3000 scanning electron microscope equipped with Bruker EDX analytical system at the University of Keele on the thin sections and using a LEO 50XVP equipped with Oxford Silicon drift X-max analytical system at the University of Bari on loose grain mount of the 2 Φ size fraction.

A subset of the thin sections was grafite coated and analysed for mineral chemistry by means of a JEOL JXA-8200 Electron Microprobe (EPMA) at the Institute für Geochemie und Petrologie, ETH Zürich. The activities were focused on major element concentrations in minerals together with sulphur and chlorine concentrations in melt inclusions. Peak counting times per element were 10–20 s, an acceleration voltage of 15 kV and a beam current of 20 nA for major element concentrations. For major elements and volatiles (Cl and S) in melt inclusions, peak counting times ranged from 20 to 40 s for major elements and 20 s for volatiles, an acceleration voltage of 15 kV and a beam current of 10 nA. Detection limits for Cl and S were 60 and 118 ppm, respectively.

Sample name	**Depositional unit**	**Lithology/Material**	**Chemistry (glass)**	**Source Area/Outcrop position**	**Minchem analysis**	**EPMA glass data**
LOWER BROWN TUFF						
LIP10/18	bt 1/2	massive ash	tephriphonolite-trachyandesite	Lipari, Canneto Dentro		x
LIP08/18	unknown	massive ash	basaltic andesite - andesite	Lipari, Canneto Dentro		
LIP04/18	bt 4	massive coarse ash, lithics at the base	trachyandesite-tephriphonolite	Lipari, Canneto Dentro	x	x
VUL10/18	unknown	laminated ash	trachyandesite	Vulcano, Grotta dei Pisani	x	x
VUL13/18	unknown	laminated ash	trachyandesite	Vulcano, Grotta dei Pisani		x
INTERMEDIATE BROWN TUFF						
bt 11/16	bt 7	massive ash	trachyandesite-tephriphonolite	Lipari, ?		x
bt 12/16	bt 8	massive ash	trachyandesite-tephriphonolite	Lipari, ?		x
LIP45/17	unknown	ash and black scoriaceous lapilli	basaltic trachyandesite	Lipari, Monterosa	x	x
LIP15/18	unknown	ash and black scoriaceous lapilli	basaltic trachyandesite - trachyandesite	Lipari, Crapazza	x	x
LIP16/18	unknown	ash and black scoriaceous lapilli	basaltic trachyandesite - trachyandesite	Lipari, Crapazza		x
LIP14/18	bt 9	massive ash	tephriphonolite	Lipari, Crapazza		x
LIP27/17	bt 9	ash and black scoriaceous lapilli	basaltic trachyandesite	Lipari, ?		x
bt 14/16	bt 10	massive ash	trachyandesite-tephriphonolite	Lipari, Vallemuria		x
bt 15/17	bt 11	massive ash	trachyandesite-tephriphonolite	Lipari, ?	x	
LIP01/18	unknown	massive ash	Trachyandesite	Lipari, Canneto Dentro		x
VUL09/18	unknown	ash, lithics at the base	Trachyandesite-tephriphonolite	Vulcano, Grotta dei Pisani	x	x
INTERMEDIATE BROWN TUFF-upper						
bt 01/16	bt 12	massive ash	tephryphonolite-trachyandesite - trachyte	Lipari, ?	x	x
LIP17/17	bt 12	massive ash	tephriphonolite - Trachyte	Lipari, Madoro	x	x
VUL09/17	bt 12	massive ash	tephriphonolite	Vulcano, Gelso	x	x
UPPER BROWN TUFF						
bt 02/16	bt 13	massive ash	tephryphonolite-trachyandesite - trachyte	Vulcano, Serra delle Telicicchie	x	x
bt 03/16	bt 13	massive ash	tephryphonolite-trachyandesite - trachyte	Vulcano, Serra delle Telicicchie		x
bt 05/16	bt 15	massive ash	tephryphonolite-trachyandesite - trachyte	Vulcano, Passo del Piano	x	x

Table 1. List of the analysed Brown Tuffs samples (componentry, morphoscopy analysis and mineral chemistry). Chemistry of glasses is from Meschiari et al. (2020).

3. Results

Hereafter the preliminary results of this analysis are described.
All the samples analysed consist of a mixture of glass fragments (from about 50 to 80 vol%), loose crystals (10–40%) and subordinate lithic fragments (3–10%) (Fig. 1). The glass shards (fragments) show similar features both in Lipari and in Vulcano islands. Color is from dark-brown to pale-brown and colorless (Fig.1), both mostly blocky and aphyric, subordinately poorly or non-vesicular with angular to platy and curviplanar surfaces (Fig. 2C) and sometimes microcrystalline. BT on Vulcano are characterized by a higher content of crystals and lithics, with percentages of lithics locally up to 8-11%, confirming the observations of De Astis et al. (1997) for the Upper BT.

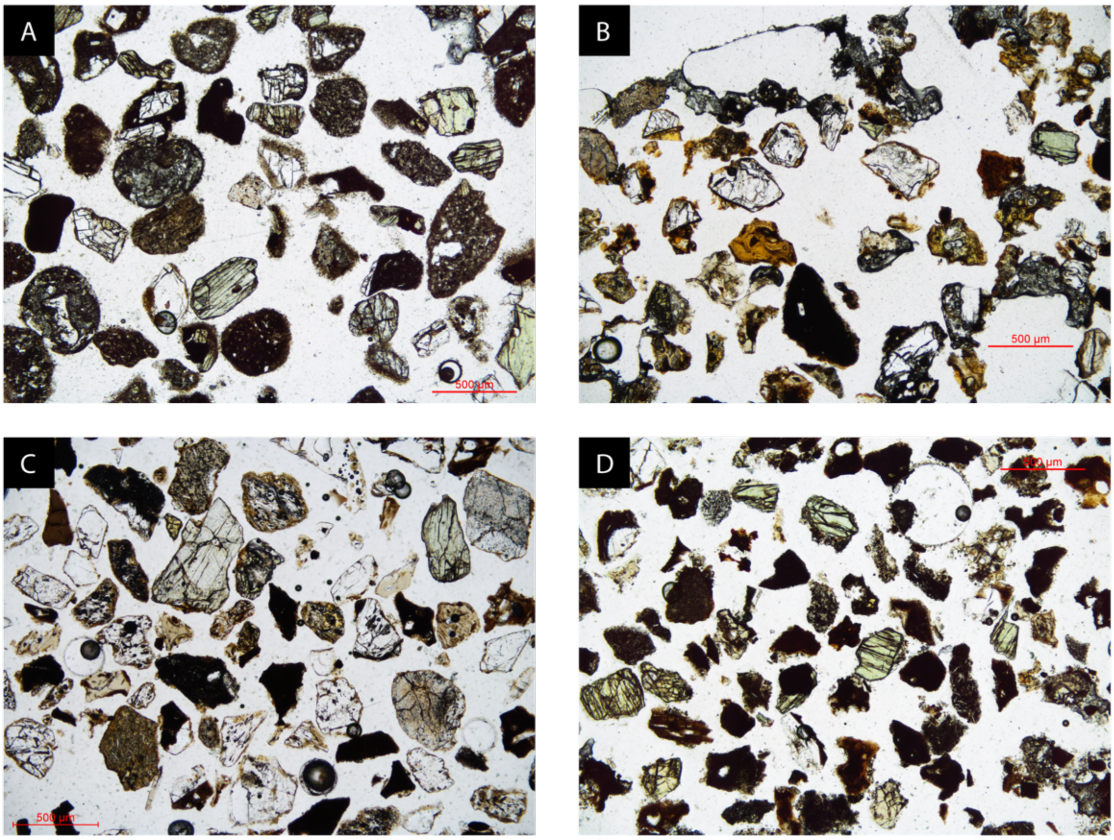

Fig.1. Microphotographs of representative samples in 2 Φ granulometrical fraction of Lower BT (A), Intermediate BT (B), Intermediate-upper BT (C) and Upper BT (D) (plane polarized light).

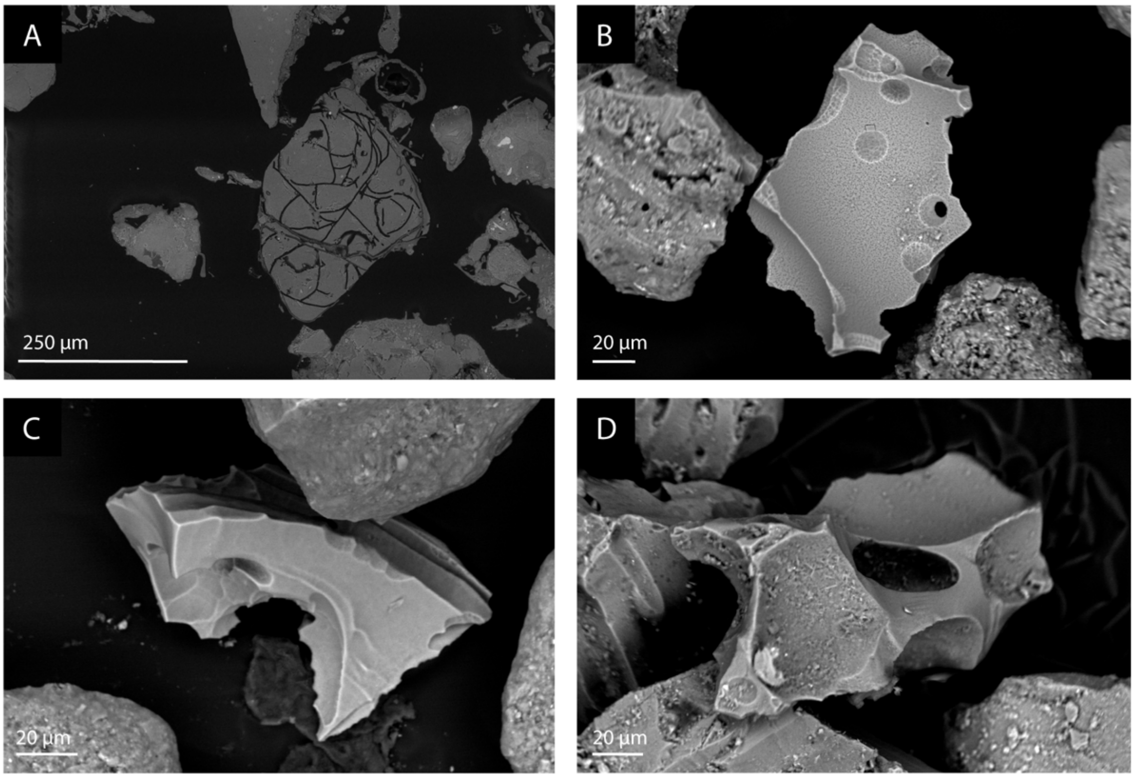

Fig. 2. SEM images of BT glasses on thin section (A) and grain mounts (B, C and D). Main features are curviplanar surfaces (C), quenching cracks (A), ash coatings (D) and pitting (B).

The crystals occur as loose components or rimmed by glass. They represent the rest of the juvenile population. Free crystals generally display a well-developed habitus, although their outline is frequently irregular. They are mainly represented by clinopyroxene, plagioclase, olivine, Fe-Ti oxides, and amphibole in order of abundance. In the Upper BT clinopyroxenes represent most of the crystals, whilst in the Intermediate BT and Lower BT the crystal fraction mostly consists of plagioclase. K-feldspar crystals are also present probably ripped and embedded from the pyroclastic levels below the sampled BT.

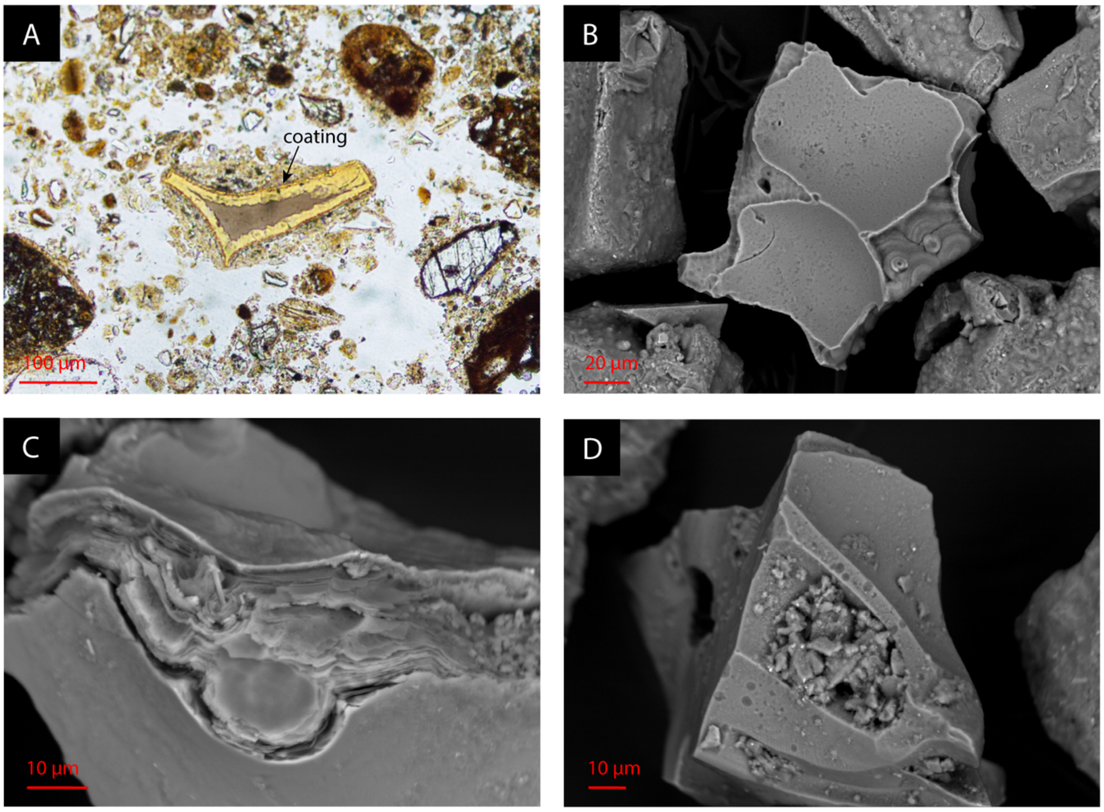

Fig.3. Microphotographs (A) and SEM images (B, C and D) of alteration features of BT glass fragments: coating (A), zeolithization-like alteration (B), multi-layer coating (C) and adhering particle (D).

3.1 Glass morphological and textural features

Morphological and textural analysis of the glass fragments in the studied BT units was conducted by using SEM on the 2 Φ fraction size. Most of the observed features are in agreement with those described by De Astis et al. (1997), Lucchi et al. (2008) and De Rosa et al. (2016). All the samples consist of <70% (estimated in thin section) of unvesiculated (Fig. 2 A-B-C) and blocky glass fragments (Fig. 2-A), with a subordinate fraction of poorly vesiculated glass (Fig.2-D), or glass shards with bubble walls and V shaped pit (Fig. 2 D-B). In some of these particles small vesicles are visible, but their low abundance indicates that they had played a minor role for the fracture processes. The surface of most of the glass fragments shows evidence of chemical pitting (Fig. 2-B) produced by dissolution processes. Hydration cracks are also common features and most present in the UBT samples analysed. Quenching cracks (Fig. 2A), ash coatings (Fig. 2D) and evidence of pitting (Fig. 2B) are sometimes visible on the shard surfaces. In a few cases brown and colourless glass fragments have a few tens of microns-thick external coating (Fig. 3), separated from the glass by a thin micrometric void, which is a sort of external quasi-coating as already described by De Astis et al. (1997) on Vulcano and De Rosa et al. (2016) in the Intermediate BT on Lipari. In some cases, glass surrounded by the coating shows a fresh core and a hydrated outer rim (Fig. 3A).

The Lower BT glasses are almost pale-brown, blocky and non-vesicular, with rare poorly vesicular clasts. Subordinately there are dark brown glass fragments, blocky with quenching cracks, and rare colorless blocky glass fragments. Glass is often surrounded by a thin coating (Fig.3-A) with some yellowish and quite altered fragments. Some glasses are microcrystalline.

The Intermediate BT glasses are almost pale-brown to colorless, blocky and poorly to non-vesicular. Adhering particles are present (Fig. 3-D). Frequently, and especially in the Lipari samples, it is observed glass alteration (Fig.3-B) and the glass is covered by few tens microns-thick external coatings (Fig.3-A). Altered glass are more yellowish in color.

The Intermediate-upper BT glasses are colorless, pale-brown and dark brown with angular and irregular shapes and are blocky, non vesiculated to poorly vesiculated. Glass shards with bubble walls and V shaped pit (Fig. 2 D-B) are frequent and adhering particles are present (Fig. 3-D). The surface of many glass fragments shows evidence of chemical pitting (Fig. 2-B).

The Upper BT glasses are dark brown, pale brown and colorless (in order of quantity). The darker glasses are generally non or poorly vesiculated. The colorless and pale brown glass fragments have angular and irregular shapes and are blocky, non vesiculated to vesiculated. Adhering particles are common (Fig.3-D). The dark brown glasses are dominant and more numerous than in the other BT macro-units.

Further SEM observations were performed on the coatings that surround many glass fragments and other alteration structures. The coatings may consist of various layers (Fig. 3-C) and do not adhere directly to the grain surfaces, but be are separated by a thin void. Coatings are also recognized around crystals and lithics, pale yellow to very pale brown in colour.

3.2 Mineral chemistry

Clinopyroxene, plagioclase and olivine were analyzed from selected samples for each BT macro-unit on Lipari and Vulcano. For a given mineral, the compositions of the crystal are compared with each other in the same macro-unit, searching for any distinctive feature.

Clinopyroxene

Euhedral clinopyroxenes generally occur both as unzoned and zoned crystals with abundant melt inclusions. Their SiO_2 content is almost constant through all the BT macro-units ranging from 50.60 to 51.68 wt% (Table 2), FeO slightly decreases from the older to most recent BT units (LBT = 9.26 wt%; IBT = 9.13 wt%; IBT-upper = 8.64 wt%; UBT = 8.49 wt%) and also TiO_2 follows a similar trend (LBT = 0.64 wt%; IBT = 0.69 wt%; IBT-upper = 0.58 wt%; UBT = 0.53 wt%). Mg# (Mg# = Mg/Mg+Fe_2+) does not show any significant variation between the macro-units (LBT = 0.73; IBT = 0.72; IBT-upper = 0.74; UBT = 0.75).

Clinopyroxenes in the Lower BT are diopsidic to augitic in composition (Fig. 4) with Wo_{41-50} En_{38-46} Fs_{9-18}, in the Intermediate BT they are diopsidic with Wo_{44-50} En_{37-47} Fs_{9-16}, in the Intermediate-upper BT they are diopsidic to augitic with Wo_{37-50} En_{37-50} Fs_{6-21} and in the Upper BT they are diopsidic with Wo_{44-47} En_{40-45} Fs_{10-15} with the max-scattering in the diopside-augite fields for Intermediate-upper BT, to a lesser extent as well as Upper BT.

Macro-unit	**Lower BT**		**Intermediate BT**		**Intermediate BT-upper**		**UpperBT**	
	mean	*1σ*	*mean*	*1σ*	*mean*	*1σ*	*mean*	*1σ*
(wt %)								
Total	99,55	0,55	99,60	0,44	99,19	6,57	99,71	0,34
SiO_2	51,04	1,11	50,69	0,62	51,36	1,97	51,68	0,46
TiO_2	0,64	0,18	0,69	0,11	0,58	0,15	0,53	0,08
Al_2O_3	3,49	1,05	3,72	0,67	3,70	2,28	3,16	0,55
Cr_2O_3	0,00	0,00	0,01	0,01	0,06	0,11	0,04	0,06
FeO	9,26	1,81	9,13	0,53	8,64	1,70	8,49	0,72
MnO	0,28	0,12	0,26	0,04	0,24	0,07	0,25	0,05
MgO	14,47	2,76	13,39	0,46	13,99	2,02	14,23	0,36
CaO	20,48	4,47	21,74	0,40	21,02	2,59	21,23	0,37
Na_2O	0,32	0,10	0,37	0,04	0,38	0,34	0,39	0,04
K_2O	0,00	0,00	0,01	0,01	0,04	0,28	0,00	0,00

Table 2. Mean and standard deviations of pyroxene compositions (wt% normalized to 100).

Plagioclase

Plagioclases appear as broken fragments and often show a typical simple twinning. Melt inclusions are present as unconnected and connected. SiO_2 content in plagioclase is almost constant through all the BT macro unit ranging from 49.82 to 52.87 wt% (Table 3), FeO slightly increases in plagioclase from the older to most recent BT units (LBT = 0.66 wt%; IBT = 0.75 wt%; IBT-upper = 0.75 wt%; UBT = 0.80 wt%), whilst Al_2O_3, CaO and Na_2O show no differences or trends between the macro-units.

The compositions of plagioclase (Fig. 5) in the Lower BT span from Ab_{4-49} and An_{44-96}, in the Intermdiate BT from Ab_{23-48} and An_{40-74}, in the Intermdiate-upper BT from Ab_{21-76} to

An_{16-77} and in the Upper BT from Ab_{35-41} and An_{54-61} with a slight change in composition from more anorthitic to more albitic from the older units to the most recent ones. In the UBT is also found an Alkali feldspar with An_{13} composition.

Olivine

Olivine show constant SiO_2, FeO and MgO wt% content (Table 4). The olivine composition in the Lower BT is Fo_{60-78} and Fa_{22-40}, those of the Intermediate BT range from Fo_{58-66} to Fa_{34-42}, for the Intermediate-upper BT between Fo_{70-71} and Fa_{29-30} and for the Upper BT from Fo_{69-73} to Fa_{27-30}.

Macro-unit	**Lower BT**		**Intermediate BT**		**Intermediate BT-upper**		**UpperBT**	
	mean	*1σ*	*mean*	*1σ*	*mean*	*1σ*	*mean*	*1σ*
(wt %)								
Total	99,86	0,53	99,98	0,44	100,25	0,61	100,09	1,22
SiO_2	50,03	3,91	52,84	1,05	54,30	2,43	53,50	0,65
TiO_2	0,03	0,02	0,04	0,02	0,04	0,02	0,04	0,02
Al_2O_3	31,41	2,69	29,45	0,72	28,56	1,59	29,33	0,49
Cr_2O_3	0,00	0,00	0,00	0,00	0,00	0,00	0,00	0,00
FeO	0,66	0,16	0,75	0,09	0,67	0,14	0,69	0,04
MnO	0,01	0,01	0,01	0,01	0,01	0,01	0,01	0,01
MgO	0,05	0,03	0,07	0,02	0,06	0,02	0,05	0,01
CaO	14,64	3,07	12,24	0,86	11,10	1,87	11,46	0,38
Na_2O	2,75	1,47	3,77	0,37	4,26	1,01	4,12	0,23
K_2O	0,42	0,37	0,82	0,25	1,00	0,31	0,79	0,09

Table 3. Mean and standard deviation of plagioclase compositions (wt% normalized to 100).

Macro-unit	**Lower BT**		**Intermediate BT**		**Intermediate BT-upper**		**UpperBT**	
	mean	*1σ*	*mean*	*1σ*	*mean*	*1σ*	*mean*	*1σ*
(wt %)								
Total	99,67	0,59	99,60	0,29	99,17	0,31	99,83	0,25
SiO_2	37,43	0,87	36,74	0,44	37,79	0,08	38,10	0,34
Al_2O_3	0,03	0,02	0,03	0,00	0,03	0,01	0,02	0,01
CaO	0,29	0,12	0,37	0,05	0,30	0,01	0,21	0,04
TiO_2	0,03	0,03	0,02	0,01	0,02	0,01	0,02	0,01
K_2O	0,00	0,00	0,00	0,00	0,00	0,00	0,00	0,00
Cr_2O_3	0,00	0,00	0,00	0,00	0,00	0,00	0,00	0,00
FeO	28,19	4,68	31,71	1,91	26,25	0,17	25,42	1,24
MnO	0,58	0,17	0,80	0,11	0,58	0,01	0,58	0,08
NiO	0,01	0,01	0,01	0,01	0,04	0,01	0,03	0,02
MgO	33,41	4,11	30,30	1,53	34,98	0,12	35,60	0,93
Na_2O	0,01	0,01	0,01	0,01	0,01	0,01	0,01	0,01

Table 4. Mean and standard deviation of olivine compositions (wt% normalized to 100).

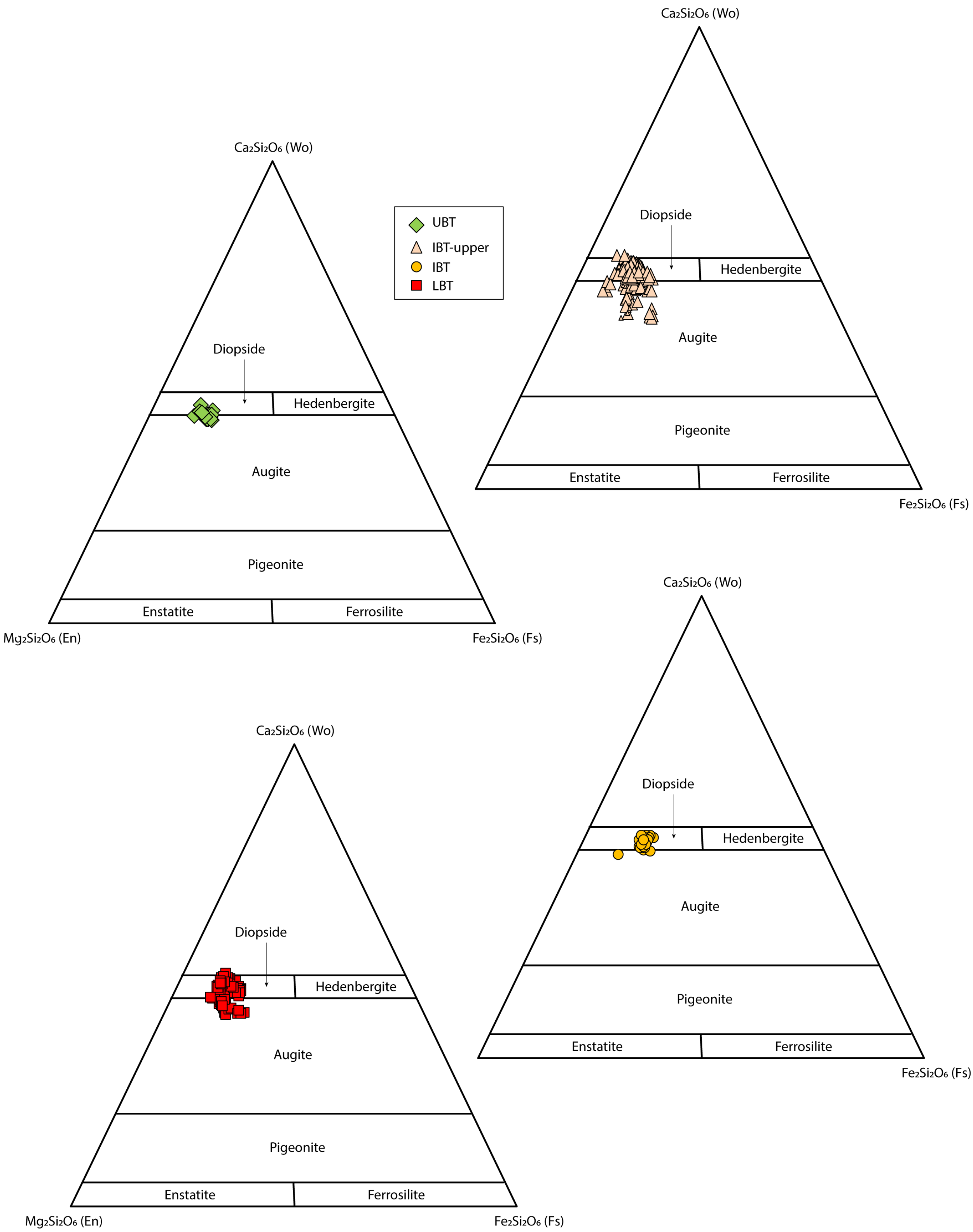

Fig. 4 Composition of pyroxenes in the Lower BT (LBT), Intermediate BT (IBT), Intermediate-upper BT (IBT-upper) and Upper BT (UBT).

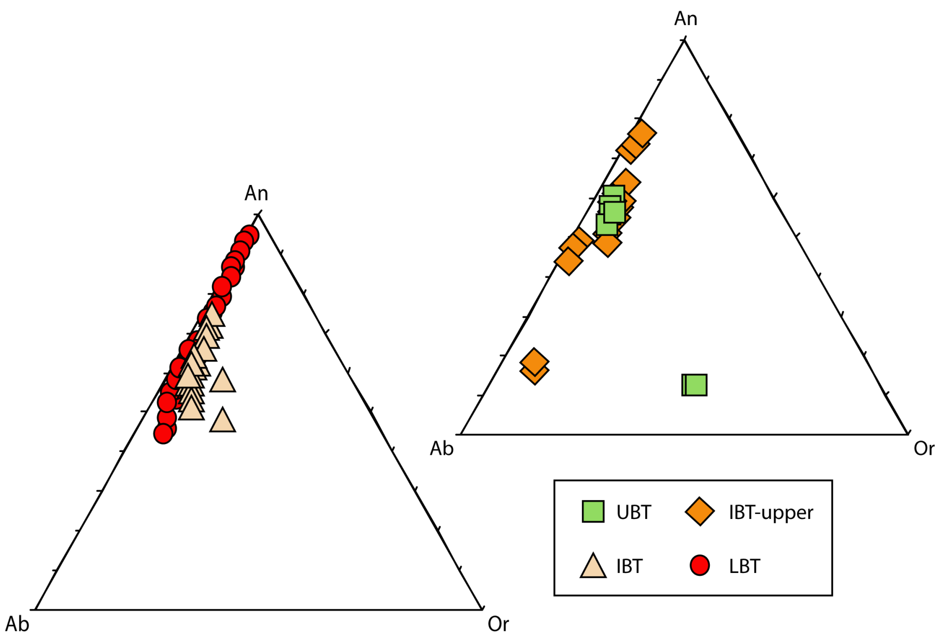

Fig. 5 Composition of plagioclase in the Lower BT (LBT), Intermediate BT (IBT), Intermediate-upper BT (IBT-upper) and Upper BT (UBT).

3.3 Melt inclusions

Melt inclusions (MI) occur in plagioclase and clinopyroxenes (rare in olivine) of the juvenile components of the Lower, Intermediate and Upper BT. MI show variable shapes and size and can be glassy or partly crystallized (Fig. 6). They tend to be rounded to elongated or irregular in shape with sizes ranging from <10 μm to a maximum of ~80 μm. The glassy MI show occasionally shrinkage bubbles inside. The inclusions that are considered as re-crystallized were not considered for the determination of major elements and volatile compositions.

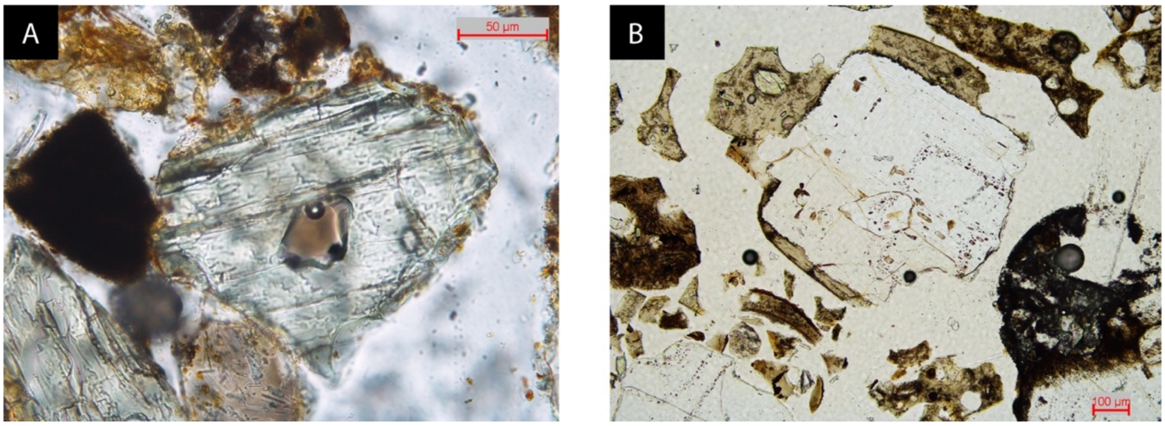

Fig. 6 Melt inclusions in clinopyroxene (A) and in plagioclase (B) from Intermediate BT-upper (A) and Lower BT (B) macro units.

Although melt inclusions are observable in all the macro units, it was not possible to analyze them in Upper Brown Tuff samples available as they occur only in very small dimensions (< 50 μm) or result to be re-crystallized.

The geochemical compositions of Lower, Intermediate and Intermediate-upper BT melt inclusions are divided in two separate clusters: one of tephriphonolitic-trachyandesitic composition (Na_2O+K_2O 9.22-11.74 wt%; SiO_2 53.88-56.48 wt%; Fig. 7) and the other of trachyandesitic-trachydacitic composition (Na_2O+K_2O 8.05-6.59 wt%; SiO_2 61.48-64.84 wt%; Fig. 7). Tree melt inclusions points are out of these clusters and show trachy-andesite, tephriphonolite and phonolite compositions. The compositions of all the BT glasses range from basaltic trachy-andesites through trachy-andesites to more evolved trachytes and show a clear K-series affinity (Meschiari et al., 2020).

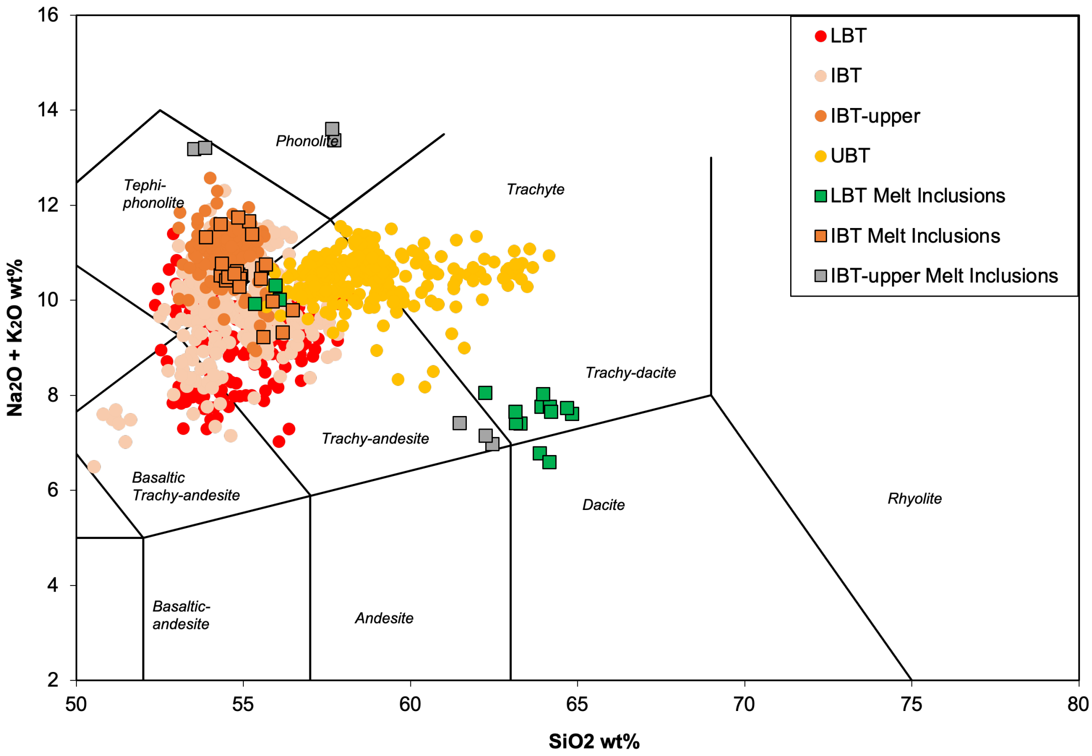

Fig. 7 TAS diagram for melt inclusions compositions in the Lower, Intermediate and Intermediate-upper BT, compared with the corresponding juvenile glass compositions from Meschiari et al. (2020).

The melt inclusion in the Lower BT samples from Lipari, in both clinopyroxene and plagioclase, are basaltic andesitic and trachydacitic to dacitic while the juvenile glass composition of this macro unit in Lipari ranging from basaltic trachy-andesites to trachy-andesites and tephri-phonolites (SiO_2 = 52.4-57.2 wt.%; Na_2O+K_2O = 7.7-11.5 wt.%; Meschiari et al., 2020). One melt inclusion is found in an enstatitic pyroxene and show basaltic andesite composition. Those of the Lower BT sample from Vulcano are trachyandesitic and compositionally are similar to the corresponding BT juvenile glass that ranges from basaltic trachy-andesite through to a dominance of trachy-andesites (SiO_2 = 54.4-58.2 wt.%; $Na_2O + K_2O$ = 7.6-10.3 wt.%; Meschiari et al., 2020).

Overall, the melt inclusions from the plagioclase of the Intermediate BT both from Lipari and Vulcano, found in plagioclase, are tephriphonolitic to trachyandesitic with a composition comparable with that of the corresponding glasses.

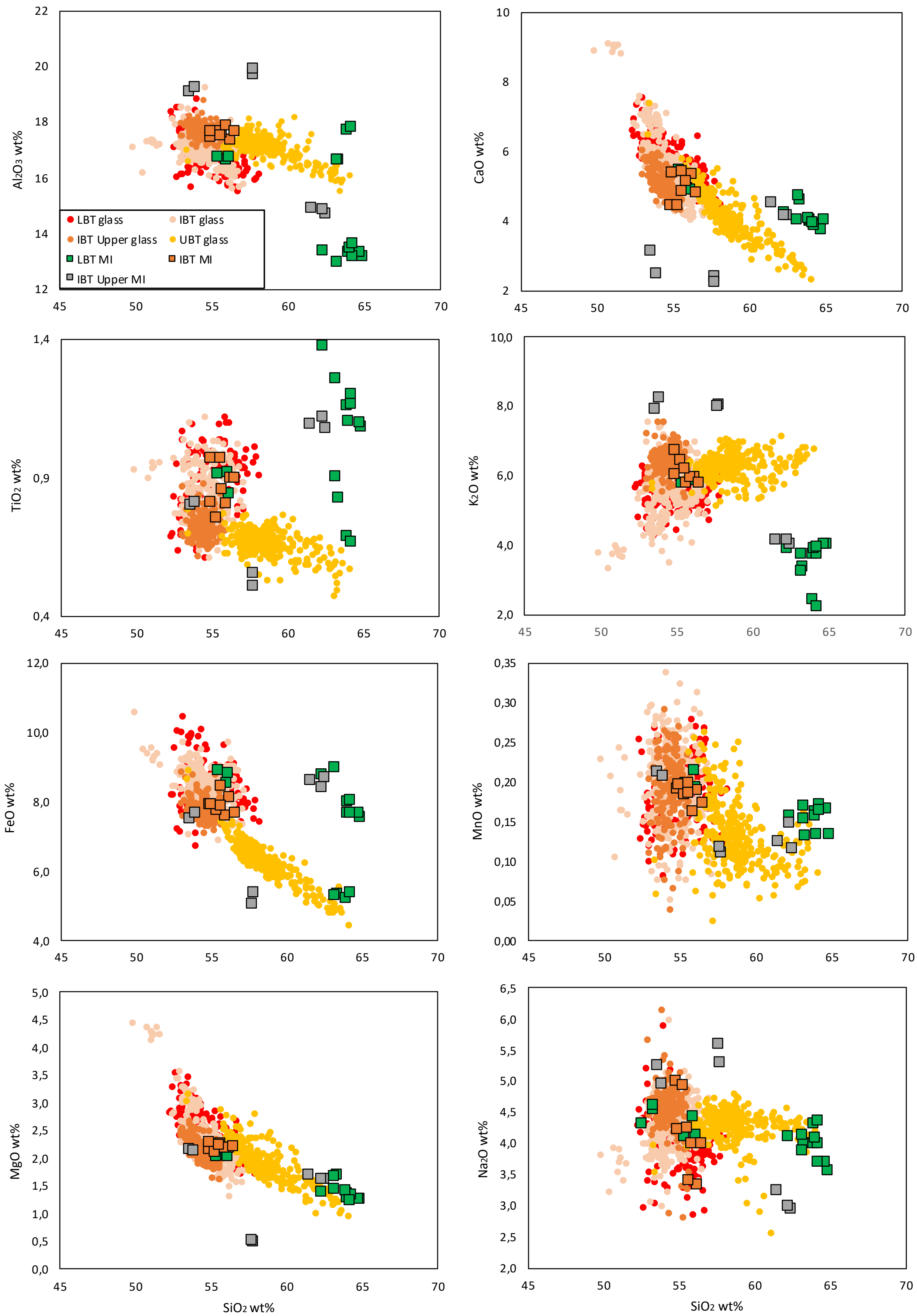

Fig. 8 Harker diagrams for MI major element compositions in the Lower, Intermediate and Intermediate-upper BT, compared with the corresponding glass compositions from Meschiari et al. (2020).

3.3.1 MI volatile contents

The concentration of sulphur in the Lower BT MI varies between 816 ppm and <100 ppm and chlorine between 3637 and 2047 ppm. In the Intermediate BT MI sulphur concentration lies in a range between 538 and <100 ppm, chlorine concentration between 2655 and 2272. MI from the Intermediate-upper BT have sulphur concentration varying from 218 to <100 ppm, and chlorine concentration is between 2289 and 1216. SO_3 concentration decreases through the BT succession, starting from the older Lower BT, until the Intermediate-upper BT (Fig. 9), while Cl concentration doesn't show particular trends. Chlorine concentrations show two principal clusters at different silica content (53.53-57.72 SiO_2 wt% and 61,47-64,83 SiO_2 wt%; Fig.8), the points at lower SiO_2 wt% are from the Lower, Intermediate and Intermediate-upper BT, and their Cl wt% is costant. They are clustered well also with K_2O wt% contents, except that for Intermediate-upper BT that show an increase of K_2O. CaO wt% range for the first cluster is less defined, ranging from 3.75-5.60 wt%. Sulphur wt% show the same two cluster of points with SiO_2 and K_2O wt% (Fig.10).

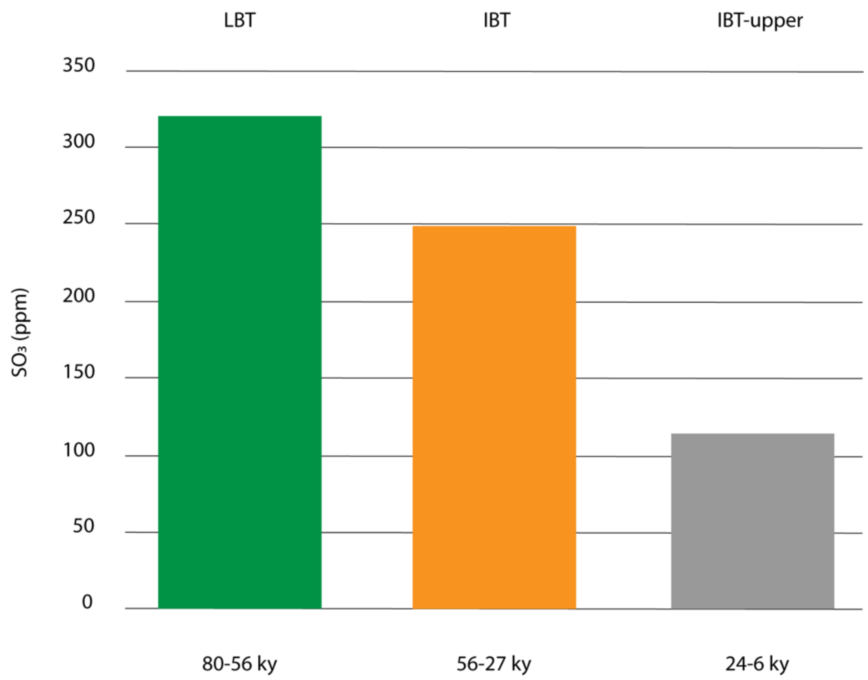

Fig. 9 Histogram for melt inclusions SO_3 mean concentrations (ppm) showing the decrease in concentration of the volatile element through time.

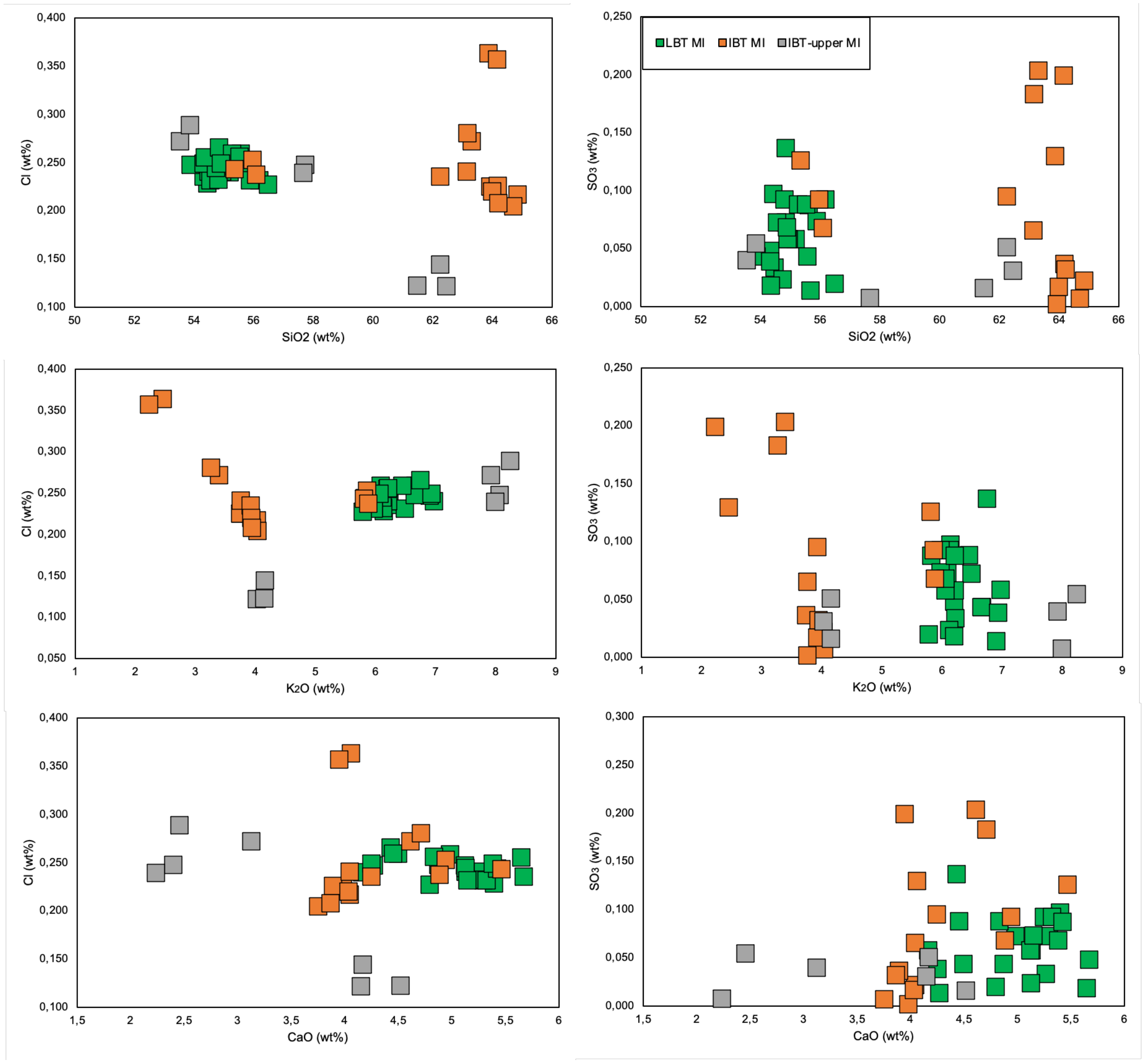

Fig. 10 Melt inclusions volatile elements Cl and SO_3 concentrations (wt%) in the Lower BT (LBT), Intermediate BT (IBT) and Intermediate-upper BT (IBT-upper).

References

De Astis, G., Dellino, P., De Rosa, R., La Volpe, L., 1997. Eruptive emplacement mechanism of fine grained pyroclastic deposits widespread on Vulcano Island. Bull. Volcanol. 59, 87-102.

De Rosa, R., Donato, P., Scarciglia, F., 2016. On the origin and post-depositional history of widespread massive ash deposits: the case of Intermediate Brown Tuffs (IBT) of Lipari (Aeolian Islands, Italy). J. Volcanol. Geotherm. Res. 327, 135-151.

Lucchi F., Tranne C.A., De Astis G., Keller J., Losito R., Morche W., 2008. Stratigraphy and significance of Brown Tuffs on the Aeolian Islands (southern Italy). J. Volcanol. Geotherm. Res. 177, 49–70.

Lucchi F., Gertisser R., Keller J., Forni F., De Astis G., Tranne C.A., 2013a. Eruptive history and magmatic evolution of the island of Salina (central Aeolian archipelago). Geol. Soc. Lond. Mem. 37, 155–211.

Lucchi F., Keller J., Tranne C., 2013b. Regional stratigraphic correlations across the Aeolian archipelago (southern Italy). Geol. Soc. Lond. Mem. 37, 55–81.

Meschiari S., Albert P.G., Lucchi F., Sulpizio R., Smith V.C., Kearney R., Tranne C.A., 2020. Stratigraphy and geochemistry of the Brown Tuffs from the Aeolian Islands (Italy) indicates Vulcano was frequently active over 80 ky and produced widespread ash dispersals. J. Volcanol. Geotherm. Res., 406, 107079.

Morimoto, N., 1988. Nomenclature of Pyroxenes. Mineralogy and Petrology 39, 55–76.

Nicotra E., Minniti M., Donato P., De Rosa R., 2020. Insights into the eruptive dynamics of small caldera-forming eruptions: the case study of the welded scoriae of Vulcano (Aeolian Islands, Italy). Frontiers in Earth Science, 8, 223.

Palummo F., Mollo S., De Astis G., Di Stefano F., Nazzari M., Scarlato P., 2020. Petrological and geochemical modeling of magmas erupted at Vulcano Island in the period 54–8 ka: Quantitative constraints on the sub-volcanic architecture of the plumbing system. Lithos 374–375, 105715

Chapter 4

New insights into the origin of external chrono-stratigraphic markers recorded on the Aeolian Islands (Southern Italy).

Albert P.G. [a,b], Meschiari S. [c], Lucchi F. [c], Sulpizio R. [d], Smith V.C. [b], C.A. Tranne [c]

[a] Department of Geography, Swansea University, Singleton Park, Swansea SA2 8PP, UK
[b] Research Laboratory for Archaeology and the History of Art (RLAHA), University of Oxford, Dyson Perrins Building, South Parks Road, Oxford OX1 3QY, UK
[c] Dipartimento di Scienze Biologiche, Geologiche e Ambientali, Università di Bologna, Piazza Porta S. Donato 1, 40126 Bologna, Italy
[d] Dipartmento di Scienze della Terra e Geoambientali, Universitá di Bari, via Orabona 4, 70125 Bari, Italy

To be submitted to Journal of Volcanology and Geothermal Research

Extended abstract

Several alkali-rich external tephra layers originating from explosive volcanism on the Italian mainland have been recognised in the proximal volcanic successions of the Aeolian Islands (Keller, 1980; Morche 1988; Kraml, 1997; Lucchi et al., 2008; Lucchi et al., 2013a). These primary ash fall layers are important stratigraphic markers and, where correlated to dated proximal source deposits, they assume the function of chronological markers. The latter is particularly important within the Aeolian Islands as the direct dating of local volcanic deposits is challenging. Salina Island preserves the most comprehensive record of major ash dispersals from the Campanian region (Keller 1980; Morche 1988; Lucchi et al. 2008), whilst other occurrences are reported on the islands of Lipari (Forni et al., 2013), Filicudi (Lucchi et al., 2013b), Panarea (Lucchi et al., 2013c) and Stromboli (Francalanci et al., 2013). These tephra layers preserved on the Aeolian Islands are the continental equivalents of some of the most widespread marine tephra layers identified in the central Mediterranean region. Their preservation in the volcanic stratigraphies of the Aeolian islands offers important chrono-stratigraphic tools used to constrain the timing of local volcanism, and at the same time allows important insights into the scale of past explosive activity at the Campanian volcanoes.

In this contribution we robustly characterise six external tephra deposits using grain-specific major (Electron microprobe [EMP]) and trace element (Laser Ablation Inductively coupled plasma mass spectrometry [LA-ICP-MS]) analysis. These data are used to examine the provenance of these external tephra layers in the context of an extensive geochemical glass dataset made available in recent years for the widespread Mediterranean tephra units (e.g., Tomlinson et al., 2012; 2014; Giaccio et al., 2017; Wulf et al., 2012; Bourne et al., 2015; Donato et al., 2016). Consequently, bringing together these datasets we aim to: (1) test the previously proposed provenance solutions of these tephra layers; (2) assess the reliability of these ash layers as chrono-stratigraphic makers for constraining the timing of eruptive activity in the Aeolian Islands; (3) provide new constraints on the distribution and scale of major ash fall events traced across the central Mediterranean by integrating these tephra beds into the regional marine and lacustrine tephrostratigraphic framework. Our investigations are centred on Salina where we characterised the following tephra layers, SAL-I, SAL-II, SAL-III, SAL-IV and the so-called Ischia tephra (IT) (Lucchi et al., 2013a, and references therein), but we also examine external ash layers on Filicudi and Panarea.

The correlation of SAL-I tephra with X-6 marine tephra (Keller et al. 1978; Keller 1981; Morche 1988) is validated by our new glass data, which include also analyses (major, trace elements) of the Ionian Sea X-6 tephra layer from its type locality (M25/4-12). Therefore, the largely accepted $^{40}Ar/^{39}Ar$ age for this tephra (108.9 ± 1.8 ka, by Iorio et al., 2014) can be reliably imported to the Salina volcano-stratigraphy.

While our chemical data clearly indicates that this tephra derives from the Campanian volcanism, its signature is seemingly more akin to those younger deposits known to have erupted Campi Flegrei (Pre-Campanian Ignimbrite (CI)), rather than Ischia activity. The origin of the SAL-II tephra correlated to the X-5 marine tephra is more complicated: this tephra differs from the composition of other distal occurrences of the X-5 (e.g., TM-25 at Lago Grande di Monticchio; Wulf et al., 2012). The X-5 tephra has a high-alkali ratio (K_2O > Na_2O; Donato et al., 2016), however the SAL-II sample collected here has a Low-alkali ratio (Na_2O > K_2O). Similarly, a reported X-5 occurrence on Panarea has a chemical signature inconsistent with the X-5 tephra, raising the possibility that the X-5 marker tephra is not yet identified in the Aeolian Islands. Previously the SAL-III and SAL-II tephra layers were assigned to generic Campanian explosive volcanism. Our new glass data reveal that these LAR tephra layers are clearly attributed to explosive activity on Ischia Island. SAL-III and SAL-IV are stratigraphically positioned below the IT on Salina, which is firmly verified here as relating to the Monte Epomeo Green Tuff (MEGT) and can be most precisely dated at 56.1 ± 1.0 ka following the $^{40}Ar/^{39}Ar$ age generated from a distal MEGT equivalent (TF-7) recorded at Lake Fucino, central Italy (Giaccio et al., 2017). SAL-III and SAL-IV are chemo-stratigraphically related to the pre-MEGT activities on the island, and clearly illustrate that Ischia produced a succession of closely spaced large-magnitude eruptions and widespread ash fall events in the lead up to the caldera-forming MEGT eruption. Our SAL-III and SAL-IV glass data can be directly compared to new analyses of the Tyrrhenian Sea marine tephra units, C(i)-8 (72.7 ka) and C(i)-7 (67.9 ka) of Paterne et al. (1988). This is important as the orbitally tuned, oxygen isotope stratigraphy, derived ages are currently the preferred age constraints for these two external tephra deposits on Salina, which ultimately constrain the timing of the highly explosive Grey Porri Tuffs erupted on the island. Finally, a bed of loose rounded pumice collected from the base of the Lower Brown Tuffs on Filicudi are attributed here to Campanian volcanism, compositionally they are more akin to the products of Ischia, although an origin from the Pre-CI activities cannot be completely excluded at this stage. Determining the precise origin of this tephra would be important for more reliably constraining the lower age limit of the Lower Brown Tuffs originating from Vulcano.

References

Bourne A.J., Cook E., Abbott P.M., Seierstad I.K., Steffensen J.P., Svensson A., Fischer H., Schüpbach S., Davies S.M., 2015. A tephra lattice for Greenland and a reconstruction of volcanic events spanning 25–45 ka b2k, Quaternary Science Reviews 118, pp 122-141.

Donato P., Albert P.G., Crocitti M., De Rosa R., Menzies M.A., 2016. Tephra layers along the southern Tyrrhenian coast of Italy: Links to the X-5 & X-6 using volcanic glass geochemistry, Journal of Volcanology and Geothermal Research 317, pp 30-41.

Forni F., Lucchi F., Peccerillo A., Tranne C.A., Rossi P.L., Frezzotti M.L., 2013. Stratigraphic and geological evolution of the Lipari volcanic complex (central Aeolian archipelago). Geol. Soc. Lond. Mem. 37, 213–279.

Francalanci L., Lucchi F., Keller J., De Astis G., Tranne C.A., 2013. Eruptive, volcanotectonic and magmatic history of the Stromboli volcano (north-eastern Aeolian archipelago). Geol. Soc. Lond. Mem. 37, 397–471.

Giaccio B., Hajdas I., Isaia R., Deino A., Nomade S., 2017. High-precision 14C and 40Ar/39Ar dating of the Campanian Ignimbrite (Y-5) reconciles the time-scales of climatic-cultural processes at 40 ka. Sci Rep 7, 45940.

Keller J., 1980. The island of Vulcano. Rendiconti della Società Italiana di Mineralogia e Petrologia. 36, pp 369-414.

Kraml M., Keller J., Henjes-Kunst F., 1997. Dating of Upper Quaternary Deep-sea Sediments from the Ionian Sea (Eastern Mediterranean) with Laser 40Ar/39Ar Analyses on Prominent Tephra Layers. EUG 9 (European Union of Geosciences), Strasbourg France, Terra Nova 9, Abstract Supplement. 1 p. 406.

Lucchi F., Tranne C.A., De Astis G., Keller J., Losito R., Morche W., 2008. Stratigraphy and significance of Brown Tuffs on the Aeolian Islands (southern Italy). J. Volcanol. Geotherm. Res. 177, 49–70.

Lucchi F., Keller J., Tranne C., 2013a. Regional stratigraphic correlations across the Aeolian archipelago (southern Italy). Geol. Soc. Lond. Mem. 37, 55–81.

Lucchi F., Santo A.P., Tranne C.A., Peccerillo A., Keller J., 2013b. Volcanism, magmatism, volcano-tectonics and sea-level fluctuations in the geological history of Filicudi (western Aeolian archipelago). Geol. Soc. Lond. Mem. 37, 113–153.

Lucchi F., Tranne C.A., Peccerillo A., Keller J., Rossi P.L., 2013c. Geological history of the Panarea volcanic group (eastern Aeolian archipelago). Geol. Soc. Lond. Mem. 37, 349–393.

Morche W., 1988. Tephrochronologie der Aolischen Inseln. Unpublished PhD Thesis. Albert-Ludwigs-Universitat Freiburg, Germany.

Paterne M., Guichard F., Labeyrie J., 1988. Explosive activity of the South Italian volcanoes during the past 80,000 years as determined by marine tephrochronology. J. Volcanol. Geotherm. Res. 34, 153–172.

Tomlinson E., Arienzo I., Civetta L., Wulf S., Smith V.C., Hardiman M., Lane C.S., Carandente A., Orsi G., Rosi M., Muller W., Thirwall M.F., Menzies M., 2012. Geochemistry of the Phlegraean Fields (Italy) proximal sources for major Mediterranean tephras: implications for the dispersal of Plinian and co-ignimbritic components of explosive eruptions. Geochimica et Cosmochimica Acta.

Tomlinson, E.L., Albert, P.G.,Wulf, S., Brown, R., Smith, V.C., Keller, J., Orsi, G., Bourne, A.J., Menzies, M.A., 2014. Age and geochemistry of tephra layers from Ischia, Italy: constraints from proximal-distal correlations with Lago Grande di Monticchio. J. Volcanol. Geotherm. Res. 287, 22–39.

Wulf S., Keller J., Paterne M., Mingram J., Lauterbach S., Opitz S., Sottil G., Giaccio B., Albert P., Satow C., Viccaro M., Brauer A., 2012. The 100-133 ka record of Italian explosive volcanism and revised tephrochronology of Lago Grande di Monticchio. Quaternary Science Reviews 58, 104-123.

Chapter 5

Sedimentological analysis of ash-rich pyroclastic density currents, with special emphasis on syn-depositional erosion and clast incorporation: the Brown Tuff eruptions (Vulcano, Italy)

F. Lucchi [a], R. Sulpizio [b,c,d], S. Meschiari [a], C.A. Tranne [a] , P.G. Albert [c,f], D. Mele [b] , P. Dellino [b].

[a] Dipartimento di Scienze Biologiche, Geologiche e Ambientali, Università di Bologna, Piazza Porta S. Donato 1, 40126 Bologna, Italy

[b] Dipartmento di Scienze della Terra e Geoambientali, Universitá di Bari, via Orabona 4, 70125 Bari, Italy

[c] INGV- Bologna section, via D. Creti, 40100, Bologna, Italy

[d] IGAG-CNR, Area della Ricerca di Roma 1- Strada Provinciale 35d, Montelibretti (Rome), Italy

[e] Department of Geography, Swansea University, Singleton Park, Swansea SA2 8PP, UK

[f] Research Laboratory for Archaeology and the History of Art (RLAHA), University of Oxford, Dyson Perrins Building, South Parks Road, Oxford OX1 3QY, UK

Submitted to Sedimentary Geology

Sedimentary Geology

Sedimentological analysis of ash-rich pyroclastic density currents, with special emphasis on syn-depositional erosion and clast incorporation: the Brown Tuff eruptions (Vulcano, Italy)

--Manuscript Draft--

Manuscript Number:	
Article Type:	Research Paper
Keywords:	Brown Tuffs Aeolian Islands Sedimentary structures Pyroclastic density current Clast embedding Shear-related granular instability structures
Corresponding Author:	Federico Lucchi University of Bologna: Universita di Bologna ITALY
First Author:	Federico Lucchi
Order of Authors:	Federico Lucchi
	Roberto Sulpizio
	Sara Meschiari
	Claudio Antonio Tranne
	Paul G. Albert
	Daniela Mele
	Piero Dellino
Abstract:	The sedimentological, lithological and textural characteristics of the Brown Tuffs (BT) pyroclastic deposits, combined with their grain-size, componentry and geochemical glass compositions, are here investigated to obtain information on the transport and depositional mechanisms of the corresponding pyroclastic density currents (PDCs). The BT are widespread reddish-brown to grey, ash-rich pyroclastic deposits generated by pulsating hydromagmatic explosive activity from the La Fossa Caldera on Vulcano island during the c. 80-6 ka time-stratigraphic interval, and then distributed on most of the Aeolian Islands and Capo Milazzo peninsula (Sicily) and in the Tyrrhenian and Adriatic Sea regions. Near the source area on Vulcano, the BT are characterized by alternating massive and planar to cross stratified lithofacies that result from the stepwise, repeating aggradation of discrete PDC pulses. This alternance is regulated by either fluid escape or granular flow depositional regimes at high clast concentration or grain by grain traction deposition in the waning diluted stages of the PDCs. Most of the BT on Vulcano show intermittently stratified and massive ash deposits result of a pervasive post-depositional disruption of the primary structures as induced by upward fluid expulsion associated to dissipation of pore pressure between layers at different grain size (fine to coarse ash) and porosity. This feature is outlined by distinctive upwards bends and pillar-type escape structures through the fluid-filled cracks and rupture points. Massive BT deposits with a faint color and grain-size banding are widely recognized on Lipari, the nearby island of Vulcano. Based on the presence, at the base of BT depositional units, of cm-thick amalgamation bands containing pumice lapilli, scoria and lithic clasts ripped-up and embedded from the loose underlying pyroclastic units, they are interpreted as deposited by ash flows laterally spreading from La Fossa Caldera and moving, over the sea, to Lipari. In this paper, the mechanism of clast erosion and incorporation is outlined across the whole island of Lipari by means of field study, grain-size, and geochemical glass analyses on the different components of the mixed basal bands of the BT. This suggests that the BT PDCs maintained enough flow power as to erode the substratum, hence likely impacting the territory, over a distance up to at least 16-17 km from the volcanic source. Evidence that the BT PDCs exerted a high shear-stress over the loose substratum is also provided by undulated, recumbent

	flame and rip-up structures at the base of some depositional units in southern and central Lipari. In order to form such bed granular instabilities between the BT and the underlying deposits we calculate that the currents had at least a shear velocity of ca. 2 m s $^{-1}$ and a shear stress in the range of 1-4.5 kPa. These results add new insights on the large-scale hazard at the Aeolian Islands and shed new lights on the widespread transport and depositional dynamics of ash flows spreading over the sea and reaching nearby islands, and their interactions with the substratum and the pre-depositional topography.
Suggested Reviewers:	Guido Giordano University of Roma 3 guido.giordano@uniroma3.it
	Damiano Sarocchi Universidad Autónoma de San Luis Potosí: Universidad Autonoma de San Luis Potosi sarocchi@gmail.com
	Brittany Brand Boise State University brittanybrand@boisestate.edu
	Jose Luis Macias UNAM: Universidad Nacional Autonoma de Mexico macias@igeofisica.unam.mx
	Greg A. Valentine University at Buffalo gav4@buffalo.edu
	Roberto Isaia INGV: Istituto Nazionale di Geofisica e Vulcanologia roberto.isaia@ingv.it
Opposed Reviewers:	Claudio Scarpati University of Naples Federico II: Universita degli Studi di Napoli Federico II claudio.scarpati@unina.it diatribes in reviews of other works

DIPARTIMENTO DI SCIENZE BIOLOGICHE, GEOLOGICHE e AMBIENTALI

11 May 2021

Manuscript submission to Sedimentary Geology

Dear Editor,

We would like our manuscript entitled '***Sedimentological analysis of ash-rich pyroclastic density currents, with special emphasis on syn-depositional erosion and clast incorporation: the Brown Tuff eruptions (Vulcano, Italy)***' to be considered for publication in your journal. Full details of all co-authors are listed at the end of this letter.

In this paper we investigate the transport and depositional behaviour of the ash-rich pyroclastic deposits known as Brown Tuffs (BT) that are generated by pulsating hydromagmatic explosive activity from the La Fossa Caldera on Vulcano island during the c. 80-6 ka time-stratigraphic interval, and then distributed on most of the Aeolian Islands and the southern Tyrrhenian Sea (southern Italy), representing the thickest and most voluminous volcanic unit in this active volcanic setting.

We present a detailed sedimentological analysis of lithofacies of the BT deposits combined with textural and grain-size characteristics, componentry and geochemical glass compositions, with a particular attention to shear-related syn-depositional sedimentary structures occurring at the base of most of the depositional units. The data show that the BT near the source area are deposited from repeating aggradation of discrete PDC pulses characterized by fluid escape (or granular flow) to grain by grain traction depositional regimes relative to varying clast concentration during the waning stages of the individual PDCs. The primary deposits are pervasively disrupted by post-depositional upward fluid escape (pore pressure) between layers at different grain size and porosity. In the nearby island

ALMA MATER STUDIORUM - UNIVERSITÀ DI BOLOGNA

PIAZZA DI PORTA SAN DONATO, 1 - 40126 BOLOGNA - ITALIA - TEL. 051-2094936 - FAX 051-2094904
Dott. Federico Lucchi
federico.lucchi@unibo.it

of Lipari most of the BT depositional units show sedimentological, grain size and geochemical evidence of distinctive mixing bands at the contact with the loose underlying pyroclastic units derived from clast embedding by laterally-spreading PDCs that moved over the sea at distances of tens of kms away from the source. These PDCs developed at the base shear-related bed granular instabilities to the underlying substratum indicating conditions of high solid concentration and basal shear velocity of the currents of up to c. 2 m s^{-1} and a shear stress in the range of 1-4.5 kPa at the time of structure formation.

These results shed new lights on the widespread mobility of ash flows spreading over the sea and reaching nearby islands, interacting with the substratum and the pre-depositional topography, thus providing new insights on large-scale volcanic hazard assessment. This information is crucial particularly for ash rich PDCs that usually have homogeneous massive structure and a challenging sedimentological interpretation. Noteworthy, our results may have a larger outcome than the volcanic environments because mechanisms of fluid expulsion related to dissipation of pore pressure and/or granular bed instabilities resulting from the shear exerted by granular flows on a loose substratum have been demonstrated in deposits of marine and fluvial sedimentary environments.

The material presented in this manuscript has not been submitted to another journal. We hope you will find the manuscript suitable for publication in Sedimentary Geology.

Yours sincerely,

Federico Lucchi

ALMA MATER STUDIORUM - UNIVERSITÀ DI BOLOGNA

PIAZZA DI PORTA SAN DONATO, 1 - 40126 BOLOGNA - ITALIA - TEL. 051-2094936 - FAX 051-2094904
Dott. Federico Lucchi
federico.lucchi@unibo.it

DIPARTIMENTO DI SCIENZE BIOLOGICHE, GEOLOGICHE e AMBIENTALI

Title:

Sedimentological analysis of ash-rich pyroclastic density currents, with special emphasis on syn-depositional erosion and clast incorporation: the Brown Tuff eruptions (Vulcano, Italy)

Authors:

Federico Lucchi [a, *], Roberto Sulpizio [b, c, d], Sara Meschiari [a], Claudio Antonio Tranne [a], Paul G. Albert [e,f], Daniela Mele [b], Piero Dellino[b]

[a] Dipartimento di Scienze Biologiche, Geologiche e Ambientali, Università di Bologna, Piazza Porta S. Donato 1, 40126 Bologna, Italy

[b] Dipartmento di Scienze della Terra e Geoambientali, Universitá di Bari, via Orabona 4, 70125 Bari, Italy

[c] INGV- Bologna section, via D. Creti, 40100, Bologna, Italy

[d] IGAG-CNR, Area della Ricerca di Roma 1- Strada Provinciale 35d, Montelibretti (Rome), Italy

[e] Department of Geography, Swansea University, Singleton Park, Swansea SA2 8PP, UK

[f] Research Laboratory for Archaeology and the History of Art (RLAHA), University of Oxford, Dyson Perrins Building, South Parks Road, Oxford OX1 3QY, UK

* Corresponding Author: federico.lucchi@unibo.it

Sedimentological analysis of ash-rich pyroclastic density currents, with special emphasis on syn-depositional erosion and clast incorporation: the Brown Tuff eruptions (Vulcano, Italy)

F. Lucchi [a, *], R. Sulpizio [b, c, d], S. Meschiari [a], C.A. Tranne [a], P.G. Albert [e,f], D. Mele [b], P. Dellino[b]

[a] Dipartimento di Scienze Biologiche, Geologiche e Ambientali, Università di Bologna, Piazza Porta S. Donato 1, 40126 Bologna, Italy

[b] Dipartmento di Scienze della Terra e Geoambientali, Universitá di Bari, via Orabona 4, 70125 Bari, Italy

[c] INGV- Bologna section, via D. Creti, 40100, Bologna, Italy

[d] IGAG-CNR, Area della Ricerca di Roma 1- Strada Provinciale 35d, Montelibretti (Rome), Italy

[e] Department of Geography, Swansea University, Singleton Park, Swansea SA2 8PP, UK

[f] Research Laboratory for Archaeology and the History of Art (RLAHA), University of Oxford, Dyson Perrins Building, South Parks Road, Oxford OX1 3QY, UK

[*] Corresponding author

ABSTRACT

The sedimentological, lithological and textural characteristics of the Brown Tuffs (BT) pyroclastic deposits, combined with their grain-size, componentry and geochemical glass compositions, are here investigated to obtain information on the transport and depositional mechanisms of the corresponding pyroclastic density currents (PDCs). The BT are widespread reddish-brown to grey, ash-rich pyroclastic deposits generated by pulsating hydromagmatic explosive activity from the La Fossa Caldera on Vulcano island during the c. 80-6 ka time-stratigraphic interval, and then distributed on most of the Aeolian Islands and Capo Milazzo peninsula (Sicily) and in the Tyrrhenian and Adriatic

Sea regions. Near the source area on Vulcano, the BT are characterized by alternating massive and planar to cross stratified lithofacies that result from the stepwise, repeating aggradation of discrete PDC pulses. This alternance is regulated by either fluid escape or granular flow depositional regimes at high clast concentration or grain by grain traction deposition in the waning diluted stages of the PDCs. Most of the BT on Vulcano show intermittently stratified and massive ash deposits result of a pervasive post-depositional disruption of the primary structures as induced by upward fluid expulsion associated to dissipation of pore pressure between layers at different grain size (fine to coarse ash) and porosity. This feature is outlined by distinctive upwards bends and pillar- type escape structures through the fluid-filled cracks and rupture points. Massive BT deposits with a faint color and grain-size banding are widely recognized on Lipari, the nearby island of Vulcano. Based on the presence, at the base of BT depositional units, of cm-thick amalgamation bands containing pumice lapilli, scoria and lithic clasts ripped-up and embedded from the loose underlying pyroclastic units, they are interpreted as deposited by ash flows laterally spreading from La Fossa Caldera and moving, over the sea, to Lipari. In this paper, the mechanism of clast erosion and incorporation is outlined across the whole island of Lipari by means of field study, grain-size, and geochemical glass analyses on the different components of the mixed basal bands of the BT. This suggests that the BT PDCs maintained enough flow power as to erode the substratum, hence likely impacting the territory, over a distance up to at least 16-17 km from the volcanic source. Evidence that the BT PDCs exerted a high shear-stress over the loose substratum is also provided by undulated, recumbent flame and rip-up structures at the base of some depositional units in southern and central Lipari. In order to form such bed granular instabilities between the BT and the underlying deposits we calculate that the currents had at least a shear velocity of ca. 2 m s^{-1} and a shear stress in the range of 1-4.5 kPa. These results add new insights on the large-scale hazard at the Aeolian Islands and shed new lights on the widespread transport and depositional dynamics of ash flows spreading over the sea and reaching nearby islands, and their interactions with the substratum and the pre-depositional topography.

KEYWORDS

Brown Tuffs, Aeolian Islands, Sedimentary structures, Pyroclastic density current, Clast embedding, Shear-related granular instability structures

1. INTRODUCTION

Pyroclastic density currents (PDCs) are ground hugging mixtures of particles and gas that flow laterally across the topography, and are among the most amazing, complex and dangerous volcanic phenomena (e.g., Carey, 1991; Druitt, 1998; Branney and Kokelaar, 2002; Sulpizio et al., 2014). Irrespective whether they are concentrated or diluted, PDCs are characterized by a very hostile nature and a complex interplay between transport and depositional mechanisms, which make their study a great challenge for volcanologists. The only way we have to get information about the processes occurring at the time of deposition is to analyze the deposit lithofacies and lithofacies associations in the field (e.g. Branney and Kokelaar, 2002; Sulpizio et al., 2008; 2010) or to replicate PDCs in the laboratory (Dellino et al., 2007; 2010; Sulpizio et al., 2016; Breard and Lube, 2017; Lube et al., 2011). This is particularly demanding for ash rich PDCs that usually have a massive structure and homogeneous lithology, which make a unique sedimentological interpretation challenging. Furthermore, quite rare is, in the volcanological literature, the analysis of the interaction between PDCs and the pre-depositional topography, which can influence the runout and the internal organization of the parent currents by means of the bulking due to substratum erosion (Roche et al., 2013; Roche, 2015; Pollock et al., 2019).

The Brown Tuffs (BT) deposits, largely outcropping over the Aeolian islands and northern Sicily (Italy), represent an exceptional case-study for shedding light on the elusive processes that drive erosion and deposition in ash-rich PDCs, and their interactions with the substratum. The BT are ash-rich, reddish-brown to grey volcaniclastic deposits from PDCs and associated fallout produced over a long-time span by pulsating hydromagmatic eruptions from the La Fossa Caldera on Vulcano island (Lucchi et al., 2008; 2013b; Cicchino et al., 2011; Meschiari et al., 2020). They usually crop out as massive, moderately to well sorted, fine to coarse ash deposits of metric thickness. Their quite ubiquitous massive appearance, recurring over a wide time span in the stratigraphy of the Aeolian Islands, and the paucity of distinctive sedimentological characteristics have long made it difficult to define the eruptive and depositional mechanisms of the BT. As such, they have been generically interpreted either as primary deposits from PDCs or fallout, reworked deposits from wind-blown volcanic ash (tuff-loess) or even paleosols (Bergeat 1899; Keller 1967, 1980a, b; Pichler 1980; Crisci et al., 1981, 1983, 1991; Manetti et al., 1988, 1995; Morche 1988; Losito 1989; Gioncada et al., 2003). The most accepted interpretation is currently that they were emplaced by mostly dilute PDCs and/or gentle (fallout) settling from accompanying ash clouds (Lucchi et al., 2008; 2013b). This is based on the occurrence of rare stratified lithofacies, internal color and grain-size banding (fine to coarse ash) and topography-controlled thickness variations on Vulcano and southern Lipari islands (De Astis et al, 1997; Lucchi et al., 2008; 2013b; Dellino et al., 2011). We present here a detailed field study of the lithological and sedimentological characteristics of the BT in the outcrops of Vulcano and Lipari islands, with the aim of investigating in detail the transport and depositional mechanisms of the corresponding PDCs.

Special attention was paid to the evidence of erosion and clast incorporation in the basal portions of some BT depositional units, which were previously signaled by Lucchi et al. (2008; 2013b). Together with the occurrence of shear-related syn-depositional sedimentary structures, this can provide information about the processes occurring in the basal portion of PDCs, which transport the vast majority of the total flow mass (Branney and Kokelaar 2002; Sulpizio et al., 2014) and determine the threat of these dangerous phenomena (Sulpizio et al. 2014; Dufek et al., 2015; Pollock et al., 2019). In recent times, the erosive capacity of PDCs was studied by means of observations in the field (e.g. Pollock et al., 2019) or small scale laboratory experiments (e.g. Roche et al., 2013), mostly focused on polydispersed, poorly sorted, concentrated PDC deposits (e.g. those related to the 1980 Mt. St. Helens eruption; Pollock et al., 2019). Nothing has been done, however, on the erosive capability of well sorted, ash-rich PDCs. In order to contribute in bridging this gap, we carried out a detail field investigation of the lower portions of the ash-rich BT depositional units supported by grain-size, componentry and geochemical analyses, which helped in deciphering the depositional dynamics of BT PDCs and shed new light on the dispersal dynamics of ash-rich PDCs.

2. GEOLOGICAL SETTING

2.1. Aeolian Islands

The Aeolian Islands (Alicudi, Filicudi, Salina, Lipari, Vulcano, Panarea and Stromboli; Fig. 1a) are the emerged portions of an active volcanic system in the Southern Tyrrhenian Sea, which also includes several seamounts (Barberi et al., 1973; Beccaluva et al., 1985; Chiarabba et al., 2008; De Astis et al., 2003; Ventura, 2013). Aeolian volcanism entirely occurred during the Quaternary, as demonstrated by the oldest radiometric age of c. 1.3 Ma of submarine lavas from the Sisifo seamount (Beccaluva et al., 1985), and then developed subaerially from ~270-250 ka to historical and present times (Leocat, 2011; Lucchi et al., 2013b, and references therein) (Fig. 1b). Successive eruptive epochs of the different volcanic islands have been subdivided by volcanic collapses or major quiescent (erosional) stages (De Astis et al., 2013; Forni et al., 2013; Francalanci et al., 2013; Lucchi et al., 2013a, c, d, e), sometimes associated with episodes of marine ingression and terrace formation during the major sea-level fluctuations (Lucchi, 2009). The marine terraces attributed to the marine (oxygen) isotope stage (MIS) 5, dated between c. 124 and 80 ka (Chappell and Shackleton, 1986; Waelbroeck et al., 2002; Rohling et al., 2014), are well constrained time-stratigraphic markers on most of the archipelago. The erupted melts in the Aeolian Islands range from basaltic andesites to rhyolites over a large range of differing magmatic suites from calc-alkaline (CA), high-K calc-alkaline (HKCA), shoshonitic (SHO) and K-Series (KS) (Ellam et al., 1988; Francalanci et al., 1993; Peccerillo et al., 2013). Major Violent Strombolian to Sub-plinian eruptions involving dacite to rhyolite magmas have occurred on Lipari, Vulcano, Salina and Stromboli during the last glacial period (from c. 80 ka) and the early Middle Ages (Crisci et al., 1981; Keller and Morche, 1993; Hornig-Kjarsgaard et al., 1993; Colella and Hiscott, 1997; De Astis et al., 1997a; De Astis et al., 2006). This is the time-stratigraphic period when the BT, the object of the present study, were erupted.

2.2. The Brown Tuffs

The BT are widespread, reddish-brown to grey, massive ash-rich volcaniclastic deposits with metric thickness recognized in the Aeolian Islands and the Capo Milazzo peninsula (Sicily).

Chemo-stratigraphic and tephrochronological studies by Lucchi et al. (2008, 2013b) and Meschiari et al. (2020) have documented the BT occurrence, with variable volumes and dispersal areas, on the islands of Vulcano, Lipari, Salina, Filicudi, Stromboli and Alicudi and the Capo Milazzo peninsula, and in Tyrrhenian and Adriatic Sea marine cores, in the c. 80-6 ka time-stratigraphic interval. The BT have been interpreted as the result of PDCs and associated gentle setting or fallout related to a pulsating hydromagmatic explosive activity from a source located inside the La Fossa caldera on Vulcano island (Fig. 1; De Astis et al, 1997; Lucchi et al., 2008, 2013b; Cicchino et al., 2011). Also the composition of BT, ranging from K-series (K_2O = 3.3-7.5 wt.%) basaltic trachy-andesites and trachy-andesites through to tephri-phonolites and trachytes (SiO_2 = 49.9-64.1 wt.%; Na_2O + K_2O = 6.5-12.6 wt.%), is entirely consistent with the Vulcano magmatic system (Meschiari et al., 2020).

The BT succession is delimited at the base by marine terraces attributed to the late marine (oxygen) isotope stage (MIS) 5 (c. 124-80 ka), and is subdivided into four macro-units: Lower BT (LBT; 80-56 ka), Intermediate BT (IBT; 56-27 ka), Intermediate-upper BT (IBT-upper; 26-24 ka) and Upper BT (UBT; 24-6 ka). This subdivision is based on the occurrence of interbedded widespread regional or local marker beds, namely the ‘Ischia Tephra’, equivalent to the Y-7 marine marker tephra (Epomeo Green Tuff, 56 ka; Keller et al., 1978; Tomlinson et al., 2014), the Monte Guardia pyroclastics from Lipari (27-26 ka) and the Spiaggia Lunga scoriae (24 ka) on Vulcano (Fig. 2; Meschiari et al., 2020). These macro-units are furtherly split into (at least) 16 depositional units, best documented on Vulcano and Lipari islands, where they have variable thicknesses ranging from a few decimeters up to a maximum of 3 m (for each depositional unit), while the entire BT succession has a (cumulated) maximum thickness of 15–25 m on Vulcano and southern Lipari. The different BT depositional units are best distinguished when they are separated by interlayered (local) volcanic units and tephra layers. Between these, the Petrazza Tuffs from Stromboli (77-75 ka) contribute to define the lower chronological constraint of the LBT, whilst the Grey Porri Tuffs (GPT, 70-67 ka) and Lower Pollara Tuffs (LPT, 27 ka) from Salina and the Vallone del Gabellotto tephra from Lipari (8.7–8.4 ka) are important for stratigraphic subdivisions in the LBT, IBT and UBT, respectively (Fig. 2). The Cugni di Molinello scoria bed is an important stratigraphic marker on Vulcano separating the lower and upper portions of the UBT (De Astis et al., 1997; Lucchi et al., 2008, 2013b), which are delimited at the top by the Punte Nere tuffs (5.5 ka). A list of the main features of the units interlayered within the BT succession is provided in Table 1. When not intercalated with other deposits, the BT generally appear as lithologically-homogeneous tephra accumulations that are unlikely to represent single depositional units, but instead they are the amalgamation of different depositional units, as also testified by the occurrence of interlayered localized erosional surfaces and reworked horizons with a limited lateral persistence.

3. METHODS AND TERMINOLOGY

Lithostratigraphic and sedimentological analysis of the BT was carried out on most of the outcrops exposed on the islands of Vulcano and Lipari (Fig. 1; Table 2), which allow identification (and correlation) of the largest number of depositional units of the BT, relative to all the distinguished BT macro-units (LBT, IBT, IBT-upper and UBT). Following Lucchi (2013), a “depositional unit” is defined as the volcanic (pyroclastic) material deposited during a single, relatively continuous depositional event from PDCs or fallout, and is delimited by evidence of interruptions of deposition (e.g. erosive surfaces, paleosols, reworked beds, angular discordances) or other sedimentological features (e.g. presence of fine “co-ignimbrite” ash, lithic-rich beds, sharp grain-size variations), and/or by interlayered exotic pyroclastic (including distal tephra layers) or lava deposits.

Outcrop description and sediment logging were based on classical lithostratigraphy and lithofacies analysis, as the main tools to infer the volcanological interpretation of the studied deposits in terms of their transport and emplacement mechanisms (see Branney and Kokelaar, 2002; Sulpizio and Dellino, 2008; Lucchi, 2013 for reviews). Sedimentological investigation of BT units was carried out through lithofacies analysis, which has commonly been used to describe and decipher the deposits of marine and non-marine environments (e.g. Miall, 1978, 1985; Lowe, 1982; Mathisen and Vondra, 1983; Smith, 1986, 1987; Waresback and Turbeville, 1990; Zanchetta et al., 2004a) and then applied to complex sequences of pyroclastic deposits (Sohn and Chough, 1989; Chough and Sohn, 1990; Colella and Hiscott, 1997; Gurioli et al., 2002; Sulpizio et al., 2007; 2010) and to lateral and vertical variations of sedimentary structures within widespread ignimbrites (e.g. Freundt and Schmincke, 1986; Druitt, 1992; Cole et al., 1993; Allen and Cas, 1998). Lithofacies have been identified in the BT deposits using a combination of texture, sedimentary structures, grain-size and sorting (Table 3). Sedimentary structures were described and measured at cm-scale, and, Grain-size and component analyses were carried out on selected samples of the mixing bands and reworked bed material at the base of various BT depositional units. Weight % of the size fractions coarser than 3 ϕ (125 μm) at 0.5 ϕ intervals ($\phi = -\log_2 d$), where d is the particle size in mm) were estimated using dry mechanical sieving. The finer fractions, from 3.5 ϕ (63 μm) to 9 ϕ (2 μm), were analysed by means of a Beckman Coulter Multisizer 4 (Mele et al. 2015), and expressed as volume % and successively converted in weight % using a constant clast density. Component analysis (juvenile, lithics and crystals) was carried out on a representative number of particles of each grain-size fraction of the bulk material. We have differentiated six main classes of components in the size fractions coarser than 3 ϕ (125 μm): i) pumice (white and grey) and ii) scoria of different porphyricity and vesicularity; iii) obsidian fragments; iv) glass fragments; v) crystals; vi) lithic clasts. The finer size fractions are undifferentiated. For the size fractions in the range from 16 to 1.4 mm, a subsample of particles of each component was hand-picked and weighted; the weight fraction of each component was calculated for each size by scaling the number of particles of the subsample to the total weight of the sample. For the grain-size range from 1 to 0.125 mm, particles of each component were counted under a stereomicroscope. The weight of each component was estimated by means of the density of each component in each size fraction. The grain-size statistical parameters by Folk and Ward (1957) were then calculated for the different sub-populations recognized in the samples from the base of BT depositional units by means of the GRADISTAT program (Blott and Pye 2001; Table 4).

Major and minor element glass data for selected samples of the basal portions of a number of BT depositional units are here provided, referring to the extensive dataset recently made available by Meschiari et al. (2020) for most of the BT depositional units and the interbedded tephra deposits. The samples were mounted in Streurs Epofix epoxy resin and mounts were ground, polished and carbon coated in preparation for chemical analysis. Glass data were determined using a wavelength-dispersive JEOL 8600 electron microprobe (WDS-EMP) hosted at the RLAHA, University of Oxford. Details of the analytical operating conditions, monitoring of data accuracy and precision, and post-analysis data treatment are provided in Meschiari et al. (2020), together with the MPI-DING reference glasses (Jochum et al., 2006). Data presented in plots are normalised (e.g. water-free) and error bars represent reproducibility, calculated as 2 x standard deviation of replicate analysis of StHs6/80-G reference glass.

4. RESULTS AND ANALYSES

4.1. Sedimentological features of the BT

Sedimentological analysis of the BT has been carried out on the outcrops exposed on Vulcano and Lipari islands (Fig. 1), which allow definition of the most complete succession of distinct depositional units of the LBT, IBT, IBT-upper and UBT macro-units (Fig. 2). Most of the outcrops are located in the flattish area of Il Piano on Vulcano island, located southeast of the La Fossa Caldera source area, and mainly belong to the UBT macro-unit. These outcrops are the most proximal today exposed, because the very proximal BT deposits within the inner part of the La Fossa Caldera were affected by the recent collapses in this area or buried below the Holocene deposits of the La Fossa cone (De Astis et al., 2013). Other outcrops of the BT are located to the west of the La Fossa Caldera, near the locality of Grotta dei Pisani, and along the southern flank of

Vulcano, near Gelso (Fig. 1). The BT have been also investigated on a number of outcrops in distinct sectors of the nearby island of Lipari at increasing distances from the source area. The main characteristics of the studied outcrops, and their distance from the source area, are summarized in Table 2.

In most outcrops the BT consist of massive (fine to coarse) ash and show, in places, internal bands of different colors (and grain-size) with gradual contacts (lithofacies mA; Table 3; Fig. 3A). Plane-parallel to cross bedding stratification and lamination (lithofacies psA-xsA; Table 3; Fig. 3B) occur in some exposures on Vulcano and southern Lipari islands, particularly in the UBT deposits (De Astis et al, 1997; Lucchi et al., 2008). Dune bedding with internal cross stratification (having ca. 2-m wavelength and 0.5-m amplitude) are observed in the outcrops of the UBT outside the southeastern rim of La Fossa Caldera. In the outcrops on Vulcano island, the BT are generally characterized by the alternation of mm to cm thick massive and stratified beds (lithofacies altpsmA), with the occurrence of some laminae of weakly consolidated reddish fine ash. The stratification (and lamination) is generally not laterally persistent and is largely disrupted (lithofacies isA; Table 3; Figs. 3C-F). A typical upward bending of the laminae is observed in many of the fragmentation points (Fig. 3E-H), and in some cases disruption of the laminae occurs in correspondence of mm-scale vertical columns of coarse ash (Fig. 3G-H). The disruption of stratification (lamination) is frequently pervasive, with fragments of laminae distributed unevenly within the massive deposits. It is noteworthy that in a number of outcrops on Vulcano, although seemingly not stratified and unstructured, the BT deposits embed scattered fragments of laminae as relicts of the original stratified/laminated lithofacies (Fig. 3I).

Syn-depositional shear structures (lithofacies mixAL, ucAL, rfAL, ruAL; Table 3) are described and measured at cm-scale at the base of most of the BT depositional units (Figs. 4 and 5), and are more abundant on Lipari rather than on Vulcano (the BT source area). This is probably because of the most common occurrence of interlayered (incoherent) exotic pyroclastic deposits within the BT succession on Lipari, which make the shear structures in the basal portions of the different BT depositional units more evident. In these cases, the basal contacts between BT and exotic deposits are transitional (Fig. 4). The base of the BT depositional units is instead sharp when the underlying units consist of lavas or welded scoriae (e.g. Spiaggia Lunga scoriae) and other not erodible pyroclastic deposits, whereas the top contact is always sharp (conformable or unconformable). The basal transitional contacts occur as bands of mixed material between the BT and the underlying incoherent pyroclastic deposit (lithofacies mixAL; Table 3). Most of the interbedded pyroclastic deposits are composed of whitish to grey pumice and obsidian (P. di Perciato, Falcone, Lip1, Monte Guardia, Vallone del Gabellotto from Lipari; Fig. 4B-H) or grey to dark-grey scoriae and pumice (Grey Porri Tuffs and Lower Pollara Tuffs from Salina; Cugni di Molinello from Vulcano) (Fig. 4A), which show a strong lithological contrast with respect to the homogeneous reddish-brown to grey, ash characterizing the BT. The mixing bands (and the other shear structures in the following) are more easily recognized where the eroded/remobilized bed is made of lapilli (due to the contrasting grain-size) or light colored clasts (due to contrasting color), whereas they are less visible when the eroded units consist of ash. The maximum dimension of the entrained clasts (either pumice or lithic) in lithofacies mixAL is of 10 cm at the base of BT9 depositional unit in southern Lipari (Fig. 4E). Thickness of the mixing bands ranges (approximately) from a few to tens of cm, with a gradual upward transition to the un-mixed BT material (Fig. 4; Table 2), and is arbitrarily measured relative to the level where we do not recognize substantial evidence of incorporated clasts from the underlying units (except for scattered lapilli at various levels). The lithofacies mixAL occurs independently of the paleo-topography, outcropping even in case of a sub-horizontal topography of the pre-BT substratum. Mixing bands are recognized in the entire study area up to the northern sector of Lipari.

Undulated structures consisting in basal layers composed of reworked bed material that appears as wavy and consisting of alternating crests and troughs (lithofacies ucAL; Table 3) are recognized in southern and central Lipari at the contact between BT and the underlying pumice deposits (Fig. 5A-C). Following Pollock et al. (2019), the length of an undulated structure is the distance between successive troughs, and its height is the distance from the lowest part of a trough to the top of the crest. Undulated structures on Lipari have length between 60 and 450 cm and height of ca. 20 cm (Table 2), and they are best exposed in outcrops arranged longitudinally with respect to the BT source area, at distances of 7-10 km (Fig. 5A-C). Crests are almost symmetric and internally massive (Fig. 6B), showing imbrication of coarser clasts.

Recumbent flame structures (lithofacies rfAL; Table 3) have an overhanging arm of entrapped clasts from the basal layer that protrudes up into the BT deposit and becomes sub-horizontal and thins in downflow direction (conforming with Pollock et al., 2019). They are common at the base of depositional unit BT9, with the best preserved one documented above the Falcone pyroclastic deposits at Spiaggia Valle Muria, south of Lipari, where the structure has a length of about 60 cm and height of about 20 cm (Fig. 5D). The length is the extent of the deformed zone and the height is the distance from root to top of the sub-horizontal tail. Lithofacies rfAL commonly occurs as trains of pumice and lithic lapilli a few cm above and parallel to the basal contact of the depositional unit BT9 (Fig. 5D). In places, only the trunk of the structure is preserved as an asymmetric deformation of the lapilli from the underlying bed (Fig. 5E).

Rip-up structures (ithofacies ruAL; Table 3), similar to recumbent flame structures, are visible at the base of some depositional units. In these cases the contact is almost planar, but there are small hook-like structures as asymmetric deformations of the underlying bed, which resemble the trunk of a flame structure (Fig. 5F). These structures are usually few cm in height and they are bended downcurrent.

4.2. Grain-size and components of the mixing bands of the BT

We collected samples of the mixing bands at the base of some BT depositional units on Lipari island, with the aim of investigating their grain-size distribution and components. The depositional units investigated here cover mostly the stratigraphic interval of the IBT and IBT-upper macro-units, but, as for the grain-size distributions, the results may be considered representative of the entire BT succession because of similar lithology and textural characteristics (Lucchi et al., 2008; De Rosa et al., 2016).

Most samples have a polymodal grain-size distribution (except for sample Lip03/17) and a large number of components (Fig. 6), as widely expected for mixing bands between BT units and the underlying tephra beds. On this respect, each grain-size distribution is the combination of two distinct sup-populations of components, one referred to the BT and the other relative to the underlying pyroclastic deposits. Considering that the Folk and Ward (1957) statistical parameters, like median diameter (Mdϕ) and sorting ($\sigma\phi$), are not useful for polymodal distributions, we then calculate them in Table 4 for the separated component distributions (and not for the bulk grain-size) recognized in the samples from the base of BT depositional units as in Figure 6.

The BT typically consist of fine (dominant) to coarse ash composed of aphiric, glass fragments (from about 65 to 90 vol. %), from dark-brown to brownish and colorless, mostly blocky or poorly vesicular, often slightly altered on their external parts (De Astis et al., 1997; De Rosa et al., 2016). The rest of the BT juvenile components (5–35%) are crystals (clinopyroxene and minor plagioclase, K-feldspar, olivine and amphibole) that are presents as loose fragments or rimmed by glass, with local abundance of mm-size clinopyroxene crystals. Lithic fragments are subordinate in the BT as components of the coarse ash fraction, for a total lithic content usually lower than 5 vol.% (De Astis et al., 1997; Lucchi et al., 2008; De Rosa et al., 2016), except for higher amounts up to 10% in some outcrops of the UBT on Vulcano (De Astis et al., 1997). Diffused dark (to yellowish) scoria lapilli are recognized in different stratigraphic levels of the BT on Vulcano and Lipari (Meschiari et al., 2020).

We attribute to the juvenile BT sub-population most of the glass fragments and crystals recognized in the fine to coarse ash fractions of the analyzed samples, and all the (undifferentiated) very fine ash. Loose crystals are considered as components of the BT sub-population, because they lack in the units interlayered to the BT succession. Lithics are kept aside from this analysis because it is not possible to establish which sub-population they belong to. The analyzed samples contain variable amounts of exotic components that are correlated to the pyroclastic deposits underlying each of the BT depositional units. These are classified here as ‘external components’ with respect to the BT sub-population. Specifically, whitish to (minor) grey pumice, and obsidian fragments are recognized in the mixing band at the base of depositional unit BT9 (outcrop L2) and they are fully consistent with the componentry of the underlying Falcone tephra (Gioncada et al., 2005; Forni et al., 2013). Poorly vesicular, highly porphyritic dark scoria and highly vesicular (subaphiric) white pumice are reported in the mixing band at the base of deposition unit BT11 in the outcrop L12, as the main components of the underlying bed of the Lower Pollara Tuffs from Salina Island (Morche 1988; Crisci et al., 1991; Calanchi et al., 1993; Lucchi et al. 2008; Forni et al. 2013). Then, the base of depositional unit BT12 sampled in the outcrops L5, L10 and L12 contain highly vesicular, white (Kf-bearing) pumice, dense to moderately vesicular grey pumice and banded pumice, and variable amounts of obsidian fragments and lithic clasts that are the typical components of the underlying Monte Guardia pyroclastic deposits (De Rosa et al., 2003). A certain amount of sub-aphyric, dark scoria ash fragments are recognized in the depositional units BT9 and BT12 (in outcrops L2, L5 and L10), and they are not present in the underlying Falcone and Monte Guardia units. These scoria fragments are thus included in the componentry of the BT depositional units, in agreement with the report of diffused dark scoria lapilli in different BT outcrops on Vulcano and Lipari (Meschiari et al., 2020).

In all the analyzed BT depositional units the exotic components are prevalent in the lapilli and block/bombs fractions (Fig. 6), and they have a polymodal grain-size distribution. Glass fragments, crystals and scoria referred to the BT are instead mainly represented in the fine ash fraction. There is not a significant variation of the relative abundance of exotic components with distance from the source area, as evident comparing the grain-size distributions of the BT12 depositional unit in the outcrops L5, L10 and L12 (Fig. 6), at distances from 10 to 14.5 km from the source. However, different quantities of the single grain-size classes and variations of the content of the individual exotic components are reported in these outcrops as a function of the variable lithological features of the underlying Monte Guardia unit in proximal to distal reaches, relatively to the eruptive vent in southern Lipari. The analyzed sub-populations of the BT have all fairly regular and unimodal grain-size distributions, with generally good to moderate sorting (σ_ϕ ranging between 1.29 and 2.07) and Md_ϕ ranging between 3.13 and 4.97 (Fig. 6), and are roughly consistent with the pattern obtained by De Astis et al. (1997) for the UBT on Vulcano. However, we argue that the data for the BT sub-populations may be not totally depurated from the presence of external components related to the embedded lapilli and ash from the underlying units. This may explain the median value of 1.98 for the LIP02/17 sample in the central sector of Lipari and the moderate sorting of some samples that do not fully fall within the defined trend of a regularly decreasing median (and better sorting) with the distance from the source.

Significant vertical variations of the grain-size parameters are reported for data from different levels of the same BT depositional unit. Specifically, BT12 in the L5 outcrop and BT11 in outcrop L12 were sampled at two stratigraphic levels (Fig. 6). Component analyses show an upward decrease of the content of exotic components, along with an increase in the amount of fine ash.

4.3. Geochemical components of the mixing bands of the BT

A number of the BT depositional units investigated on both Lipari and Vulcano islands contain minor populations of exotic volcanic glass compositions that mostly plot well outside the dominant K-series compositional field of the BT, which ranges from basaltic trachy-andesites and trachy-andesites through to tephri-phonolites and trachytes. The exotic glass compositions are here named ‘secondary components’ consistent with Meschiari et al. (2020) (Fig. 7A, B). These secondary components are generally reported from the basal portions of the individual BT depositional units, characterized by mixing bands with the underlying pyroclastic deposits (lithofacies mA), and chemically similar to these deposits. Figure 7 provides clear evidence of the geochemical correspondence between the secondary components identified within depositional units belonging to the LBT, IBT, IBT-upper and UBT macro-units and the underlying pyroclastic units sourced from eruptions on Salina (Grey Porri Tuffs), Lipari (P.del Perciato, Falcone, Lip1, M. Guardia, Vallone del Gabellotto) and Vulcano (Cugni di Molinello), following the reconstructed stratigraphic succession (Fig. 2). Major and minor element glass analyses of representative samples relative to different BT depositional units and their secondary components are reported in Table 4.

Among the analysed samples there is only one apparent lack of geochemical agreement between a BT secondary component and the underlying deposits. Specifically, the BT8 depositional unit (sample bt12/16), belonging to the IBT, directly rests above the Punta del Perciato pumice and ash in the L2 outcrop of Lipari. While it contains secondary rhyolitic glasses that are compositionally similar at a major element level to the Punta del Perciato glasses, some of these secondary glasses exhibit significantly higher K_2O and lower Na_2O contents relative to the Punta del Perciato glasses (Figs. 7C, D, E). These offsets could reflect compositional variability in the underlying Punta del Perciato tephra unit which may have been previously undetected, considering that its previous chemical characterisation targeted only the pumice component (Albert et al., 2017). An alternative explanation is that hydration has resulted in alkali exchange within these particular glass fragments. This is apparently supported by previous IBT investigations by De Rosa et al. (2016) who identified physical evidence of fluid induced alteration (hydration) of the juvenile glass particles relating to the syn-eruptive interaction of magma and hot fluids or sea-water. Indeed, our attempt to chemically analyse juvenile glass components of BT8 was entirely precluded by the significant alteration of the dominant glass component.

It is noteworthy that in some cases secondary components are also reported in BT depositional units where mixing with underlying pyroclastic deposits is not visible at a macroscopic scale. In south Lipari (outcrop L2) we sampled the IBT (sample bt14/16) that rests above the Falcone pumice succession, which are commonly subdivided into the depositional units BT9 and BT10 by the interlayered Lip1 tephra unit (Fig. 2). The sample bt14/16 contains HKCA rhyolitic secondary glass components that are broadly consistent with the Lip 1 ash (Figs. 7C, D, E), although this tephra layer is not visible in the investigated outcrop. A possible correlation of the

HKCA rhyolitic secondary glass components found in bt14/16 with the underlying Falcone pumice unit is considered not probable because this sample was taken close to the base of the (overlying) Lower Pollara Tuffs, at about 2 meters above the contact with the Falcone unit. A similar situation is noticed at the Punta della Crapazza outcrop (L0) in the IBT sampled above the Falcone domes (samples LIP15/18, LIP16/18). In these samples we do observe HKCA rhyolitic secondary glasses which are chemically consistent with the Lip1 tephra layer (Figs. 7C, D, E), although the latter is not visible in the investigated stratigraphic succession. A correlation of these secondary components with the Falcone unit, which could be chemically possible, is considered unreasonable because the sampled IBT rests above the thick lava domes erupted after the Falcone pumice succession. Finally, at the outcrop of Monterosa (L7) we sampled the IBT (sample LIP45/17) above the Ischia Tephra, and none of the interbedded stratigraphic makers from southern Lipari are visible (e.g., the Punta di Perciato, Falcone and Lip1). However, in sample LIP45/17 we do find chemical evidence of secondary HKCA rhyolitic glass components that could be attributed to any of the above-mentioned tephra units (Figs. 7C, D, E).

5. DISCUSSION

5.1. Model for deposition from the BT PDCs

PDC deposits record processes occurring in the flow boundary zone, which includes the lowermost part of the current interacting with the forming deposits or with the topography (Branney and Kokelaar, 2002). Most PDC deposits originated from stratified flows in which the segregation of the particles with higher terminal velocities in the lowermost part can result in the development of a high concentration zone (Valentine, 1987; Branney and Kokelaar, 2002; Dellino et al., 2004; Sulpizio et al., 2014). This basal portion of the flow can move downslope developing different depositional regimes, which can span from traction- to granular flow-dominated (Branney and Kokelaar, 2002; Sulpizio et al., 2014). In polydisperse mixtures, including a wide range of sizes (from ash to blocks) and componentry (lithics, pumice, crystals), sedimentary structures may help in deciphering the depositional regime at time of deposition, defining the lithofacies of the deposit. As an example, sedimentary structures like parallel to cross stratification and dune-bedding are indicative of traction-dominated depositional regime from a flow-boundary zone of a diluted PDC. At the other end of PDC spectrum, reverse grading of blocks may indicate a granular flow-dominated depositional regime in a concentrated PDC, in which grain interaction can induce kinetic sieving and kinematic squeezing of the largest particles. If the porosity within the flow-boundary zone is sufficiently low to maintain the gas entrapped in the mixture, a fluid escape-dominated depositional regime may develop, with deposits that appears massive and poorly sorted. Well selected, ash dominated deposits are generally interpreted as gentle settling of fine grained particles from a diluted cloud, defining a direct fallout regime.

These sedimentological hints are poorly useful for PDCs formed only by well selected ash particles, as in the case of most of the BT deposits (Figs. 3-5). This is because of the impossibility to develop sedimentary structures from very fine grain-sizes (Dellino et al., 2019), which makes difficult to interpret the depositional regimes of ash-rich PDCs from lithofacies analysis. This is one of the reasons why it is complicated to decipher the transport and depositional mechanisms of the PDCs of the BT eruptions, which were previously generically interpreted as mostly dilute PDCs associated to gentle setting or fallout from the co-ignimbrite ash clouds or accompanying eruptive columns (De Astis et al., 1997; Lucchi et al., 2008).

Most of the information on the depositional mechanisms of the BT presented here is derived from distinctive lithofacies mA, psA and xsA (Table 3) recognized in the proximal outcrops of the UBT macro-unit on Vulcano island (outcrops V1-V4; Fig. 1). Massive deposits of the lithofacies mA are interpreted as the result of the gentle settling from slow-moving, ground-hugging ash-rich PDCs, and their homogeneous appearance is indicative of fluid escape or granular flow depositional regimes from a fine-grained, concentrated flow-boundary zone. The abundant ash aggregates present in these deposits at the microscopic scale (Lucchi et al., 2008) indicate the occurrence of steam in the ash cloud or fine ash aggregation driven by electrostatic force during the gentle settling of ash from the more diluted portions (or the phoenix cloud) of the PDCs. Lithofacies psA and xsA instead indicate grain by grain deposition from dilute and turbulent PDCs, mainly formed by coarse and fine ash, in which suspension and traction are the main transport (and depositional) mechanisms. Notably, in the UBT deposits investigated here, the most common is lithofacies altpsmA (Fig. 3; Table 3). This is a combination of lithofacies mA and lithofacies psA, and is indicative of a stepwise, repetitive aggradation of discrete PDC pulses developed within each depositional unit of the BT. Massive beds are deposited from granular- or fluid-escape dominated depositional regimes of concentrated PDCs and alternate with stratified ash from the turbulent and diluted ash cloud accompanying the underflow during the waning stage of each pulse. This depositional behaviour is consistent with the long-lasting, pulsating eruptive activity that is assumed to have characterised the emplacement of the UBT macro-unit (and the rest of the BT) on Vulcano island (Lucchi et al., 2008; 2013b).

However, intermittently stratifed ash deposits of the lithofacies isA (Fig. 3) are the most prominent on Vulcano island and characterise most of the BT outcrops on Il Piano area. This lithofacies is not interpreted as a primary feature acquired at time of deposition of the PDCs during the BT eruptions, but as the result of pervasive post-depositional disruption of the primary deposits of lithofacies altpsmA. The disruption of stratified beds here is explained as due to fluid escape related to dissipation of pore pressure from the underlying massive beds (Fig. 8). This mechanism of fluid expulsion resembles that largely described in marine and fluvial sedimentary environments (Allen, 1977; Owen, 1987; 1996; Selker, 1993; Odonne et al., 2011), and even in pyroclastic deposits (Douillet et al., 2015). Experiments have demonstrated that fluid expulsion structures can be produced by an unstable fluidization behavior where a lower base layer of granular material is inhibited from releasing intergranular fluids by the presence of an overlying low porosity top layer (Nichols et al., 1994). The weight of the overlying material is balanced by an increased fluid pressure in the basal layer. If the load exceeds a critical threshold, a fluid-filled crack forms and, as it grows, instability causes the top layer to bend (Fig. 3G). Rupture occurs at the apex of fluid crack, allowing the underlying fluid and fluidized material to burst out through the top layer. The fluidized base layer material then flows through the rupture until the fluid overpressure is fully dissipated. The top layer material is bent upwards around the rupture (Figs. 3E, G, H), and the resulting pillar-type escape structure is preserved (Figs. 3G, H). The vigor of the burst out is greatest when the base layer material has a grain-size 15% of the top layer material (Nichols et al., 1994), as in the case of the BT investigated here that are composed of coarse to fine ash deposits. If the base layer grain-size is less than 8% of the top layer then base layer material will pass through the top layer pore spaces, without forming an escape structure. Depending on how much the disruption mechanism was pervasive, the BT deposits in the investigated outcrops have either largely preserved the original lithofacies (Fig. 3F) or they are almost entirely massive with only fragments of laminae distributed unevenly as relicts of the original stratified lithofacies (Fig. 3I). It is therefore important to note that in many cases the massive deposits of the BT on Vulcano are not a primary lithofacies but they are instead the result of pervasive post-depositional fluid escape processes. De Astis et al. (1997) suggested that the fragments of stratified ash embedded in some massive BT deposits was due to fragmentation of a stratified layer due to an external trigger (earthquakes), with subsequent sinking of the denser and heavier fragments into the soft massive deposits. We consider this explanation less probable because the evidence of disrupted stratification and fragments of stratified ash is recognized in a number of BT depositional units at different stratigraphic levels, which makes it difficult to assume a repetitive trigger external to the depositional system. Moreover, the upward bending of the fragmentation points and pillar-type structures observed in the lithofacies isA are more consistent with a model of fluid escape. Small ash diapirs were explained by De Astis et al. (1997) as a result of a significant amount of (liquid) water in the massive deposits, but we consider more probable a process of fluid escape due to dissipation of the pore pressure during deposition of the BT and subsequent compaction.

Most of the BT outcrops on Lipari and southern Vulcano are characterized by homogeneously massive lithofacies that are referred to deposition from PDCs on the base of significant thickness variations as function of paleo-topography of the individual BT depositional units, which is not fully consistent with primary fallout processes (Lucchi et al., 2008). Progressive aggradation of different PDC pulses can be argued from faint banding due to colour differences or subtle grain-size variations within massive deposits. Also in this case the deposits are mostly formed by ash, which raises the issue if they were erupted as mixtures of fine particles or if the coarse particles were deposited in very proximal areas. It was suggested that an efficient hydromagmatic fragmentation have produced a large amount of fine ash with respect to lapilli and blocks. Evidence that fragmentation was driven mostly by magma-water interaction is provided by SEM results showing that equant blocky fragments, with quenching cracks and abundant adhering particles are dominant in the BT deposits (De Astis et al., 1997; Lucchi et al., 2008). This is consistent with a location of eruptive vents inside the La Fossa Caldera, the floor of which has been below or near sea level during most of its evolution starting from c. 80 ka (De Astis et al., 2013). Another possible explanation, which may be concomitant with efficient hydromagmatic fragmentation, is that coarse-grained material has been probably deposited in the caldera depression, which is now filled and completely covered with the more recent deposits of La Fossa cone (De Astis et al., 1997; Lucchi et al., 2008).

The massive BT deposits can be interpreted either as the result of direct fallout-dominated flow-boundary zones or fluid-escape (or even granular flow) depositional regimes in well sorted, ash-dominated pyroclastic mixtures (cf. Branney and Kokelaar, 2002; Sulpizio et al., 2007; 2010). Direct fallout implies mainly vertical gentle settling of particles in a slow moving or motionless pyroclastic cloud, whilst deposition from fluid-escape (or granular flow) dominated flow-boundary zones implies lateral movement of the moving flow. The key feature for establishing a depositional mechanism from laterally-spreading PDCs is the evidence at the base of the BT depositional units of bands containing a substantial component of lapilli (and ash) of pumice, scoria and lithics from the underlying pyroclastic deposits (lithofacies mixAL; Fig. 4). These mixing bands indicate erosion and incorporation of loose material from the underlying beds into the moving ash flows that deposited the BT. The general poor sorting and massive appearance of the mixed deposits are suggestive of sedimentation from a current in which the rate of supply (Rs) is higher than the rate of deposition (Rd), which induces rapid development of a highly concentrated zone above the flow boundary, dominated by fluid escape or granular flow regimes. The moving flows relative to the BT exerted shear stress over the loose, erodible pyroclastic deposits that represented their substratum, causing entrapment of exotic clasts into the flow body (Fig. 9). Clast embedding was previously signaled by Lucchi et al. (2008) only in the outcrops of southern Lipari and Gelso (south Vulcano; Fig. 1), as an evidence of substrate erosion exerted by the PDCs during the BT eruptions in proximal areas. The mixing bands are formed by a dominant ash component from the BT, which forms the matrix of the deposit, and embedded lapilli (and ash) fraction made up of pumice, scoria and lithics ripped-up from the loose underlying units (Fig. 5). This is supported by component and geochemical analyses of selected base layers of BT depositional units, showing that they are composed of BT ash fragments and crystals and exotic clasts from the stratigraphically underlying pyroclastic deposits. When the mixing material is not visible at visual inspection, it can be documented by different glass geochemistry. Secondary glass components plotting outside of the main compositional field of the BT were described in Meschiari et al. (2020) (Fig. 7). As an example, the rhyolitic Lip1 (ash) tephra layer from an eruptive vent in southern Lipari is characterized by a very discontinuous areal distribution. This can be due to processes of wind-reworking or post-depositional erosion, as typically occurs for ash beds, but the role played by processes of erosion and clast incorporation by the BT currents is clearly outlined by the finding of secondary components chemically correlated to Lip1 within the BT depositional unit above, even where there is no direct evidence of the Lip1 tephra layer in the field.

Overall, sedimentological analyses, combined with grain-size, componentry and geochemical investigation, provide unequivocal evidence that the BT were deposited from PDCs laterally spreading from the La Fossa caldera all over the islands of Lipari and Vulcano. De Rosa et al. (2016)

suggested that mixing bands are the result of post-eruptive remobilization of the BT deposits on pre-existing steep slopes. The occurrence of mixing bands even on flat topography make us confident in excluding reworking as a primary mechanism. Notably, this enlarges the area where the PDCs that deposited the BT had a potential of eroding the substratum and embedding clasts from the underlying units up to distances of 16-17 km from the source area, therefore substantially increasing the estimate of the maximum run-out of currents of this type. This is coherent with the experimental model of Dellino et al. (2019) showing that PDCs transporting mostly fine ash, like those of the BT on Lipari, may travel further and possess a higher capacity of impact over the territory with respect to those characterized by coarser material.

5.2 Physical characteristics of the PDCs inferred from shear structures

In addition to the mixed lithofacies, also the sedimentary structures of lithofacies ucAL, rfAL, ruAL recognized in outcrops of southern and central Lipari are indicative of an effective lateral transport and shear stress exerted by the ash flows of the BT over the substratum (Fig. 9).

In particular, the undulated contacts (lithofacies ucAL) between the BT depositional units and the underlying lapilli beds in outcrops L1 and L5 may be referred to conditions of high shear stress exerted by the overriding currents to the loose lapilli substratum, which induces remobilization of its upper part and formation of waves with variable wavelength. Recumbent flame structures (lithofacies rfAL) also indicate high shear stress exerted by the overriding PDCs of the BT eruptions over the underlying lapilli beds, which produce incorporation of lapilli that are aligned downflow and bended to form an alignment of lapilli within the BT ash deposit for a distance up to some meters. Instead, the small hook-like structures of the lithofacies ruAL is related to conditions of moderate shear stress exerted from the overriding ash flow, which was able to rip-up lapilli from the underlying bed into the BT unit but with no significant lateral displacement of the upper part of the structure. The formation of the different shear structures depends on both flow and erodible deposit characteristics, like flow velocity, depositional regime, perpendicular load component of the moving flow, grain packing in the deposit, and terminal velocity of erodible clasts, among others. Currently, there are no laboratory or field study able to unravel these complex interplays to gain flow conditions responsible of the various structures, and the description have to be maintained at the first order of approximation. Nevertheless, some hints may be gained from published studies on PDC erosion. Following Pollock et al. (2019), the recumbent flame structures are referred to PDCs of similar concentration to the undulated structures, and the latter represent an earlier phase of growth of the recumbent flame structures. Moreover, the recumbent flame structures are a reliable indicator of the approximate local direction of the currents. Additionally, the recumbent flame structures are related to conditions of high concentration in the flow boundary zone (Pollock et al., 2019), indicating that the BT were deposited by mostly concentrated PDCs.

By a physical point of view, the undulated (lithofacies ucAL), recumbent flame (lithofacies rfAL) and rip-up structures (lithofacies ruAL) recognized at the base of BT depositional units are a signature of instabilities occurring at the boundary of two sheared granular media, and they may represent the frozen record of granular, pseudo Kelvin–Helmholtz instabilities. Waves and overturned stratification like those described at the base of BT are usually the result of simple shear exerted by the overriding flow on the loose substratum (Allen and Banks, 1972; Mills, 1983; Valentine et al. 1989; Røe and Hermansen, 2006; Douillet et al., 2015; Pollock et al., 2019). They have been also described in several analogue experimental studies with granular flows over grain beds (Goldfarb et al., 2002; Mangeney et al., 2010; Rowley et al., 2011; Roche et al., 2013; Farin et al., 2014).

Shear stress τ is defined as:

$$\tau = u_*^2 \rho_{PDC} \quad (1)$$

where u_* is the shear velocity, and ρ_{PDC} is the current density. The minimum velocity needed for starting bed instability is given by:

$$u_{*min} = \left[\frac{g\lambda}{2\pi}\frac{(1-x^2)}{x}\right]^{1/2} \quad (2)$$

where g is the gravity acceleration, λ is the wavelength of bed instability, and x the relative flow concentration (ρ_{PDC} /ρ_{bed}) (Doulliet et al., 2015). Eq. (2) states that the wavelength of the instabilities depends on shear velocity and the ratio between particle concentrations of the PDC and the underlying bed. It is interesting to note that Eq. (2) holds for $0 \leq x \leq 1$ (Douillet et al., 2015), which means that instabilities can form only if particle concentration in the bed is greater than that in the flow. Figure 10 shows that the more diluted the flow is (lower numbers of x), the more is the velocity required to form bed instabilities. In concentrated PDCs characterized by a granular flow or fluid-escape dominated flow-boundary zone the solid-void ratio and flow density (ρ_{PDC}) can vary greatly with height, producing flow stratification (e.g. Valentine, 1987; Dellino et al., 2004). The fluid and solid components abundance and densities determine the physical properties of the flow, which greatly depend on grain-size distributions and relative abundance of the different solid componentry. Without direct measurements, a gross estimate of particle concentration and ρ_{PDC} can be obtained from the deposits for granular/fluid escape-dominated flows. Assuming a characteristic solid-fluid ratio of 50-60% for ash rich deposits and a mean solid density of 2400 kg m^{-3} (e.g. Sulpizio et al., 2007; Breard and Lube, 2017), it results a range of ρ_{PDC} of ca. 1100-1400 kg/m^{-3}. We prefer the lower limit of this range as we know the currents needed to flow, for some distance, on sea water as to reach Lipari coast. Considering that the solid volume fraction can reach 70% in PDC deposits (Gase et al., 2018), it results in a relative flow concentration *(x)* of 10-20%, which can be used to constrain the minimum shear velocity to form the observed bed instabilities. For wavelength number of 0.16 (l=40 cm) the minimum basal shear velocity is less than 1 m s^{-1}, while for wavelength number of 0.72 (l=450 cm) it is less than 2 m s^{-1} (Fig. 10). It is to note that the calculated velocities do not reflect velocities at the flow front, but instead reflect the basal slip velocity at the time of instability formation. The resulting minimum basal shear stress, which refers the very base of the stratified current (a few mm-cm) may be calculated in the range of 1-4.5 kPa using Eq. (1).

6. CONCLUSIONS

A sedimentological analysis of lithofacies, combined with grain-size and componentry investigation and grain-specific volcanic glass compositional data, for a large number of the different depositional units of the ash-rich Brown Tuffs (BT) has been carried out on Lipari and Vulcano to provide constraints on their transport and depositional mechanisms and dispersal area. We rely on the framework of knowledge acquired so far according to which the BT were generated over a long time interval between c. 80 and 6 ka by pulsating hydromagmatic eruptions from eruptive vent(s) inside the La Fossa caldera on Vulcano. The following are the main outcomes of the present work:

1. The UBT on Vulcano (24-6 ka) are deposited from ground-hugging ash-rich pyroclastic density currents (PDCs) that have surmounted the caldera walls. Alternating massive and planar to cross stratified deposits reflect a repetitive aggradation of PDC pulses characterized by either fluid escape or granular flow depositional regimes from a fine-grained, concentrated flow-boundary zone (lithofacies mA) or grain by grain deposition from diluted and turbulent PDCs (lithofacies psA-xsA) during the waning stage of each pulse.
2. Intermittently stratified ash deposits of the UBT on Vulcano, with distinctive upwards bends and pillar- type escape structures through the rupture points are interpreted as the result of post-depositional disruption of the primary deposits due to fluid escape related to dissipation of pore pressure between layers at different porosity. This process can be pervasive to

produce almost entirely massive UBT deposits with only fragments of laminae distributed unevenly as relicts of the original stratified lithofacies.

3. Most of the individual BT depositional units on Lipari (and Vulcano) are characterized at the base by mixing bands containing pumice, scoria and lithic clasts ripped-up and embedded from the loose underlying pyroclastic units, as outlined by field study supported by grain-size and component analyses and geochemical glass investigation of the different components. These mixing bands indicate erosion and incorporation of loose material from the underlying beds into the laterally-spreading ash flows that deposited the BT. The recognition of these structures up to the northern sector of Lipari indicates that the PDCs during the BT eruptions travelled up to distances of (at least) 16-17 km from the source area and possessed a high capacity of impact over the territory.
4. Undulated, recumbent flame and rip-up structures are recognized at the base of some BT depositional units on southern and central Lipari as the result of effective lateral transport and moderate to high shear stress exerted by the ash flows of the BT to the substratum. These structures provide indications on the approximate local south-to-north direction of the currents, and the conditions of high solid concentration of the PDCs that deposited these BT. Moreover, they can be adopted to estimate a basal shear velocity of the currents of up to c. 2 m s^{-1} and a shear stress in the range of 1-4.5 kPa at the time of structure formation.

In conclusion, massive ash deposits of the BT can actually result from the spreading of PDCs that possess a high erosive power and shear strength at the flow base, representing a substantial hazard for tens of km away from the source area, which is amplified by the fine grain size that helps maintaining fluidization and increasing flow mobility.

ACKNOWLEDGEMENTS

SM funded through a PhD Scholarship of the University of Bologna-Alma Mater Studiorum. PGA is funded through a UKRI Future Leaders Fellowship (MR/S035478/1).

REFERENCES

Albert, P.G., Tomlinson, E.L., Smith, V.C., Di Traglia, F., Pistolesi, M., Morris, A., Donato, P., De Rosa, R., Sulpizio, R., Keller, J., Rosi, M., Menzies M., 2017. Glass geochemistry of pyroclastic deposits from the Aeolian Islands in the last 50 ka: a proximal database for tephrochronology. Journal of Volcanology and Geothermal Research 336, 81-107.

Allen, J.R.L., 1977. The possible mechanics of convolute lamination in graded sand beds. Journal of the Geological Society London 134, 19–31.

Allen, J.R.L., Banks, N.L., 1972. An Interpretation and Analysis of Recumbent Folded Deformed cross Bedding. Sedimentology 19, 257-283.

Allen, S.R., Cas, R.A.F., 1998. Rhyolitic fallout and pyroclastic density current deposits from a phreatoplinian eruption in the eastern Aegean Sea, Greece. Journal of Volcanology and Geothermal Research 86, 219–251.

Barberi, F., Gasparini, P., Innocenti, F., Ferrara, G., Villari, L., 1973. Volcanism of the southern Tyrrhenian Sea and its geodynamic implications. Journal of Geophysical Research 78, 5221-5232.

Beccaluva, L., Gabbianelli, G., Lucchini, F., Rossi, P.L., Savelli, C., 1985. Petrology and K/Ar ages of volcanics dredged from the Aeolian seamounts: implications for geodynamic evolution of the Southern Tyrrhenian basin. Earth and Planetary Science Letters 74, 187–208.

Bergeat, A., 1899. Die Äolischen Inseln (Stromboli, Panaria, Salina, Lipari, Vulcano, Filicudi und Alicudi). Abhandlungen der Mathematisch-Physikalischen Klasse der Königlich Bayerischen Akademie der Wissenschaften, vol. 20 I. Abt., München, 274 pp.

Blott, S.J., Pye, K., 2001. GRADISTAT: a grain size distribution and statistics package for the analysis of unconsolidated sediments. Earth Surface Processes and Landforms 26, 1237–1248. https://doi.org/10.1002/esp.261.

Branney, M.J., Kokelaar, P., 2002. Pyroclastic Density Currents and the Sedimentation of Ignimbrites. Geological Society London, Memoirs 27, 143 pp.

Breard, E. C. P., Lube, G. (2017). Inside pyroclastic density currents—Uncovering the enigmatic flow structure and transport behaviour in large- scale experiments. Earth and Planetary Science Letters 458, 22–36. https://doi.org/10.1016/j.epsl.2016.10.016.

Calanchi, N., De Rosa, R., Mazzuoli, R., Rossi, P.L., Santacroce, R., Ventura, G., 1993. Silicic magma entering a basaltic magma chamber: eruptive dynamics and magma mixing – an example from Salina (Aeolian Islands, southern Tyrrhenian Sea). Bulletin of Volcanology 55, 504–522.

Cas, R.A.F., Wright, J.V., 1987. Volcanic Successions. Unwin Hyman, London, pp. 528.

Carey, S.N., 1991. Transport and deposition of tephra by pyroclastic flows and surges. SEPM, Society for Sedimentary Geology, Special Publications 45, 39–57.

Chappell, J., Shackleton, N.J., 1986. Oxygen isotopes and sea level. Nature 324, 137–140.

Chiarabba, C., De Gori, P., Speranza, F., 2008. The Southern Tyrrhenian Subduction Zone: deep geometry, magmatism and Plio-Pleistocene evolution. Earth and Planetary Science Letters 268, 408–423.

Chough, S.K., Sohn, Y.K., 1990. Depositional mechanics and sequences of base surges, Songaksan tuff ring, Cheju Island, Korea. Sedimentology 37, 1115–1135.

Cicchino, A., Zanella, E., De Astis, G., Lanza, R., Lucchi, F., Tranne, C.A., Airoldi, G., Mana S., 2011. Rock magnetism and compositional investigation of Brown Tuffs deposits at Lipari and Vulcano (Aeolian Islands – Italy). Journal of Volcanology and Geothermal Research 208, 23-28.

Cole, P.D., Guest, J.E., Duncan, A.M., 1993. The emplacement of intermediate volume ignimbrite: a case study from Roccamonfina volcano, southern Italy. Bulletin of Volcanology 55, 467–480.

Colella, A., Hiscott, R.N., 1997. Pyroclastic surges of the Pleistocene Monte Guardia sequence (Lipari Island, Italy): depositional processes. Sedimentology 44, 47–66.

Crisci, G.M., De Rosa, R., Lanzafame, G., Mazzuoli, R., Sheridan, M.F., Zuffa, G.G., 1981. Monte Guardia Sequence: a Late-Pleistocene Eruptive Cycle on Lipari (Italy). Bulletin of Volcanology 44, 241-255.

Crisci, G.M., Delibrias, G., De Rosa, R., Mazzuoli, R., Sheridan, M.F., 1983. Age and petrology of the Late-Pleistocene Brown Tuffs on Lipari, Italy. Bulletin of Volcanology 46, 381-391.

Crisci, G.M., De Rosa, R., Esperanca, S., Mazzuoli, R., Sonnino, M., 1991. Temporal evolution of a three component system: the island of Lipari (Aeolian Arc, southern Italy). Bulletin of Volcanology 53, 207-221.

De Astis, G., Dellino, P., De Rosa, R., La Volpe, L., 1997. Eruptive emplacement mechanism of fine grained pyroclastic deposits widespread on Vulcano Island. Bulletin of Volcanology 59, 87-102.

De Astis, G., Ventura, G., Vilardo, G., 2003. Geodynamic significance of the Aeolian volcanism (Southern Tyrrhenian Sea, Italy) in light of structural, seismological and geochemical data. Tectonics 22, 1040–1057. https://doi.org/10.1029/2003TC001506.

De Astis, G., Lucchi, F., Dellino, P., La Volpe, L., Tranne, C.A., Frezzotti, M.L., Peccerillo, A., 2013. Geology, volcanic history and petrology of Vulcano (central Aeolian archipelago). Geological Society London, Memoirs 37, pp. 281–348.

De Rosa, R., Donato, P., Gioncada, A., Masetti, M., Santacroce, R. 2003. The Monte Guardia eruption (Lipari, Aeolian Islands): an example of a reversely zoned magma mixing sequence. Bulletin of Volcanology 65, 530–543.

De Rosa, R., Donato, P., Scarciglia, F., 2016. On the origin and post-depositional history of widespread massive ash deposits: the case of Intermediate Brown Tuffs (IBT) of Lipari (Aeolian Islands, Italy). Journal of Volcanology and Geothermal Research 327, 135-151.

Dellino, P., Isaia, R., Veneruso, M., 2004. Turbulent boundary layer shear flows as an approximation of base surge at Campi Flegrei (Southern Italy). Journal of Volcanology and Geothermal Research 133, 211–228.

Dellino, P., Zimanowski, B., Buttner, R., La Volpe, L., Mele, D., Sulpizio, R., 2007. Large-scale experiments on the mechanics of pyroclastic flow: design, engineering, and first results. Journal of Geophysical Research 112, B04202. https://doi.org/10.1029/2006JB004313.

Dellino, P., Buttner, R., Dioguardi, F., Doronzo, D.M., La Volpe, L., Mele, D., Sonder, I., Sulpizio, R., Zimanowski, B., 2010. Experimental evidence links volcanic particle characteristics to pyroclastic flow hazard. Earth and Planetary Science Letters 295, 314–320.

Dellino, P., De Astis, G., La Volpe, L.,Mele, D., Sulpizio, R., 2011. Quantitative hazard assessment of phreatomagmatic eruptions at Vulcano (Aeolian Islands, Southern Italy), as obtained by combining stratigraphy, event statistics and physical modelling. Journal of Volcanology and Geothermal Research 201, 264-384.

Dellino, P., Dioguardi, F., Doronzo, D.M., Mele, D., 2019. The rate of sedimentation from turbulent suspension: An experimental model with application to pyroclastic density currents and discussion on the grain-size dependence of flow runout. Sedimentology 66, 129–145.

Douillet, G.A., Taisne, B., Tsang-Hin-Sun, M.S.K., Kueppers, U., Dingwell, D.B., 2015. Syn-eruptive, soft-sediment deformation of deposits from dilute pyroclastic density current: triggers from granular shear, dynamic pore pressure, ballistic impacts and shock waves. Solid Earth 6, 553-572. https://doi.org/10.5194/se-6-553-2015.

Druitt, T. H. (1998). Pyroclastic density currents. Geological Society London, Special Publications 145, 145–182.

Dufek, J., Esposti Ongaro, T., Roche, O., 2015. Pyroclastic density currents: processes and models. In: Sigurdsson, H., Houghton, B., McNutt, S., Rymer, H., Stix, J. (Eds.), The Encyclopedia of Volcanoes (second edition). Academic Press, Elsevier, pp. 631–648.

Ellam, R.M., Menzies, M.A., Hawkesworth, C.J., Leeman, W.P., Rosi, M., Serri, G., 1988. The transition from calc-alkaline to potassic orogenic magmatism in the Aeolian Islands, Southern Italy. Bulletin of Volcanology 50, 386–398.

Farin, M., Mangeney, A., Roche, O., 2014. Fundamental changes of granular flow dynamics, deposition, and erosion processes at high slope angles: insights from laboratory experiments. Journal of Geophysical Research-Earth 119, 504–532.

Forni, F., Lucchi, F., Peccerillo, A., Tranne, C.A., Rossi, P.L., Frezzotti, M.L., 2013. Stratigraphic and geological evolution of the Lipari volcanic complex (central Aeolian archipelago). Geological Society London, Memoirs 37, 213-279.

Folk RL, Ward WC., 1957. Brazos River bar: a study in the significance of grain size parameters. Journal of Sedimentary Petrology 27, 3–26.

Francalanci, L., Lucchi, F., Keller, J., De Astis, G., Tranne, C.A., 2013. Eruptive, volcano-tectonic and magmatic history of the Stromboli volcano (north-eastern Aeolian archipelago). Geological Society London, Memoirs 37, 395–469.

Francalanci, L., Taylor, S.R., Mcculloch, M.T., Woolhead, J.D., 1993. Geochemical and isotopic variations in the calc-alkaline rocks of Aeolian arc, southern Tyrrhenian Sea, Italy: constraints on magma genesis. Contributions to Mineralogy and Petrology 113, 300–313.

Freundt, A., Schmincke, H.U., 1986. Emplacement of small-volume pyroclastic flows at Lacher See (East Eifel, Germany). Bulletin of Volcanology 48, 39–59.

Gase, A., Bradford, J.H., Brand, B., 2018. Estimation of porosity and water saturation in dual porosity pyroclastic deposits from joint analysis of compression, shear, and electromagnetic velocities. Geophysics 83(3), 1-39. https://doi.org/10.1190/geo2017-0234.1.

Gioncada, A., Mazzuoli, R., Bisson, M., Pareschi, M.T., 2003. Petrology of volcanic products younger than 42 ka on the Lipari-Vulcano complex (Aeolian Islands, Italy): an example of volcanism controlled by tectonics. Journal of Volcanology and Geothermal Research 122, 191–220.

Gioncada, A., Mazzuoli, R., Milton, A.J., 2005. Magma mixing at Lipari (Aeolian Islands, Italy): insights from textural and compositional features of phenocrysts. Journal of Volcanology and Geothermal Research 145, 97–118.

Goldfarb, D.J., Glasser, B.J., Shinbrot, T., 2002. Shear instabilities in granular flows. Nature 415, 302–305.

Gurioli, L., Cioni, R., Sbrana, A., Zanella, E., 2002. Transport and deposition of pyroclastic density currents over an inhabited area: the deposits of the AD 79 eruption of Vesuvius at Herculaneum, Italy. Sedimentology 49, 1–26.

Hornig-Kjarsgaard, I., Keller, J., Koberski, U., Stadlbauer, E., Francalanci, L., Lenhart, R., 1993. Geology, stratigraphy and volcanological evolution of the island of Stromboli, Aeolian arc, Italy. Acta Vulcanologica, 3, 21–68.

Keller, J., 1967. Alter und Abfolge der vulkanischen Ereignisse auf den Aolischen Inseln. Berichte der Naturforschenden Gesellschaft zu Freiburg i. Br. 57, 33–67.

Keller, J., 1980a. The island of Salina. Rendiconti della Società Italiana di Mineralogia e Petrologia 36, 489-524.

Keller, J., 1980b. The Island of Vulcano. Rendiconti della Società Italiana di Mineralogia e Petrologia 36, 369-414.

Keller, J., Ryan, W.B.F., Ninkovich, D., Altherr, R., 1978. Explosive volcanic activity in the Mediterranean over the past 200 000 yr as recorded in deep-sea sediments. Geological Society of America Bulletin 89, 591–604.

Leocat, E., 2011. Histoire eruptive des volcans du secteur occidental des Iles Eoliennes (Sud de la Mer Tyrrhenienne, Italie). Unpublished PhD thesis, University of Paris 11, Orsay.

Losito, R., 1989. Stratigrafia, caratteri deposizionali e aree sorgente dei tufi bruni delle Isole Eolie. Unpublished PhD Thesis, University of Bari, Italy.

Lowe, D.R., 1982. Sediment gravity flows: II. Depositional models with special references to deposits of high-density turbidity currents. Journal of Sedimentary Petrology 52, 279–297.

Lube, G., Cronin, S.J., Platz, T., Freundt, A., Procter, J.N., Henderson, C., Sheridan, M.F., 2007. Flow and deposition of pyroclastic granular flows: a type example from the 1975 Ngauruhoe eruption, New Zealand. Journal of Volcanology and Geothermal Research 161, 165–186.

Lube, G., Huppert, H.E., Sparks, R.S.J., Freundt, A., 2011. Granular column collapse down rough, inclined channels. Journal of Fluid Mechanics 675, 347–368.

Lucchi, F., 2009. Late-Quaternary marine terrace deposits as tools for wide-scale correlation of unconformity-bounded units in the volcanic Aeolian archipelago (southern Italy). Sedimentary Geology 216, 158–178.

Lucchi, F., 2013. Stratigraphic methodology for the geological mapping of volcanic areas: insights from the Aeolian archipelago (southern Italy). Geological Society London, Memoirs 37, 37–55.

Lucchi, F., Tranne, C.A., De Astis, G., Keller, J., Losito, R., Morche, W., 2008. Stratigraphy and significance of Brown Tuffs on the Aeolian Islands (southern Italy). Journal of Volcanology and Geothermal Research 177, 49-70.

Lucchi, F., Gertisser, R., Keller, J., Forni, F., De Astis, G., Tranne, C.A., 2013a. Eruptive history and magmatic evolution of the island of Salina (central Aeolian archipelago). Geological Society London, Memoirs 37, 155-211.

Lucchi, F., Keller, J., Tranne, C., 2013b. Regional stratigraphic correlations across the Aeolian archipelago (southern Italy). Geological Society London, Memoirs 37, 55-81.

Lucchi, F., Tranne, C.A. et al. 2004. Stratigraphic constraints to date late-Quaternary ancient shorelines and to evaluate vertical movements at Lipari (Aeolian Islands). Quaternary International 115/116, 105–115.

Lucchi, F., Tranne, C.A., Peccerillo, A., Keller, J., Rossi, P.L., 2013c. Geological history of the Panarea volcanic group (eastern Aeolian archipelago). Geological Society London, Memoirs 37, 349-393.

Lucchi, F., Peccerillo, A., Tranne, C. A., Rossi, P. L., Frezzotti, M. L. & Donati, C. 2013d. Volcanism, calderas, and magmas of the Alicudi composite volcano (western Aeolian archipelago). Geological Society London, Memoirs 37, 83–111.

Lucchi, F., Santo, A.P., Tranne, C.A., Peccerillo, A., Keller, J., 2013e. Volcanism, magmatism, volcano-tectonics and sea-level fluctuations in the geological history of Filicudi (western Aeolian archipelago). Geological Society London, Memoirs 37, 113-153.

Mangeney, A., Roche, O., Hungr, O., Mangold, N., Faccanoni, G., Lucas, A., 2010. Erosion and mobility in granular collapse over sloping beds, Journal of Geophysical Research-Earth 115, F03040. https://doi.org/10.1029/2009JF001462.

Manetti, P., Pasquaré, G., Tibaldi, A., Tsegaye, A., 1988. Geology of the island of Filicudi (Aeolian arc). Bollettino G.N.V. (Gruppo Nazionale di Vulcanologia, Italia), IV, 368-382.

Manetti, P., Pasquaré, G., Tibaldi, A., Tsegaye, A., 1995. A new geo-vulcanological map of Filicudi island (Aeolian arc, Italy). Acta Vulcanologica 7, 1-5.

Mathisen, M.E., Vondra, C.F., 1983. The fluvial and pyroclastic deposits of the Cagayan basin, Northern Luzon, Philippines—an example of non-marine volcaniclastic sedimentation in an interarc basin. Sedimentology 30, 369–392.

Mele, D., Dioguardi, F., Dellino, P., Isaia, R., Sulpizio, R., Braia, G., 2015. Hazard of pyroclastic density currents at the Campi Flegrei Caldera (Southern Italy) as deduced fromthe combined use of facies architecture, physical modeling and statistics of the impact parameters. Journal of Volcanology and Geothermal Research 299, 35–53.

Meschiari, S., Albert, P.G., Lucchi, F., Sulpizio, R., Smith, V.C., Kearne, R., Tranne, C.A., 2020. Frequent activity on Vulcano (Italy) spanning the last 80 ky: New insights from the chemo-stratigraphy of the Brown Tuffs. Journal of Volcanology and Geothermal Research 406. https://doi.org/10.1016/ j.jvolgeores.2020.107079.

Miall, A.D., 1978. Lithofacies types and vertical profiles models in braided river deposits: a summary. In: Miall, A.D. (Ed.), Fluvial Sedimentology. Canadian Society of Petroleoum Geologists, Memoirs 5, 597–604.

Miall, A.D., 1985. Architectural-element analyses: a new method of facies analyses applied to fluvial deposits. Earth-Science Reviews 22, 261–308.

Mills, P.C., 1983. Genesis and diagnostic value of soft-sediment deformation structures: a review. Sedimentary Geology 35, 83–104.

Morche, W., 1988. Tephrochronologie der Aolischen Inseln. Unpublished PhD Thesis, Albert-Ludwigs-Universitat Freiburg, Germany.

Nichols, R., Sparks, R., and Wilson, C., 1994. Experimental studies of the fluidization of layered sediments and the formation of fluid escape structures. Sedimentology 41, 233–253.

Odonne, F., Callot, P., Debroas, E.-J., Sempere, T., Hoareau, G., and Maillard, A., 2011. Soft-sediment deformation from submarine sliding: Favourable conditions and triggering mechanisms in examples from the Eocene Sobrarbe delta (Ainsa, Spanish Pyrenees) and the mid-Cretaceous Ayabacas Formation (Andes of Peru). Sedimentary Geology 235, 234–248.

Owen, G., 1987. Deformation processes in unconsolidated sands. Geological Society London, Special Publications 29, 11–24.

Peccerillo, A., De Astis, G., Faraone, D., Forni, F., Frezzotti, M.L., 2013. Compositional variations of magmas in the Aeolian arc: implications for petrogenesis and geodynamics. Geological Society London, Memoirs 37, 489–508.

Pichler, H., 1980. The Island of Lipari. Rendiconti della Società Italiana di Mineralogia e Petrologia 36, 415-440.

Pollock, N.M., Brand, B.D., Rowley, P.J., Sarocchi, D., Sulpizio, R., 2019. Inferring pyroclastic density current flow conditions using syn-depositional sedimentary structures. Bulletin of Volcanology 81, 46.

Roche, O., Niño, Y., Mangeney, A., Brand, B.D., Pollock, N.M., Valentine, G.A., 2013. Dynamic pore-pressure variations induce substrate erosion by pyroclastic flows. Geology 41: 1107–1110. https://doi.org/10.1130/G34668.1.

Rohling, E.J., Foster, G.L., Grant, K.M., Marino, G., Roberts, A.P., Tamisiea, M.E., Williams, F., 2014. Sea-level and deep-sea-temperature variability over the past 5.3 million years. Nature 508, 477–482.

Røe, S.-L., Hermansen, M., 2006. New aspects of deformed cross-strata in fluvial sandstones: examples from Neoproterozoic formations in northern Norway. Sedimentary Geology 186, 283–293.

Rowley, P.J., Kokelaar, P., Menzies, M., Waltham, D., 2011. Shear derived mixing in dense granular flows. Journal of Sedimentary Research 81, 874–884.

Selker, J.S., 1993. Expressions for the formation of load casts in soft sediment. Journal of Sedimentary Research 63, 1149–1151.

Smith, G.A., 1986. Coarse-grained nonmarine volcaniclastic sediment: terminology and depositional process. Geological Society of America Bulletion 97, 1–10.

Smith, G.A., 1987. The influence of explosive volcanism on fluvial sedimentation: the Deschutes formation (Neogene) in central Oregon. Journal of Sedimentary Petrology 57, 613–629.

Sohn, Y.K., Chough, S.K., 1989. Depositional processes of the Suwolbong Tuff Ring, Cheju Island (Korea). Sedimentology 36, 837–855.

Sulpizio, R., Dellino, P., 2008. Sedimentology, depositional mechanisms and pulsating behaviour of pyroclastic density currents. Developments in Volcanology 10, 57–96.

Sulpizio, R., Bonasia, R., Dellino, P., Mele, D., Di Vito, M.A., La Volpe, L., 2010. The Pomici di Avellino eruption of Somma-Vesuvius (3.9 ka BP). Part II: Sedimentology and physical volcanology of pyroclastic density current deposits. Bulletin of Volcanology 72, 559–577.

Sulpizio, R., Castioni, D., Rodriguez-Sedano, L.A., Sarocchi, D., Lucchi, F., 2016. The influence of slope-angle ratio on the dynamics of granular flows: insights from laboratory experiments. Bulletin of Volcanology 78: 77

Sulpizio, R., Dellino, P., Doronzo, D.M., Sarocchi D., 2014. Pyroclastic density currents: state of the art and perspectives. Journal of Volcanology and Geothermal Research 283, 36–65.

Sulpizio, R., De Rosa, R., Donato, P., 2008. The influence of variable topography on the depositional behaviour of pyroclastic density currents: the examples of the Upper Pollara eruption (The island of Salina, southern Italy). Journal of Volcanology and Geothermal Research 175, 367–385.

Sulpizio, R., Mele, D., Dellino, P., La Volpe, L., 2007. Deposits and physical properties of pyroclastic density currents during complex Subplinian eruptions: the AD 472 (Pollena) eruption of Somma-Vesuvius, Italy. Sedimentology 54, 607–635.

Tomlinson, E.L., Albert, P.G., Wulf, S., Brown, R., Smith, V.C., Keller, J., Orsi, G., Bourne, A.J., Menzies, M.A., 2014. Age and geochemistry of tephra layers from Ischia, Italy: constraints from proximal-distal correlations with Lago Grande di Monticchio. Journal of Volcanology and Geothermal Research 287, 22-39.

Valentine, G.A., 1987. Stratified flow in pyroclastic surges. Bulletin of Volcanology 49, 616–630.

Valentine, G.A., Buesch, D.C., Fisher, R.V., 1989. Basal layered deposits of the Peach Springs Tuff, northwestern Arizona, USA. Bulletin of Volcanology 51, 395–414.

Ventura, G., 2013. Kinematics of the Aeolian volcanism (Southern Tyrrhenian Sea) from geophysical and geological data. Geological Society London, Memoirs 37, 3–11.

Waelbroeck, C., Labeyrie, L., Michel, E., Duplessy, J.C., McManus, J.F., Lambeck, K., Balbon, E., Labracherie, M., 2002. Sea-level and deep water temperature changes derived from foraminifera isotopic records. Quaternary Science Reviews 21, 295–305.

Waresback, D.B., Turbeville, B.N., 1990. Evolution of a Plio-Pleistocene volcanogenic alluvial fan: the Puye formation, Jemez Mountains, New Mexico. Geological Society America Bulletin 102, 298–314.

TABLES

Tab. 1. Main characteristics of tephra units used for the subdivisions of the BT succession and showing evidence of syn-depositional clast incorporation within distinct BT depositional units (listed in stratigraphic order starting from the older one). Chemical composition of juvenile glass fragments (w.r=whole rock) and mineralogy are reported by referring to: (1) present work; (2) Meschiari et al. (2020); (3) Albert et al (2017); (4) Sulpizio et al. (2016); (5) Tomlinson et al. (2014); (6) De Astis et al (2013); (7) Gioncada et al. (2005); (8) De Rosa et al. (2003); (9) Calanchi et al. (1993). Labels for compositions: CA=calcalkaline, HKCA=high-k calcalkaline, SHO=shoshonite series; Bas-And=basaltic andesite, And=andesite, Dac=dacite, Rhy=rhyolite, Sho=shoshonite. Labels for phenocrysts: pl=plagioclase, kf=K-feldspar; cpx=clinopyroxene; opx=orthopyroxene, bt=biotite; ol=olivine; amp=amphibole; ox=oxides; ap=apatite; zr=zircon; ti=titanite; acm=acmite). Proximal stratigraphic units refer to: (1) Lucchi et al. (2008); (2) Forni et al. (2013); (3) Lucchi et al., 2013a; (4) De Astis et al. 2013. Age references: (1) Morche, 1988; (2) Soligo et al 2000; (3) Siani et al., 2004; (4) Leocat, 2011; (5) Lucchi et al., 2013a, b; (6) Sulpizio et al. 2016; (7) Giaccio et al. 2017; (8) Meschiari et al. 2020.

Tab. 2. Selected outcrops, stratigraphy and measurements of the syn-depositional sedimentary structures. The distance from the source area is arbitrarily measured relative to the centre of the La Fossa Caldera. The sample names refer to the BT depositional units selected for chemical analyses. Labels for the sedimentary structures: MB=mixing band; US=undulated structure; FS=recumbent flame structure; RS=rip-up structure. In the column of sedimentary structures the symbol / indicates that there is no direct evidence in the field of mixed lithofacies but the process of clast-embedding is outlined by means of geochemical analyses.

Tab. 3. Lithofacies codes, description and interpretation of the lithofacies recognized in the BT investigated in the present work. The first letters of the lithofacies code indicate the general appearance of the deposit (m = massive, ps = planar stratified, xs = cross-stratified, is = intermittently stratified, etc.) and the capital letters indicate the grain size (A = ash, L = lapilli).

Tab. 4. Representative major and minor element compositions of samples relative to the mixing bands recognized in this study at the base of different Brown Tuffs (BT) units, according to LBT, IBT, IBT-upper and UBT macro-units. Totals are pre-normalised analytical totals.For each of the samples, we include representative analyses for the main BT juvenile component and the secondary components (sec. comp.) relative to the process of clast embedding from the underlying pyroclastic units. Representative analyses for the proximal pyroclastic units used for the correlation of the secondary components are reported for comparison (in grey): gpt=Grey Porri Tuffs, Salina; pe=Punta del Perciato, Lipari; fa=Falcone, Lipari; Lip1 tephra layer, Lipari; mg=Monte Guardia, Lipari; cm=Cugni di Molinello, Vulcano; vg=Vallone del Gabellotto, Lipari. Compositions of the proximal pyroclastic units and the BT conform to Meschiari et al. (2020), except for "pe", "fa" and "mg" which are from Albert et al. (2017).

FIGURES

Fig. 1. Sketch maps of the islands of Vulcano and Lipari showing the areal distribution of the BT deposits and the location of outcrops where the sedimentary structures object of the present study have been observed (L1-13, V1-6). The inset (A) shows the location of the Aeolian Islands and seamounts in the southern Tyrrhenian sea (depth contour lines in metres below sea level). Coordinates conform to the Gauss-Boaga System (IGM). In (B) there is a sketch chronostratigraphic framework showing the development of Aeolian subaerial volcanism and the time-stratigraphic interval of BT deposition. Labels for the main tephra layers are: pt = Petrazza Tuffs; gpt = Grey Porri Tuffs; it =

Ischia Tephra; lpt = Lower Pollara Tuffs; gu = Monte Guardia pumice; vg = Vallone del Gabellotto pumice; pn = Punte Nere tuffs. References: Alicudi = Lucchi et al., 2013c; Filicudi = Lucchi et al., 2013d; Salina = Lucchi et al., 2013a; Lipari = Forni et al., 2013; Panarea = Lucchi et al., 2013b; Vulcano = De Astis et al., 2013; Stromboli = Francalanci et al., 2013.

Fig. 2. Generalized stratigraphic succession of the BT derived from correlations between the islands of Lipari and Vulcano. The BT succession is subdivided into (at least) 16 depositional units (BT1-16) superposed to the LBT, IBT, IBT-upper and UBT macro-units by means of interlayered volcanic units and tephra layers, erosive surfaces and reworked horizons (see also Meschiari et al., 2020). The individual depositional units of the UBT on Vulcano have a different name because they can not be directly correlated with those on Lipari. References for the stratigraphy of the two islands are: Forni et al., 2013 (Lipari); De Astis et al., 2013 (Vulcano). The stratigraphic units interlayered within the BT that are characterized by the sedimentary structures object of this work are described in Table 1.

Fig. 3. Outcrop photographs of the BT and their distinctive lithofacies. A) Massive deposits (lithofacies mA) of the BT on Lipari (outcrop L5). The BT in this outcrop correspond to the IBT-upper and UBT macro-units developed above the Monte Guardia marker bed. B) UBT deposits on Vulcano (outcrop V1) characterized by planar to cross-stratified lithofacies (psA-xsA). C) Alternating massive (mA) and intermittently stratified (isA) lithofacies of the UBT on Vulcano (outcrop V3). D) Detailed view of the deposits of Figure 3C. E) Detail of the ruptured laminae of the intermittently stratified deposits of UBT. The arrows indicate distinctive upward bending of the laminae in the rupture points. F) Intermittently stratified ash (isA) deposits of the UBT on Vulcano (outcrop V2). G) Close view of the deposits of Figure 3G showing ruptured laminae with typical upward deformation and columns of coarse ash (arrow) and inflated deformation of the laminae before the rupture (*). H) Close view of the deposits of Figure 3G showing ruptured laminae with typical upward

deformation (arrow). I) Massive deposits of the UBT on Vulcano near to Grotta dei Pisani that contain fragments of laminae (arrows) representing relicts of the stratified lithofacies.

Fig. 4. Field evidence of the mixing bands recognized at base of different BT depositional units on Lipari and Vulcano, shown in stratigraphic order (starting from the oldest) according to Fig. 2. A) Vallone dei Lacci, Lipari (outcrop L8): mixing band (*) between the BT4 depositional unit and the Grey Porri Tuffs (gpt). B) Valle Muria, Lipari (outcrop L2): mixing band (*) between the BT8 depositional unit and the Punta del Perciato pumice (pe). C) Mixing band (*) between the BT9 depositional unit and the Falcone pumice (pe) at Valle Muria, Lipari (outcrop L2). D) Detail of the mixing band in Figure 4C. E) Spiaggia Valle Muria, Lipari (outcrop L1): mixing band (*) between the BT9 depositional unit and the Falcone pumice (pe). F) Valle Muria, Lipari (outcrop L2): scattered pumice lapilli of the Falcone unit (fa) embedded within the overlying BT9 depositional unit. G) Gelso, Vulcano (outcrop V5): mixing band (*) between the BT12 depositional unit and the Monte Guardia tephra layer (gu). H) Passo del Piano, Vulcano (outcrop V1): mixing band (*) between the BT16(V) depositional unit and the Vallone del Gabellotto pumice (vg).

Fig. 5. Field evidence of shear structures on Lipari. A) Tunnel Canneto, Lipari (outcrop L5): undulated structure (lithofacies ucAL) along the contact between the BT12 depositional unit and the underlying Monte Guardia pumice succession. B) Detail of the crest of the undulated structure of Figure 5A. C) Spiaggia Valle Muria, Lipari (oucrop L1): panoramic view of the undulated structure (lithofacies ucAL) along the contact between the BT9 depositional unit and the underlying Falcone pumice succession. D) Trail of pumice and lithic lapilli of the Falcone pumice succession embedded within the overlying BT9 depositional unit (see C for location), representing the tail of a recumbent flame structure (lithofacies rfAL). E) Deformed bed of lapilli along the boundary between the BT9 depositional unit and the underlying Falcone pumice succession, representing the trunk of a not fully

developed recumbent flame structure (lithofacies rfAL). F) Detail of the undulated contact in Figure 5C showing a hook-like structure of rip-up lapilli from the underlying Falcone unit (lithofacies ruAL).

Fig. 6. Grain-size and components frequency histograms of weight % at half-phi intervals and pie charts of the components of representative samples of the mixing bands at the base of distinct BT depositional units in outcrops L2, L5, L10 and L12 on Lipari (see Fig. 1 for location). Representative photographas of the outcrops are also shown. The outcrops are displayed relative to an increasing distance from the inferred source area of La Fossa Caldera on Vulcano from base to top.

Fig. 7. TAS (A) and K_2O/SiO_2 (B) classification diagrams of the BT glasses compared to the volcanic glasses of explosive eruption deposits produced on Vulcano, Lipari and Salina during the last 50 ky. Data for the BT glasses are from Meschiari et al. (2020), whislt the data for Vulcano, Lipari and Salina are from Albert et al. (2017). Error bars represent 2*standard deviations of replicated analyses of the StHs6/80-G secondary standard glass run alongside the BT samples. The secondary components recognized in distinct BT depositional units referred to the LBT, IBT, IBT-upper and UBT macro-units are compared to the compositions of the underlying proximal pyroclastic units in distinct major element glass geochemical variation diagrams (A-N). The stratigraphic succession of BT depositional units (BT3, BT4, BT8, BT9, BT10, BT12, BT14-V, BT16-V) refers to Fig. 2. Data for the BT glasses are from Meschiari et al. (2020). References for the pyroclastic units used for comparison are: Grey Porri Tuffs (w.r.) = Sulpizio et al. (2016); Grey Porri Tuffs, Salina, proximal = Albert et al. (2017); Grey Porri Tuffs, Lipari medial, Vulcano medial-distal and Panarea, distal = Sulpizio et al., 2016; Meschiari et al. (2020); Lip1 = Meschiari et al. (2020); Falcone = Albert et al. (2017); Punta del Perciato = Albert et al. (2017); Monte Guardia field = Albert et al. (2017) and Meschiari et al. (2020); Monte Guardia (1) = Albert et al. (2017); Monte Guardia (2) = Meschiari et al. (2020); Cugni di Molinello = Meschiari et al. (2020); Vallone del Gabellotto (1) = Albert et al. (2017); Vallone del Gabellotto (2) = Meschiari et al. (2020).

Fig. 8. Sketch of the transport and depositional behaviour of the PDCs during the UBT eruptions on Vulcano island when interacting with the La Fossa Caldera wall (arrows indicate the flow direction). In the inbox, a model explaining the formation of lithofacies altpsmA (alternance of planar stratified and massive ash) as continuous aggradation of deposits from different PDC pulses (a, b, c, d) in the area of il Piano to the south of the source area, and the lithofacies isA (intermittently stratified ash) as disruption of the deposits due to fluid escape (d, e, f). Not to scale.

Fig. 9. Sketch of the formation of syn-depositional sedimentary structures (mixing bands, undulated structures and recumbent flame structures) at the base of the BT deposits as the result of lateral transport and high shear stress exerted by the PDCs of the BT on the loose underlying pyroclastic (pumice) material along downslope and upslope paths on the island of Lipari, to the north of the La Fossa Caldera source area. Arrows indicate the flow direction. Not to scale.

Fig. 10. Diagrams showing variations of minimum basal shear velocity (u_*) vs. relative flow concentration between PDCs and an underlying bed ($\boldsymbol{x} = \rho_{PDC} / \rho_{bed}$) for different wavelength numbers ($\lambda/2\pi$) of basal instabilities. Dashed lines indicate the minimum basal shear velocity for the observed wavelength of undulated structures of 40 cm ($\lambda/2\pi$=0.16) and 450 cm ($\lambda/2\pi$=0.72 as example of bed instabilities in the case study of the BT eruptions.

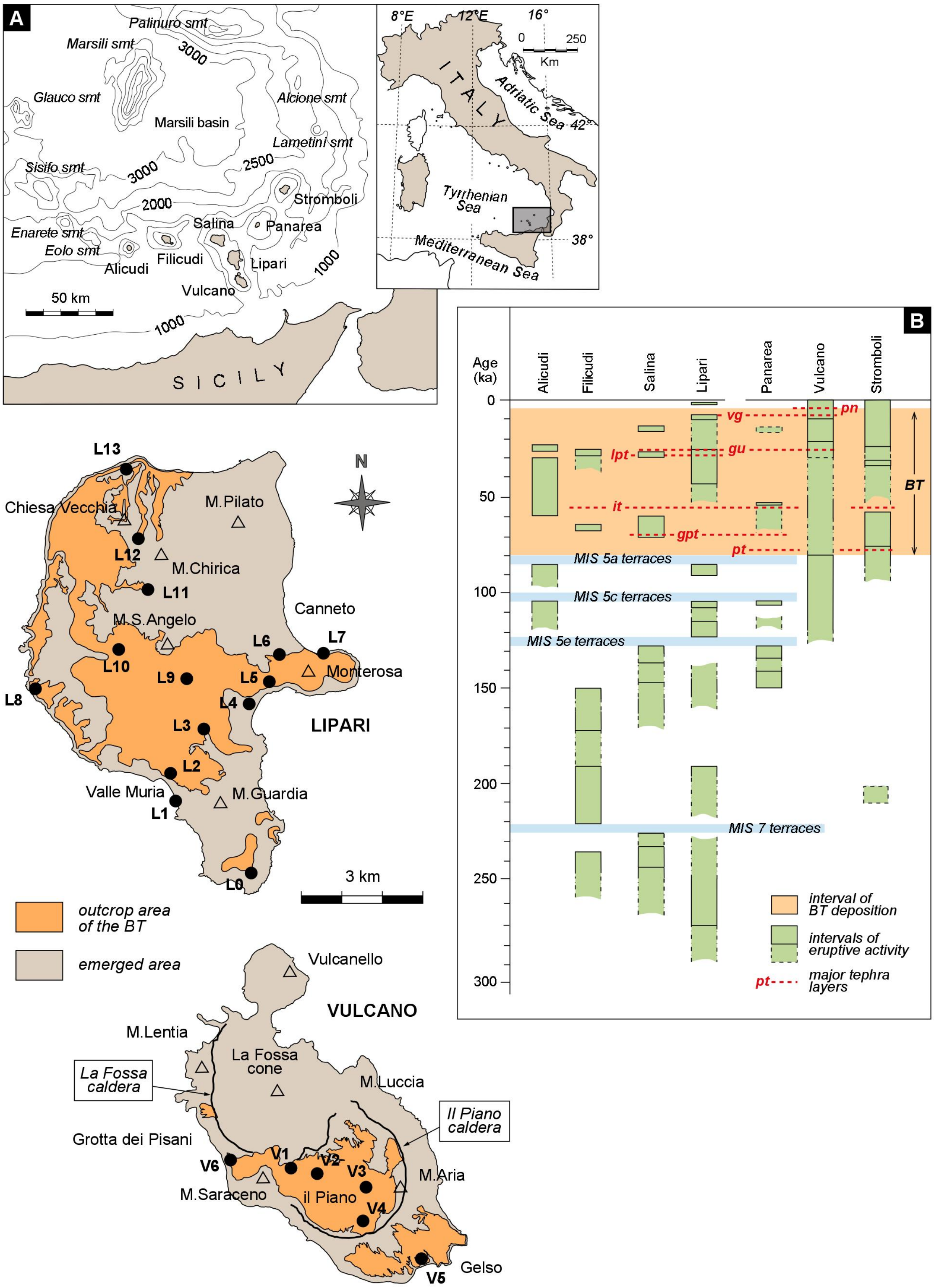
A
Palinuro smt
Marsili smt
3000
Glauco smt
Alcione smt
Marsili basin
Lametini smt
Sisifo smt
3000
2500
2000
Stromboli
Salina
Panarea
Enarete smt
Eolo smt
Alicudi
Filicudi
Lipari
1000
Vulcano
50 km
1000
SICILY
8°E
12°E
16°
0
250
Km
ITALY
Adriatic Sea
42°
Tyrrhenian Sea
38°
Mediterranean Sea
B
Age (ka)
Alicudi
Filicudi
Salina
Lipari
Panarea
Vulcano
Stromboli
vg
pn
lpt
gu
it
gpt
pt
BT
MIS 5a terraces
MIS 5c terraces
MIS 5e terraces
MIS 7 terraces
interval of BT deposition
intervals of eruptive activity
major tephra layers
L13
N
Chiesa Vecchia
M.Pilato
L12
M.Chirica
L11
Canneto
M.S.Angelo
L6
L7
L10
L9
L5
Monterosa
L8
L4
L3
LIPARI
L2
Valle Muria
M.Guardia
L1
L0
3 km
outcrop area of the BT
emerged area
Vulcanello
VULCANO
M.Lentia
La Fossa cone
La Fossa caldera
M.Luccia
Il Piano caldera
Grotta dei Pisani
V6
V1
V2
V3
M.Aria
M.Saraceno
il Piano
V4
Gelso
V5

Fig. 1

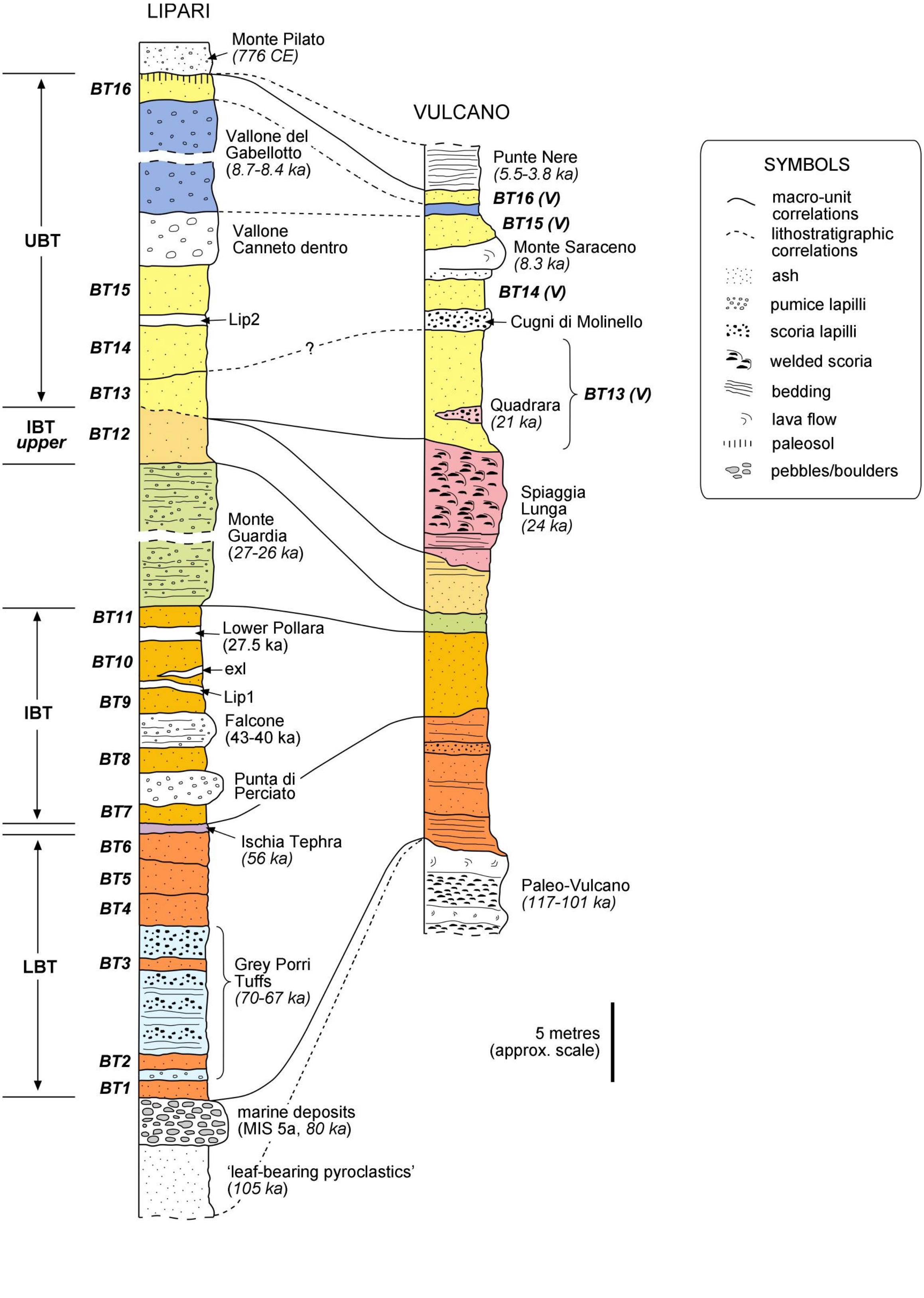
LIPARI
VULCANO
Monte Pilato
(776 CE)
UBT
IBT
upper
IBT
LBT
BT16
BT15
BT14
BT13
BT12
BT11
BT10
BT9
BT8
BT7
BT6
BT5
BT4
BT3
BT2
BT1
Vallone del
Gabellotto
(8.7-8.4 ka)
Vallone
Canneto dentro
Lip2
?
Monte
Guardia
(27-26 ka)
Lower Pollara
(27.5 ka)
exl
Lip1
Falcone
(43-40 ka)
Punta di
Perciato
Ischia Tephra
(56 ka)
Grey Porri
Tuffs
(70-67 ka)
marine deposits
(MIS 5a, 80 ka)
'leaf-bearing pyroclastics'
(105 ka)
Punte Nere
(5.5-3.8 ka)
BT16 (V)
BT15 (V)
Monte Saraceno
(8.3 ka)
BT14 (V)
Cugni di Molinello
Quadrara
(21 ka)
BT13 (V)
Spiaggia
Lunga
(24 ka)
Paleo-Vulcano
(117-101 ka)
5 metres
(approx. scale)
SYMBOLS
macro-unit
correlations
lithostratigraphic
correlations
ash
pumice lapilli
scoria lapilli
welded scoria
bedding
lava flow
paleosol
pebbles/boulders

Fig. 2

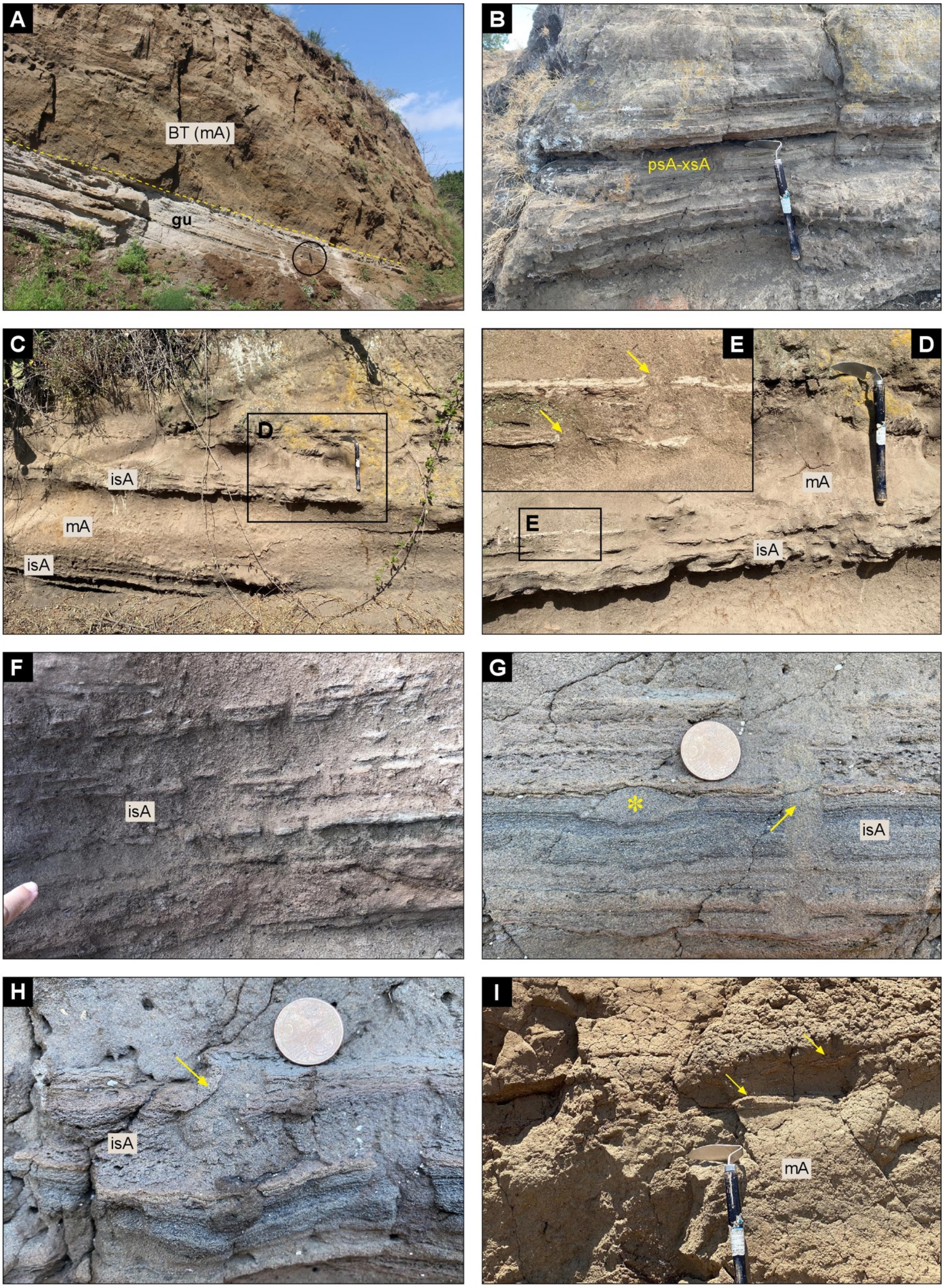

Fig. 3

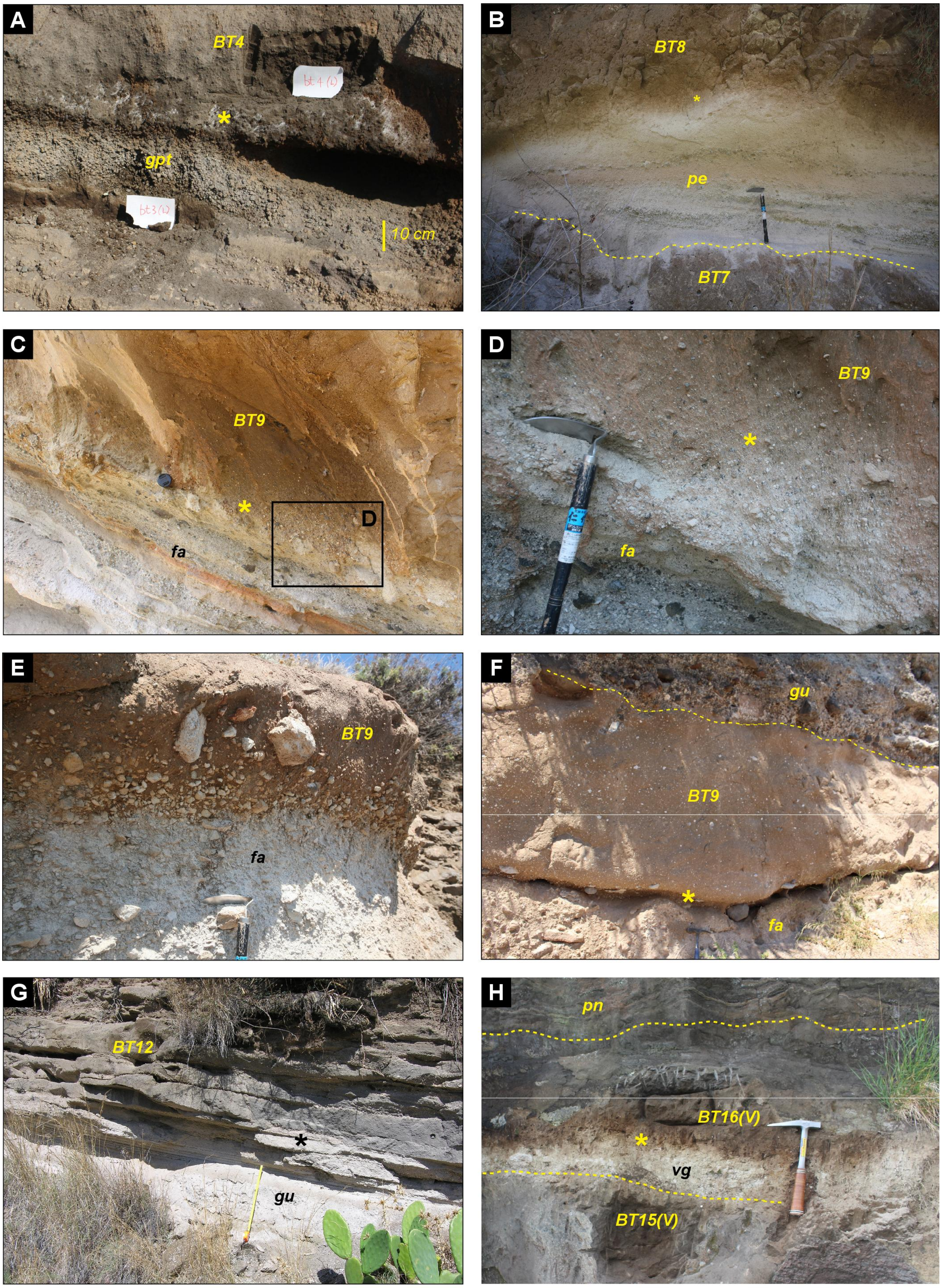
A
BT4
bt4 (2)
gpt
bt3 (2)
10 cm
B
BT8
pe
BT7
C
BT9
D
fa
D
BT9
fa
E
BT9
fa
F
gu
BT9
fa
G
BT12
gu
H
pn
BT16(V)
vg
BT15(V)

Fig. 4

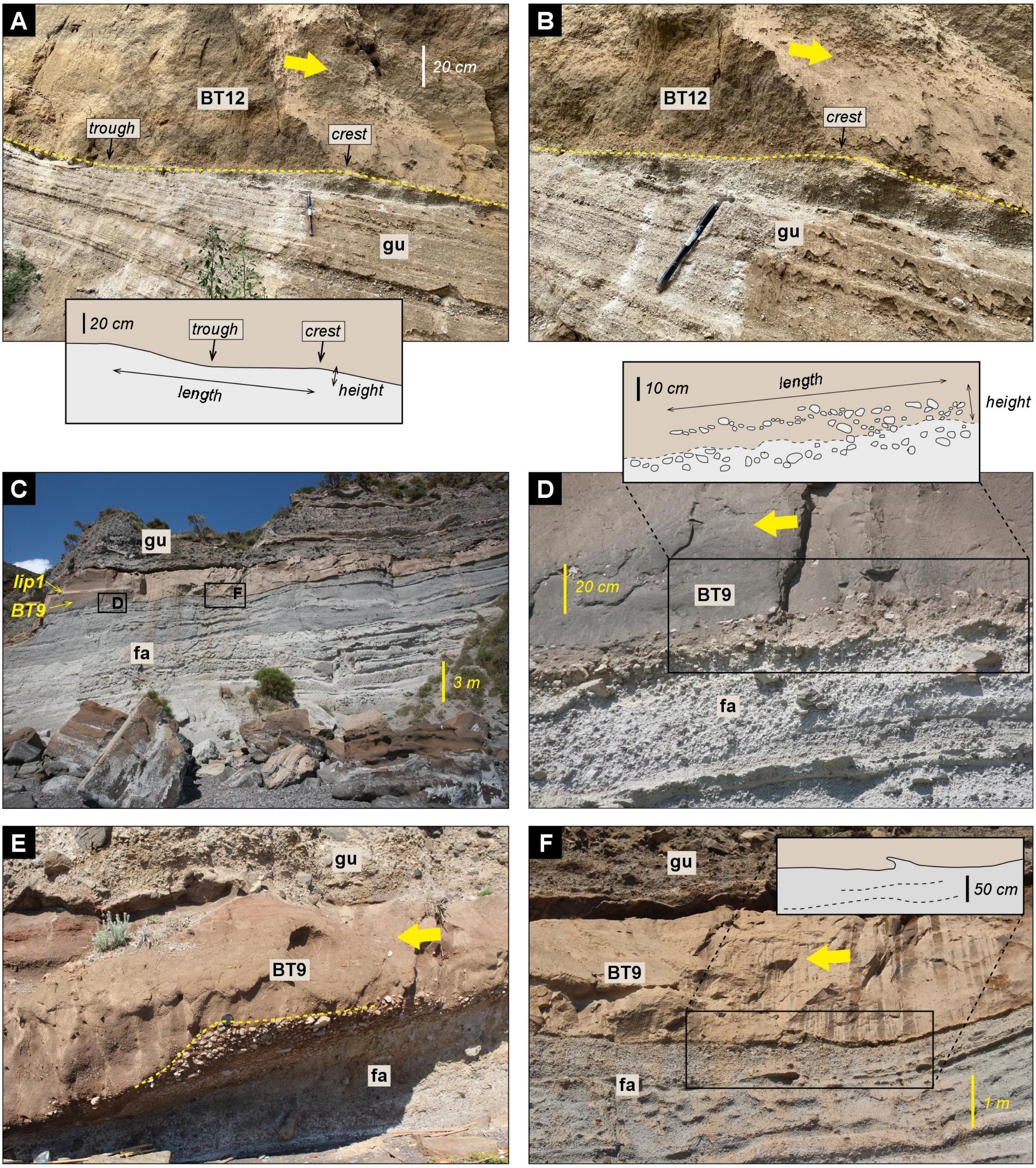
A
BT12
20 cm
trough
crest
gu
20 cm
trough
crest
length
height
B
BT12
crest
gu
10 cm
length
height
C
gu
lip1
BT9
D
F
fa
3 m
D
20 cm
BT9
fa
E
gu
BT9
fa
F
gu
50 cm
BT9
fa
1 m

Fig. 5

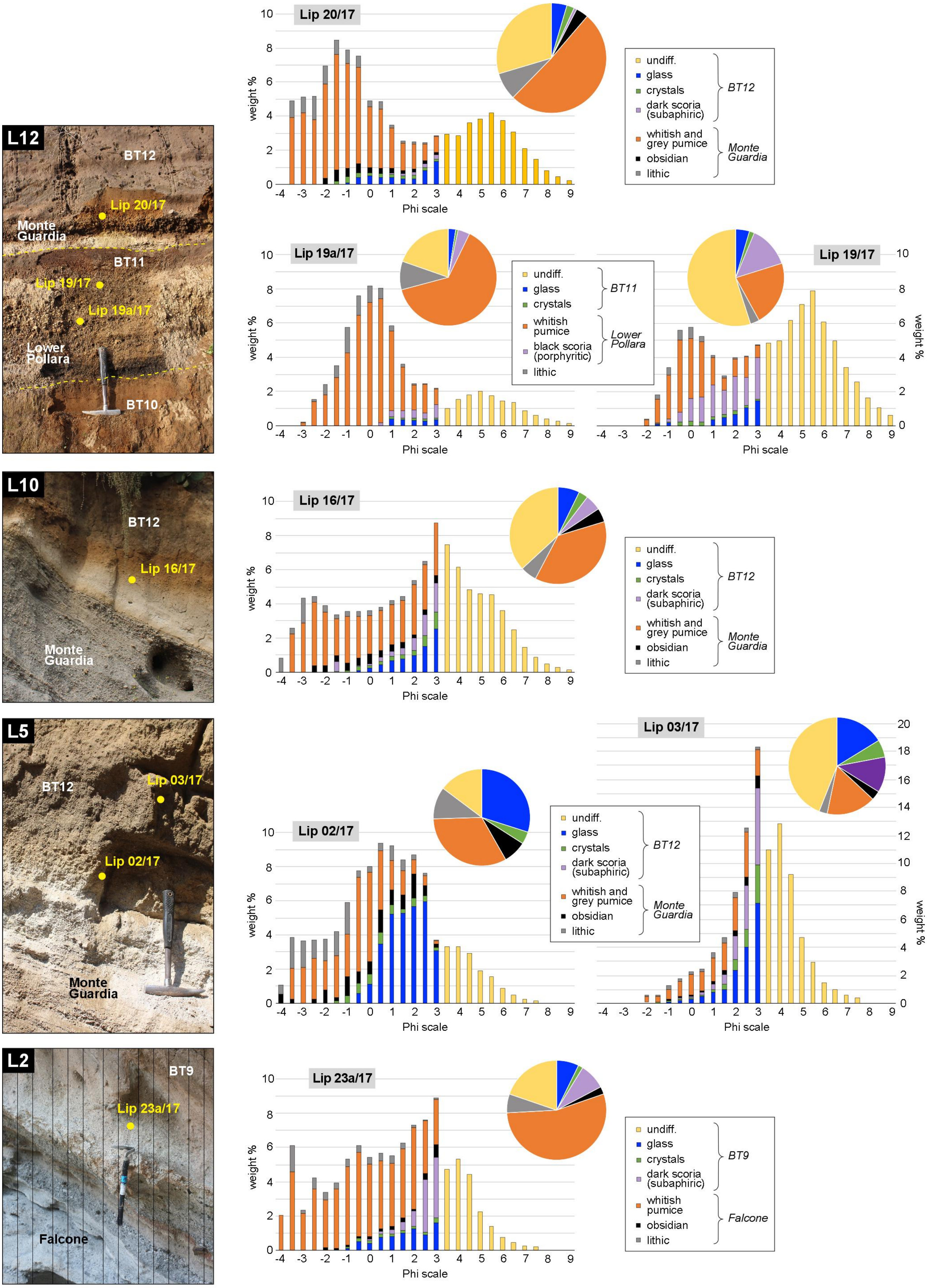
L12
BT12
Lip 20/17
Monte Guardia
BT11
Lip 19/17
Lip 19a/17
Lower Pollara
BT10
L10
BT12
Lip 16/17
Monte Guardia
L5
BT12
Lip 03/17
Lip 02/17
Monte Guardia
L2
BT9
Lip 23a/17
Falcone
weight %
Phi scale
undiff.
glass
crystals
dark scoria (subaphiric)
whitish and grey pumice
obsidian
lithic
BT12
Monte Guardia
whitish pumice
black scoria (porphyritic)
BT11
Lower Pollara
BT9
Falcone

Fig. 6

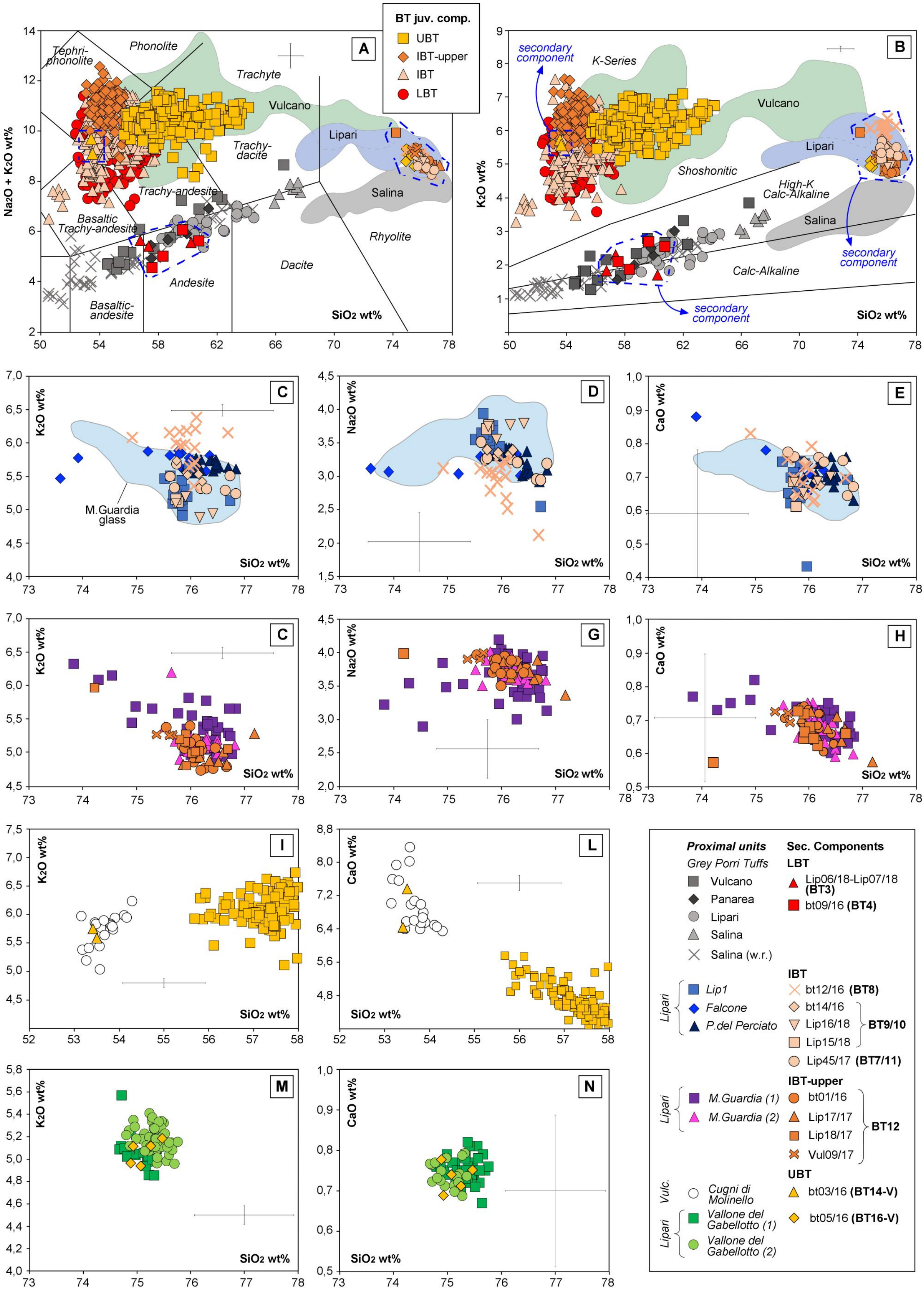

BT juv. comp.
UBT
IBT-upper
IBT
LBT
Tephri-phonolite
Phonolite
Trachyte
Vulcano
Lipari
Trachy-dacite
Trachy-andesite
Basaltic Trachy-andesite
Salina
Rhyolite
Dacite
Andesite
Basaltic-andesite
$Na_2O + K_2O$ wt%
SiO_2 wt%
secondary component
K-Series
Shoshonitic
High-K Calc-Alkaline
Calc-Alkaline
K_2O wt%
M.Guardia glass
Na_2O wt%
CaO wt%
Proximal units
Grey Porri Tuffs
Vulcano
Panarea
Lipari
Salina
Salina (w.r.)
Lipari
Lip1
Falcone
P.del Perciato
M.Guardia (1)
M.Guardia (2)
Vulc.
Cugni di Molinello
Vallone del Gabellotto (1)
Vallone del Gabellotto (2)
Sec. Components
LBT
Lip06/18-Lip07/18 (BT3)
bt09/16 (BT4)
IBT
bt12/16 (BT8)
bt14/16
Lip16/18
Lip15/18
BT9/10
Lip45/17 (BT7/11)
IBT-upper
bt01/16
Lip17/17
Lip18/17
Vul09/17
BT12
UBT
bt03/16 (BT14-V)
bt05/16 (BT16-V)

Fig. 7

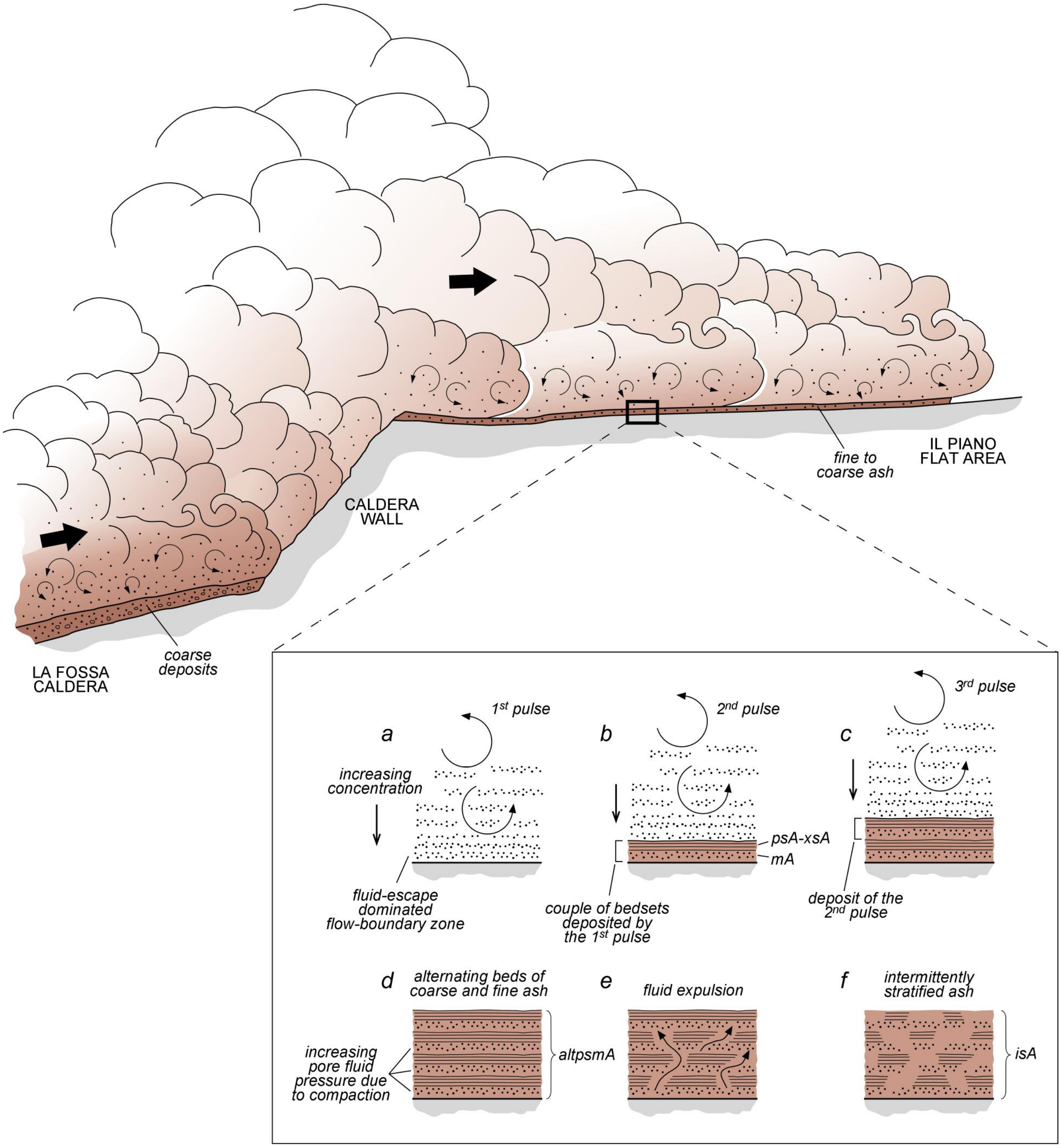
LA FOSSA
CALDERA
coarse
deposits
CALDERA
WALL
fine to
coarse ash
IL PIANO
FLAT AREA
a
1st pulse
increasing
concentration
fluid-escape
dominated
flow-boundary zone
b
2nd pulse
psA-xsA
mA
couple of bedsets
deposited by
the 1st pulse
c
3rd pulse
deposit of the
2nd pulse
d
alternating beds of
coarse and fine ash
increasing
pore fluid
pressure due
to compaction
altpsmA
e
fluid expulsion
f
intermittently
stratified ash
isA

Fig. 8

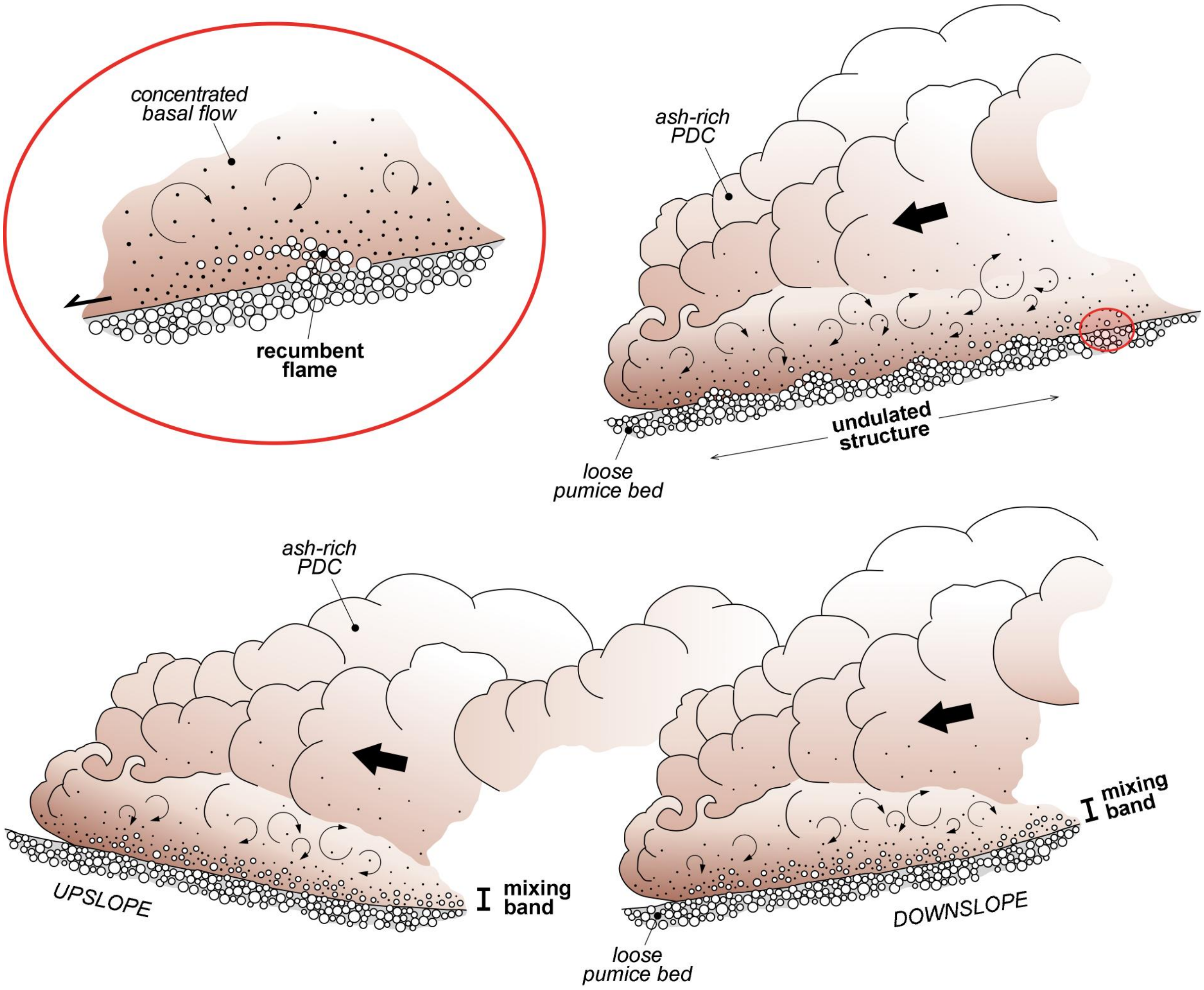
concentrated basal flow
recumbent flame
ash-rich PDC
undulated structure
loose pumice bed
ash-rich PDC
mixing band
UPSLOPE
mixing band
DOWNSLOPE
loose pumice bed

Fig. 9

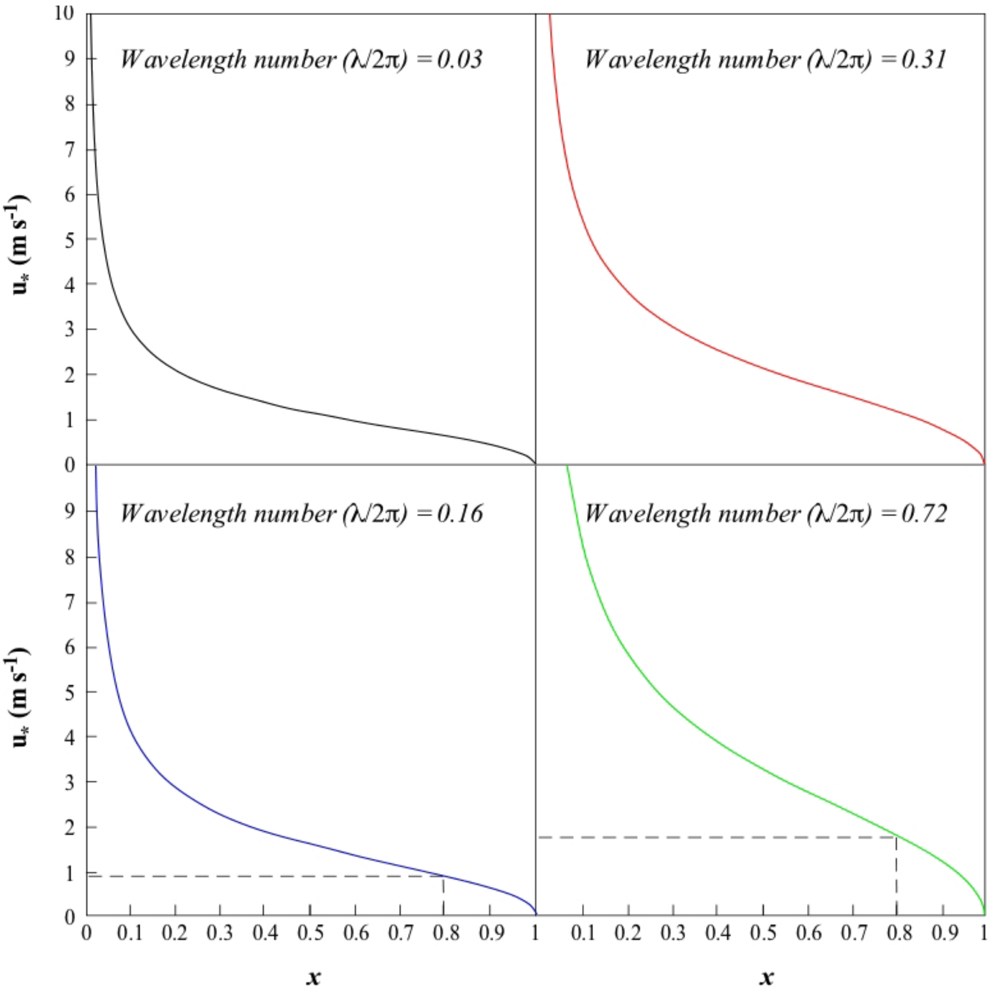
Wavelength number (λ/2π) = 0.03
Wavelength number (λ/2π) = 0.31
Wavelength number (λ/2π) = 0.16
Wavelength number (λ/2π) = 0.72
u* (m s-1)
u* (m s-1)
x
x
0
1
2
3
4
5
6
7
8
9
10
0.1
0.2
0.3
0.4
0.5
0.6
0.7
0.8
0.9

Fig. 10

Table 1 - Main characteristics of tephra units used for the subdivisions of the BT succession and showing evidence of syn-depositional clast incorporation within distinct BT depositional units (listed in stratigraphic order starting from the older one). Chemical composition of juvenile glass fragments (w.r=whole rock) and mineralogy are reported by referring to: (1) present work; (2) Meschiari et al. (2020); (3) Albert et al (2017); (4) Sulpizio et al. (2016); (5) Tomlinson et al. (2014); (6) De Astis et al (2013); (7) Gioncada et al. (2005); (8) De Rosa et al. (2003); (9) Calanchi et al. (1993). Labels for compositions: CA=calcalkaline, HKCA=high-k calcalkaline, SHO=shoshonite series; Bas-And=basaltic andesite, And=andesite, Dac=dacite, Rhy=rhyolite, Sho=shoshonite. Labels for phenocrysts: pl=plagioclase, kf=K-feldspar; cpx=clinopyroxene; opx=orthopyroxene, bt=biotite; ol=olivine; amp=amphibole; ox=oxides; ap=apatite; zr=zircon; ti=titanite; acm=acmite). Proximal stratigraphic units refer to: (1) Lucchi et al. (2008); (2) Forni et al. (2013); (3) Lucchi et al., 2013a; (4) De Astis et al. 2013. Age references: (1) Morche, 1988; (2) Soligo et al 2000; (3) Siani et al., 2004; (4) Leocat, 2011; (5) Lucchi et al., 2013a, b; (6) Sulpizio et al. 2016; (7) Giaccio et al. 2017; (8) Meschiari et al. 2020.

Pyroclastic unit	Main components	Chemistry (glass)	Mineralogy	Source area	Proximal stratigraphic unit	Age
Grey Porri Tuffs	Moderately vesicular to dense brown/grey pumice + dark scoria + highly vesicular, whitish pumice + variable content of lithic clasts	CA Bas-And and And to Dac	Porphyritic pumice and scoria (pl, cpx, opx, ol, ox, ap and scarse amp) (4)	Salina	Rocce di Barcone Fm. (3)	70–67 (1,5,6)
Ischia Tephra (Y-7)	White-yellowish ash	Tra-Pho (2)	kf, bt, pl, cpx, ti, acm (5)	Ischia	Epomeo Green Tuff –Monte Sant'Angelo (1)	56.1±1.0 (7)
Punta del Perciato	Highly to moderately vesicular whitish pumice and ash + scarce obsidian fragments	Rhy (1,2,3)	Scarcely porphyritic (kf, pl, amp, bt, ti) (7)	Lipari	Punta del Perciato Fm., member pe2 (2)	
Falcone	Highly vesicular, whitish pumice + dense to moderately vesicular grey pumice (and banded pumice) + obsidian fragments + minor lava lithics	Tra (minor) to Rhy (1,2,3)	Porphyritic grey pumice (cpx, pl, ol, ti) + low porphyritic whitish pumice (pl, kf, amp, bt) (7)	Lipari	Falcone Fm., member fa1 (2)	43-40 (4)
Lip1	Whitish ash	Rhy (1,2,3)		Lipari		
Lower Pollara Tuffs	Grey vesicular pumice (partly banded) + dense, highly porphyritic, poorly vesicular scoria + highly vesicular, white pumice (in the upper portion)	CA- to HKCA Bas-And to And Bas to Bas-And (black scoria) + And (grey pumice) + Rhy (white pumice) (9)	Porphyritic grey pumice and black scoria (pl, cpx, ox, ol with amp in the pumice) + subaphyric to aphyric white pumice (9)	Salina	Punta Fontanelle Fm. (3)	27.6-26.4 (8)
Monte Guardia	White, highly vesicular pumice + grey, dense to moderately vesicular pumice and banded pumice + obsidian fragments + abundant lithic clasts in some breccia levels	Rhy (1,2,3)	Low porphyritic white pumice (kf, cpx, amp, bt, ti, ap, zr) + porphyritic grey pumice (cpx, pl, ol, ti, ap) (8)	Lipari	Monte Guardia Fm. (2)	27-26 (8)
Spiaggia Lunga	Red-brownish weakly to intensely welded scoria lapilli and bombs + laminated ash at the base	SHO Bas to Sho (w.r.) (6)	pl, cpx, ol, ox (6)	Vulcano	Spiaggia Lunga Fm. (4)	24±5 (2)
Cugni di Molinello	Black, highly vesicular scoria lapilli	Tra-And (2)		Vulcano	Cugni di Molinello Fm. (4)	
Vallone del Gabellotto	Whitish pumice, from highly vesicular to moderately vesicular and blocky, and minor obsidian clasts	Rhy (1,2,3)	Aphyric	Lipari	Vallone del Gabellotto Fm. (2)	8.7 – 8.4 (3)

Table 2 - Selected outcrops, stratigraphy and measurements of the syn-depositional sedimentary structures. The distance from the source area is arbitrarily measured relative to the centre of the La Fossa Caldera. The sample names refer to the BT depositional units selected for chemical analyses. Labels for the sedimentary structures: MB=mixing band; US=undulated structure; FS=recumbent flame structure; RS=rip-up structure. In the column of sedimentary structures the symbol / indicates that there is no direct evidence in the field of mixed lithofacies but the process of clast-embedding is outlined by means of geochemical analyses.

Island	Outcrop	Location	Distance (km)	Sedimentary structure	BT dep. unit	Sample name	underlying unit	Thickness - MB (cm)	Length (cm)	Height (cm)
Lipari	L0	Punta della Crapazza	5,5	/	BT10	Lip15/18, Lip16/18, Lip17/18	Lip1*	/		
	L1	Spiaggia Valle Muria	7,7	MB, US, FS, RS	BT9		Falcone	≈30 (max)	≈450 (US)	≈20 (US)
									≈60 (FS)	≈20 (FS)
				MB	BT10		Lip1	≈5		
	L2	Valle Muria	8.5	MB	BT11		Lower Pollara	10		
				/	BT10	bt14/16	Lip1	/		
				MB	BT9		Falcone	25-30		
				MB	BT8	bt12/16	P. di Perciato	≈10		
	L3	Chiesa dell'Annunciazion	9.5	MB	BT12		Monte Guardia	≈25		
	L4	Portinente	10	MB	BT12	bt01/16	Monte Guardia	n.v.		
	L5	Tunnel Canneto	10.5	MB, US	BT12		Monte Guardia	≈15	≈250	≈20
	L6	Vallone Canneto dentro	11	MB	BT11		Lower Pollara Tuffs	≈5		
				MB	BT9		Falcone	≈10		
				MB	BT7		Ischia Tephra	≈5		
				MB	BT3-BT4	Lip06/18, Lip07/18	Grey Porri Tuffs	≈5		
	L7	Monterosa	11	/	BT9-10-11	Lip45/17	Lip1, Falcone or P. del Perciato	/		
				MB	BT7		Ischia Tephra	≈3		
	L8	Vallone dei Lacci	12	MB	BT4	bt09/16	Grey Porri Tuffs	≈5		
	L9	Santa Margherita	11	MB	BT11		Lower Pollara Tuffs	≈10		
	L10	Madoro	12	MB	BT12	Lip17/17, Lip18/17	Monte Guardia	≈25		
				MB	BT11		Lower Pollara Tuffs	≈10		
				MB	BT9		Falcone	≈5		
	L11	Vallone Fiume Bianco	13.5	MB	BT16		Vallone del Gabellotto	≈15		
	L12	Chiesa Vecchia	14.5	MB	BT12		Monte Guardia	≈5		
				MB	BT11		Lower Pollara Tuffs	≈5		
	L13	Acquacalda	16.5	MB	BT16		Vallone del Gabellotto	≈20		
					BT12		Monte Guardia	≈10		
Vulcano	V1	Passo del Piano	2	MB	BT16 (V)	bt05/06	Vallone del Gabellotto	≈10		
	V2	Il Piano	2.5	MB	BT14 (V)		Cugni di Molinello	≈10		
	V3	Il Piano	3	MB	BT14 (V)		Cugni di Molinello	≈10		
	V4	Serra dei Pisani	4	MB	BT14 (V)	bt03/16	Cugni di Molinello	≈15		
	V5	Gelso	5.7	MB	BT12	Vul09/17	Monte Guardia	≈20		
	V6	Grotta dei Pisani	2	/	BT13(V)		Spiaggia Lunga	/		

Table 3 - Lithofacies codes, description and interpretation of the lithofacies recognized in the BT investigated in the present work. The first letters of the lithofacies code indicate the general appearance of the deposit (m = massive, ps = planar stratified, xs = cross-stratified, is = intermittently stratified, etc.) and the capital letters indicate the grain size (A = ash, L = lapilli).

Lithofacies code	Description	Interpretation	Reference
mA	Massive, fine to coarse ash, sometimes with scattered pumice and lapilli. Abundant ash aggregates. Geochemically homogeneous. Moderate to poor sorting.	Gentle settling from a slow-moving, ground-hugging ash cloud. The homogeneous massive appearance suggests deposition from a fine-grained, concentrated flow-boundary zone dominated by fluid escape or granular flow regime. Ash aggregates indicate the presence of steam in the ash cloud or fine ash aggregation driven by electrostatic force during gentle settling of ash from the phoenix cloud of the PDCs.	Figs. 4A, C-D, I
xsA	Cross-stratified ash, sometimes with laminae. Dune bedded, medium to coarse ash. Moderate to good sorting	Dune-bedding and internal cross stratification indicate grain by grain deposition from a diluted, turbulent current in which suspension and traction are the main transport mechanisms.	Fig. 4B
psA	Planar stratified ash, sometimes with laminae. Moderate to good sorting	Planar stratification indicate grain by grain deposition from a diluted, turbulent current in which suspension and traction are the main transport mechanisms	Fig. 4B
altpsmA	Alternating planar stratified and massive ash. Planar stratified ash sometimes contains laminae. Moderate to good sorting.	The alternating beds of planar stratified and massive ash testifies for stepwise aggradation of discrete pulses developed within each depositional unit. The massive beds indicate that the flow-boundary zone of each pulse was dominated by granular- or fluid-escape dominated depositional regime. Planar stratified ash beds testify for sedimentation from the waning stage of each pulse, mainly in the traction regime.	
isA	Intermittently stratified ash. Alternation of mm to cm thick massive and stratified beds. The stratified beds are disrupted with distinctive upward deformation and vertical columns of coarse ash at the disruption points. Moderate to good sorting	Massive beds indicate deposition from a fluid-escape dominated flow boundary zone, whilst the stratified beds indicate deposition from a dilute, turbulent current in which suspension and traction are the main transport mechanisms. The disruption of stratified beds is driven by fluid escape structures related to post depositional dissipation of pore pressure from the underlying massive beds.	Figs. 4C-H
Shear structures			
mixAL	Mixed ash and lapilli from different units. The ash component is homogeneous and forms the matrix of the deposit. The lapilli (and ash) fraction is made by pumice and scoriae eroded from the loose underlying units. Usually are white pumice and dark scoriae in a brown ash matrix. Distribution of pumice and scoria may be homogeneous or their abundance decreases regularly upwards within the overlying ash. General poor sorting.	Mixing of material from different units indicate erosion and incorporation of loose material from the underlying beds into the moving ash flows. The general poor sorting and massive appearance are suggestive of sedimentation from a current in which the rate of supply (Rs) is higher than the rate of deposition (Rd). This induces the rapid development of a highly concentrated zone above the flow boundary, dominated by fluid escape or granular flow regimes. The moving flow exerted shear stress over the loose substratum, causing entrapment of clasts into the flow body.	Figs. 5A-H

Tab.4 - Representative major and minor element compositions of samples relative to the mixing bands recognized in this study at the base of different Brown Tuffs (BT) units, according to LBT, IBT, IBT-upper and UBT macro-units. Totals are pre-normalised analytical totals.For each of the samples, we include representative analyses for the main BT juvenile component and the secondary components (sec. comp.) relative to the process of clast embedding from the underlying pyroclastic units. Representative analyses for the proximal pyroclastic units used for the correlation of the secondary components are reported for comparison (in grey): gpt=Grey Porri Tuffs, Salina; pe=Punta del Perciato, Lipari; fa=Falcone, Lipari; Lip1 tephra layer, Lipari; mg=Monte Guardia, Lipari; cm=Cugni di Molinello, Vulcano; vg=Vallone del Gabellotto, Lipari. Compositions of the proximal pyroclastic units and the BT conform to Meschiari et al. (2020), except for "pe", "fa" and "mg" which are from Albert et al. (2017).

Macro-unit	IBT							
Unit	BT3				BT4		gpt	
Sample	Lip06/18		Lip07/18		bt09/16			
Component	BT	sec.comp.	BT	sec.comp.	BT	sec.comp.		
(wt%)								
Total	96,42	97,34	98,63	98,56	96,79	98,61	98,72	97,75
SiO2	56,37	60,25	55,73	57,38	56,32	60,76	54,53	64,51
TiO2	0,85	0,48	0,95	1,38	0,91	0,87	0,98	0,80
Al2O3	16,48	19,60	16,22	15,65	16,38	15,38	17,17	14,70
FeO	8,32	4,64	8,60	8,79	8,79	8,25	9,31	6,61
MnO	0,12	0,14	0,21	0,12	0,23	0,22	0,17	0,07
MgO	2,18	1,55	2,36	3,56	2,23	2,32	4,79	1,61
CaO	5,23	7,38	5,59	7,05	5,40	5,92	7,69	4,43
Na2O	3,93	3,85	3,82	3,09	3,81	3,08	3,26	3,62
K2O	5,5	1,7	5,6	2,3	5,08	2,55	1,44	2,93
P2O5	0,72	0,20	0,76	0,54	0,68	0,35	0,51	0,38
Cl	0,26	0,24	0,19	0,17	0,16	0,30	0,15	0,34

Macro-unit	IBT			IBT									
Unit	BT8		pe	BT9-10 (?)						BT7-8-9-10-11 (?)		fa	Lip1
Sample	bt12/16			Lip15/18		Lip16/18		bt14/16		Lip45/17			
Component	BT	sec.comp.		BT	sec.comp.	BT	sec.comp.	BT	sec.comp.	BT	s.c		
(wt%)													
Total	99.51	96,57	96,22	97,84	97,58	93,35	94,63	98,33	96,83	99,05	96,37	94,06	95,30
SiO2	56.30	75,92	76,35	54,12	75,72	53,53	75,90	53,21	75,73	51,14	76,19	76,35	75,84
TiO2	0.87	0,08	0,07	0,84	0,07	0,86	0,07	0,87	0,05	0,78	0,10	0,04	0,07
Al2O3	1.67	12,39	12,55	17,56	12,67	16,73	12,65	18,16	12,69	17,25	12,40	12,62	12,93
FeO	8.04	1,35	1,29	8,19	1,47	8,91	1,42	8,12	1,30	9,21	1,51	1,35	1,13
MnO	0.16	0,06	0,03	0,20	0,14	0,21	0,10	0,15	0,10	0,19	0,04	0,10	0,01
MgO	1.87	0,00	0,00	3,01	0,01	3,20	0,04	2,38	0,00	4,25	0,05	0,00	0,01
CaO	5.36	0,73	0,70	6,79	0,69	7,28	0,66	5,52	0,64	9,02	0,76	0,70	0,66
Na2O	3.72	2,91	3,25	3,78	3,71	4,09	3,60	3,06	3,40	3,67	3,25	3,00	3,54
K2O	6.08	6,20	5,75	4,65	5,18	4,28	5,26	7,53	5,75	3,88	5,34	5,83	5,46
P2O5	0.79	0,04	-	0,58	0,02	0,62	0,01	0,73	0,01	0,46	0,01	-	0,03
Cl	0.09	0,31	-	0,28	0,33	0,29	0,30	0,28	0,32	0,15	0,35	-	0,32

Chapter 6

Laboratory experiments on ash rich granular flows

1. Introduction

Understanding the mechanisms and physical laws that govern the dynamics of pyroclastic flows is one of the primary objectives in the field of modern volcanology. The study and characterization of these events have great importance in the assessment of the natural risk because pyroclastic density currents (PDCs) are the most hazardous volcanic phenomena for population living near volcanic edifices (e.g., Cas and Wright, 1987; Carey, 1991; Branney and Kokelaar, 2002). PDCs are composed of fragmented magma, gases, lithic clasts derived from the vent, conduit and substrate, and they have a rapid propagation over the ground characterized by high dynamic pressures and temperatures. The direct observation of these events is very complicated due to their dangerous nature and their study is difficult because the impossibility of expressing their rheological behavior through a single equation, due to the wide range of clast concentrations and forces that govern these phenomena. For this reason, the study of PDCs is limited to remote observation and observations on the deposits, but in the last decades studies based on experimental equipment have seen a great development in the field of stratigraphic-sedimentary analysis and modeling. Models and experiments may play an important role in quantifying the eruptive parameters of PDCs, but this record remains incomplete as many processes are non-depositional and the deposits may only record the conditions in the lower flow boundary immediately prior to deposition.

In this section, the experimental approach is applied to fine-grained granular flows for the purpose of reproducing the transport and depositional behavior of ash-rich PDCs like those produced during the Brown Tuffs eruptions from Vulcano, thus contributing to define the main parameters of velocity and maximum run-out. Here are present the results of properly-designed laboratory experiments carried out using the GRANFLOW Simulator at the Instituto de Geología of the University of San Luis Potosi (Mexico) (Fig. 1). Small-medium scale experiments were performed on ash granular flows in order to investigate their erosional behavior on a loose substratum, by comparison with the specific shear-related sedimentary structures observed at the base of the BT depositional units. This provides information on the processes occurring in the basal region of PDCs, which is challenging due to the difficulty of making direct observation in real time. On this, it is to be noticed that deposits from PDCs give only an incomplete record of what happens in the basal region of the corresponding PDCs, because the processes occurring in the moments prior to, during, and following deposition (Branney and Kokelaar 2002). Moreover, this information is generally difficult to be obtained for the deposits of fine-grained PDCs because they generally lack of sedimentary structures. Special emphasis will be devoted to the potential of erosion and clast incorporation of ash PDCs. A number of studies identified depositional evidence for erosional channels (Sparks et al. 1997; Calder et al. 2000; Brand et al. 2014; Gase et al. 2018) or substrate derived lithics in PDC deposits (Buesch 1992; Bernard et al. 2014; Brand et al. 2016; Pollock et al. 2016), both of which may be related to shear stress exerted on the bed by the PDCs. However, observations on fine grained deposits are lacking and little is known yet on how substrate erosion can occur in fine-grained PDCs.

2. Methods

The experiments were carried out using a flume facility designed and built up at the Instituto de Geología of the University of San Luis Potosi, Mexico. The instrumentation is able to reproduce dry or wet granular flows at mesoscale and its geometric characteristics can be readily modified to satisfy different experimental needs. The characteristics of the experimental instrumentation are described below.

2.1 Material used for the experiments

The choice of the material to be used for the experiments is very important in order to minimize the number of physical-mechanical variables considered and therefore to use the results obtained for purposes like the development of a physical-theoretical model reproducible at full scale. For the experiments object of this work, both natural and artificial material were used. The granular material to reproduce the flows was represented by moderately vesicular dacitic pyroclastics from the Nevado de Toluca volcano (Mexico), whilst the clast carpet that simulates the pyroclastic substratum over which the flows travelled and deposited was composed by colored plastic clasts of different grain-size.

2.2 Experimental structure

The experiments are performed by using the flume facility known as “Granular Flow Simulator” (GRANFLOW-sim; Bartali et al., 2012; Fig.1a). It consists of 5 sections that can move independently one from another, which gives the instrument a great versatility and the possibility of performing different experiments at different conditions of inclination of the transport and depositional planes. The structure is waterproof and allows to carry out both dry and wet experiments. The structure is 10 m long, 5 m wide and has a vertical development of 7 m, for a total weight of about 2 tons.

The structure consists of the following parts:

1) *Support tower*: it is a metal structure with a 2x2 meters base and a height of 7 meters. The main function is to support the flow channel and the expansion box (depositional area), and to allow the operators to climb up to fill the container with the granular material. Since the container rises and lowers according to the inclination of the channel, the tower has been divided into three floors at a distance of 2 meters from each other. At the end of the tower, three plastic coverages have been placed, the first covering the surface of the tower itself, while the second starts from the top of the tower and reaches the outer end of the laying surface, in order to guarantee the waterproofing of the entire structure. In addition to these covering, others have been added in a lateral position in order to protect from wind and bad weather conditions

2) *Charge system*: this is a container with a square base of 20 cm per side wand height of 90 cm, built up in PVC in order to ensure greater pressure of the material on the external walls and greater resistivity to atmospheric agents over time. The maximum capacity of the container is 50 kg of material, and it is equipped with a side window to dose the filling of the container. For each experiment of this work 43 kg of material were used. The charge system has the ability to move and adjust, through a pulley, with respect to the inclination of the channel and the intention of the operator. The distance from the inclined channel can vary from a minimum of 40 cm to a maximum of 1 m. The upper part of the container is open to facilitate recharging during the experiments, while in the lower part there are doors electronically controlled by the system so that the immediate and simultaneous emission of the loaded material can be controlled.

3) *Delivery system*: it is a wooden plank inclined by 20°, placed below the container of the charge system in order to reduce the dispersion of energy upon impact between the released material and the channel. The unit is fixed on the channel and can allow a further increase in inclination if required. At the base of the acceleration unit, exactly in the point where there is the first contact between the granular material and the channel, a piezoelectric sensor is installed connected to the electronic system that provides the time interval that the material takes from the moment it is released into the container until it comes in contact with the channel (the moment it begins to flow).

4) *Channel system*: it is a channel composed of two metal bars to which supports have been added transversely to increase its rigidity and load-bearing capacity. Overall, it has a width of 30 cm and a total length of 4.9 m. The side walls are made entirely of glass to make possible to observe the phenomenon from multiple points of view, while the surface is covered with a particular plastic that gives a specific basic roughness. Extensions have been added along the entire structure to allow the installation of sensors to record the kinematics of flow. The inclination can vary from a minimum of 10° to a maximum of 42°.

5) *Expansion box:* it is a 1.2 m wide and 2.40 m long plastic top bordered by glass side walls. The entire surface lies on a mobile structure with wheels on rails so, as the inclination of the channel varies, it can be perfectly aligned with the rest of the structure. The deposition top can also vary in inclination up to a maximum of 20°. There are side supports to install lasers and load cells to record kinematics. Above the deposition top there is a rod on which cameras are mounted to record the depositional process.

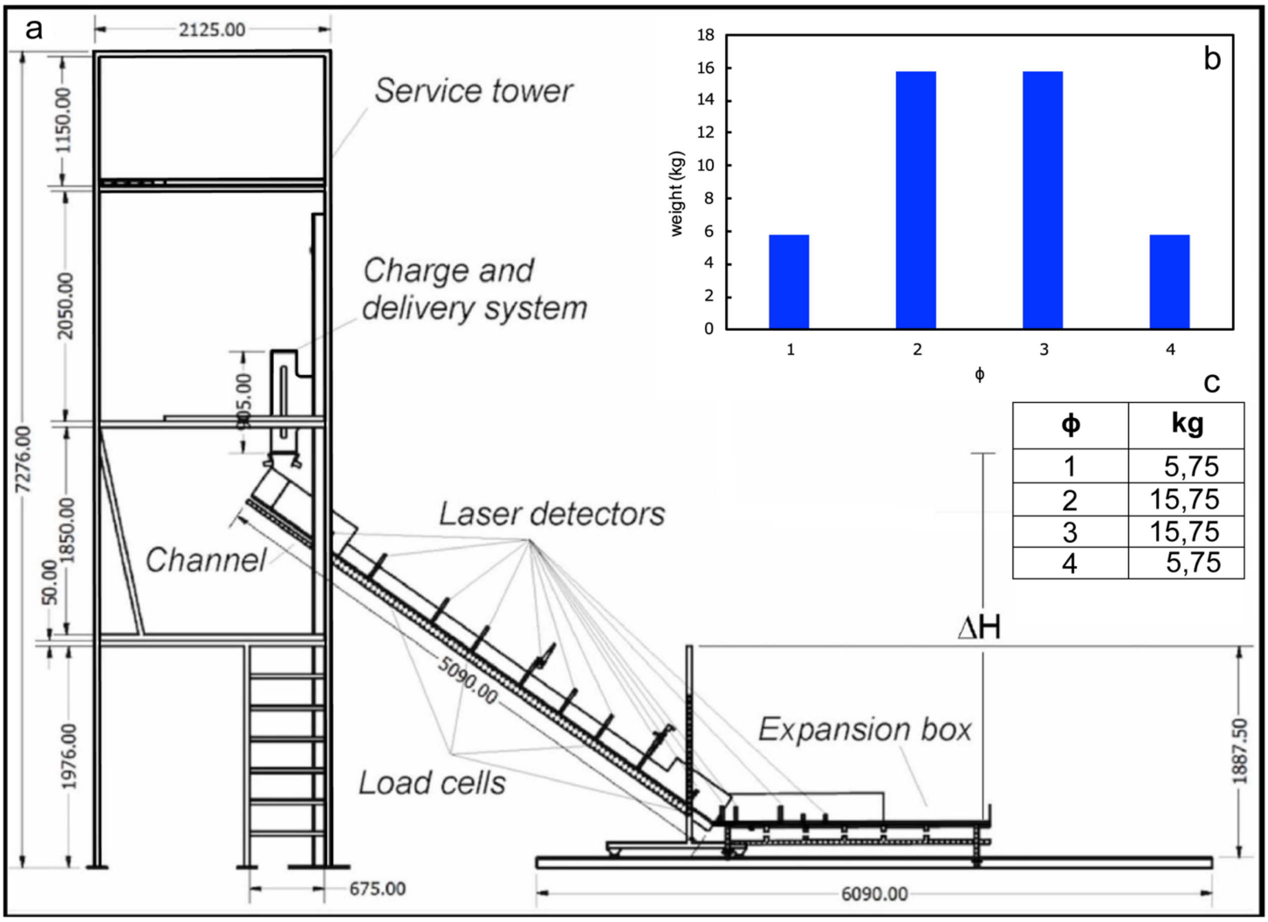

ϕ	kg
1	5,75
2	15,75
3	15,75
4	5,75

Fig.1 Design of the laboratory apparatus used for experimental runs. a) Sketch of the charge and delivery system, flume and expansion box (see Bartali et al. 2012 for more details); b) grain size histogram for material used in the experiments of the first batch; c) table of grain size distribution at 1ϕ intervals.

2.3 Experimental setup

Two types of experiments were conducted. The first batch of experiments has been carried out to characterize the erosive potential of fine-grained granular flows as an analogue of the PDCs that deposited the Brown Tuffs. The second batch had the purpose of building up a physical model that allow to describe the motion of fine-grained granular flows, to discuss their predictive potential by comparison with other cases and check the the influence of grain size and channelization on the mobility of volcanic granular flows.

To record the experiments the instrumentation consisted of three medium-speed (60 fps) high-resolution (1920 × 1080 pixel) camcorders (SONY HDR-CX240), a GoPro (Hero3 model) with fish-eye vision, and, for the first batch of experiments, slow motion videos with high-speed cameras (PHOTRON FASTCAM MINI AX and FASTEC IL5) were recorded to better describe how these flows behave and how they interact with the substratum. These high-speed cameras have been designed to meet the requirements of specialized imaging techniques employed also in fluid dynamics including Particle Image Velocimetry (PIV), Laser Induced Fluorescence (LIF) and others.

2.3.1 First batch experiments

Channelized flow experiments were carried out in order to study the behavior of fine-grained granular flows passing over a loose clast carpet and the resulting deposit. Two principal experimental setups in terms of inclinations of channel and expansion box were chosen, and for each of these 3 launches were made for a different grain size of the clast carpet. We define slope-angle ratio (SR) the ratio between the slope angle in the expansion box (depositional area) and that in the upstream channel (charge area), so that lower SRs indicate greater breaks in slope. The experiments were also repeated with a different covering of the channel to check if the texture of the substratum can affect the flow. The height of the clast carpet is determined by the particle size itself as it is arranged in a single-particle layer. The material used for the granular flow for the purpose of reproducing the characters of the Brown Tuffs was sieved at 1φ interval in order to obtain four grain size classes between 4 and 1φ (0.063 to 0.5 mm; Fig. 1b) ($\varphi = -\log_2 d$, where d is the particle diameter) in the ash size fractions. The sieved material was assembled in order to obtain a fine-grained Gaussian distribution (Fig. 1b-c). The clast carpet that simulates the pyroclastic substratum over which the flows travelled and deposited was composed by a single layer of colored plastic clasts, with different grain-size classes used for each experiment. The grain sizes choose for the plastic clasts are 0φ (1 mm), −1φ (2 mm) and −2φ (4 mm), for the purpose of reproducing the coarse ash to lapilli dimensions of the clasts of the pyroclastic units that in most cases represent the substratum in the natural case of the Brown Tuffs. The density of the 0φ particles is assumed as 2.53 ± 0.07 while that of −1φ and −2φ is 2.74 ± 0.03 (average value of 5 measurements).

A summary of the experimental condition is provided in Table 1.

Experiment number	Slope ratio (SR)	Clast carpet grain size	Channel coating material
SET 4			
4	42-10	4 mm (-2φ)	plastic
5	42-10	2 mm (-1φ)	plastic
6	42-10	1 mm (0φ)	plastic
SET 3			
7	42-10	2 mm (-1φ)	polycarbonate
8	42-10	4 mm (-2φ)	polycarbonate
9	42-10	1 mm (0φ)	polycarbonate
SET 2			
10	44-5	4 mm (-2φ)	polycarbonate
11	44-5	2 mm (-1φ)	polycarbonate
12	44-5	1 mm (0φ)	polycarbonate
SET 1			
13	44-5	2 mm (-1φ)	plastic
14	44-5	4 mm (-2φ)	plastic
15	44-5	1 mm (0φ)	plastic

Table 1. Experimental setup of the first batch of experiments. The experiments 1 to 3 (here not reported) are those performed without the clast carpet to verify the system. Labels for the slope ratios (e.g. 42-10) give indication of the angles of inclination of the channel (42°) and the expansion box (10°).

2.3.2 Second batch

The experimental runs of the second batch of experiments aimed at studying the influence of grain size and channelization on the mobility of volcanic granular flows, and they are the object of the manuscript in preparation of Chapter 6. These experiments were performed with a (constant) channel inclination of 40°, whereas the inclination of the expansion box varied between 0° and 20°, at steps of 5°. Three experiments for each slope ratio (SR) were carried out. Two grain size distributions (coarse and fine grained) of the granular material were used to run the experiments (Fig. 2). The material (43 kg for each experiment) was released from the hopper by means of a remotely controlled electromagnetic trap door and dropped vertically from a height of 0.40 m above the channel top. The granular material for the experiments was sieved at 1φ interval in order to obtain eight grain size classes (between 4 and −3φ, 0.063 to 8 mm; Fig. 2). The sieved material was assembled in order to obtain a coarse-grained Weibull distribution, modified with the addition of coarse-grained material (−3φ), and a fine-grained Gaussian distribution (Fig. 2). The conditions for these experiments are channelized and not channelized to shed light on the effect of grain size and channelization of volcanic granular flows (e.g. concentrated PDCs, lahars) moving over a break in slope, as the main (internal and external) factors that control flow dynamics, inundated area and deposit thickness.

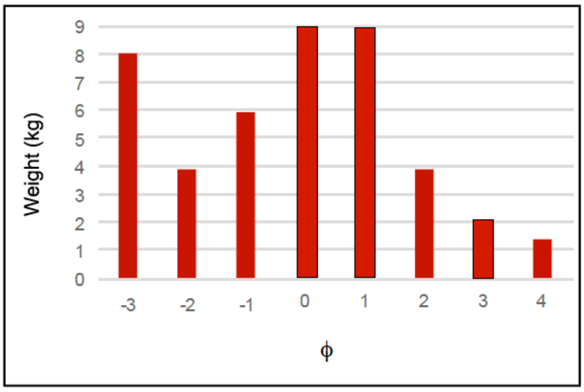

ϕ	Weight (kg)
-3	8.05
-2	3.85
-1	5.9
0	9
1	9
2	3.85
3	2
4	1.4

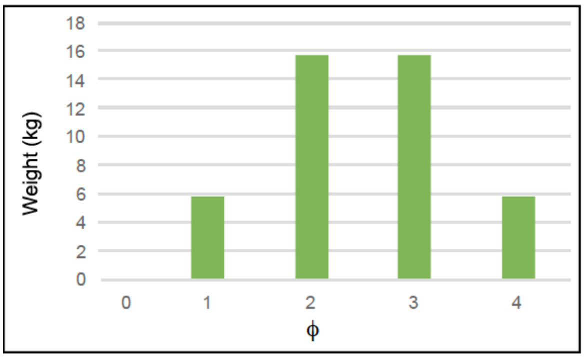

ϕ	Weight (kg)
1	5.75
2	15.75
3	15.75
4	5.75

Fig. 2 Grain size histogram of the material used in the experiments of the second batch with tables of the grain size (weight) distributions at 1ϕ intervals.

3. Results

The results described here are those from the first batch of experiments and focus on the behavior of the flows passing over a loose clast carpet and the resulting deposit. The results of the second batch of experiments are fully described and examined in the manuscript under preparation of Chapter 6.

In the experiments, the material charged in the hopper was released into the channel system after a 0.40 cm of free fall, and it accelerated until the break in slope. After the break in slope, the granular flow started to interact with the loose clast carpet and decelerated confined in the expansion box. At any experimental conditions and for any grain size of the carpet, particles were substantially incorporated in the basal portion of the flows and the corresponding deposits. All the experiments produced shear-related structures at the base of the deposits. Recumbent flame structures (Fig. 3A) and convex, undulated structures were formed (Fig. 3B) at the contact between the flow deposit and the loose clast carpet in different experimental conditions. In particular, recumbent flame structures are well visible for erodible carpets at both 1 mm and 2 mm grain sizes with the expansion box at inclinations of 5° and 10° (Fig. 4). The sedimentary structures produced in the deposits of the experimens are fully comparable with those observed in the field at the base of the Brown Tuffs depositional units (cf. Chapter 4) (Fig. 5).

Fig. 3. Recumbent Flame (A) and undulated (B) structures in deposits formed after experiments in different conditions: A) slope-ratio 42-10 and 1 mm clast carpet size; B) slope-ratio 44-5 and 4 mm clast carpet size.

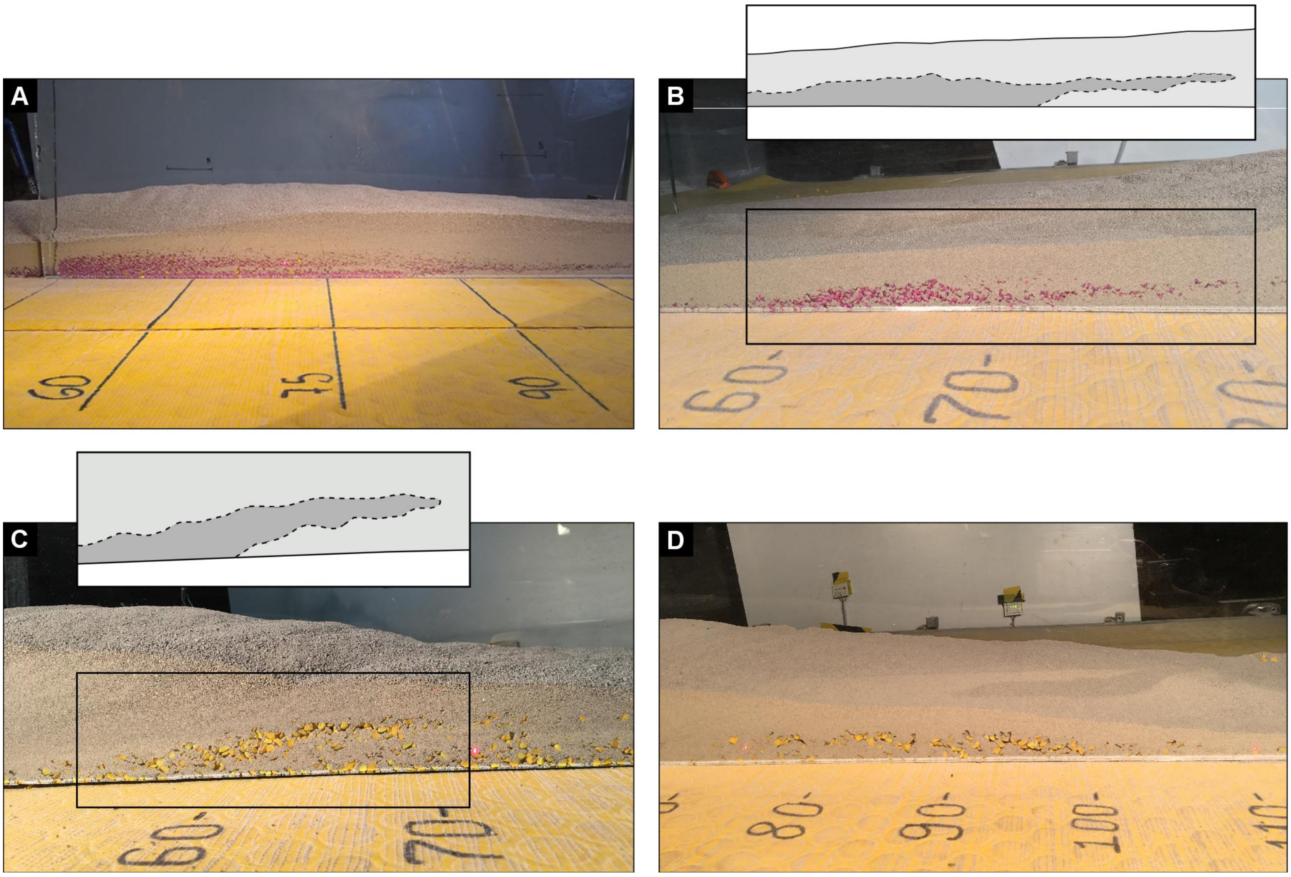

Fig. 4. Examples of recumbent flame structures formed in the deposits at different experimental conditions: A) slope-ratio 40-20, 1 mm clast carpet size; B) slope-ratio 42-10, 1 mm clast carpet size; C) slope-ratio 44-5, 2 mm clast carpet size; D) slope-ratio 44-5, 4 mm clast carpet size.

Fig. 5. Rip-up structure formed in the deposits of an experiment at slope-ratio 42-10 and 2 mm clast carpet size (A) compared with a similar structure observed at the base of a Brown Tuffs depositional unit in southern Lipari (B)

The runout of the flow deposits during the experiments are reported in Table 2. Runouts of the flow deposits do not show any major differences at different slope ratios and grain sizes of the clast carpet, whilst an increase of the runouts is observed in experiments with channel and expansion box coated with a polycarbonate sheet (experiments 7, 8, 9, 10, 11, 12).

Experiment	Slope ratio (SR)	Clast carpet grain size	Runout (cm)
4	42-10	4 mm (-2φ)	147
5	42-10	2 mm (-1φ)	180
6	42-10	1 mm (0φ)	220
7	42-10	2 mm (-1φ)	286
8	42-10	4 mm (-2φ)	300
9	42-10	1 mm (0φ)	300
10	44-5	4 mm (-2φ)	300
11	44-5	2 mm (-1φ)	300
12	44-5	1 mm (0φ)	300
13	44-5	2 mm (-1φ)	270
14	44-5	4 mm (-2φ)	200
15	44-5	1 mm (0φ)	196

Table 2. Sumary of the runouts of the flow deposits at different experimental conditions. Labels for the slope ratios (e.g. 42-10) give indication of the angles of inclination of the channel (42°) and the expansion box (10°).

In a first instance, it can be highlighted an exponential decay of the run-outs as a function of the particle size of the substratum in experiments with a plastic coat (SET 1 and SET 5, Table 1; Fig. 6). With a polycarbonate sheet the function is inverse and an exponential growth of the run-outs can be estimated (SET 2 and SET 3, Table 1; Fig. 6). The runouts as a function of slope-ratios are reported and discussed in Chapter 5.

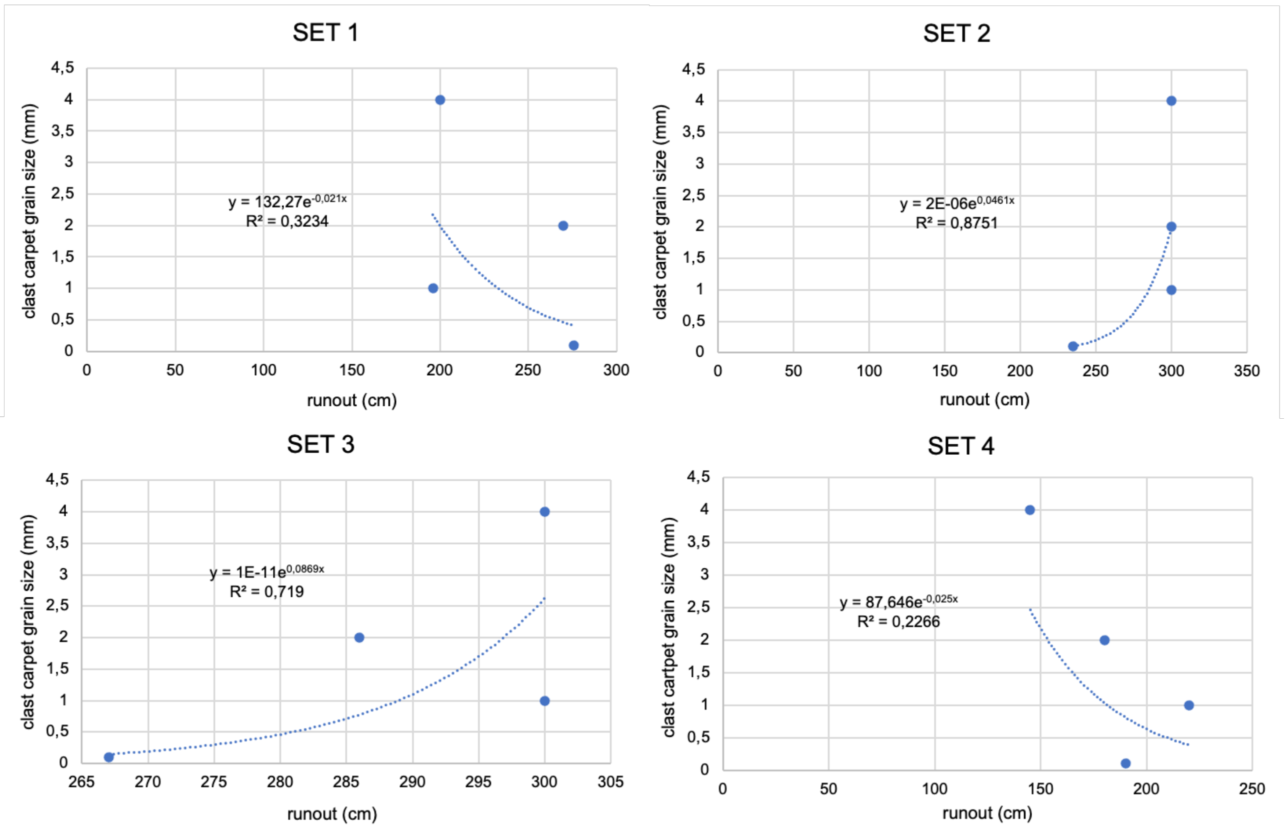

Fig. 6. Diagrams of run-outs (cm) as a function of the grain size (mm) of the clast carpet for different sets of experiments, and exponential functions for the relationships. Each set has one slope ratio and one type of channel coating material (cf. Table 1).

4. Preliminary discussion

The undulated and recumbent flame structures observed in the experimental flow deposits comprise a lower layer that is deformed and elongated, suggesting that the channelized flows interacted with and deformed the clast carpet during transport and deposition. The elongation of the structures suggests some amount of shear exerted on the flow-bed interface by the overriding flows, as observed in the deposits of other high-energy currents including tsunamis (cf. Matsumoto et al. 2008). Other examples, a few order of magnitude higher than those estimated with these experiments, are from the the PDC deposits of the May 18, 1980 eruption of Mount St. Helens (WA, USA) that contain sedimentary structures consisting of bed material reworked into undulose structures and recumbent flame structures (Pollock et al., 2019), but this type of shear-related structures were never described before for fine-grained granular flows. We can also assume the elongation direction of the undulated and recumbent flame structures can be used a reliable indicator of the approximate local flow directions, because in our experiments the flame structures have a concave lee surface with an overhanging arm that thins in downflow direction.

Further elaboration of the available data and new experiments in different conditions are needed to give contraints on the main parameters of velocity of the flows and thickness of the deposits compared with the natural case study, and also to have information on the influence of the process of clast incorporation on the final run-out of the flow deposits.

References

Bartali R, Sarocchi D, Nahmad-Molinari Y., Rodríguez-Sedano L.A., 2012. Estudio de flujos granulares de tipo geológico por medio del simulador multisensor GRANFLOW-SIM. Bol. Soc. Geol. Mex., 64, pp. 265-275

Bergeat, A., 1899. Die Äolischen Inseln (Stromboli, Panaria, Salina, Lipari, Vulcano, Filicudi
und Alicudi). Abh. Math. Phys. Kl. Kgl. Bayer. Akad. Wiss. 20, 274 I. Abt., München.

Bernard J., Kelfoun K., Le Pennec J.L., Vallejo Vargas S., 2014. Pyroclastic flow erosion and bulking processes: comparing field-based vs. modeling results at Tungurahua volcano, Ecuador. Bull Volcanol 76:858.

Brand B.D., Mackaman-Lofland C., Pollock N.M., Bendaña S., Dawson B., Wichgers P., 2014. Dynamics of pyroclastic density currents: conditions that promote substrate erosion and self-channelization—Mount St Helens, Washington (USA) J. Volcanol. Geotherm. Res., 276, pp. 189-214

Brand B.D., Bendaña S., Self S., Pollock N.M., 2016. Topographic controls on pyroclastic density current dynamics: Insight from 18 May 1980 deposits at Mount St. Helens, Washington (USA), J. Volcanol. Geotherm. Res., 321, pp 1-17.

Branney M., Kokelaar B., 2002. Pyroclastic density currents and the sedimentation of ignimbrites. Geol Soc London Mem 27:1–143

Buesch D.C., 1992. Incorporation and redistribution of locally derived lithic fragments within a pyroclastic flow, Geol. Soc. Am. Bull., 104, pp. 1193-1207.

Calder E.S., Sparks R.S.J., Gardeweg M.C., 2000. Erosion, transport and segregation of pumice and lithic clasts in pyroclastic flows inferred from ignimbrite at Lascar Volcano, Chile. J Volcanol Geotherm Res 104:201–235

Cas R.A.F., Wright J.V., 1987. Volcanic Successions: Modern and Ancient. Allen & Unwin, St. Leonards, NSW, Australia, 528 pp

Carey S.N., 1991. Transport and deposition of tephra by pyroclastic flows and surges. R.V. Fisher, G.A. Smith (Eds.), Sedimentation in Volcanic Settings, SEPM, Special Publications, vol. 45, pp. 39-57

Crisci G.M., De Rosa R., Lanzafame G., Mazzuoli R., Sheridan M.F., Zuffa G.G., 1981.
Monte guardia sequence: a late-pleistocene eruptive cycle on lipari (Italy). Bull. Volcanol. 44, 241–255.

Crisci G.M., Delibrias G., De Rosa R., Mazzuoli R., Sheridan M.F., 1983. Age and petrology
of the Late-Pleistocene Brown Tuffs on Lipari. Italy. Bull. Volcanol 46, 381–391.

Crisci G.M., De Rosa R., Esperanca S., Mazzuoli R., Sonnino M., 1991. Temporal evolution
of a three component system: the island of Lipari (Aeolian Arc, southern Italy). Bull. Volcanol. 53, 207–221.

De Astis G., Dellino P., De Rosa R., La Volpe L., 1997. Eruptive emplacement mechanism of fine grained pyroclastic deposits widespread on Vulcano Island. Bull. Volcanol. 59, 87–102.

De Rosa R., Donato P., Scarciglia F., 2016. On the origin and post-depositional history of
widespread massive ash deposits: the case of Intermediate Brown Tuffs (IBT) of Lipari (Aeolian Islands, Italy). J. Volcanol. Geotherm. Res. 327, 135–151.

Gase A., Bradford J.H., Brand B., 2018. Estimation of porosity and water saturation in dual porosity pyroclastic deposits from joint analysis of compression, shear, and electromagnetic velocities. Geophysics 83(3).

Gioncada A., Mazzuoli R., Bisson M., Pareschi M.T., 2003. Petrology of volcanic products
younger than 42 ka on the Lipari–Vulcano complex (Aeolian Islands, Italy): an example of volcanism controlled by tectonics. J. Volcanol. Geotherm. Res. 122, 191–220.

Keller, J., 1967. Alter und Abfolge der vulkanischen Ereignisse auf den Äolischen Inseln Bericht Naturforschenden Gesellschaft Freiburg. 57 pp. 33–67.

Keller J., 1980a. The island of Vulcano. Rendiconti della Società Italiana di Mineralogia e Petrologia. 36, pp 369-414.

Keller J., 1980b. The island of Salina. Rendiconti della Società Italiana di Mineralogia e Petrologia. 36, pp 489–524.

Losito R., 1989. Stratigrafia, caratteri deposizionali e aree sorgente dei Tufi bruni delle isole Eolie. Dissertation, University of Bari

Lucchi F., Tranne C.A., De Astis G., Keller J., Losito R., Morche W., 2008. Stratigraphy and significance of Brown Tuffs on the Aeolian Islands (southern Italy). J. Volcanol. Geotherm. Res. 177, 49–70.

Lucchi F., Keller J., Tranne C., 2013. Regional stratigraphic correlations across the Aeolian archipelago (southern Italy). Geol. Soc. Lond. Mem. 37, 55–81.

Manetti P., Pasquaré G., Tibaldi A., Tsegaye A., 1988. Geology of the island of Filicudi (Aeolian arc). Bollettino G.N.V. IV 368–382.

Manetti P., Pasquaré G., Tibaldi A., Tsegaye A., 1995. A new geo-vulcanological map of Filicudi island (Aeolian arc, Italy). Acta Vulcanol. 7, 1–5.

Matsumoto D., Naruse H., Fujino S., Surphawajruksakul A., Jarupongsakul T., Sakakura N. and Murayama M., 2008. Truncated flame structures within a deposit of the Indian Ocean Tsunami: evidence of syn-sedimentary deformation. Sedimentology, 55: 1559-1570.

Meschiari S., Albert P.G., Lucchi F., Sulpizio R., Smith V.C., Kearney R., Tranne C.A., 2020. Stratigraphy and geochemistry of the Brown Tuffs from the Aeolian Islands (Italy) indicates Vulcano was frequently active over 80 ky and produced widespread ash dispersals. J. Volcanol. Geotherm. Res., 406, 107079.

Morche W., 1988. Tephrochronologie der Aolischen Inseln. Unpublished PhD Thesis. Albert-Ludwigs-Universitat Freiburg, Germany.

Pichler H., 1980. The Island of Lipari. Rend. Soc. Ital. Mineral. Petrol. 36, 415–440.

Pollock N.M., Brand B.D., Roche O., 2016. The controls and consequences of substrate entrainment by pyroclastic density currents at Mount St Helens, Washington (USA), J. Volcanol. Geotherm. Res., 325, 135-147.

Pollock, N.M., Brand, B.D., Rowley, P.J., Sarocchi, D., Sulpizio, R., 2019. Inferring pyroclastic density current flow conditions using syn-depositional sedimentary structures. Bull. Volcanol. 81, 46

Sparks R.S.J., Gardeweg M.C., Calder E.S., Matthews S.J., 2017. Erosion by pyroclastic flows on Lascar Volcano, ChileBull. Volcanol., 58, pp. 557-565

Chapter 7

The influence of grain size and channelization on mobility of volcanic granular flows: insights from laboratory experiments

Sulpizio R.[1,2,3], Meschiari S.[4], Sarocchi D.[5], Rodriguez-Sedano L.A.[5], Lucchi F.[4]

[1] Dipartimento di Scienze della Terra e Geoambientali, via Orabona 4, 70125, Bari, Italy

[2] IGAG-CNR, Via Mario Bianco, 9, 20131 Milano, Italy

[3] INGV section of Bologna, Via Franceschini 31, 40128 Bologna, Italy

[4] Dipartimento di Scienze Biologiche Geologiche ed Ambientali, Piazza di Porta San Donato, 1, 40126, Bologna, Italy

[5] Instituto de Geologia, Fac. De Ingegneria, UASLP, Av. Dr. M. Nava No 5, 78290 San Luis Potosí, México.

Submitted to Bulletin of Volcanology

Bulletin of Volcanology

The influence of grain size and channelization on mobility of volcanic granular flows: insights from laboratory experiments

--Manuscript Draft--

Manuscript Number:	BUVO-D-21-00019
Full Title:	The influence of grain size and channelization on mobility of volcanic granular flows: insights from laboratory experiments
Article Type:	Research Article
Corresponding Author:	ROBERTO SULPIZIO Universita degli Studi di Bari Aldo Moro Bari, ITALY
Corresponding Author Secondary Information:	
Order of Authors:	ROBERTO SULPIZIO
	Sara Meschiari
	Damiano Sarocchi
	Luis Angel Rodriguez-Sedano
	Federico Lucchi
Funding Information:	
Abstract:	Laboratory experiments on granular flows using natural material were carried out using different experimental conditions, in order to investigate the behavior of fine to coarse-grained, channelized and not channelized granular flows passing over a break in slope. Morphometric parameters of channelized and not channelized experiments were compared for both fine-grained and coarse-grained grain size distributions. After normalization, morphometric data provided empirical relationships that highlight the major influence of grain size vs. channelization of the experimental flows. Normalized velocity data show third-order polynomial fit for both coarse-grained and fine-grained experiments, as well as for not channelized and channelized ones. This highlights similar complex behavior of the different experimental flows, which differs only for different partition of inertial and frictional forces at changing grain size of experimental mixtures. Finally, we discussed the applicability of the experimental results to natural granular flows, highlighting the difficulties to directly apply the experimental equations to fine-rich pyroclastic density currents and volcaniclastic flows due to the influence of fluidization processes in many fine-grained natural flows.
Suggested Reviewers:	Greg Valentine gav4@buffalo.edu expert of natural flows
	Gert Lube G.Lube@massey.ac.nz expert on experiments on volcanic flows
	Guido Giordano guido.giordano@uniroma3.it expert on volcanic flows
Author Comments:	Dear Editor, we would ask not to select the following colleagues for the revision of the manuscript, due to competing research: i) B. Cagnoli (INGV Bologna); ii) researchers of the group or collaborating with P. Kokelaar (Un. of Liverpool); iii) O. Roche (Lab Magma et Volcans, Clermont Ferrand)

The influence of grain size and channelization on mobility of volcanic granular flows: insights from laboratory experiments

Sulpizio R.[1,2,3], Meschiari S.[4], Sarocchi D.[5,6], Rodriguez-Sedano L.A.[5], Lucchi F.[4]

[1] Dipartimento di Scienze della Terra e Geoambientali, via Orabona 4, 70125, Bari, Italy

[2] IGAG-CNR, via M. Bianco 9, Milan, Italy

[3] INGV section of Bologna, via D. Creti, Bologna, Italy

[4] Dipartimento di Scienze Biologiche, Geologiche ed Ambientali, Piazza di Porta San Donato, 1, 40126, Bologna, Italy

[5] Instituto de Geología. Universidad Autónoma de San Luis Potosí, Dr. M. Nava No. 5, Zona Universitaria, San Luis Potosí, 78240, México.

[6] CONACYT-Instituto de Geología, Universidad Autónoma de San Luis Potosí, Av. Dr. M. Nava No 5, Zona Universitaria, 78240, San Luis Potosí, México

Abstract

Laboratory experiments on granular flows using natural material were carried out using different experimental conditions, in order to investigate the behavior of fine to coarse-grained, channelized and not channelized granular flows passing over a break in slope. Morphometric parameters of channelized and not channelized experiments were compared for both fine-grained and coarse-grained grain size distributions. After normalization, morphometric data provided empirical relationships that highlight the major influence of grain size vs. channelization of the experimental flows.

Normalized velocity data show third-order polynomial fit for both coarse-grained and fine-grained experiments, as well as for not channelized and channelized ones. This highlights similar complex behavior of the different experimental flows, which differs only for different partition of inertial and frictional forces at changing grain size of experimental mixtures.

Finally, we discussed the applicability of the experimental results to natural granular flows, highlighting the difficulties to directly apply the experimental equations to fine-rich pyroclastic

density currents and volcaniclastic flows due to the influence of fluidization processes in many fine-grained natural flows.

Keywords: granular flows; experiments; pyroclastic density currents; volcaniclastic flows

Introduction

Many hazardous natural processes, like snow avalanches, landslides, debris flows and pyroclastic density currents (PDCs) are dominated by granular flow processes (Iverson 1997; Branney and Kokelaar 2002; Zanchetta et al. 2004; Louge et al. 2012; Sulpizio et al. 2014), being characterized by complex interactions between solid grains and an accessory fluid phase that ultimately control their motion, deposition and final runout (Campbell 2006; Iverson and Vallance 2001). In volcanic settings, the physics of granular flows particularly controls the dynamics of concentrated PDCs and debris flows, which are among the most dangerous phenomena related to volcanic activity, threatening life and producing great economic loss around the world (Tilling and Lipman 1993; Tanguy et al. 1998; Gurioli et al. 2010). Mobility of natural volcanic granular flows (e.g. concentrated pyroclastic density currents, debris flows) is a major topic in volcanology since long times (Hayashi and Self 1992; Dade and Huppert 1998; Calder et al. 2000; Breard et al. 2018; Palladino and Giordano 2019), but it has relevance also for snow avalanches (Vallet et al. 2004; Turnbull et al. 2007; Louge et al. 2012) and granular flow studies (e.g. Gray et al. 1999; Pudasaini and Hutter 2007; Pudasaini 2012).

The dynamics of (dry) granular flows, in terms of particle segregation, erosion and rate of deposition, is directly influenced by local variations of the topographic slopes, as documented in volcanic areas and other sedimentary settings (e.g. Macias et al. 1998; Calder et al. 2000; Denlinger and Iverson 2001; Mulder and Alexander 2001; Felix and Thomas 2004; Zanchetta et al. 2004; Cole et al. 2005; Gray et al. 2005; Lube et al. 2007; 2011; Sulpizio et al. 2007; 2010; Bernard et al. 2014). However, accurate physical models describing the motion of granular flows over topography are few and unsatisfactory (Gray et al. 1999; Denlinger and Iverson 2001; Iverson et al. 2004), due to the complex feedbacks between moving particulate and real topography at a millimeter to decameter scale. This implies that the effects of grain size distribution of the granular flow and length of confinement within valleys and channels is largely undetermined, as well as their influence on flow dynamics and runout.

The motion of natural volcanic granular flows is hardly observable, because of their very hostile nature, and the collection of geological data from past deposits is very extensive but not decisive for reconstructions of the behavior of the corresponding avalanches. It descends that laboratory experiments are usually the best compromise between observable and measurable processes and natural scale of phenomena. Here we present the results of a number of laboratory experiments that simulate the behavior of granular flows engineered and carried out using a 5-m-long flume (Fig. 1a) and natural volcanic particles. The experiments deal with the runouts of channelized and unconfined flows using coarse and fine-grained volcanic material moving across a break in slope. In particular, the results of coarse-grained granular flows in unconfined conditions provided by Sulpizio et al. (2016) are here complemented and compared with experiments carried out using fine-grained material and channelized coarse-grained one. The results highlight some significant feedbacks on flow mobility among slope changes, grain size and flow channelization, which may provide important insights for the comprehension of natural granular flows.

Experimental setup

The laboratory experiments were carried out using a flume facility, designed and built up at the

Instituto de Geología of Universidad Autónoma de San Luis Potosí (Mexico), using an acrylic rough-bottom flume with transparent glass sidewalls, which allows real-time observation of the moving granular avalanches (see Sulpizio et al., 2016 for details). It is a modular apparatus, whose geometric characteristics can be modified to arrange different experimental setups. The facility consists of the following sections (Fig. 1a): (1) a charge system, consisting of a container of granular material (hopper) with a remotely controlled electromagnetic opening system; (2) a delivery system, where the granular material is delivered to the channel; (3) a channel with constant slope (which can be changed by the operator), where the flow starts and develops; and (4) an expansion box with transparent sidewalls, with inclination that can vary between 0° and 20°, where the granular material decelerates and deposits. We run two different types of experiments where the deceleration of the granular flows occurred in i) confined and ii) unconfined conditions. In the first case, the channel was prolonged within the expansion area using glass walls that delimited a channel of the same width, whilst in the second case the granular material was left to expand unconfined in the expansion box (Sulpizio et al. 2016). In the first set of experiments (see also Sulpizio et al., 2016), instrumentation consists of three medium-speed (60 fps) high-resolution (1920 × 1080 pixel) camcorders (SONY HDR-CX240) and a GoPro (Hero3 model) with fish-eye zenithal vision. In the second set of experiments (with channelized deposition area), three Nikon1 J1 cameras (400 fps and 640 × 240 pixel resolution) were used, as well as a GoPro hero 7 camera for a zenithal panoramic view.

The experimental runs were performed with a (constant) channel inclination of 40°, whereas the inclination of the expansion box varied between 0° and 20°, at steps of 5°. We define slope-angle ratio (SR) the ratio between the slope angle in the expansion box (depositional area) and that in the upstream channel (charge area), so that lower SRs indicate greater breaks in slope. Three experiments for each SR were carried out. We used two grain size distributions of the granular material to run the experiments (Fig. 1b): coarse grained (30° internal and 35° basal friction angle of material) and fine grained (32° internal and 37° basal friction angle of material). The material (43 kg for each experiment) was released from the hopper by means of a remotely controlled electromagnetic trap door and dropped vertically from a height of 0.40 m above the channel top.

The granular material for the experiments is represented by moderately vesicular, dacitic pyroclastics from the Nevado de Toluca volcano (Mexico), sieved at 1φ interval ($\varphi = -\log_2 d$, where d is the particle diameter). The sieved material was assembled in order to obtain a coarse-grained Weibull distribution, modified with the addition of coarse-grained material (−3φ; 8 mm), and a fine-grained Gaussian distribution (Fig. 1b).

Results

We describe here the original results of experiments carried out using fine-grained material in confined and unconfined conditions and channelized coarse-grained material, which are compared with the dynamics of coarse grained unconfined granular flows described by Sulpizio et al. (2016). In our experiments the material charged in the hopper falls into the flume after 0.40 m of free fall. Following the impact with the flume bottom the material accelerates until the break in slope, beyond which the granular flow starts to spread unconfined (then decelerating) in the expansion box (Fig. 2a) or decelerates confined in the channel (Figs. 2b, c).

The results of experiments using two different grain sizes in channelized or not channelized conditions, highlight similar behaviors in terms of the relationships between runout and SR. Here we define the normalized runout as the ratio between the distance travelled beyond the break in slope for each experiment (D), which is the effective runout of the flows, and the difference in height between the hopper gate and the deposit in the expansion box (ΔH) (Fig. 1a). Not channelized experiments show a linear dependence of the normalized runout on SR for experiments carried out with both coarse grained and fine grained material (Fig. 3a). The runouts are similar for low SR values (0 to 0.125), but they diverge at increasing SR values (Fig. 3a). This is clearly expressed by the different angular coefficients of the two regression lines, passing from 1.1 for the fine-grained grain size to 1.5 for the coarse-grained one. Channelized experiments show a behavior very similar to not channelized ones, with angular coefficients that vary from 1.2 for fine-grained material to 1.6 for coarse-grained one (Fig. 3b). The comparison of experiments using the same grain size in channelized and not channelized conditions shows quite similar regression lines, with only a limited increase shift of 5-10% in favor of channelized experiments (Figs. 3c, d).

To investigate the depositional behavior in the different experimental conditions, we plotted also the position of the normalized maximum thickness relative to SR (Fig. 4). The position of the normalized maximum thickness is expressed as the ratio between the distance at which the maximum thickness of the deposits is recorded (MT) and the difference in height between the hopper gate and the deposit in the expansion box (ΔH). The MT represents the position of the main mass of the granular material and, due to the geometry of the deposits in channelized and not channelized experiments, it can be considered as a proxy of the center of mass of the deposits. From Figure 4a it is evident how the general behavior described by the normalized maximum thickness vs. SR in not channelized conditions is similar to that described for the runout, but there is a marked divergence at increasing SRs between coarse grained and fine grained material highlighted by different angular coefficients (from 0.55 to 1.05). Whilst, in channelized conditions the behavior of the normalized maximum thickness vs. SR is largely different, with data that are best fitted by power laws (Fig. 4b). Experiments for both coarse-grained and fine-grained material show almost constant $MT/\Delta H$ values (0.08-0.11 for coarse grained and 0.05 for fine grained material) at low (coarse grained flows) and low to intermediate (fine-grained flows) SRs (shaded areas in Fig. 4b). Data at increasing SRs may be linearly fitted (Fig. 4b).

The depositional behavior is also described by means of geometric parameters, such as perimeter

(2p) and area (A) of the deposit (Table 1), measured from images of the (fine-grained) material deposited in the not channelized experiments (Fig. 2a). In order to generalize these morphometric data and to compare them with those obtained from coarse-grained experiments (Sulpizio et al. 2016), perimeter and area of the deposit were normalized with respect to the difference in height between the hopper gate and the deposit in the expansion box (ΔH; Table 1). Both areas and perimeters in the different experimental conditions are linearly correlated with SR (Fig. 5a).

Similarly to Sulpizio et al. (2016), we also plotted the velocity profiles versus the travelled distance for different SRs (Fig. 5b). Velocities of the flows (v) measured in the expansion box were normalized with respect to the maximum velocity of each experimental run (v_{max}), the latter measured at the end of the inclined channel. The normalized distance (D) is instead expressed with respect to the difference in height between the hopper gate and the deposit in the expansion box (ΔH). The patterns of the (normalized) velocity vs. (normalized) distance in not channelized conditions are complex but quite similar between experiments for fine-grained (color lines in Fig. 5b) and coarse grained flows (grey lines in Fig. 5b), although the normalized values are quite different at equal SRs. The normalized data show a very good fit to a third-order polynomial, with an inflection point defining an intermediate runout region of relatively limited change in velocity (Fig. 5b). As in the case of coarse grained experiments from Sulpizio et al. (2016), the inflection point coordinates have a positive correlation with SR, and depend on the polynomial coefficients *m*, *n* and *p*, defined as in Figure 6a. These coefficients are controlled by the variables *a*, *b* and *c*, which depends of the third-order polynomial at changing SR, and can be calculated as functions of SR:

$$\begin{cases} -a = 6.4e^{-2SR} \\ b = 25e^{-3.3SR} \\ -c = 32.2e^{-4.6SR} \end{cases} \tag{1}$$

In order to compare channelized and not channelized experiments, we also plotted the normalized velocity profiles vs. normalized distance for coarse grained (Fig. 5c) and fine-grained flows (Fig. 5d). The general behavior of channelized and not channelized experiments for coarse grained and fine grained flows is similar, with only slightly longer runouts of channelized flows with respect to not channelized ones. It is worth noting that major difference between channelized and not channelized patterns is observed in the final decelerating paths of the experimental granular flows, and is more evident for SRs greater than 0.125 (Figs. 5c, d). As for the not channelized experiments of Figure 5b, the correlation between (normalized) velocity and distance of channelized flows can be expressed as a function of the variables *a*, *b* and *c*:

$$\begin{cases} -a = 3.2e^{-1SR} \\ b = 8.4e^{-1.9SR} \\ -c = 9.2e^{-3.3SR} \end{cases} \tag{2}$$

for coarse grained flows and:

$$\begin{cases} -a = 4.9e^{-1.6SR} \\ b = 17.8e^{-3SR} \\ -c = 21.5e^{-4.3SR} \end{cases} \tag{3}$$

for fine grained flows

Discussion

The mobility of granular flows is a major topic in volcanic areas and other sedimentary settings. It is generally expressed as the ratio between the horizontal distance travelled (D) and the height of generation (ΔH), which also helps to define the friction coefficient μ (Hayashi and Self 1992). Many factors influence the friction coefficient, and are either internal or external to the granular mixture. Internal factors comprise the grain size distribution (Cagnoli and Romano 2010; 2012) and mass (volume) of the material (Rodriguez-Sedano et al. 2016). External factors include channelization (Kokelaar et al. 2014) and the break in slope between the flume and the expansion area, defined here as SR (Sulpizio et al. 2016). The passage over a break in slope is generally claimed as one of the major factors influencing the dynamics of volcanic granular flows (Denlinger and Iverson 2001; Iverson et al. 2004; Zanchetta et al. 2004; Sulpizio and Dellino 2008; Sulpizio et al. 2007; 2008; Sarocchi et al. 2011; Sulpizio et al. 2014). Beyond the break in slope, the reduction in flow velocity induces deposition of material and partial transfer of momentum into the generation of turbulence and elutriation of fines (Gray et al. 2005).

The experiments reported in the present paper for coarse-grained and fine-grained volcanic material in channelized and not channelized conditions shed light on the effect of grain size and channelization of volcanic granular flows (e.g. concentrated PDCs, volcaniclastic debris flows) moving over a break in slope, as the main (internal and external) factors that control flow dynamics, inundated areas and deposit thickness. In the following, the different outputs of the experiments will be discussed in the light of runout and inundated areas, of velocity decay in the depositional area and, finally, of their predictive potential for natural cases.

Runout and inundated areas

Runout and inundated areas are discussed based on the morphometric parameters derived from image analysis of the deposits obtained in the different experimental conditions. Results for coarse grained, not channelized flows provided by Sulpizio et al. (2016) are here compared and complemented with those for experimental flows made up of fine-grained material (both channelized and not channelized) and coarse grained material in channelized conditions. The elliptical approximation of deposit contours estimated by Sulpizio et al. (2016) holds also for fine-grained deposits in the present experiments (Fig. 2a), which allows for easy extraction of morphometric parameters at changing SRs (Figs. 2a, 5a; Table 1). In particular, the major axis measured in elliptical deposits coincides with the runout of not channelized deposits, which were compared with channelized ones (Fig. 3a). It is worth noting how, starting from a common value at SR=0, the channelized and not channelized runout diverges at a rate of 0.4 SR (difference between the angular coefficients of the two regression lines in Fig. 3a, b) in coarse grained flows compared to fine grained ones (Fig. 3a, b), indicating the strong sensitivity of the reciprocal of the apparent coefficient of friction (μ=D/ΔH) from grain size at increasing SR. This means that curvature radius effects are prevailing at low SR on the dynamics of granular flows, irrespective of their grain size. Whilst, having the two adopted grain mixtures (coarse and fine grained) similar internal and basal friction angles, the divergence of runouts for coarse and fine grained flows at increasing SR needs to be related to other internal effects than energy dissipation by friction. We cannot advocate a mass dependence of the runout difference (Rodriguez-Sedano et al. 2016) because the mass of the fine and coarse grained material in the different experiments is the same (Fig. 1b). What is different is only the mass distribution along the vertical profile of the moving flow, which shows clear reverse grading of the larger clasts in the case of coarse grained experimental flows (Sulpizio et al. 2016). This flow stratification concentrates the maximum of momentum at the top of the moving granular mixture, which is the least influenced by friction. This also explains why the grain size effect is more evident at increasing SR, being the momentum partitioning of a flow moving over a break in slope less effective passing from low to high SR values (Denlinger and Iverson 2001), according to the equation:

$$q_{bs} = (m2\pi r - \frac{mv^2}{r}) \qquad (4)$$

where q_{bs} is the momentum breakdown passing over a break in slope of radius *r* (with increasing *r* corresponding to higher SR), $2\pi r$ and v^2/r are the tangential and centripetal accelerations per unit time.

In this respect, there is a limited influence of flow channelization, with confinement effect that impacts on flow runout only for 0.1 SR for both the grain size distributions (Figs. 3c, d). We can consider this slight difference as due to the energy dissipated for the lateral spreading in not channelized experimental flows.

The dependence of the reciprocal of the apparent coefficient of friction from grain size is even more evident when it is considered relative to the center of mass of the deposit (MT) rather than to the run-out ($\mu_{MT} = MT/\Delta H$) for not channelized experiments (Fig. 4a). In this case the linear fittings for coarse grained and fine grained flows yield a difference in angular coefficients of 0.5 SR. The almost constant value of μ_{MT} at low SRs (Fig. 4b) suggests that increased SR (increasing curvature radius, i.e. smoother transition between channel and depositional area) is less effective than an increased area over which friction applies, represented by the lateral walls of the channel. If we consider the balance between inertial vs. frictional forces it is evident how the first are prevalent for SR>0.125 for coarse grained mixtures, or 0.250 for fine grained ones (Fig. 4b), indicating again how abundance of fine grained grain sizes increase effectiveness of frictional forces.

Finally, the values of normalized perimeter and area for fine-grained not channelized flows relative to SR have linear fittings similar to those for the coarse-grained ones (Sulpizio et al. 2016), but they yield lower angular coefficients (Fig. 5a). This indicates a higher internal friction between the (fine) grains, which limited the surface covered by the deposits (corresponding to the inundated area) with respect to the coarse-grained experimental flows.

Velocity decay beyond the break in slope

The deceleration paths of experimental coarse and fine grained granular flows in channelized and not channelized conditions show the same trends, independently on SR. The normalized velocity profiles show three distinct phases of deceleration: (i) initial strong deceleration due to sudden drop in the driving force; (ii) almost invariant, inertia-dominated deceleration; iii) final, friction-dominated rapid deceleration (Fig. 5b). The runout decreases in fine grained flows with respect to coarse-grained ones at increasing SR, as already discussed in the previous paragraph. The same holds when comparing normalized velocity profiles for channelized vs. not channelized experimental flows. All the profiles show third order polynomial fits according to the general form:

$$v/v_{max} = 1 + mD + nD^2 + pD^3 \quad (5)$$

where m=a/ΔH, n=b/$ΔH^2$, p=c/$ΔH^3$, and a, b, c are the parameters of the third-order polynomial at changing SR (Table 2).

The passage from the initial drop in momentum and the final friction-dominated deceleration tract can be identified in the position of the flex of the third order polynomials (X_f; Fig. 5b). Figure 6 shows how X_f increases with SR, with no significant differences between channelized and not channelized experimental flows and only a slight difference between coarse- and fine-grained flows.

Implication for natural granular flows

The empirical relationships extracted from laboratory experiments provide useful insights for better understand the dynamics of transportation and deposition of natural granular flows. In particular, experiments demonstrated how, at equal boundary conditions, channelization has not a decisive effect in increasing flow runouts. On the other hand, fine grained mixtures show shorter runouts at increasing SR with respect to coarse grained mixtures (Fig. 3), indicating how grain size distribution is prevalent with respect to topographic control for determining the flow runout.
The experiment outputs seem to contradict some data from natural cases, which suggest higher mobility for fine grained PDCs or volcanoclastic flows (i.e. mud flows). As an example, fine grained PDCs generated from column/fountain collapse during the Montserrat eruption in the period 1995-1998 were reported to have longer runout and inundate larger areas with respect to coarse grained PDCs from dome collapses (Calder et al. 1999). In volcanoclastic flows, mud flows are considered more mobile than coarse grained debris flows, as in the case of Osceola mud flow from Mount Rainier (USA; Vallance and Scott 1997).
This apparent contradiction between experiments and natural flows may be explained by other mechanisms that in nature may alter the simple relationships found in the experiments. First of all, fine grain size of the solid particles can promote fluid (gas or water) retention within the mixture, promoting fluidization (Druitt et al. 2006; Iverson 1997). Fluidization reduces granular contacts, which are the primary source of energy consumption due to frictional forces. As an example, fluidization was claimed as main mechanism explaining the longer runouts of slow moving,

ignimbrite-forming concentrated PDCs (Roche et al. 2016). Efficiency of fluidization depends on many factors, including topographic roughness, amount of gas in eruptive mixture or water in volcaniclastic flow, and type of substratum. In any case, the most prevalent parameter is the permeability of the solid mixture, which controls the rate of fluid escape from the moving flow (Burgisser 2012; Sulpizio et al. 2014). Permeability is the combination of different physical properties of the moving mixture, including flow expansion, grain size distribution and shape and sorting of solid particles (Burgisser 2012). Flow expansion depends mainly on granular temperature, which measures the state of agitation of solid particles, and is proportional to the square of flow velocity. Higher is the flow expansion, easier is the gas escape. This effect reduces effectiveness and duration of fluidization state in the flow. Grain size distribution controls the rate of fluidization vs. elutriation of very fine grained particles, which impinge on the retention of fluid within the moving flow. Finally, shape of particles determines the tortuosity of fluid paths, which rules the time of fluid escape from the solid mixture (Burgisser 2012).

From the parameters discussed above, it is evident how the fluidization strongly depends on availability of fluid sources and characteristics of solid particles. Applying these characteristics to our experiments, it emerges how there are not internal (e.g. magmatic gas from breakage of juvenile clasts) nor external (e.g. water filled sediments, vegetation) fluid sources to the moving mixture. Also, the air ingestion of air from flow front is not effective, except for the expanded front, as demonstrated by inspection of experiment video-records (Sulpizio et al. 2016).

The coarse grain size distribution of the experimental material show more than 90% of particles coarser than 0.5 mm and ca. 20% coarser than 2 mm (Fig. 1b), which seems not adequate to retain the (small) amount of gas (air) available within the moving flow. On the other hand, the mixture used for fine grained experiments shows a very good sorting, which increases permeability.

This justifies why our experimental flows largely appear non-fluidized granular flows, and the apparent contradiction of experimental results with some natural cases described in the literature.

All these points alerts on apodictic and acritical applicability of experimental results to nature, which has to be intended appropriate only for non-fluidized, fine- to coarse-grained granular flows.

Conclusion

Experimental runs were performed in order to investigate the behavior of coarse-grained and fine-grained volcanic material passing over a break in slope. Channel inclination was maintained fixed at 40°, whereas the inclination of the expansion box was varied between 0° and 20°, at steps of 5°. This experimental setup allowed to measure flow parameters at different SR, defined as the ratio between the slope angle in the expansion box (depositional area) and that in the upstream channel (charge area), so that lower SRs indicate greater breaks in slope. Experiments were carried out using two grain size distributions of the granular material: coarse grained (30° internal and 35° basal friction angle of material) and fine grained (32° internal and 37° basal friction angle of material).

Experiments results highlight linear dependence of runouts of both coarse-grained and fine-grained mixtures to SR. The two regression lines differs of 0.4 SR, indicating the strong sensitivity of the reciprocal of the apparent coefficient of friction (μ=D/ΔH) from grain size at increasing SR. This means that curvature radius effects are prevailing at low SR on the dynamics of granular flows, irrespective of their grain size.

The effect of flow channelization is less effective, with confinement effect that impacts on flow runout only for 0.1 SR for both the grain size distributions.

The deceleration paths of experimental coarse and fine grained granular flows in channelized and not channelized conditions show the same trends, independently on SR. The normalized velocity profiles show three distinct phases of deceleration: (i) initial strong deceleration due to sudden drop in the driving force; (ii) almost invariant, inertia-dominated deceleration; iii) final, friction-dominated rapid deceleration.

Finally, caution was recommended for direct application of experimental results to nature, because of the more complex behavior of real fine-rich flows due to the superimposition of fluidization effects that can alter the energy dissipation within the moving flow.

Acknowledgments

References

Bartali R, Sarocchi D, Nahmad-Molinari Y, Rodríguez-Sedano LA (2012) Estudio de flujos granulares de tipo geológico por medio del simulador multisensor GRANFLOW-SIM. Bol Soc Geol Mex 64:281–291

Bernard J, Kelfoun K, Le Pennec J-L, Vallejo Vargas S (2014) Pyroclastic flow erosion and bulking processes: comparing field-based vs. modeling results at Tungurahua volcano, Ecuador. Bull Volcanol 76:858. doi:10.1007/s00445-014-0858-y

Bourgisser A (2012) A semi-empirical method to calculate the permeability of homogeneously fluidized pyroclastic material. J Volcanol Geotherm Res 243–244: 97–106

Branney M, Kokelaar B (2002) Pyroclastic density currents and the sedimentation of ignimbrites. Geol Soc London Mem 27:1–143

Cagnoli B, Romano GP (2010) Effect of grain size on mobility of dry granular flows of angular rock fragments: An experimental determination. J Volcanol Geotherm Res 193:18-24.

Cagnoli B, Romano GP (2012) Effects of flow volume and grain size on mobility of dry granular flows of angular rock fragments: a functional relationship of scaling parameters. J Geophys Res 117, B2. doi: 10.1029/2011JB008926

Calder ES, Cole PD, Dade WD, Druitt TH, Hoblitt RP, Huppert HE, Ritchie L, Sparks RSJ, Young SR (1999) Mobility of pyroclastic flows and surges at the Soufriere Hills Volcano, Montserrat. Geophys res Lett 26, 5: 537-540

Calder ES, Sparks RSJ, Gardeweg MC (2000) Erosion, transport and segregation of pumice and lithic clasts in pyroclastic flows inferred from ignimbrite at Lascar Volcano, Chile. J Volcanol Geotherm Res 104:201–235

Campbell CS (2006) Granular material flows—an overview. Powder Tech 162:208–229

Cole PD, Fernandez E, Duarte E, Duncan AM (2005) Explosive activity and generation mechanisms of pyroclastic flows at Arenal volcano, Costa Rica between 1987 and 2001. Bull Volcanol 67:695–716

Dade WB, Huppert HE (1998) Long-runout rockfalls. Geology 26 (9): 803–806.

Denlinger RP, Iverson RM (2001) Flow of variably fluidized granular masses across three-dimensional terrain. II. Numerical predictions and experimental tests. J Geophys Res 106:553–566

Druitt TH, Avard G, Bruni G, Lettieri P, Maez F (2007) Gas retention in fine-grained pyroclastic flow materials at high temperatures. Bull Volcanol 69, 881–901.

Felix G, Thomas N (2004) Relation between dry granular flow regimes and morphology of deposits: formation of levees in pyroclastic deposits. Earth Planet Sci Lett 221:197–213

Gray TE, Alexander J, Leeder MR (2005) Quantifying velocity and turbulence structure in depositing sustained turbidity currents across breaks in slope. Sedimentology 4:1–22

Gray JMNT, Wieland M, Hutter K. (1999) Free surface flow of cohesionless granular avalanches over complex basal topography. Proc R Soc A 455:1841–74.

Gurioli L, Sulpizio R, Cioni R, Sbrana A, Santacroce R, Luperini W, Andronico D (2010) Pyroclastic flow hazard assessment at Somma–Vesuvius based on the geological record. Bull Volcanol 72:1021–1038. doi:10.1007/s00445-010-0379-2

Hayashi JN, Self S (1992) A comparison of pyroclastic flow and debris avalanche mobility. J Geophys Res 97:9063-9072.

Iverson R (1997) The physics of debris flows. Rev Geoph 35:245–296

Iverson RM, Vallance JW (2001) New views of granular mass flows. Geology 29:115–118

Iverson RM, Logan M, Denlinger RP (2004) Granular avalanches across irregular three-dimensional terrain: 2. Experimental tests. J Geophys Res Earth Surf 109:F01015

Kokelaar BP, Graham RL, Gray JMNT, Vallance JW (2014) Fine-grained linings of leveed channels facilitate runout of granular flows. Earth Planet Sc Lett 385:172-180.

LougeM, Turnbull B, Carroll C (2012) Volume growth of a powder snow avalanche. Ann Glaciol 53:57–60

Lube G, Cronin SJ, Platz T, Freundt A, Procter JN, Henderson C, Sheridan MF (2007) Flow and deposition of pyroclastic granular flows: a type example from the 1975 Ngauruhoe eruption, New Zealand. J Volcanol Geotherm Res 161:165–186

Lube G, Huppert HE, Sparks RSJ, Freundt A (2011) Granular column collapse down rough, inclined channels. J FluidMech 675:347–368

Macias JL, Espindola JM, Bursik MI, Sheridan MF (1998) Development of lithic-breccias in the 1982 pyroclastic flow deposits of El Chichon volcano, Mexico. J Volcanol Geotherm Res 83:173–196

Mulder T, Alexander J (2001) The physical character of subaqueous sedimentary density flows and their deposits. Sedimentology 48: 269–299

Sulpizio R, Dellino P (2008) Sedimentology, depositional mechanisms and pulsating behaviour of pyroclastic density currents: Caldera volcanism: analysis, modelling and response. Developments in Volcanology 10, (Eds J. Gottsman and J. Marti): 58–96. Elsevier, Amsterdam

Palladino DM, Giordano G (2019) On the mobility of pyroclastic currents in light of deposit thickness and clast size trends. J Volcanol Geotherm Res 384:64-74.

Pudasaini SP (2012) A general two-phase debris flow model. J Geophys Res 117: F03010.

Pudasaini SP, Hutter K (2007) Avalanche Dynamics—Dynamics of Rapid Flows of Dense Granular Avalanches, Springer-Verlag, Berlin.

Roche O, Buesch DC, Valentine GA (2016) Slow-moving and far-travelled dense pyroclastic flows during the Peach Spring super-eruption. Nat Comm, 7: 10890, DOI 10.1038/ncomms10890

Sarocchi D, Sulpizio R, Macías J L, Saucedo R (2011) The 17 July 1999 block-and-ash flow (BAF) at Colima Volcano: new insights on volcanic granular flows from textural analysis. J Volcanol Geotherm Res 204 (1-4): 40-56

Sulpizio R, Zanchetta G, Demi F, Di Vito MA, Pareschi MT, Santacroce R (2006) The Holocene syneruptive volcaniclastic debris-flows in the Vesuvian area: geological data as a guide for hazard assessment. *In:* Siebe C, Macias JL, Aguirre-Diaz GJ eds, Neogene–Quaternary continental margin volcanism: a perspective from Mexico. GSA Special Paper 402: 203-221

Sulpizio R, Mele D, Dellino P, La Volpe L (2007) Deposits and physical properties of pyroclastic density currents during complex Subplinian eruptions: the AD 472 (Pollena) eruption of Somma-Vesuvius, Italy. Sedimentology 54:607–635

Sulpizio R, De Rosa R, Donato P (2008) The influence of variable topography on the depositional behaviour of pyroclastic density currents: the examples of the Upper Pollara eruption (Salina Island, southern Italy. J Volcanol Geotherm Res 175:367–385

Sulpizio R, Bonasia R, Dellino P, Mele D, Di Vito MA, La Volpe L (2010) The Pomici di Avellino eruption of Somma-Vesuvius (3.9 ka BP). Part II: sedimentology and physical volcanology of pyroclastic density current deposits. Bull Volcanol 72:559–577

Sulpizio R, Dellino P, Doronzo DM, Sarocchi D (2014) Pyroclastic density currents: state of the art and perspectives. J Volcanol Geotherm Res 283:36–65

Sulpizio R, Castioni D, Rodriguez-Sedano LA, Sarocchi D, Lucchi F (2016) The influence of slope-angle ratio on the dynamics of granular flows: insights from laboratory experiments. Bull Volcanol 78:77. DOI 10.1007/s00445-016-1069-5

Tanguy JC, Ribiere C, Scarth A, Tjetjep WS (1998) Victims from volcanic eruptions: a revised database. Bull Volcanol 60:137–144

Tilling RI, Lipman PW (1993) Lessons in reducing volcanic risks. Nature 364:77–280

Turnbull B, McElwaine JN, Ancey C (2007) Kulikovskiy–Sveshnikova–Beghin model of powder snow avalanches: Development and application. J Geophys Res 112, F1. Doi: 10.1029/2006JF000489

Vallance JW, Scott KM (1997) The Osceola mudflow from Mount Rainier: Sedimentology and hazard implications of a huge clay-rich debris flow. Geol Soc Am Bull, 109(2), 143–163.

Vallet J, Turnbull B, Joly S, Dufour F (2004) Observations on powder snow avalanches using videogrammetry. Cold Reg Sci Technol 39(2-3): 153–159. Doi:10.1016/j.coldregions.2004.05.00

Zanchetta G, Sulpizio R, Pareschi M, Leoni F, Santacroce R (2004) Characteristics of may 5–6, 1998 volcaniclastic debris flows in the Sarno area (Campania, southern Italy): relationships to structural damage and hazard zonation. J Volcanol Geotherm Res 133:377–393

Figure captions

Figure 1 – Design of the experimental flume. a) Sketch of the charge and delivery system, flume and expansion box; b) grain size histograms and tables for material used for coarse-grained and fine-grained experiments;

Figure 2 – View of not channelized and channelized deposits using different SR values. a) Deposits of fine-grained experiments. The red contours were used for calculation of morphological parameters listed in Table 1; b) examples of channelized deposits for coarse-grained (two pictures on the left) and fine-grained (two pictures on the right) experiments.

Figure 3 – Diagrams of reverse apparent coefficient of friction (D/ΔH) vs. slope ratio (SR). a) Not channelized experiments, comparing fine-grained (red) and coarse-grained (blue) experiments. Equation for linear interpolation of data are also reported; b) channelized experiments, comparing fine-grained (green) and coarse-grained (orange) experiments. Equation for linear interpolation of data are also reported; c) comparison of channelized and not channelized coarse-grained experiments; d) comparison of channelized and not channelized fine-grained experiments

Figure 4 - Diagrams of reverse apparent coefficient of friction of the maximum thickness of the deposits (MT/ΔH) vs. slope ratio (SR). a) Not channelized experiments, comparing fine-grained (red) and coarse-grained (blue) experiments. Equation for linear interpolation of data are also reported; b) channelized experiments, comparing fine-grained (red) and coarse-grained (blue) experiments. Green and grey shaded areas indicate the almost constant MT/ΔH values. Equation for power law interpolation (solid lines) of data are reported, while dashed lines indicate linear interpolation of data beyond the constant MT/ΔH values.

Figure 5 - Diagrams of a) morphometric parameters vs. slope-angle ratio of fine-grained, not channelized experiments (in red). In grey are reported the morphological data of coarse-grained experiments (from Sulpizio et al. 2016); b) diagram of normalized velocity (velocity/maximum velocity) vs. normalized distance (D/ΔH) for not channelized experiments. The general form of the third-order polynomial regression is also shown, along with the general expression of parameters m, n and p; c) diagram of normalized velocity vs. normalized distance for coarse-grained experiments; d) diagram of normalized velocity vs. normalized distance for fine-grained experiments.

Figure 6 – Diagram showing the position of flex of third order polinomials of Figure 5 vs. SR for the different combinations of grain size and channelization and not channelization.

Table captions

Table 1 – Morphological parameters of deposits from fine-grained experiments.

Table 2 - Variations of parameters *a*, *b* and *c* of the third-order polynomial fit at changing SR and for the various combination of grain size and channelization

Figure 1

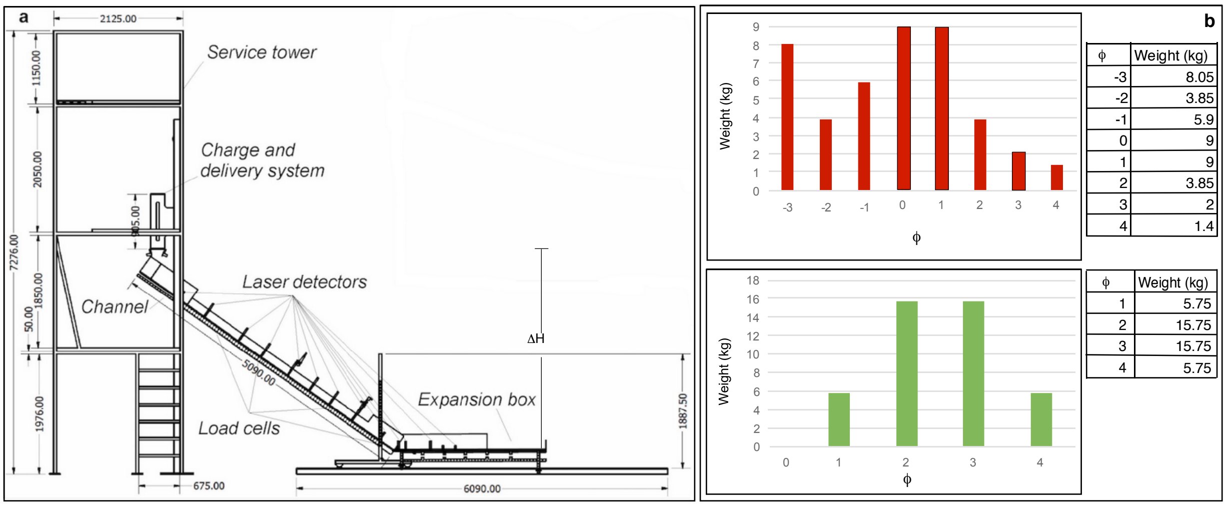
a
2125.00
Service tower
Charge and
delivery system
Laser detectors
Channel
Load cells
Expansion box
ΔH
5090.00
1887.50
675.00
6090.00
7276.00
1150.00
2050.00
1850.00
50.00
1976.00
b
Weight (kg)
ϕ
ϕ Weight (kg)
-3 8.05
-2 3.85
-1 5.9
0 9
1 9
2 3.85
3 2
4 1.4
ϕ Weight (kg)
1 5.75
2 15.75
3 15.75
4 5.75

Figure 2

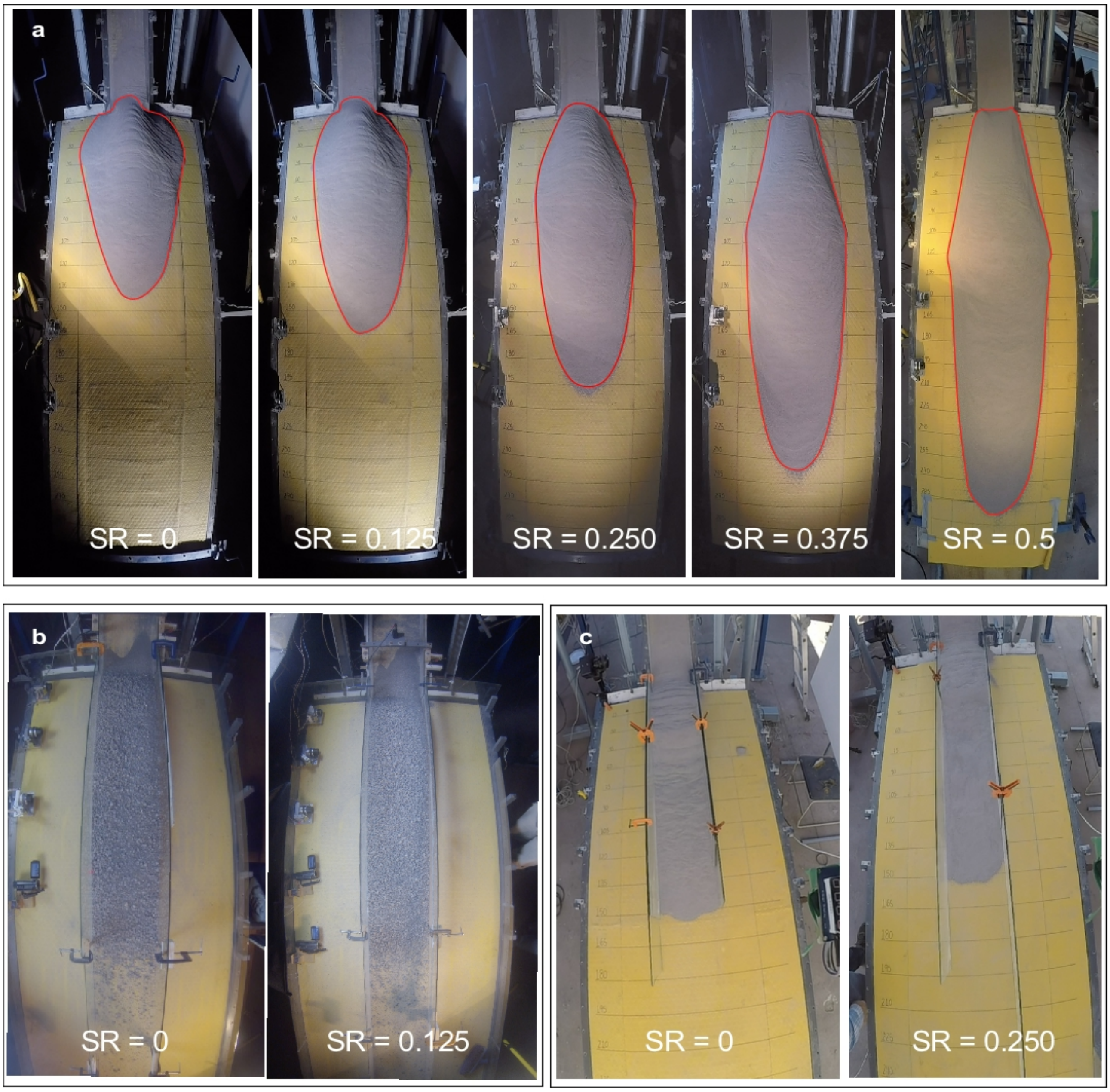

Figure 3

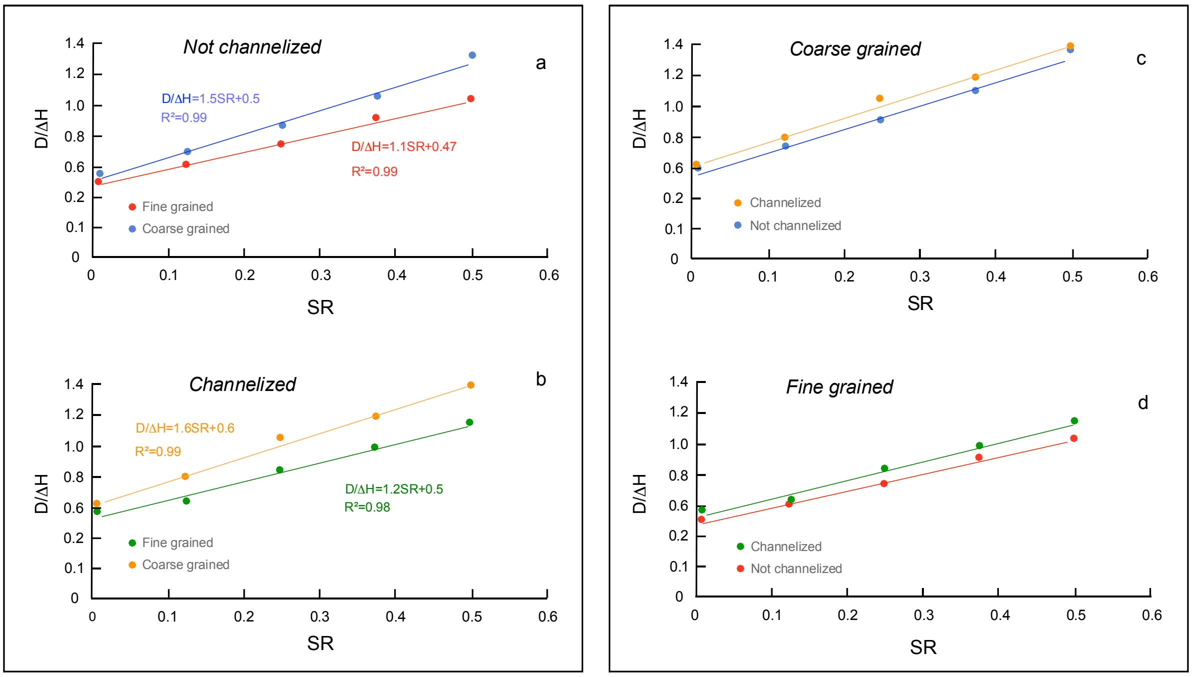

Figure 4

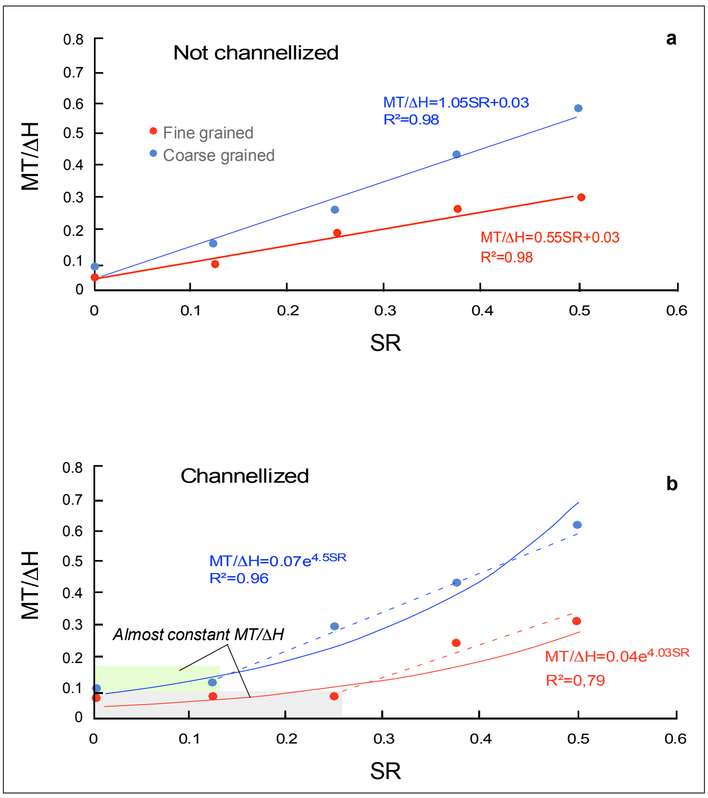

Figure 5

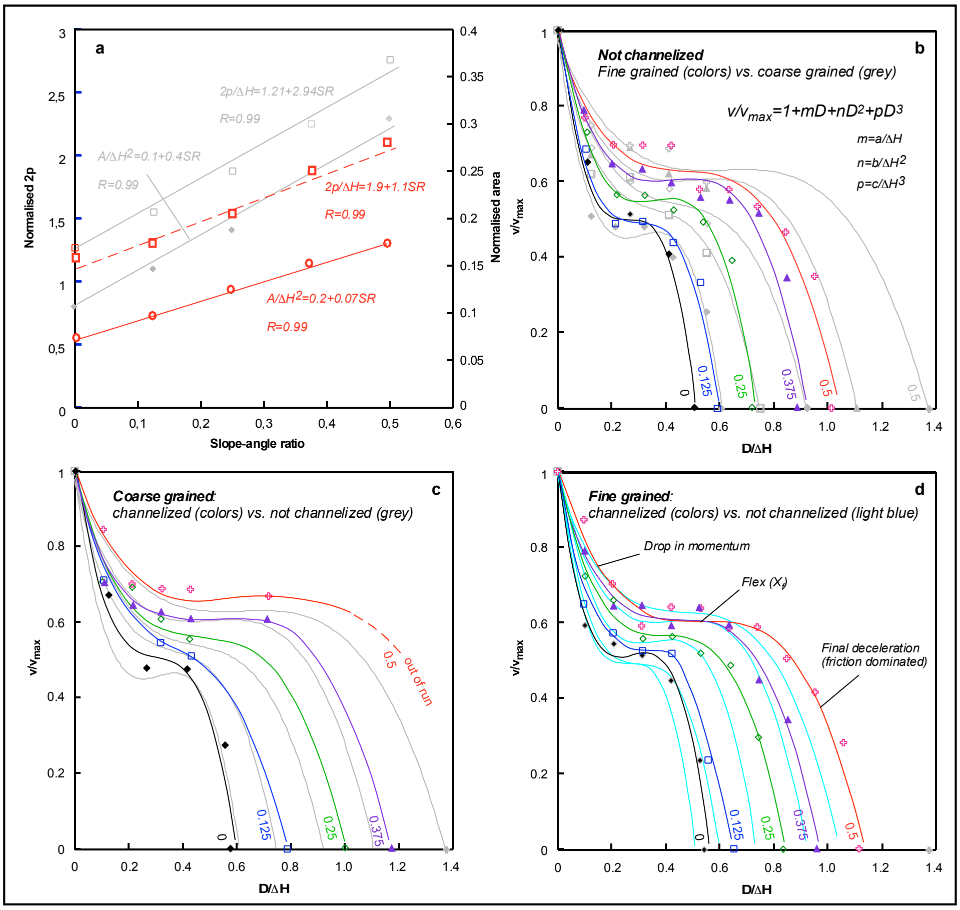

Figure 6

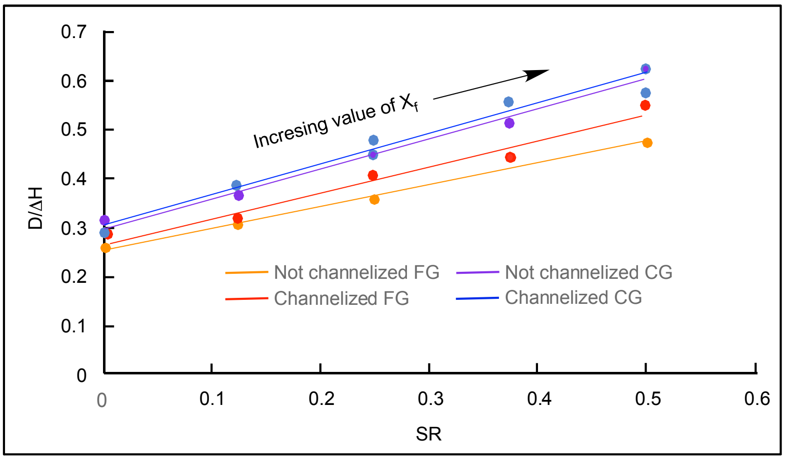

Table 1

Non-normalized			Normalized	
SR	**2p (m)**	**area (m^2)**	**2p norm**	**area norm**
0	323,9	5500	1,16	0,07
0,125	357,9	7383,7	1,28	0,09
0,25	417,6	9298,2	1,49	0,12
0,375	515,3	11729,5	1,84	0,15
0,5	579,6	13292,9	2,07	0,17

Table 2

	Coarse grained channelized			*Fine grained channelized*		
SR	**a**	**b**	**c**	**a**	**b**	**c**
0,0001	3,3	9,3	11	5,5	20,4	24,3
0,125	2,7	5,9	5,2	3,7	11	11,7
0,25	2,5	5,1	3,6	3,1	7,6	6,3
0,375	2,3	4,3	2,6	2,6	5,8	4,4
0,5	1,9	3,4	2	2,4	4,4	2,7
	Coarse grained not channelized			*Fine grained not channelized*		
SR	**a**	**b**	**c**	**a**	**b**	**c**
0,0001	5,5	18,29	19,57	6	23,5	30,6
0,125	3,3	8,51	7,8	5,1	16,8	18,5
0,25	2,7	5,8	4,34	4,2	12,1	11,4
0,375	2,2	4,48	2,93	3	7,1	5,4
0,5	1,72	2,81	1,51	2,2	4,5	3,2

Chapter 8

Conclusions

This multidisciplinary study of the Brown Tuffs (BT) in the Aeolian Islands, combining field stratigraphic and sedimentological analyses together with geochemical investigations, new radiocarbon ages and laboratory experiments on granular flows, has provided new insights on the characterization of their source area of La Fossa Caldera on Vulcano and definition of the transport and depositional mechanisms and dispersal area, with special emphasis on the role of the BT as proximal-distal correlatives. The following are the main results of this research.

1) A large dataset of grain-specific major element volcanic glass compositional data for the different BT depositional units on Vulcano and Lipari has defined the juvenile compositions ranging from basaltic trachyandesite and trachy-andesite to trachytes compositions, broadly evolving to higher SiO_2 contents through the succession. These compositional feature largerly correspond with those of the Vulcano magmatic system. This reinforces the correlation of the BT with the Vulcano magmatic system.
2) Stratigraphic analyses, combined with glass compositional data for the different BT depositional units on Vulcano and Lipari, have defined correlations between the Lower BT, Intermediate BT, Intermediate-upper BT and Upper BT macro-units and proximal units on Vulcano, providing a more robust framework for the long-term hazard assessment related to explosive activity within the La Fossa Caldera. in particular, a clear geochemical link is suggested between the UBT and the early products of the La Fossa cone, indicating a shared magmatic system during the last 24 ka, and thus extending the life cycle of this currently active eruptive source area
3) Unequivocal proximal-to-distal correlations of the BT with ash deposits preserved across the Aeolian archipelago and in Tyrrhenian and Adriatic Sea marine cores with important insights into the scale of these eruptions and the associated hazard in the region under study.
4) Stratigraphic and geochemical data, combined with new radiocarbon ages and correlations with distal tephra layers, have allowed to re-define the the time interval of the eruptions that deposited the Upper BT to between 24 and 6 ka based on the

observed chemostratigraphic transitions which coincides with the age of the Spiaggia Lunga marker bed on Vulcano.

5) The UBT on Vulcano are interpreted as the result of a repetitive aggradation pyroclastic density currents (PDCs) pulses characterized by either fluid escape or granular flow depositional regimes from a fine-grained, concentrated flow-boundary zone or grain by grain deposition from diluted and turbulent PDCs, and are characterized by distinctive intermittent stratification induced by post-depositional disruption of the primary deposits due to fluid escape related to dissipation of pore pressure between layers at different porosity.
6) Distinctive sedimentary structures (mixing bands, undulated, recumbent flame and rip-up structures) are documented at the base of a number of BT depositional units on Vulcano and Lipari by sedimentological, grain-size and geochemical investigations, and also verified in the behaviour of ash-rich granular flows in properly desgined laboratory experiments. These structures indicate effective lateral transport and moderate to high shear stress exerted by the BT ash currents to the substratum producing erosion and incorporation of loose material from the underlying beds up to distances of even 16-17 km from the source area. They highlight and enhance the potential hazard and impact capacity of this kind of eruptions over the territory of this kind of eruptions.
7) Properly designed laboratory experiments for fine-grained granular flows, which reproduce the behaviour of ash-rich PDCs during the BT eruptions, indicate that flow mobility is directly inlfuenced by slope ratio (SR) variations, grain size and channelization, thus providing insights on the comprehension of their behaviour.

Chapter 9

Future perspectives

This section contains some perspectives on research lines that could be developed in the coming months by taking advantage of the completion of some sets of analyses (in addition to the ones already acquired) and the path of interpretation of the data relating to them, which may lead to an increase in knowledge on some aspects related to the geology and magmatology of the Brown Tuffs (BT). Some of these research lines are already in an advanced stage, but temporarily halted due to the limitations imposed by the Covid-19 health crisis.

9.1. Eruptive parameters of ash-rich granular flows (PDCs)

Laboratory experiments on granular flows using natural ash volcanic particles were performed to check the depositional behaviour and potential erosive capability of ash-rich PDCs similar to those responsible of the emplacement of the BT. All the experiments reveal the potential of fine-grained PDCs of entrapping clasts from a loose substratum, and the entrapped particles are concentrated in the basal to middle portion of the deposit, forming shear-related sedimentary structures similar to those recognized at the base of some BT depositional units. Further experiments are needed to characterize the behaviour of fine-grained granular flows depending on slope-ratio variations, as well as elaboration of the available data to obtain values of velocity and run-out of the PDCs in the different experimental conditions.

9.2. Brown Tuff dispersal area and tephrostratigraphy

In order to assist the definition of proximal-distal and mid-distal correlations of the BT in the region under study the marine tephra layers sampled in seven deep-sea cores by ISMAR (CNR, Bologna) from the Gioia Basin (NE Sicily) and the Paola Basin (NW Calabria), in the surroundings of the Aeolian Islands, should be analyzed and completed. Distinct tephra levels within the cores were already identified through visual observation combined with magnetic susceptibility profiles and XRF logs and 92 samples of tephra and cripto-tephra layers were taken. The completion of the major element compositions of some of these tephra layers, together with trace element data on selected tephras, is expected to provide a set of correlations with the BT and other pyroclastic units in the Aeolian region, providing insights into the scale of the eruptions and the associated hazards, and offering further contribution to investigate slope instability processes in the area based on the age of the correlated tephra layers.

9.3 Brown Tuff magmatic system

The processing of the available data on the mineral chemistry of the BT, together with the major elements glass compositional data of the BT and new trace element compositions, will be carried out with the the purpose of reconstructing the magma feeding and system shallow conduit processes of the BT eruptions, and the main magmatic parameters of temperature, pressure and depth of crystallization. These aspects will be investigated in the framework of the magma plumbing system of Vulcano in the long time interval during which the eruption of the BT took place, with a special emphasis on the relationships between the BT eruptions and the subsequent development of the active La Fossa cone inside the La Fossa caldera.